STROMATOLITES AND THE BIOSTRATIGRAPHY OF THE AUSTRALIAN PRECAMBRIAN

with appendices on pseudofossils from Australian Precambrian iron-formation and greywacke

Volume II

by

M. R. Walter, B.Sc. (Hons)

Department of Geology and Mineralogy

University of Adelaide

April 1970

Contents

Volume II

APPENDICES

TABLES

FIGURES

PLATES

APPENDIX I

PSEUDOFOSSILS FROM THE BROCKMAN IRON FORMATION (PRECAMBRIAN, WESTERN AUSTRALIA) AND THEIR DIAGENETIC SIGNIFICANCE

ABSTRACT

Colloidal processes were of paramount importance during diagenesis of the Brockman Iron Formation.

The presence of large lobate and concentric medusiform pseudofossils that formed by the diffusion and rhythmic precipitation of silica and of numerous septarian nodules and their moulds and casts (some medusiform) indicates that the iron-formation was gelatinous during diagenesis. The large medusiform structures, numerous small diapirs of quartz, and other features show that during diagenesis the silica was mobile. Shrinkage during diagenesis is indicated by the common presence of septarian nodules and chalcedonic quartz, and the irregular lamination of some beds is due to this and other factors. Finely laminated quartz-iron oxide can form by the loss of silica from coarsely laminated iron oxide-poor chert; the ultimate products of this process are massive magnetite beds. "Fossils" previously described from the Brockman Iron Formation are abiogenic.

The pseudofossils indicate that the iron-formation was siliceous at a very early stage of diagenesis, when it was also gelatinous, and at this stage there was much re-organization, particularly of the silica distribution.

INTRODUCTION

The Precambrian Brockman Iron Formation occupies an area of nearly 80,000 square kilometres in the Hamersley Ranges of Western Australia (fig.47). Over a very large area it is only slightly folded and extremely well exposed. It is very little metamorphosed, if at all. Such unique preservation makes its importance in the study of iron-formation[1] great.

Several "fossils" and pseudofossils were described from this formation by Edgell (1964). He considered the apparent fossils to be stromatolites and possibly two types of meduseae. Since 1964 petrological, chemical and stratigraphic (including bore hole) information on the formation has increased greatly, and interest in Precambrian fossils and the origin of iron-formations has led to a critical field and laboratory re-examination of the evidence for biogenic activity within the formation. All specimens figured and described by Edgell were re-examined and a detailed study was made of much new material collected during several weeks in the Hamersley Ranges.

Glaessner (1962, 1966) has discussed the problems of distinguishing Precambrian fossils from pseudofossils, particularly those resulting from colloidal processes. The examination of supposed fossils from iron-formations highlights these problems because, as is shown below,

---

[1] Iron-formation is used throughout this appendix in the sense of James (1954) to mean the banded iron-rich rock largely restricted to the Precambrian.

colloidal processes were of great importance during the diagenesis of these rocks. Structures were considered abiogenic if at least one of the following criteria was satisfied: 1) Abiogenic processes necessary to form such a structure were shown to have happened in the iron-formation. 2) An appropriate physical or chemical process by which such a structure could form is known. 3) Morphology made biogenesis unlikely. It might be thought that these conditions would exclude some true fossils; this possibility was always considered and in some cases it was with reluctance that possibilities of biogenesis were finally abandoned.

Full interpretation of the pseudofossils awaits a more detailed study than this but already they have provided information on the physical and chemical systems acting during diagenesis of the iron-formation. Although experimental duplication of the complex colloidal systems operating during diagenesis would be difficult such an approach could lead to a much better understanding of these extraordinary rocks. The structures described here will be significant in any study of this sort.

As indicated in the plate captions, the illustrated specimens are kept in the Department of Geology and Mineralogy of the University of Adelaide, South Australia (numbers without prefixes), the Geological Survey of Western Australia (prefixed F), and the Western Australian Museum (prefixed WAM).

THE BROCKMAN IRON FORMATION AND ITS REGIONAL GEOLOGICAL ENVIRONMENT

A detailed account of the geology of the Hamersley Ranges with particular reference to the ore deposits is given by MacLeod (1967)

and a concise summary of the stratigraphy and structure is to be found in Daniels (1966). The Brockman Iron Formation has been described by Ryan & Blockley (1965), Trendall (1965, 1966a, 1966b) and Trendall & Blockley (1968), and Trendall (1968) has compared it with other iron-formations. The petrology of some of the "shales" within the formation is the subject of a paper by La Berge (1966). References to older literature are given in all of these publications. A summary of relevant facts is presented below.

The stratigraphic classification and nomenclature is shown in Table 7 (modified after Daniels; 1966).

		Lithology	Thickness (m)
	Wyloo Group	clastics, carbonates, chert	4,500(?)
H	Boolgeeda Iron Formation	iron-formation, shale, silt-stone	210
a			
m	Woongarra Volcanics	dacite, rhyolite	570
e			
r	Weeli Wolli Formation	iron-formation, shale, dolerite, basalt	480
s			
l	Brockman Iron Formation	iron-formation, shale, dolomite, chert	600
e	Mount McRae Shale	shale, siltstone, dolomite, chert	90
y			
G	Mount Sylvia Formation	iron-formation, shale, dolomitic shale, chert	33
r			
o	Wittenoom Dolomite	dolomitic shale, chert	150
u			
p	Marra Mamba Iron Formation	chert, iron-formation	180
	Fortescue Group	basalts, pyroclastics, arenites, cherts, dolomites	c.7,000 max.

Table 7: Content of the Mount Bruce Supergroup

The Woongarra Volcanics of the Hamersley Group have been dated by the Rb-Sr total-rock method at 2000±100 m.y. (Compston & Arriens, 1968).

The Brockman Iron Formation (fig.47) outcrops over an area approximately 480km by 160km. Folding in the Hamersley Range is very gentle and has formed large dome and basin structures. Most of the pseudofossils to be described came from the northern part of the ranges where dips are generally less than 5^{o}, although steeper dips occur locally (Trendall, 1965, p.55). In harmony with the low degree of structural disturbance metamorphism is of a very low grade, or absent. Concerning the Brockman Iron Formation in the Wittenoom Gorge area of the Hamersley Ranges La Berge (1966, p.159) stated that the predominance of ferrostilpnomelane and "the occurrence of montmorillonite in some layers with stilpnomelane, and the fact that many volcanic textures are preserved in minute detail suggests a very low grade of metamorphism". Organic matter with a high sulphur content found in the Jeerinah Formation 500m conformably below the Brockman Iron Formation indicates a low thermal history (fairly certainly less than $200^{o}C$) for the Shale, and therefore even lower for the overlying Iron Formation (Trendall, 1966b).

The Iron Formation has been divided into four members (Ryan & Blockley, 1965, Dr A. J. Trendall, pers. comm., 1968) which in descending order are the

Yandicoogina Shale Member		60m
Joffre Member	iron-formation	342-352m
Whaleback Shale Member	-	49-58m
Dales Gorge Member	iron-formation	107-180m

The Dales Gorge Member, which has been studied in greatest detail, consists of an alternation of seventeen units of iron-formation with sixteen shales. These units, termed macrobands by Trendall (1965, p.56), are apparently all coextensive with the member. Isopach maps figured by Ryan & Blockley (1965) indicate that the Dales Gorge Member was deposited in a linear basin approximating the present outcrop area, although the edges are missing. No lateral facies changes within iron-formation macrobands have been reported; on the contrary, several authors (e.g. Trendall, 1965, p.57; Trendall & Blockley, 1968) have noted the remarkable lateral persistence of units, e.g. individual chert beds 2cm thick have been recognized at localities up to about 300km apart. While breccias (Trendall, 1965), graded-bedding (La Berge, 1966), scours and cross-bedding occur in the shales, such evidence of energetic currents is absent from the iron-formation macrobands; the extraordinary persistence of beds is clear evidence of a very low energy environment, but the "cross-podded" structures of Trendall (1966a) may be ripple marks. ("Ripplemarks" earlier reported from the iron-formation macrobands are now known to be tectonic in origin; J. H. Lord, pers. comm., 1966). La Berge (1966) considers the shales to be largely pyroclastic in origin; his evidence for cyclic volcanicity is disputed by Trendall (1966b).

Detailed study of the Dales Gorge Member has led Trendall (1965, 1966a) to recognize that each macroband is composed of a large number of mesobands (individual, persistent, thin beds) which in turn consist of microbands (laminations), as shown in plates 34a and 36c-f.

The mesobands, typically 0.5 to 5cm thick, are composed of chert, chert plus iron oxides, magnetite, carbonate (commonly siderite), or rarely stilpnomelane. Combinations of these types and the inclusion of minor amounts of other minerals is normal. Microbands are usually marked by concentrations of iron oxides, carbonates, stilpnomelane or combinations of these.

COLLOIDAL PHENOMENA

A discussion of diagenesis and the formation of pseudofossils in the Brockman Iron Formation requires a brief description of two processes which commonly occur in gels. For recent discussions on the geological importance of colloids, see Chukhrov (1955), a very detailed and copiously illustrated book with an extensive bibliography, and Krauskopf (1967).

On standing a hydrous gel may spontaneously dehydrate and contract, a phenomenon known as syneresis (Graham, 1864). The syneresis of silica gels has been studied by Graham and by Holmes, Kaufmann & Nicholas (1919); the latter authors demonstrated that syneresis can occur under water, and that strong tensional forces are involved. The formation of septarian nodules (which have a radially and concentrically cracked interior) is considered to be due to the syneresis of a mass of gel (Pettijohn, 1957). The formation of syneresis cracks in deposits of clay under water has recently been described (White, 1961).

Secondly, the Liesegang phenomenon: this is much studied but not well understood, as shown by the fact that two recent reviews (Stern,

1954; Matalon & Packter, 1955) favour different mechanisms. One of Liesegang's classic experiments was to place a drop of silver nitrate solution onto gelatine gel impregnated with potassium dichromate, with the resultant precipitation of silver dichromate in a system of concentric annuli around a central patch (Leveson, 1963). A gelatinous medium is usual but not essential for this phenomenon (Hedges, 1932; Stern, 1954). The formation of the rings or shells of precipitate necessitates reaction of the outwardly diffusing substance with another that will give an insoluble or sparingly soluble precipitate, such as the reaction between two electrolytes (as in Liesegang's experiments), two oppositely charged colloids (e.g. ferric hydroxide and silica) or a colloid and an electrolyte. The zones of precipitate are spaced in geometric progression, usually closest together at the centre, although they may become closer outwards or rarely remain equidistant (Stansfield, 1917a; Stern, 1954). Weaker secondary zones of precipitate may form inbetween the main zones (Isemura, 1939). The spacing of the zones depends on the concentration of the reacting substances, the temperature, pH, viscosity and age of the gel, the presence of "impurities", and possibly other factors as well (Isemura, 1939; Stern, 1954; Matalon & Packter, 1955). Shells or rings of precipitate with large diameter and radial structures form in fluid gels; in more viscous gels radial structures, which are probably formed by diffusion currents, occur less and less frequently (Leveson, 1963). The zones of precipitate are spherical or circular in a homogeneous medium but in gels under tension may be elongate (Burton & Bell, 1921). Hedges (1932) and Isemura (1939) stress the generality of the phenomenon

of rhythmic precipitation but point out that it is controlled by many factors, as mentioned above, and all must be favourable before such a precipitate can form. A comprehensive bibliography is given by Stern (1967).

Even before Liesegang described his experiments Johnston-Lavis & Gregory (1894) proposed a process of rhythmic precipitation to explain the formation of the pseudofossil "Eozoon". Since then the geological importance of rhythmic precipitation has been demonstrated by Liesegang (1913), and more recently by Leveson (1963), and others.

Leveson discusses a simple mathematical method for recognizing Liesegang precipitates. Since the precipitate zones are nearly always spaced in geometric progression the logarithm of the spacing will be a linear function which will plot as a straight line graph. Precipitates controlled by external processes, such as the shells of some orbicules and oolites, lack this characteristic.

DIAGENESIS OF IRON-FORMATIONS

Before describing the pseudofossils it is necessary to summarize some of the evidence used previously in support of the postulate that colloids were important during the genesis of iron-formations, and to describe Trendall's (1965, 1966a) hypothesis regarding the diagenesis of the Brockman Iron Formation.

Many authors have suggested that colloidal processes were important during the precipitation and diagenesis of iron-formations (e.g.

Harington & Cilliers, 1963; Huber, 1959) but few have presented objective evidence in support of their ideas. Among the few are Spencer & Percival (1952): two types of structures contribute most to their arguments favouring the action of colloidal processes during the genesis of the Indian iron-formations. The first is the presence in the iron-rich cherts of microscopic polygonal structures interpreted as shrinkage cracks; in a general discussion of structures which can be used to infer the former gelatinous state of rocks Park & MacDiarmid (1964) illustrate similar cracks. The second is the occurrence of microscopic spherulites of radially crystallised chert with iron oxide cores. James (1951, 1954) described microscopic spherulites and spherites from North American iron-formations and considered (1954, p.268) that Spencer & Percival's interpretation for those in the Indian iron-formations as having formed in a gel was also applicable to the iron-formations he was describing. Recently, similar polygonal and spherical structures from the Brockman Iron Formation have been figured (Percival, 1967). Spherulites commonly form in gels (Chukhrov, 1955, p.198; Kurz, 1965), although a gel is not essential (Pettijohn, 1957, p.202). The geological importance of the formation from silica sols of ultramicroscopic spherical aggregates of silica is demonstrated by recent work on opal (Jones & Segnit, 1966). Such processes, and the adsorption of dispersed organic material or iron compounds on to spherical particles of silica gel, must be considered when interpreting apparent microfossils (such as "type G" of La Berge, 1967) from iron-formations. Goodwin (1956, p.581) is one of the many authors who have suggested that iron-formation granules formed through

colloidal processes, which suggestion he supported with the observation that shrinkage cracks occur in some granules. La Berge (1967) has shown that some microscopic granular and spherical structures in iron-formations are probably biogenic.

Goodwin (1956) also noted the common occurrence of cracks in chert beds and lenses in the Gunflint Iron-Formation and ascribed these to the drying and shrinkage of gelatinous silica, as did Gershoig (1965) for similar structures in the iron-formation of Krivoi Rog. The common occurrence of septaria in the Upper Slaty member of the Biwabik Iron-Formation was documented by Gruner (1946). It is important to note that syneresis can occur under water.

Trendall (1965, 1966a) has developed an hypothesis regarding the diagenesis of the iron-formation macrobands in the Brockman Iron Formation. The starting point is a relatively homogeneous sediment most nearly represented now by "primitive" chert mesobands. These are cherts with conspicuous and comparatively coarse microbanding (pl.36d) which "is defined by ankerite bands about 0.25mm thick, made up of a virtually continuous mosaic of rhombs about half this dimension across, alternating with bands of chert with an irregular quartz mosaic of average grain diameter about 5μ. Within the quartz are thin green streaks of stilpnomelane flakes". Such cherts have about equal proportions of chert and ankerite in microband pairs about 0.5mm thick (Trendall, 1965, p.63). The primitive chert was modified in either of two ways, both involving the extensive removal of silica and carbonate. One type of change

produced "flat-modified" chert mesobands, in which the thickness has been reduced evenly with a volume reduction of perhaps 80%. During this modification: 1. The stilpnomelane was changed to haematite platelets about 5μ across. 2. The carbonate bands decreased in thickness and part of the ankerite was replaced by quartz; siderite rhombs appeared. 3. The microbanding became finer and its continuity more difficult to follow. 4. Concertina-shaped lines of solid magnetite with crystal faces appeared. In the other, "podded", form of modification similar mineralogical changes occurred, but there was differentiation into chert pods ("lenses") with intervening quartz-iron oxide (pls 34a,36f). The alteration of the chert in the pods is similar to flat-modification but there is comparatively little microband compression and little magnetite growth. The quartz-iron oxide typically contains:

quartz	35%	carbonates	10%
magnetite	45%	stilpnomelane	10%

Microbands are sometimes continuous from chert pods into the intervening quartz-iron oxide but are much closer together in the latter (in an example quoted by Trendall a number of microbands occupy a thickness of 7mm in a chert pod but only 1.5mm in the contiguous quartz-iron oxide; see pl. 36f for similar examples). More recent work has led to the abandonment of the terms "primitive chert" and "flat-modified chert", and the rocks so called are no longer considered to lie on a direct line of diagenetic descent; despite this the types of changes outlined above are still considered to have happened (Trendall, pers. comm., 1968; to be published in Bull. geol. Surv. West Austral., 119). The term

"quartz-iron oxide" was also abandoned in favour of "chert-matrix" but is retained here because it is convenient and unambiguous.

The postulated diagenetic sequence seems compatible with La Berge's (1964) findings indicating the secondary formation of magnetite after carbonate in North American iron-formations (although metamorphism is apparently not necessary), and according to Trendall (1966a) has received "strong chemical support", although this has not been published. It explains simply some of the processes of formation of unusual structures described by Trendall (1966a). Where possible the formation of the pseudofossils here described is discussed separately from this hypothesis, although they are considered to provide further evidence indicating the mobility and localised removal of silica during diagenesis.

PSEUDOFOSSILS FROM THE BROCKMAN IRON FORMATION

The Brockman Iron Formation contains numerous unusual structures some of which have been described by Edgell (1964) and Trendall (1966a). The descriptions to follow are mainly of forms that have been or could possibly be confused with fossils.

On the basis of their mode of formation the pseudofossils are classified into four groups. Sub-groups are provided for morphologically and genetically distinct types.

1. Structures formed by the migration of silica and/or carbonates during diagenesis
   - 1.1 Liesegang precipitates
   - 1.2 Diapirs and associated medusiform structures

1.3 Sponge-like nodes

1.4 Quartz discs

2. Structures formed by the retention of silica during diagenesis

2.1 Nodules previously described as stromatolites, and structures formed by compaction over them

2.2 Macules, and structures formed by compaction over them

3. Structures formed by the shrinkage and moulding of gelatinous silica during diagenesis

3.1 Septaria and their moulds and casts (some medusiform)

3.2 "Medusae incertae sedis" of Edgell (1964)

4. Compound structures

Several terms used here require explanation: Diapir is used for small allochthonous masses of silica and carbonates with a shape and mode of formation similar to the large structures to which that term is usually applied. Medusiform is used for any structure consisting of a system of concentric ridges lying essentially in one plane (the bedding plane) and indicates a resemblance to fossil medusae but does not imply biogenesis. Macule is explained below (p. 433).

1.1 Liesegang precipitates

Only two medusiform Liesegang precipitates are known (pl.34b,c) both from the Joffre Member 10km east of Mount Brockman. The larger is more completely preserved. It is oval with the two principal axes about 40cm and 50cm long, and consists of about ten flat-topped, concentric, oval ridges, the inner ones mostly narrower, and all divided by radial

grooves into numerous lobes. Some radial grooves continue through several ridges but often are restricted to only one. An oval area 10cm by 20cm in the middle of the structure is featureless. The outer limit of the structure is not clear: poorly defined concentric grooves extend outwards about 28cm. Concentric with the structure are cylindrical fractures several centimetres deep (pl.34b,d).

The lobes are composed of fine-grained martite, continuous downwards with a mesoband consisting almost entirely of martite; in this mesoband the chert content decreases upwards (pl.34d). Within the martite mesoband are two sets of planar zones of structural dislocation, oriented at between 20 and 45° to the mesoband surface; the two sets intersect at about 120°, and the displacement (maximum 0.3mm) across the two is sometimes in the same sense. In detail they consist of an en echelon pattern of chalcedonic quartz-filled slightly sinusoidal fractures. The radial and concentric grooves (pl.34b-d) are rectangular in section and nearly filled with chert containing many scattered grains of martite. The contacts between the martite lobes and the intervening chert are gradational over about 0.75mm. In the centre of each concentric groove examined is a secondary concentration of martite, also continuous with the underlying mesoband (pl.34d). The surfaces of most lobes have adherent patches of chalcedonic quartz, apparently the remnants of a more continuous cover.

The mesoband bearing the medusiform structure thins from about 2.0cm at the centre of the oval to 1.7cm in its outer part. Concomitant

with the thickness change is a compositional variation from about 50% chert and 50% iron oxide at the centre to less than 10% chert in the upper part of the mesoband continuous with the lobes near the edge of the structure (visual estimations).

Both examples are crossed by small ridges and lineations of tectonic origin which in the large one trend at about 95° and in the small one at about 110° east of true north. Deformation of lobes is visible in the small example (pl.34c). These trends are near those of the major structures of the region, about 120° true. The long axis of the larger example is aligned at about 80° true; that of the smaller one is not accurately determinable, but is approximately the same.

The medusiform structures have obviously been affected by deforming stresses but their morphology and the distribution of visible zones of structural dislocation are not consistent with them having been formed mechanically.

The spacing of the concentric, partly chert-filled grooves (measured on a large photograph from the centre of the grooves) is very nearly in geometric progression (fig.48), being closest together at the centre of the oval. This, the presence of a featureless central area with a greater proportion of chert than the outer areas, the gradational contact between the martite and the chert and the rectangular cross-sectional shape of the chert concentrations are good evidence for the structures having formed by Liesegang precipitation of silica (as described above). The radial arrangement of chert can be attributed

to radial diffusion currents, although it is less continuous than is usual in such structures; the mesoband must have been fairly fluid when the medusiform structure formed (p.414). Their oval shape is probably due to later tectonic deformation. The medium supporting diffusion was probably gelatinous iron carbonate or hydroxide, now martite (Fe_2O_3 after Fe_3O_4); Trendall (1965) has also suggested that water-rich mixtures of carbonates and iron hydroxide may have formed part of the original sediment. Since silica in true solution is very difficult to precipitate unless it is greatly supersaturated (Krauskopf, 1959; White et al., 1956) it was most likely coagulated from a sol. Coagulation could have been caused by reaction with an electrolyte. The most likely of these in the iron-formation are phosphates and carbonates; X-ray spectrographic analysis revealed no significant difference in phosphate content between the martite lobes and the chert in the concentric grooves. In addition, there is little carbonate in the chert and calcite does not cause coagulation (Krauskopf, 1959) so precipitation by electrolytes is unlikely. Reaction with an oppositely charged iron hydroxide sol could have coagulated the silica. The mutually precipitated iron hydroxide and silica must then have segregated; their very different mechanical properties (Jirgenson & Straumanis, 1954) may have been the cause of this. This segregation accounts for the chert concentrations being thinner than contiguous martite lobes (pl.34d).

The rarity of such medusiform structures in the iron-formation is a natural consequence of the diversity of factors controlling the Liesegang phenomenon.

1.2 Diapirs and associated medusiform structures

The structure illustrated in plate 35a consists of coarse grained quartz that transgresses 3.5cm through an iron oxide mesoband from a chert mesoband, and slightly in the opposite direction. The quartz contains numerous carbonate inclusions a few microns wide. Microbands in the iron oxide are cut off against the edges of the quartz mass and near its top are domed over it. The medusiform structures of plate 35c are concentrically arranged folds centred over similar quartz masses; these latter are folded and cracked internally and have irregular borders (pl.35b). The enclosing iron oxide-rich mesoband is thickened about them. The mesoband below one of the quartz structures is depressed about 2.5cm and an iron oxide-rich mesoband lower still pinches out completely. No microbands are present in the quartz. A layer of chalcedonic quartz about 1mm thick coats much of the folded medusiform surface.

Several examples of medusiform structures overlying quartz masses were seen in the field and in each case they were on an upper bedding surface (however, few lower surfaces were visible). The impression left on the contiguous mesoband would also resemble a medusa and lacking a diapir at its centre would be difficult to interpret. The circular structures associated with ripple mark-like microfolds in plate 35d are possibly of this latter type: some have quartz masses at their centres but the only one collected does not. They are on the surfaces of a quartz-iron oxide mesoband. Possibly similar structures are figured by Campana et al. (1964) as "algal(?)".

The quartz structures superficially resemble macule cores (p. 433) but their transgressive contacts, lack of microbanding and contorted inner structure distinguish them. They are intrusive masses analogous to diapirs, and here that term is applied to them. Other, even more clearly intrusive, diapiric structures are described in the next section (on sponge-like nodes). The diapirs probably formed because a weakness (perhaps due to syneretic cracking) in a mesoband allowed the penetration of silica and/or carbonates which were plastic during diagenesis and activated by the weight of overlying sediment. In the example in plate 35b, where no chert mesoband is present, the silica probably segregated from the enclosing mesoband during diagenesis. Some of the diapirs may originally have been largely carbonates which were later replaced by silica. The act of penetration of the diapirs may have caused the concentrically arranged folds of the medusiform structures or these may be the result of later compression over the rigid quartz pillars. In either case there would have been a radially directed component of the stress capable of causing such folds. During diagenesis differential compaction about some diapirs resulted in expulsion of material from beneath them; similar examples of pressure effects are described later (p.433,438).

The diapirs are common in the field, but only a few medusiform structures were seen associated with them. Whitten (1966) figured as "fossils (?)" circular structures several centimetres in diameter and with depressed rims from Precambrian iron-formation in South Australia. Their similarity to structures here described is notable, but they have

not been available for study.

1.3 Sponge-like nodes

Very similar to the diapirs are nodes such as those shown in plate 35e. The one sectioned (pl.35f) has a core of chert, much contorted and with included irregular patches of iron oxides. The chert on the edge of the nodule is puckered into small folds (1mm amplitude) lying in planes perpendicular to the long axis of the node. Microbands in the quartz-iron oxide mesoband below the node are fractured and buckled irregularly, and the spaces so formed are filled with chalcedonic quartz. The node has abrupt fault contacts against the partly enclosing chert mesoband. Small mounds beside the nodes (a section of one can be seen in plate 35f) resemble the "pit and mound" structures of Shrock (1948, p.132) but microbands continue through the "cones" and therefore these are probably diagenetic structures.

The nodes are concentrations of silica that apparently formed during diagenesis and were injected into the overlying chert mesoband during compaction, the resultant disturbance being shown by the contortion of surrounding sediment and the growth of chalcedonic quartz. The chalcedonic quartz was probably originally chalcedony, which may have formed from silica gel (White & Corwin, 1961) in low pressure areas (Taliaferro, 1934) resulting from distortion of the sediment. Swarbrick (1968) discusses the formation of similar injection structures in Carboniferous sediments, including cherts, from England.

1.4 Quartz discs

Discoidal to spherical quartzose structures up to 10mm in diameter

and up to 5m thick (pl. 34e-g) occur rarely in the iron-formation. They have quartz walls 0.5 to 1.2mm thick of radially arranged slightly elongate grains about 0.5mm wide. Most are embedded in and infilled with chert and limonite with a grain size of from 2 to 30μ. Limonite is concentrated on the inner side of the quartz walls and small (5μ) euhedral magnetite and possibly haematite grains on the outer side (or within the quartz wall near its outer edge). The quartz grains are unusually large for the Brockman Iron Formation, and contain numerous small (2-3μ) inclusions of a carbonate. Boundaries between quartz grains are serrated. Some discs are solid quartz and in some of these the peripheral quartz grains are smaller than those at the centre.

Associated with the well formed discs are some small accumulations of quartz with only a poorly developed concentric layering, and some discs which are only swellings in quartz layers that parallel microbanding. Most discs are arranged parallel to microbanding, which is deformed about them.

The best formed chert-filled discs seen were in the central chert cores of magnetite-walled cylinders about 2cm high orientated perpendicularly to bedding (pl.34f). In some of the cylinders several discs occur one above the other. Others occur in magnetite mesobands or in solid magnetite nodes similar to the chert-cored cylinders.

The presence of numerous carbonate inclusions suggests that the silica has replaced carbonate. The considerable morphological variation within these structures makes biogenesis unlikely, as does

their presence in magnetite nodes, since magnetite is a secondary mineral. It is probable that they formed during diagenesis by the segregation of carbonates and/or silica. The process of segregation (due perhaps to the different mechanical properties of iron-rich and silica gels) or the crystallization of the silica to quartz caused the expulsion of iron compounds to give the layering now present. No adequate explanation for the hollow discoidal shape is available.

Closely similar, but ellipsoidal, structures have been described from iron-formation of the Kursk Magnetic Anomaly, Baltic Shield, by Dmitriev & Gritsay (1964); these they considered as probable fossils. However, similarity with the Brockman forms makes it most likely that they are abiogenic.

2.1 Nodules previously described as stromatolites, and structures formed by compaction over them

Stromatolites have been found in a Carboniferous iron-formation in Ireland (Schultz, 1966) and within Precambrian iron-rich sediments in North America, China and the USSR (e.g. Hoffman, 1969; Moorhouse & Beales, 1962; Tegengren, 1921-23; Starostina, 1959). Structures reported by Edgell (1964) as stromatolites from the Brockman Iron Formation have been re-examined and here are attributed to diagenetic (and possibly tectonic) processes. A search for true stromatolites has so far been unsuccessful.

Typical Brockman Iron Formation is shown in plate 34a: the light coloured mesobands are chert-rich. All gradations from chert mesobands

with only minor thickness variations to those consisting of widely spaced and isolated "lenses" (pods) are present. Edgell (1964) called chert mesobands of markedly variable thickness "Collenia cf. kona" and isolated chert pods "Collenia brockmani". In the plan the chert pods range in shape from discoid to irregular (pl.36a,b). Locally, long axes of elongate pods are aligned; an alignment parallel to fold axes of "pinch and swell structures" in the iron-formation (Daniels, 1967) may be similar. Extraordinary continuity (300km) has been claimed for the mesobands (p.412). The microbands in some chert mesobands of even thickness are themselves even and thick while those in chert pods are irregular and thinner (pl,36c,d). Cases where microbands in the chert are clearly continuous with those in the enclosing quartz-iron oxide are known (pl. 36f) but often microbands are too indistinct to be traced. Several variants of microband relationship are illustrated in figure 49. Edgell stated (p.241) that "Fine clastic layers within the ferruginized sediment often dichotomize around these silicified, discoidal stromatolites" indicating their "primary nature". A study of Edgell's specimens and others has revealed no bifurcation of microbands; in fact microbands in the quartz-iron oxide nearly always trend into those of the chert, as described above.

Septarian cracks commonly occur in the chert pods; the process which causes the cracking can also crenulate the microbands (p.434; pl.37c).

Analyses reported by Trendall (1966a, p.85) show that some chert

pods have a greater apatite content (0.45% P_2O_5) than the enclosing quartz-iron oxide (0.09% P_2O_5). To test the generality of these analyses chert pods and the contiguous quartz-iron oxide were sampled in a core from about 300m below the ground surface in the Australian Blue Asbestos Company's bore hole 63, near Wittenoom Gorge; analyses were done in duplicate by R. Wilson-Smith of the Australian Mineral Development Laboratories. Two composite samples consisting of portions of approximately equal volume from ten chert pods and the contiguous quartz-iron oxide were analysed. The chert was found to contain less than 0.05% P_2O_5 and the quartz-iron oxide 0.31%. These analyses combined with Trendall's show that the phosphate distribution is not as simple as previously supposed, and may be random.

One of the reasons given for interpreting the chert pods as stromatolites is the wrinkled structure of the microbands, stated to be typical of stromatolites (Edgell, 1964, p.240). Other explanations are available. There is abundant evidence in the iron-formation of the movement of silica and carbonate (e.g. Liesegang medusiform structures and diapirs and compound structures described below). This and syneresis (of which the septarian cracks are evidence) provide adequate mechanisms for the wrinkling of microbands: firstly by slightly irregular removal of addition of components and volume charges resulting from mineral replacements, secondly by contortion accompanying shrinkage.

That chert pods and mesobands of constant thickness are not fundamentally different is shown by the continuum of variation between

them. Two segments of the continuum were selected by Edgell as stromatolites. The formation of lenticular chert mesobands from those of constant thickness has been discussed by Trendall (1965, 1966a; p.417 herein): an essential process is the localized depletion of silica eventually leaving quartz-iron oxide between chert remnants (pods). Such processes did operate, as is demonstrated by the presence of the compound structures described on p.439 and the continuity of laminae between chert pods and contiguous quartz-iron oxide. The process was silica removal from between the pods, not concretion into the pods (which Gershoig, 1965, considered for similar structures), since in cases where lenticular mesobands grade laterally into ones of even thickness the maximum thickness of each pod is the general thickness of the even mesoband. The presence of septarian cracks in many chert pods strongly suggests that the pods were formerly gelatinous. Trendall suggested that phosphate ions may have exerted some control during diagenesis since he found apatite concentrated in some chert pods and other chert nodules ("macules" - see p.433). But the analyses reported above cast doubt on the significance of those findings. Trendall (1965, p.62) also reported that the chert pods contain more carbonate than the surrounding quartz-iron oxide but whether this is a result of diagenetic processes or a controlling factor cannot at present be answered. However, it is interesting to note that Hatschek (1925) reports that phosphates and carbonates cause the rapid coagulation of silica sols (Krauskopf, 1959, found that calcite has no such effect). The aggregation of such electrolytes (the cations of which cause coagulation) in some cases could have hastened the lithification of the

colloidal silica in the pods and could thus have reduced its subsequent loss during diagenesis. The various shapes of chert mesobands may have resulted from the patchy distribution of phosphates and carbonates but confirmation of this is beyond the scope of this study.

Since processes which could have formed the "stromatolites" were acting during diagenesis and tectonism it is unnecessary to invoke an organic agency. Furthermore, these structures differ from all known stromatolites (including those in iron-formations) in two ways: 1) They form thin beds (mesobands) of extraordinary continuity, whereas stromatolitic beds on such a scale are much less continuous. 2) The microbands in pods continue into the intervening quartz-iron oxide (except where banding has been destroyed), yet the composition of the microbands in these two components is quite different (in the one dominantly chert or carbonate, in the other iron oxide). Where laminae continue across an interspace between individual stromatolites their composition remains constant. This makes any primary origin for the pods unlikely. Finally, Edgell's (1964, p.242) comparison of chert mesobands of markedly variable thickness with Collenia kona Twenhofel has little basis. Collenia kona Twenhofel is a stromatolite consisting of interconnected columns the laminae of which are strongly convex upwards (Twenhofel, 1919). A cross-section of the "Collenia kona" shown in Edgell's plate 2, figure 1 shows (pl.36e herein) that the microbands are not convex upwards under the thickenings that he called growth centres (with the specimen in the same orientation as Edgell figured it), and are dis-

continuous between those thickenings. The other specimen he illustrated as C. cf kona (his pl.2, fig.3) does show slight doming of microbands in the thickened areas.

Chert pods such as those which have been described can cause the formation of other pseudofossils. The raised structures shown in plate 36g are bulges formed by compaction over chert lenses in a quartz-iron oxide mesoband, as shown in plate 36h . The prominent domed bands are rich in chert on the flanks of the structures but in the central areas are chert-poor; microbands within the domed chert bands are continuous with those in the quartz-iron oxide overlying the chert lenses. These are another example of the localized expulsion of silica (in this case from above the chert lenses) due to differential compaction, probably during diagenesis (p. 425,438).

2.2 Macules, and structures formed by compaction over them

Trendall (1966a) described from the Brockman Iron Formation unusual nodules, very common at some localities, which he called "macules". These have a central cylindrical core, usually of chert, oriented perpendicularly to bedding. The microbands of the core are continuous with those of the enclosing mesoband(s) but are more widely spaced. Contiguous mesobands are folded over and under the core (pl. 37a). The size of macules varies greatly, from less than 1cm to several metres in height (e.g. see MacLeod, 1967, fig.12), but those about 20cm high are prominent in the field. Some mesobands may be thickened above a macule (Trendall, p.77), producing a discoid structure. Radial and concentric crack patterns commonly form in the mesobands above macules

(Trendall, fig.27); a section through another example on the same slab shows that the radiating haematite (at least partly martite) filaments shown in plate 37b are most likely infilled cracks above a chert mass similar to a macule core.

Trendall concluded that macules formed during diagenesis by the retention of silica in the core while it was expelled from the enclosing mesoband(s). He noted that apatite is common in the chert cores and suggested that macules are essentially phosphate concretions. They may have resulted from the coagulation of colloidal silica by an electrolyte as discussed above. The radiating cracks formed by compaction over the rigid core at a stage when some mesobands were brittle.

3.1 Septaria and their moulds and casts (some medusiform)

A good example of a septarian nodule is shown in plate 37c-e. This specimen was kindly lent by the Geological Survey of Western Australia. It is a laminated mass of chert, semicircular in outline, 5.0 to 5.5cm thick and 13.5cm in diameter. One side is convex and the other concave, but the original orientation is unknown. The convex side has a shallow central depression surrounded by a low, broad ridge; crossing the ridge and the area outside of it are radial narrow depressions, the surface expression of deep fractures. The convex side, and the impression that it must have left on the formerly enclosing beds, is superficially like a medusa. The microbands within the chert conform to the surface structure, i.e. they are arched into a series of concentrically arranged folds. On the concave surface are quartz-infilled

septarian cracks with the same central axis as the folds. There are numerous cracks, the larger of which penetrate almost completely through the chert (pl.37c).

The folding and cracking, arranged about a common centre, probably had a common cause. Stansfield (1917b) suggested that syneresis of a silica gel could have formed apparently similarly folded cherts. Holmes, Kaufmann & Nicholas (1919) have shown that silica gels are under tension and it was noted above that syneresis is the likely cause of septarian cracks. The fact that syneresis and shrinkage can cause the crinkling of microbands is important in the interpretation of the iron-formation "stromatolites".

More chert lenses with septarian cracks are illustrated in plate 37f; in these the cracks are only shallow. Septarian nodules are common in the Brockman Iron Formation; many of Edgell's (1964) "Collenia brockmani" are good examples (see for instance his pl.1, figs 3,4; pl.2, fig.7). This is further evidence for the formerly gelatinous state of the Formation.

Related to septarian structures are those shown in plate 37g,h ; both are in shales from the Dales Gorge Member. That in plate 37g was donated by Mr D. McKenna of Conzinc Riotinto of Australia Limited. It consists of a sub-circular depression 1-3mm deep and 14cm wide in the central part of which is an irregular pattern of mounds and depressions with a relief of up to 5mm. V-shaped cracks about 4mm deep in the shale are arranged radially and concentrically about the central deformed area;

the radial cracks taper out beyond the depression. The counterpart of this specimen fits very closely. The structures illustrated in plate 37h are on the surface of a large fallen block the original orientation of which is unknown (this photograph by Mr N. Beeck was kindly lent to Prof. M. F. Glaessner by the Western Australian Museum). A later search for this block proved fruitless; a specimen from it lent by the Western Australian Museum had several individuals with irregular radial and concentric ridges in shallow subcircular depressions. Both of these types are best explained as moulds of discoidal septarian nodules. In the first case the gel must either have adhered strongly to or penetrated the surface of the shale (which because it is fine-grained may also have been subject to syneresis) causing it to crack also. The gel must then have been expelled during diagenesis and the contiguous shale forced into the mould and cracks that were left. The radial and concentric ridges of the other examples are infillings of syneresis cracks.

Septarian nodules from iron-formation in the Pretoria Series of South Africa are figured by von Backström (1964?). In addition to having typical septarian crack systems these also show a colour banding resembling those produced by the Liesegang phenomenon; this is added evidence for the originally gelatinous state of the nodules.

3.2 "Medusae incertae sedis" of Edgell (1964)

The most biogenic-looking medusiform structures from the Brockman Iron Formation are those described by Edgell (1964, p.249; pl.3, fig.1)

as "*medusae incertae sedis*" (pl.38a,b herein). Edgell's two specimens were re-examined, and the locality from which they came was visited but no more were found. The structures are on an upper bedding surface (J. H. Lord, pers. comm., 1967). They apparently came from the same small outcrop on which occur the small concentrically folded structures described below.

A polished radial section of the small example is shown in plate 38b. The concentric medusiform structure is restricted to a chert microband 0.3 to 1.0mm thick but the central nodes are due to chert concentrations several millimetres below the surface. The four nodes are grouped two on each of two parallel ridges. The ridges extend almost to the edge of the medusiform structure. Below the chert mircoband is a quartz-iron oxide mesoband. Ten millimetres beneath the centre of the medusiform structure is a basinal structure similar to those within the concentrically folded pseudofossils described below, but the similarity is not close and no such structure could be seen in the larger example. Edgell noted the presence of a "hemispherical" protrusion on one side of the small medusiform structure; this has a vague concentric structure which seems to overlap that of the "parent" (pl.38a).

Whereas the small medusiform structure occupies a slight depression, the larger covers a mound the limits of which approximate its own boundaries. So far as can be seen the concentric ridges of the large example contain concentrations of iron oxides; Edgell's (p.250) description of them as partly silicified is misleading. Some microbands

present in the ridges seem to be absent between them (but it was thought advisable not to section this specimen as well as the other because they are the only two of this kind known). Weathering has revealed that the ridges are continuous downwards for at least 1.5mm. The nodular central part is irregular and contains more than four nodes.

Since the nodes and concentric ridges have a constant spatial relationship they are probably genetically related. The nodes of the small example are chert lenses such as are common in the iron-formation and which are thought to have formed during diagenesis. The concentric structure of this specimen probably did not form by compression over the nodes and ridges since it is not elongated parallel to the ridges; no nodes are associated with its semi-ciroular protrusion. Comparison with pseudofossils described earlier (septarian nodules and their moulds and casts) suggests that these medusiform structures are moulds or counterpart casts (Wade, 1968, p.255) of discoid masses of gel. The nodular central parts are comparable with the irregular areas in the centre of some of the septaria and associated moulds. The structure of the nodes indicates that they formed during diagenesis; this does not preclude biogenesis for the medusiform structures as it is feasible that the overlying bed was competent enough to retain a mould during diagenesis (as happened in the preservation of some animals in the Precambrian Pound Quartzite of Ediacara; Wade, 1968), and the nodes could have formed by differential compaction during counterpart casting (cf. p.425,433). The specimen figured by Edgell (his pl.3, fig.2) as a pseudofossil also has a concentric arrangement of ridges and several irregular ridges at its centre. Sectioning showed that the body of the pseudofossil is

a lens of chert-rich iron-formation around which the contiguous meso-band has been deformed, giving the concentric structure.

While it is likely that the "medusae" are moulds or casts of discoid masses of gel, there are at present no sound reasons for assuming that the gelatinous masses were biogenic; If in the future a number of other specimens with a structure closely similar to Edgell's "medusae" (particularly in the nodular part) are found then biogenesis would become more likely, but because of the similarity with other structures demonstrated to have formed by the casting of gelatinous silica an inorganic origin is strongly favoured.

Given a reason to assume biogenesis for such structures the possibility of plant "jellies" such as those described by Weed (1889) must be assessed. In this regard it is notable that Glaessner (1966) suggested that medusiform impressions from the Grand Canyon (Alf, 1959) might be algal in origin. Recent algal colonies (pl. 38c) collected from a salt lake in the SE of South Australia bear a remarkable resemblance to some medusiform fossils; they have concentrically arranged ridges formed by superimposed growth layers and are as firm as, or firmer than, medusae. These consist largely of diatoms but the same growth form could probably be achieved by other types of algae.

4. Compound structures

Edgell (1964, pl.3, fig.4) figured as a pseudofossil a concentrically ringed structure from about 30m above the base of the Dales Gorge Member 1.6km N by E of Hamersley Homestead. Many of these unusual

structures occur at this locality (pl.38d); most are isolated but some coalesce with those adjacent to form a pattern like an interference figure of a biaxial mineral (pl.38e).

A cross-section of one of the biaxial forms is shown in plate 38g and figure 50. The mesoband "a" is flat-modified chert (see p.418), with microbands of average thickness 0.35mm; "b" is finely banded quartz-iron oxide consisting mainly of fine grained magnetite, the average microband thickness being 0.1mm. Magnetite octahedra up to 0.5mm wide are scattered throughout the unit "b" and tend to obliterate the banding; these become common towards the upper edge of the unit where it is in contact with "c", which is a mesoband of non-banded, dense, coarsely crystalline magnetite. Capping this is unit "d", several microbands of quartz-iron oxide. Locally are units "c" and "d" separated by a discontinuous layer of chalcedonic quartz up to 0.3mm thick. The surficial concentric ridges are asymmetric folds (visible only in "d") with the steeper sides facing outwards. Some folds are overthrust along fracture planes which are concave outwards and extend through "c" into the upper part of "b". The fractures change from reverse faults in "d" to normal faults in "b". In biaxial forms fractures between the axes are planar, but are uniformly curved in isolated forms. In some examples narrow radial depressions cross the surface ridges: these are minor downfolds in "d".

The microbands in the basal parts of "b" are continuous with those in "a", but whereas about sixteen microbands occupy a thickness

of 5.5mm in "a" the same microbands are compressed to 2.5mm in "b". In isolated forms the central structure ("b") is circular in transverse section; in all cases the basal part of "b" is circular in transverse section. The phosphate contents of these areas were analysed (by R. Wilson-Smith, Australian Mineral Development Laboratories) and both the basal part of "b" and the enclosing chert mesoband were found to contain 0.07% P_2O_5; both "c" and the upper part of "b" contained less than 0.05%.

Even apparently minor features are consistently developed; for example, the small chert blebs in the base of "b" (one is visible in pl.38g) occurred in all four individuals sectioned. All of the well-formed examples from the Hamersley Homestead locality are from the same mesoband, and even individual mircobands a fraction of a millimetre thick can be recognized in specimens collected from localities over a metre apart. The specimen figured by Edgell apparently came from the same mesoband since the same microbands were recognized in a section.

The specimen from 10km east of Mount Brockman figured by Edgell (his pl.3, fig.7) as a "medusoid indeterminate or concentric pseudofossil" was sectioned and found to closely resemble the central part ("b") of the pseudofossils described above. The medusiform structure is planoconvex (he figured the planar side) and microbanded. It is clearly not a fossil medusa.

The main differences between units "a", "b" and "c" are their silica content, the fineness of the microbanding which reflects that and the prevalence of large magnetite octahedra. It seems clear that the

basal part of the finely banded quartz-iron oxide ("b") formed from the coarsely banded iron oxide-poor chert ("a") by loss of silica during diagenesis. Similarly the magnetite mesoband ("c") could be the end product of such a process, with not as much silica being expelled from the upper part of "b" as from the rest of that mesoband. There is a clear sequence from "a" to "b" to "c", with gradational boundaries between them. The shape of these units (in particular their thickness) is a reflection of the volume reduction accompanying silica loss. The greatest reduction occurred in the magnetite mesoband. These same changes Trendall (1965, 1966a) postulated to have occurred on a large scale in the iron-formation. But the explanation for the mushroom shape of unit "b", the quartz-iron oxide, is not known; once these formed, the folds in "d" could have resulted from compression due to sediment overlying the mounds "b". The fractures associated with the folds show displacements in unit "b" suggesting that this unit was formed before the folds and hence may have been their cause.

The medusiform structure of plate 38f probably had a similar origin, although it could be a variant of the diapiric type, but the central part is not preserved. The concentric ridges are on a non-banded magnetite mesoband.

There are other similar but much larger structures consisting of concentrically arranged asymmetric folds (Halligan & Daniels, 1964, fig.1). They are up to 2m wide and adjacent ones interfere as in their small analogues. Cross sections exposed in outcrop reveal no

central structures, fractures or elevations of the central area such as in the small forms, but the folded part is very similar. The folds have an amplitude of several centimetres and affect several mesobands.

DISCUSSION

Since many of the specimens used in this study came from surface outcrops the mineral composition has been affected by weathering (oxidation of ferrous oxides, silification). Some chalcedonic quartz may have formed by alteration of crocidolite. However, only where the iron-formation has been intensively weathered under a dissected Tertiary land surface (MacLeod, 1967) is its structure different from that which occurs at the bottom of bore holes over 300m deep, and so the pseudo-fossils are neither products of weathering nor are they structurally altered by moderate weathering. Chert pods and quartz diapirs were studied from bore hole and mine samples as well as outcrop samples.

Although no stromatolites are now known from the Brockman Iron Formation they are common in North American granular iron-formations (e.g. Hoffman, 1969; Moorhouse & Beales, 1962). Several authors, among them Edgell (1964, p.237, 254-257), have cited the presence of siliceous stromatolites as evidence for the wholesale secondary silification of calcareous sediments to give iron-formations. They assume that these stromatolites were originally calcareous. Since siliceous stromatolites do occur in some iron-formations it is worth briefly discussing the possibility of them being primary. As is discussed in chapter 3, siliceous stromatolites are at present growing in hot pools in the

volcanic terrain of Yellowstone, USA. There the main process seems to be silica trapping, just as detrital carbonate trapping is important in the growth of other modern stromatolites. Siliceous stromatolites in a Carboniferous iron-formation probably formed in this manner (Schultz, 1966). The excellent preservation of micro-organisms within the cherty stromatolites of the Gunflint Formation has led Barghoorn & Tyler (1965) and Cloud (1965) to the conclusion that the silica is a primary sediment. Although siliceous stromatolites are known to be forming only in a very restricted modern environment it is considered that fossil examples do not necessarily indicate secondary silification, especially since those in iron-formations probably formed in a silica-rich environment. However, the suggestion of Barghoorn (pers. comm. quoted in Brock, 1967) that the Gunflint Formation algae lived in hot springs seems unlikely because of the wide distribution of the stromatolite-bearing units. There is of course other evidence in favour of the hypothesis that the silica in banded iron formations is a primary sediment or at least was introduced very soon after deposition of the sediment (see, e.g. James, 1954; White, 1954).

In connection with the origin and precipitation of the iron and silica it is interesting to note the deposition of colloidal iron hydroxides and biogenic silica in the Mediterranean Sea near Santorin volcano (Butuzova, 1966), and the conversion of sedimentary sodium silicates to bedded chert in an alkaline lake in a volcanic terrain in Kenya (Eugster, 1967). Interpretation of the original form of the Brockman Iron Formation is made difficult by the pervasive diagenetic

re-organization of which the pseudofossils are by-products. The micro-organisms found by La Berge (1967) may have caused some of this re-organization: the decay of trapped organic matter can produce highly alkaline conditions during early diagenesis (Berner, 1968) and may account for the massive removal of silica for which there is much evidence in the iron-formation.

CONCLUSIONS

All of the "fossils" previously described from the Brockman Iron Formation are abiogenic. The presence of large lobate and concentric medusiform pseudofossils shown to be the result of diffusion and rhythmic precipitation of silica (by the Liesegang phenomenon) and of numerous septarian nodules and their moulds and casts (some medusiform) provides strong evidence indicating that the sediments were gelatinous during diagenesis.

The Liesegang medusiform structures, numerous small diapirs of quartz, and evidence of the loss of silica nodules that caused septarian cracks indicates that the silica was mobile during diagenesis. Some carbonates may have been replaced by silica. Some of the mobile silica formed septarian crack infillings, small lenses of quartz and chalcedony patches. Small basin-shaped structures at the centre of concentrically folded medusiform structures show that finely laminated quartz-iron oxide can form by the loss of silica from coarsely laminated chert poor in iron oxide; further loss of silica and the enlargement of magnetite octahedra results in massive magnetite mesobands.

Besides the common presence of septarian cracks, small patches of chalcedonic quartz common in the iron-formation may indicate shrinkage during diagenesis. The irregular microbanding of some mesobands is probably due to shrinkage and the irregular removal of silica and carbonates, volume changes caused by alteration and replacement of minerals and also to the fact that silica and iron hydroxide gels have very different mechanical properties and thus adjacent microbands may have reacted differently to the same physical forces.

These structures indicate that the iron-formation was siliceous at a very early stage of diagenesis, when it was also gelatinous, and at this stage there was much re-organization, particularly of the silica distribution. Only a detailed study of the colloidal processes operating during diagenesis will allow an interpretation of the primary form of non-granular banded iron-formations: the pseudofossils are but a by-product of pervasive diagenesis.

REFERENCES

Alf, R. M., 1959 : Possible fossils from the Early Proterozoic Bass Formation, Grand Canyon, Arizona. Plateau 31, 60-63.

Barghoorn, E. S. & S. A. Tyler, 1965 : Microorganisms from the Gunflint chert. Science N.Y. 147, 563-577.

Berner, R. A., 1968 : Calcium carbonate concretions formed by the decomposition of organic matter. Science N.Y. 159, 195-197.

Brock, T. D., 1967 : Life at high temperatures. Science N.Y. 158, 1012-1019.

Burton, E. F. & G. C. Bell, 1921 : Note on Liesegang rings in strained gel. J. Phys. Chem. 25, 526.

Butuzova, G. Yu., 1966 : Zhelezorudnyye osadki fumarol'nogo polya vulkana Santorin, ikh sostav i genezis (Iron ore sediments of the fumarole field of Santorin volcano, their composition and origin). Dokl. Akad. Nauk SSSR, 168, 1400-1402 (Dokl. Acad. Sci. USSR, Earth Sci. Secn 168, 215-217).

Campana, B., F. E. Hughes, W. G. Burns, I. G. Whitcher & E. Muceniekas, 1964 : Discovery of the Hamersley iron deposits. Proc. Austral. Inst. Min. Met. 210, 1-30.

Chukhrov, F. V., 1955: Kolloidy v zemnoy kore (Colloids in the Earth's crust). Izdat. Akad. Nauk SSSR, Moscow, 671p. (in Russian).

Cloud, P. E. Jr, 1965 : Significance of the Gunflint (Pre-cambrian) microflora. Science N.Y. 148, 27-35.

Compston, W. & P. A. Arriens, 1968 : The Precambrian geochronology of Australia. Can. J. Earth Sci. 5, 561-583.

Daniels, J. L., 1966 : The Proterozoic geology of the North-West Division of Western Australia. Proc. Aust. Inst. Mining Metall. 219, 17-26.

Daniels, J. L., 1967 : Explanatory notes of the Turee Creek 1:250,000 Geological Sheet, Western Australia. Rec. geol. Surv. West. Austral. 1967/7, 28p.

Dmitriev, E. V. & Yu. L. Gritsay, 1964 : O problematicheskom obrazovanii iz dokembriya Yakovlevskogo zhelezorudnogo mestorozhdeniya KMA (Problematic structure from the Precambrian Yakolev iron-ore deposit, Kursk Magnetic Anomaly). Dokl. Akad. Nauk SSSR 154, 833-835 (Dokl. Acad. Sci. USSR, Earth Sci. Secn 154, 57-58).

Edgell, H. S., 1964 : Precambrian fossils from the Hamersley Range, Western Australia, and their use in stratigraphic correlation. J. Geol. Soc. Aust. 11, 235-261.

Eugster, H. P., 1967 : Hydrous sodium silicates from Lake Magadi, Kenya: Precursors of bedded chert. Science N.Y. 157, 1177-1180.

Gershoig, Yu. G., 1965 : Osobennosti sloistosti zhelezistykh porod Krivorozh'ya (Characteristics of the lamination in ferruginous rocks from Krivoi Rog). Izv. Akad. Nauk SSSR, ser. geol., 1965 no. 8, 45-60.

Glaessner, M. F., 1962 : Pre-Cambrian fossils. Biol. Rev. 37, 467-494.

Glaessner, M. F., 1966 : Precambrian palaeontology. Earth-Sci. Rev. 1, 29-50.

Glaessner, M. F. & Mary Wade, 1966 : The late Precambrian fossils from Ediacara, South Australia. Palaeontology 9, 599-628.

Goodwin, A. M., 1956 : Facies relations in the Gunflint iron formation. Econ. Geol. 51, 565-595.

Graham, T., 1864 : On the properties of silicic acid and other analogous colloidal substances. J. Chem. Soc. London 17, 318-327.

Gruner, J. W., 1946 : The mineralogy and geology of the taconites and iron ores of the Mesabi Range, Minnesota. Office of the Commissioner of the Iron Range Resources and Rehabilitation, St. Paul, Minnesota, 127p.

Halligan, R. & J. L. Daniels, 1964 : Precambrian geology of the Ashburton Valley region, North-West Division. Ann. Rep. geol. Surv. W. Austral. 1963, 38-46.

Harington, J. S. & J. J. Le R. Cilliers, 1963 : A possible origin of the primitive oils and amino acids isolated from amphibole asbestos and banded ironstone. Geochim. cosmochim. Acta 27, 411-418.

Hatschek, E., 1925 : Laboratory manual of elementary colloid chemistry, 2nd ed. Churchill, London, 153p.

Hedges, E. S., 1932 : Liesegang rings and other periodic structures. Chapman & Hall, London, 122p.

Hofmann, H. J., 1969 : Stromatolites from the Proterozoic Animikie and Sibley Groups, Ontario. Geol. Surv. Pap. Can. 68-69, 32p.

Holmes, H. N., W. E. Kaufmann & H. O. Nicholas, 1919 : The vibration and syneresis of silicic acid gels. J. Amer. Chem. Soc. 41, 1329-1336.

Huber, N. K., 1959 : Some aspects of the origin of the Iron-wood iron-formation of Michigan and Wisconsin. Econ. Geol. 54, 82-118.

Iler, R. K., 1955 : The colloid chemistry of silica and the silicates. Cornell Univ. Press, Ithaca, N.Y., 324p.

Isemura, T., 1939 : Studies on rhythmic precipitates. Bull. chem. Soc. Jap. 14, 179-237.

James, H. L., 1951 : Iron Formation and associated rocks in the Iron River district, Michigan. Bull. geol. Soc. Amer. 62, 251-266.

James, H. L., 1954 : Sedimentary facies of iron-formation. Econ. Geol. 49, 235-293.

James, H. L., 1966 : Chemistry of the iron-rich sedimentary rocks in Data of geochemistry, 6th ed. U.S. geol. Surv. Prof. Pap. 440-W, W1-W60.

Jirgensons, B. & M. E. Straumanis, 1954 : A short textbook of colloid chemistry. Pergamon Press, London, 420p.

Johnston-Lavis, H. J. & J. W. Gregory, 1894 : Eozoonal structure of the ejected blocks of Monte Somma. Sci. Trans. roy. Dubl. Soc. 2(5), 259-286.

Jones, J. B. & E. R. Segnit, 1966 : The occurrence and formation of opal at Coober Pedy and Andamooka. Austral. J. Sci. 29, 129-133.

Krauskopf, K. B., 1959 : The geochemistry of silica in sedimentary environments in Silica in Sediments. Spec. Publ. Soc. econ. Pal. Min., Tulsa 7, 4-19.

Krauskopf, K. B., 1967 : Introduction to geochemistry. McGraw-Hill Book Co., New York, 721p.

Kurz, P., 1965 : Frozen reactions. Int. Sci. Technol. March 1965, 81-82.

LaBerge, G. L., 1964 : Development of magnetite in iron-formations of the Lake Superior region. Econ. Geol. 59, 1313-1342.

LaBerge, G. L., 1966 : Altered pyroclastic rocks in iron-formation in the Hamersley Range, Western Australia. Econ. Geol. 61, 147-161.

LaBerge, G. L., 1967 : Microfossils and Precambrian iron-formations. Bull. geol. Soc. Amer. 78, 331-342.

Leveson, D. J., 1963 : Orbicular rocks of the Lonesome Mountain area, Beartooth Mountains, Montana and Wyoming. Bull. geol. Soc. Amer. 74, 1015-1040.

Liesegang, R. E., 1913 : Geologische diffusionen. T. Steinkopff, Dresden & Leipzig, 180p.

MacLeod, W. N., 1967 : The geology and iron deposits of the Hamersley Range area, Western Australia. Bull. geol. Surv. W. Austral. 117, 170p.

Matalon, R. & A. Packter, 1955-1956 : The Liesegang phenomenon. J. Colloid Sci. 10, 46-62; 11, 96-106, 150-157.

Moorhouse, W. W. & F. W. Beales, 1962 : Fossils from the Animikie, Port Arthur, Ontario. Trans. roy. Soc. Canada 3(56), 97-110.

Park, C. F. Jr & R. A. MacDiarmid, 1964 : Ore deposits. W. H. Freeman Co., San Francisco & London, 475p.

Percival, F. G., 1967 : Texture of Brockman Iron Formation jaspilite, Western Australia. Econ. Geol. 62, 431-432.

Pettijohn, F. J., 1957 : Sedimentary rocks, 2nd ed. Harper & Brothers, New York, 718p.

Ryan, G. R. & J. G. Blockley, 1965 : Progress report on the Hamersley Range blue asbestos survey. Rec. geol. Surv. W. Austral. 1965/32, 63p. (unpubl.).

Schultz, R. W., 1966 : Lower Carboniferous oherty ironstones at Tynagh, Ireland. Econ. Geol. 61, 311-342.

Shrock, R. R., 1948 : Sequence in layered rocks. McGraw-Hill Book Co., New York, 507p.

Siever, R., 1962 : Silica solubility, 0^{o}-200^{o}C., and the diagenesis of siliceous sediments. J. Geol. 70, 127-150.

Spencer, E. & F. G. Percival, 1952 : The structure and origin of the banded hematite jaspers of Singhbhum, India. Econ. Geol. 47, 365-383.

Stansfield, J., 1917a : Retarded diffusion and rhythmic precipitation. Amer. J. Sci. 4(43), 1-26.

Stansfield, J., 1917b : Concentric rings in naturally occurring silica. Trans. roy. Soc. Can. ser. 3, v. 11, sect. 4, 117-120.

Starostina, Z. M., 1959 : Ob usloviyakh razmeshcheniya sideritovykh rud vo vmeshchayushchikh porodakh bakal'skoy gruppy mestorozhdeniy (yuzhnyy ural) (Conditions of distribution of siderite ores throughout the host rocks of the Baikal group of ore deposits, southern Urals). Izv. Akad. Nauk SSSR, Ser. Geol. 1959 no. 7, 40-59 (Izv. Acad. Sci. USSR, Geol. Ser. 1959, 33-50).

Stern, K. H., 1954 : The Liesegang phenomenon. Chem. Rev. 54, 79-99.

Stern, K. H., 1967 : Bibliography of Liesegang rings, 2nd ed. Misc. Publ. Nat. Bur. Stand., U.S. Dept. Commerce, 292, 61p.

Swarbrick, E. E., 1968 : Physical diagenesis; intrusive sediment and connate water. Sediment. Geol. 2, 161-175.

Taliaferro, N. L., 1934 : Contraction phenomena in cherts. Bull. geol. Soc. Amer. 45, 189-232.

Tegengren, F. R., 1921-23 : The iron ores and iron industry of China: including a summary of the iron situation of the Circum-Pacific region, Pts. 1, 2. Mem. geol. Surv. China, Ser. A, no. 2 (1921), no. 2 (1923), Atlas.

Trendall, A. F., 1954 : Progress report on the Brockman Iron Formation in the Wittenoom-Yampire area. Rep. geol. Surv. W. Austral. 1964, 55-65.

Trendall, A. F., 1966a : Second progress report on the Brockman Iron Formation in the Wittenoom-Yampire area. Rep. geol. Surv. W. Austral. 1965, 75-87.

Trendall, A. F., 1966b : Altered pyroclastic rocks in iron-formation in the Hamersley Range, Western Australia. Econ. Geol. 61, 1451-1458.

Trendall, A. F., 1968 : Three great basins of Precambrian banded iron formation: a systematic comparison. Bull. geol. Soc. Am. 79, 1527-1544.

Trendall, A. F. & J. G. Blockley, 1968 : Stratigraphy of the Dales Gorge Member of the Brockman Iron Formation, in the Precambrian Hamersley Group of Western Australia. Rep. geol. Surv. W. Austral. 1967, 48-53.

Twenhofel, W. H., 1919 : Pre-Cambrian and Carboniferous algal deposits. Amer. J. Sci. 4(48), 339-352.

von Backström, J. W., 1964? : Septarian concretions in the Lower Griquatown Stage of the Pretoria Series near Kuruman, Cape Province. Ann. geol. Surv. S.Af. 2 (for 1963), 79-81.

Wade, Mary, 1968 : Preservation of soft-bodied animals in the Precambrian at Ediacara Hills. Lethaia, 1, 238-267.

Weed, W. H., 1889 : Formation of travertine and siliceous sinter by the vegetation of hot springs. Ann. Rep. U.S. geol. Surv. 9 (1887-1888), 613-676.

White, D. A., 1954 : The stratigraphy and structure of the Mesabi Range, Minnesota. Bull. Minnesota geol. Surv. 38, 92p.

White, D. E., W. W. Brannock & K. J. Murata, 1956 : Silica in hot-spring waters. Geochim. cosmochim. Acta 10, 27-59.

White, J. F. & J. F. Corwin, 1961 : Synthesis and origin of chalcedony. Amer. Mineral. 46, 112-119.

White, W. A., 1961 : Colloidal phenomena in the sedimentation of argillaceous rocks. J. sed. Pet. 31, 560-570.

Whitten, G. F., 1966 : Suggested correlation of iron ore deposits within South Australia. Quart. Geol. Notes, Geol. Surv. S. Austral. 18, 7-11.

APPENDIX II

TECTONICALLY DEFORMED SAND VOLCANOES IN A PRECAMBRIAN GREYWACKE, NORTHERN TERRITORY OF AUSTRALIA

INTRODUCTION

The structures here described were previously considered as probable fossils (Robertson, 1962) and because of their antiquity (between 1,760 and 2,550 m.yrs : Dunn, Plumb & Roberts, 1966) and unusual form aroused much interest (Glaessner, 1966).

They occur within the 1500m thick Noltenius Formation of the Finniss River Group, a sequence of siltstones, greywackes, sandstones and quartz pebble conglomerate that occur within the Pine Creek Geosyncline. Some of these rocks exhibit graded bedding (Malone, 1962). In the areas under consideration they are apparently unmetamorphosed.

OCCURRENCE

The modified sand volcanoes are known from three localities: near George Creek and Tumbling Waters, respectively about 80 miles and 40 miles south of Darwin (precise localities are given by Robertson, 1962) and 3/4 mile north of Adelaide River, 70 miles south of Darwin (B. Tapp, pers. comm., 1967). This last occurrence was unknown when I visited the area.

George Creek

At this locality the structures are well exposed in a sequence of massive greywacke interbedded with siltstone. The rocks are deformed into upright, open, shallow-plunging folds with dips of up to 60^{o}. The sand volcanoes are in the upper 30cm or so of a steeply dipping 4m thick bed of coarse grained greywacke. There appear to be two such

beds, on opposite sides of a small creek, but this probably due to slight displacement along a fault. Overlying the greywacke with a sharp contact is a red-weathering siltstone with load casts on its lower surface; the exact nature of the contact was obscured because the siltstone outcropped only poorly. The sand volcano cones make up the bulk of the upper part of the greywacke (pl.39a), contiguous ones often deforming each other (pl.39e). In all cases the infilled feeder pipes (cores) of the volcanoes are approximately at right angles to the bedding, and penetrate downwards for at least 30cm.

Tumbling Waters

Although a bed containing the volcanoes is exposed here the direction of bedding and hence the orientation of the structures is in doubt. It was thought in the field that the structures were at a low angle to, or parallel to, the bedding, but it now seems likely that this was jointing, not bedding. Outcrop is poor and the contiguous beds are not exposed. A fault cuts off one end of the outcrop. However, this exposure is valuable in that many oblique longitudinal sections of the volcanoes are visible (pl.39f). In this area the Noltenius Formation is deformed into tight, upright, shallow-plunging folds with dips of up to 90°.

At both localities are many circular cones which have been little distorted by tectonism.

MORPHOLOGY AND PETROLOGY

All of the structures present are variations on one type. This

is cylindrical or conical (widening upwards), the base merging with the enclosing rock. Axially placed is a core of coarse-grained greywacke; surrounding this is coarse-grained greywacke grading peripherally into fine grained greywacke. The outer edge of the core is a fracture zone at the outermost extension of coarse grained sediment. Radiating from the core, but not occurring within it, are longitudinal planar structures visible on weathered surfaces as grooves; these also fade out near the base of the cone. Each of the structural elements is described in detail below.

In order of decreasing abundance, the framework constituents of the greywacke are quartz, quartzite, chert and mica. Grains are angular but roughly equidimensional (except the mica), with a maximum diameter of 1.0mm. The matrix consists of smaller grains of quartz and abundant sericite. Some quartz grains have been partially replaced by clayey and sericitic minerals. The quartz grains where in contact are interlocking, with sutured contacts. There is much very fine grained limonite and some small grains of haematite.

Core

Only rarely is there more than one core but nine were seen in one cone (pl.39a). The core is the most continuous part of the volcanoes: cores up to 30cm long have been observed, and never was a lower end visible. In transverse section the cores are circular to subquadrangular, their diameter being 15 to 25% of that of the cones. Separating the core from the cone is a narrow zone of concentric fractures and, in

some cases, finer grained sediment. The fractures split framework grains and the resultant inequidimensional grains are tangentially arranged. Because of the fractures this is a weak area which weathers easily and is often lost in thin-section preparation (pl.39b).

No persistent longitudinal grain size trends have been observed. The bulk of the core is coarse grained, with the framework constituents of the greywacke predominating. In some examples the outer part of the core is finer grained (other than because of grain size diminution due to fracturing). Rarely there are weak saucer-shaped laminations arranged at right angles to the core axis, and concave upwards. These are only apparent because of concentrations of limonite in them, and do not reflect grain size variations. No cores were seen in which the axial region is finer grained than the periphery, but Robertson (1962) recorded one such example.

Cone

The cones are 10-50cm wide, the inner two-thirds or so (by radius) consisting of a concentration of coarse grained greywacke; this always passes outwards into a fine grained outer zone (pls 39b,40a,b). Distinct tongues of sediment are sometimes present, but often the change in grain size is gradational. Several of the specimens sectioned contained distinct laminations due to grain size variations in the sediment of the cone. In one the laminations are concave upwards and dip outwards from the core at 10 to 30^{o} near the centre, flattening outwards (pl.40b). These laminae are deflexed near the core, there dipping inwards at 55 to 60^{o},

forming a crater (this is faintly visible in pl.40a). In another core the laminations were slightly convex upwards (pl.40a). In most cases the laminae are sharply deflexed at the outer edge of the cones, but occasionally they bend upwards there. The laminations are also slightly deflexed where they intersect the radial structures.

Outer Margin of the Cones

The structural break at the edge of the cones is similar to that at the edge of the cores. It consists of a narrow zone of concentric fractures at the outermost extension of tongues of coarse grained sediment (pl.40a,b). It also includes a tangential arrangement of inequidimensional grains. The sediment between the cones is fine grained like that in their peripheries, and is sometimes faintly laminated, the laminae being deflexed at the edge of the cones.

Radial Structures

It is these that are the most unusual feature of the modified sand volcanoes. Appearance on weathered surfaces suggested that the radially disposed grooves marked concentrations of fine grained sediment. Oblique longitudinal sections exposed at the Tumbling Waters locality revealed that the radial structures are not just grooves but are penetrative and planar (pl.39f). The development of these varies, some cones having none, others up to about 70 (pl.39d).

While the radial structures are obvious on weathered surfaces, in thin sections often they are almost invisible. As with the structurally weak areas on the peripheries of the cores and cones the grains within

the radial structures were often lost during thin section preparation. The structures consist of roughly planar fractures, or braided series of fractures, along which are concentrations of limonite. The limonite is dark coloured, causing the illusion that the fractures are concentrations of fine sediment. Many quartz grains are split by the fractures (pl.40d).

MODE OF FORMATION

The presence of a central pipe, laminations within the cone and the intertonguing of the coarse grained interior and fine grained periphery clearly shows that these are primary sedimentary structures similar to sand volcanoes (Gill & Kuenen, 1957) and spring pits (Quirke, 1930). They have been distorted by tectonism, as discussed below.

The grain size variations in the cones are as expected, with the coarsest sediment near the source - the crater. The grain size variations in cores are attributable to the winnowing action of water moving up through sediment in the feeder pipe, perhaps accompanied by some flow differentiation (Bhattacharji, 1967) and variation in the grain size of sediment being supplied from the lower part of the greywacke bed. The weak laminations within the cores formed later, during compaction. In one example laminae at the periphery of the cone are bent upwards, but most are sharply deflexed there. The upwardly bent laminae could be explained if the structures were spring pits, but not the deflexed ones and all such flexures are best explained as due to later deformation.

These structures very closely resemble the sand volcanoes described

from the Carboniferous of Ireland by Gill & Kuenen (1957), the only major difference being the possession by the Australian examples of fracture zones with their associated lamina flexures. The sand volcanoes from both regions have narrow central vents into which laminae dip steeply and away from which dips are gentle, the laminae in the cones being very gently convex or concave. The volcanoes from both regions can be very closely spaced and always occur at the tops of beds (at least where their position in a bed is known). The Irish examples all occur on slumped beds, or are closely associated with them. At George Creek, where exposure is good, the Australian sand volcanoes are in the upper 30cm or so of a 4m thick bed of coarse greywacke, in which no internal structures were visible in the field.

Gill & Kuenen (1957) quote experimental evidence to support their interpretation that the Irish sand volcanoes were built because of the rapid extrusion of water from the underlying sediment. They consider that the water extrusion was a result of the process which caused the slumping; the slumping may have been accompanied by little horizontal movement and possibly was due to sudden compaction resulting from disturbance by earthquakes. The sediment may have been thixotropic. In interpreting the Australian volcanoes their apparently rare occurrence must be considered. Because of this and the grain size distribution of the sediment it is possible that the extrusion of water resulted from an earthquake induced thixotropic change from solid to liquid sediment.

The fracturing and lamina flexuring resulted from stress systems arranged radially about each volcano core. The stress systems probably

developed during folding of the host rock. Some cones have slightly elliptical transverse sections, with the long axes of the ellipses aligned with a weak foliation in the host rock. The arrangement of the stress systems must have resulted from the anisotropy of the rock, i.e. the stress distribution was controlled by the distribution of the sand volcanoes. The lamina flexuring could have resulted from centripetal forces caused during the folding of the host rocks but the fractures are tensional features which may have formed when the folding stresses were unloaded. Similar fractures form when experimentally stressed quartzites are unloaded (Carter, Christie & Griggs, 1964). There are probably only two concentric fractures because there are only two concentric structural discontinuities to concentrate the stresses. The stresses have also caused deformation of quartz grains, resulting in undulose extinction. Quartz veins cut the fractured volcanoes (pl.39d), indicating that the fractures formed at an earlier stage than the veins.

SIMILAR STRUCTURES

It is interesting to briefly note that structures described from Precambrian carbonates by Walcott (1912) as "Atikokania lawsoni" and "A. irregularis" are similar to those described here in being about the same size and shape and having comparable radial structures. These have long been considered pseudofossils and also appear to have had a partly mechanical origin (some resemble cone in cone structures).

SUMMARY

Structures which before were considered to be umbrella-shaped and probable fossils have been found to be cylindrical to conical sand volcanoes. Tectonic deformation to which their host rock has been subjected affected them in an unusual way, resulting in the production of concentric and radial fractures, the latter up to about 70 in number.

REFERENCES

Bhattacharji, S., 1967 : Mechanics of flow differentiation in ultramafic and mafic sills. J. Geol. 75, 101-112.

Carter, N. L., J. M. Christie & D. T. Griggs, 1964 : Experimental deformation and recrystallization of quartz. J. Geol. 72, 687-733.

Dunn, P. R., K. A. Plumb & H. G. Roberts, 1966 : A proposal for time-stratigraphic subdivision of the Australian Precambrian. J. geol. Soc. Aust. 13, 593-608.

Gill, W. D. & P. H. Kuenen, 1957 : Sand volcanoes on slumps in the Carboniferous of County Clare, Ireland. Geol. Soc. Lond. Q. Jl 113, 441-464.

Glaessner, M. F., 1966 : Precambrian palaeontology. Earth-Sci. Rev. 1, 29-50.

Malone, E. J., 1962 : Explanatory notes to the Darwin 1:250,000 sheet, N.T. Explan. Notes Bur. Min. Resour. Geol. Geophys. Aust. D/52-4, 20p.

Oldershaw, W., 1960 : Probable sand volcanoes in the Lower Proterozoic at Tennant Creek, N.T. J. geol. Soc. Aust. 6, 197-199.

Quirke, T. T., 1930 : Spring pits, sedimentation phenomena. J. Geol. 38, 88-91.

Robertson, W. A., 1962 : Umbrella-shaped fossils(?) from the Lower Proterozoic of the Northern Territory of Australia. J. geol. Soc. Aust. 9, 87-90.

Walcott, C. D., 1912 : Notes on fossils from limestone of Steeprock series, Ontario. Mem. Geol. Surv. Can. 28, 16-20.

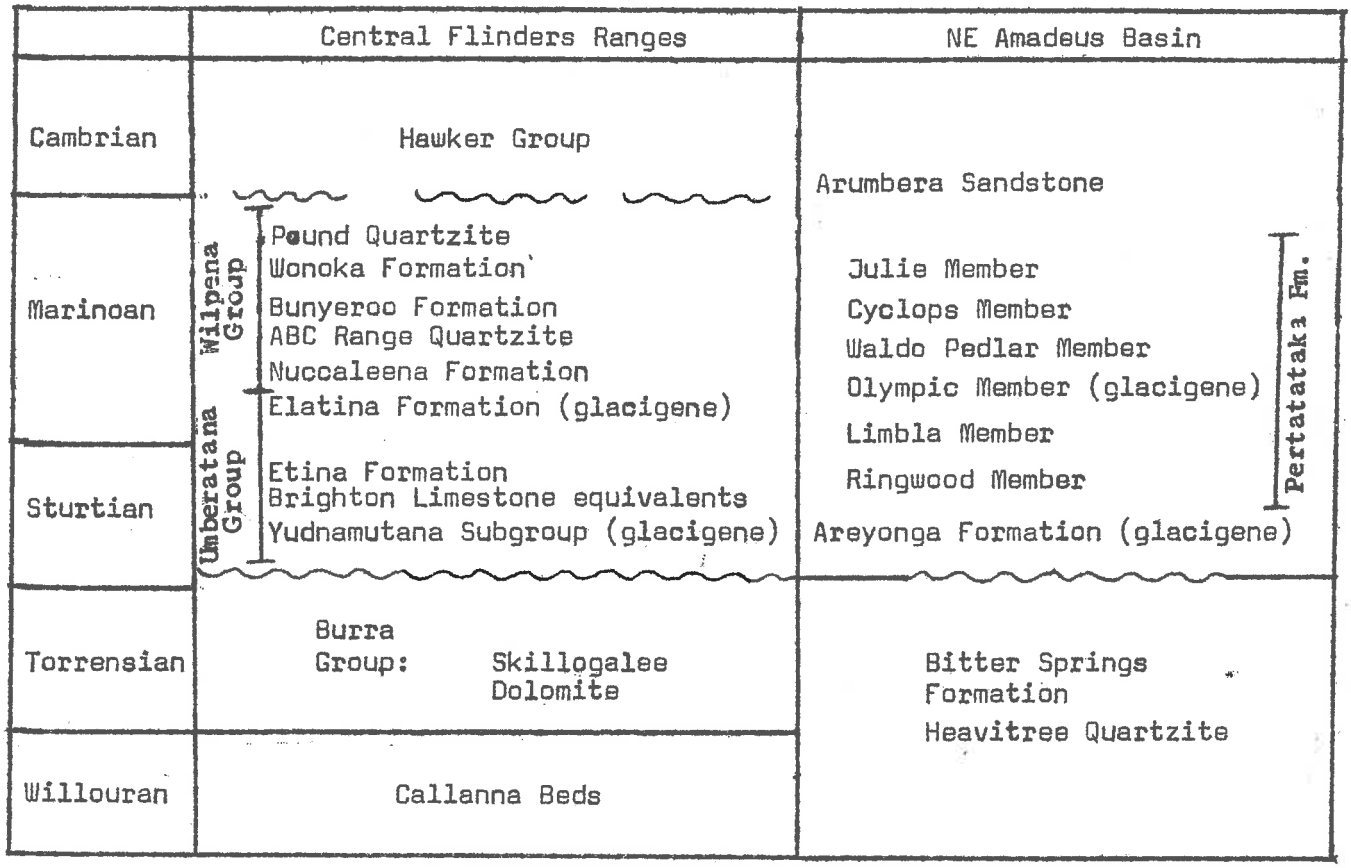

Table 1: Tentative correlation of the sequences in the Adelaide Geosyncline and Amadeus Basin; made by Wells et al. (1967b) in their text and figure P614. Though the correlation of the upper units is acceptable the conventional correlations of the lower units are now modified, as shown in table 2. Only selected units are shown.

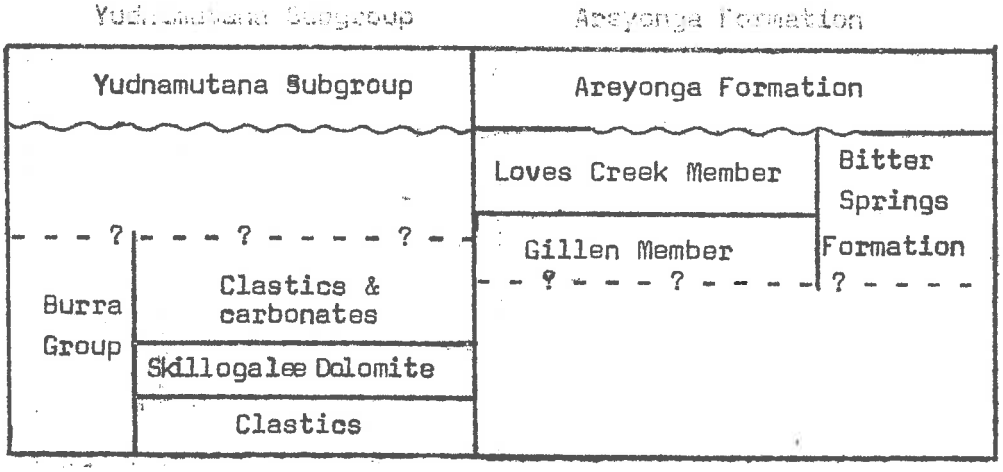

Table 2: New correlation of the lower units of the Adelaide Geosyncline and Amadeus Basin, based on a comparison of stromatolite assemblages (modified after Glaessner, Preiss & Walter, 1969).

	UNCONFORMITY			
WYLOO	Capricorn Formation	Sandstone, greywacke, dolomite shale	1,200 min.	
	Ashburton Formation	Shale, greywacke	Unknown; large	
	Duck Creek Dolomite	Dolomitic limestone, chert	300	*Pilbaria perplexa* *Patomia* f. indet.
	Mount McGrath Formation	Conglomerate, sandstone, quartzite, siltstone, shale, basalt	2,000	
	Beasley River Quartzite	Quartzite	90	+2020±165 m.y.
	Turee Creek Formation	Greywacke, conglomerate, shale, basalt	300	
HAMERSLEY	Boolgeeda Iron Fmn	Siltstone, ferruginous shale, banded iron-formation	200	
	Woongarra Volcanics	Dacite, rhyolite, pyroclastics	570	+2000±100 m.y.
	Weeli Wolli Formation	Banded iron-formation, shale, dolerite	480	
	Brockman Iron Fmn	Banded iron-formation, chert, shale	660	
	Mount McRae Shale	Shale, siltstone, dolomite, dolomitic shale, chert	90	
	Mount Sylvia Shale	Banded iron-formation, shale	30	
	Wittenoom Dolomite	Dolomite, dolomitic shale	150	
	Marra Mamba Iron Fmn	Chert, banded iron-formation	180	
FORTESCUE	Jeerinah Formation	Shale, chert, banded iron-formation, mudstone, quartzite, dolomite, dolerite	900	
	Mount Jope Volcanics	Pillow lavas, pyroclastics (including as correlatives Pillingini Tuff and Tumbiana Pisolite)	2,000	+2190±100 m.y. *Alcheringa narrina*
	Hardey Sandstone	Sandstone, arkose, conglomerate, quartzite, basalt	1,200	
	UNCONFORMITY			

Table 3. Content of the Mount Bruce Supergroup, based on a stratigraphic table for the Mount Bruce 1:250,000 Sheet area (de la Hunty, 1965), with modifications from Daniels (1968) and Kriewaldt & Ryan (1967). Thicknesses are in metres. Group names are on the left. +Rb-Sr whole rock datings; the stratigraphic positions of the dated rocks in the Fortescue and Wyloo Groups were not specified by Compston & Arriens (1968).

Kurabuka Formation	Sandstone, silty shale, shale	?	
Fords Creek Shale	Greenish shale, with some greywacke and chert	1700	
Coodardoo Formation	Greywacke with minor silt and shale	150-360	
Curran Formation	Shale with siltstone and chert	75	*1080±80 m.y.
Ullawarra Formation	Shale, siltstone, rare sandstone and dolomite	?1500-1800	(thickness includes dolerite sills)
Devil Creek Formation	Dolomite, dolomitic shale and dolomite breccia	60-360	Baicalia capricornia
Discovery Chert	Thin-bedded black or grey chert	60-360	
Kiangi Creek Formation	Sandstone with minor shale and chert	?600	
Irregully Formation	Dolomite, dolomitic shale, sandstone, chert, conglomerate and breccia	?900+	Baicalia capricornia Conophyton garganicum australe

UNCONFORMITY

Folded and metamorphosed Ashburton and Capricorn Formations, Wyloo Group, Mount Bruce Supergroup

Table 4. Content of the Bangemall Group in the Edmund 1:250,000 Sheet area (after Daniels, 1968). Thicknesses are in metres. *Rb-Sr whole-rock dating on shale.

Table 6:

Time ranges of stromatolites in the USSR. Colonnella, Conophyton and Jacutophyton are placed first, followed by columnar branching forms and then noncolumnar stromatolites. The ranges have been assembled from all available literature and incorporate modifications made since the names were first published. The widths of the columns representing the Early, Middle and Late Riphean, Vendian and Cambrian are proportional to the time spans of these units; this is not so for the other, minor subdivisions. The subdivisions within the Middle and Late Riphean and the Vendian are apparently not yet widely accepted; where I have been unable to exactly determine ranges relative to these subdivisions the line representing the range is dotted (•••). If in addition doubts about the range are expressed in the Russian literature this is indicated with queries (?). The positions of the ends of ranges should not be taken as precise. Taxa of doubtful validity are enclosed by quotation marks ("). Taxa whose classification is in doubt are indicated with a query.

\+ Komar & Semikhatov (1969) do not show B. lacera extending into the Late Riphean

* Komar & Semikhatov (1969) do not show B. prima in the early Middle Riphean

** In contrast to previous workers Raaben (1969a) places K. karatavica in the late Late Riphean rather than the early Late Riphean

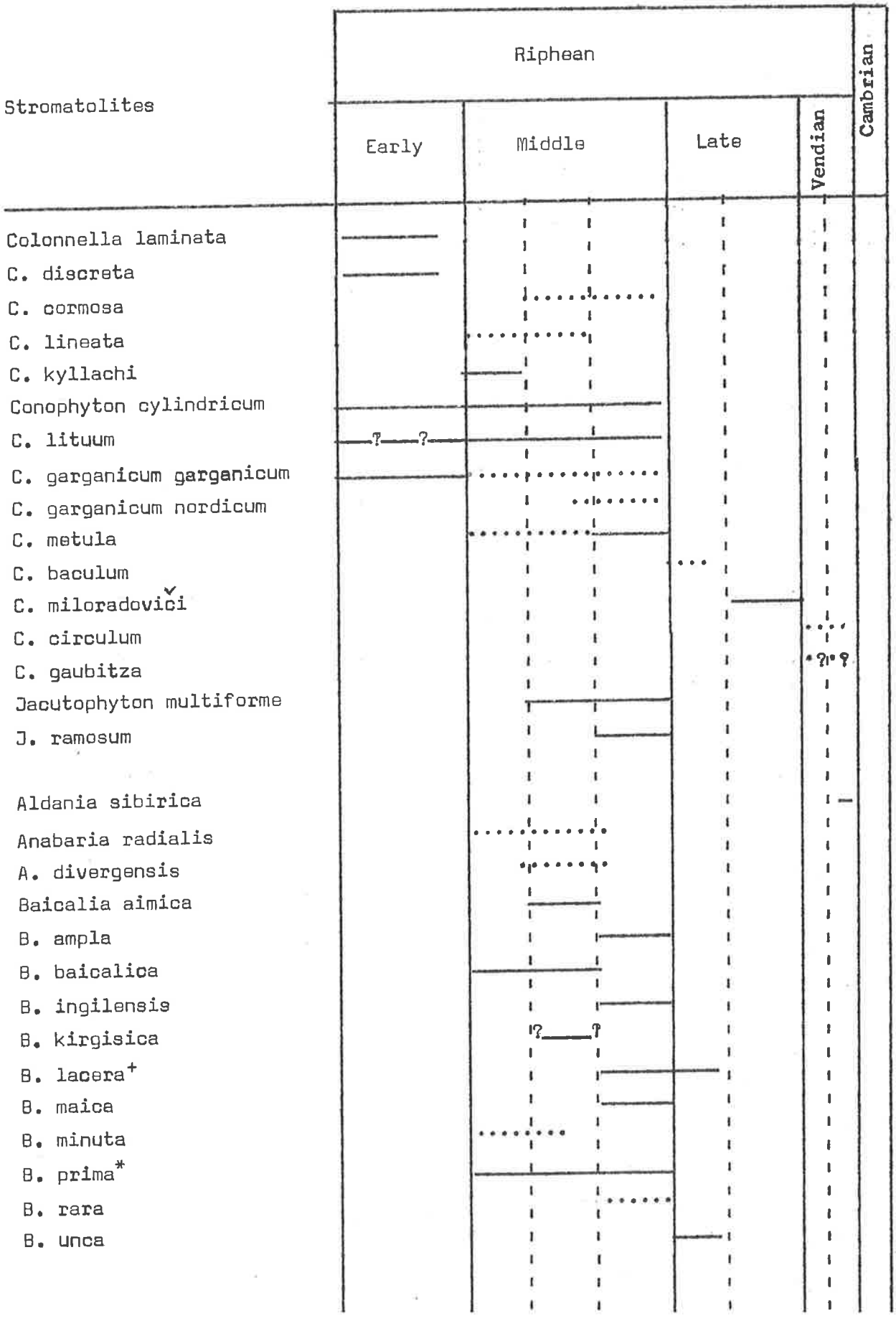
Stromatolites
Riphean
Early
Middle
Late
Vendian
Cambrian
Colonnella laminata
C. discreta
C. cormosa
C. lineata
C. kyllachi
Conophyton cylindricum
C. lituum
C. garganicum garganicum
C. garganicum nordicum
C. metula
C. baculum
C. miloradovici
C. circulum
C. gaubitza
Jacutophyton multiforme
J. ramosum
Aldania sibirica
Anabaria radialis
A. divergensis
Baicalia aimica
B. ampla
B. baicalica
B. ingilensis
B. kirgisica
B. lacera+
B. maica
B. minuta
B. prima*
B. rara
B. unca

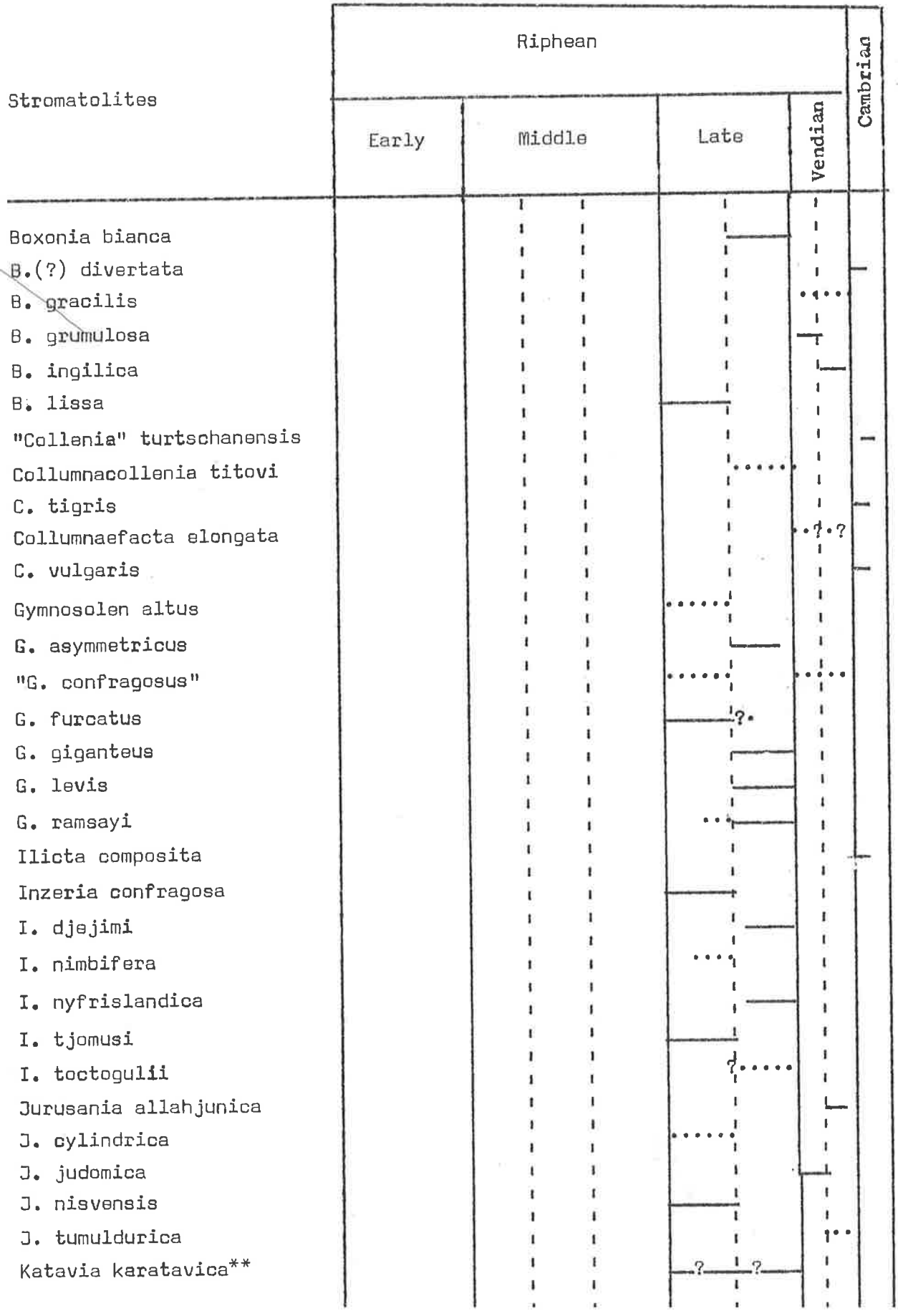
Stromatolites
Riphean
Early
Middle
Late
Vendian
Cambrian
Boxonia bianca
B.(?) divertata
B. gracilis
B. grumulosa
B. ingilica
B. lissa
"Collenia" turtschanensis
Collumnacollenia titovi
C. tigris
Collumnaefacta elongata
C. vulgaris
Gymnosolen altus
G. asymmetricus
"G. confragosus"
G. furcatus
G. giganteus
G. levis
G. ramsayi
Ilicta composita
Inzeria confragosa
I. djejimi
I. nimbifera
I. nyfrislandica
I. tjomusi
I. toctogulii
Jurusania allahjunica
J. cylindrica
J. judomica
J. nisvensis
J. tumuldurica
Katavia karatavica**

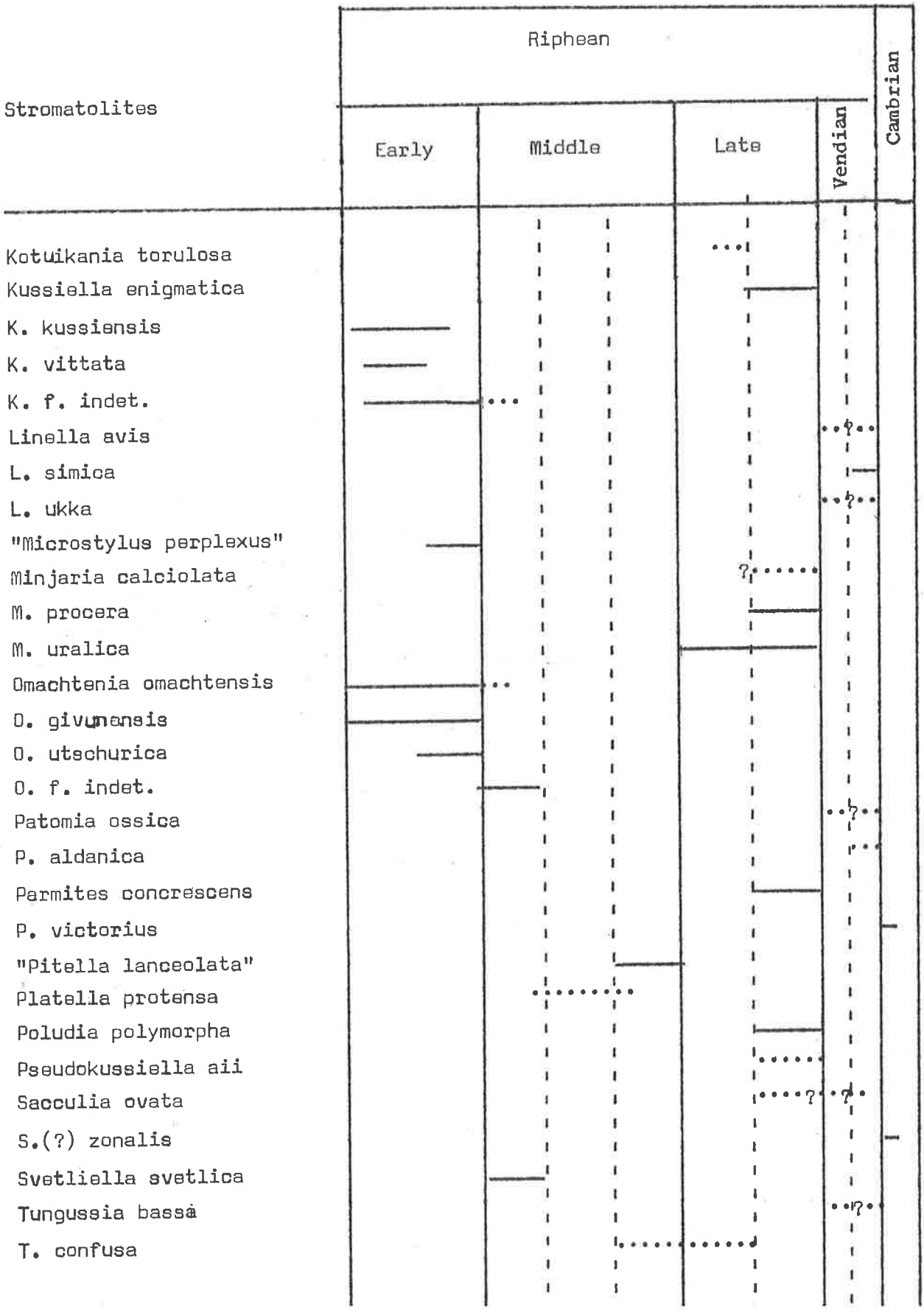
Stromatolites
Riphean
Early
Middle
Late
Vendian
Cambrian
Kotuikania torulosa
Kussiella enigmatica
K. kussiensis
K. vittata
K. f. indet.
Linella avis
L. simica
L. ukka
"Microstylus perplexus"
Minjaria calciolata
M. procera
M. uralica
Omachtenia omachtensis
O. givumensis
O. utschurica
O. f. indet.
Patomia ossica
P. aldanica
Parmites concrescens
P. victorius
"Pitella lanceolata"
Platella protensa
Poludia polymorpha
Pseudokussiella aii
Sacculia ovata
S.(?) zonalis
Svetliella svetlica
Tungussia bassa
T. confusa

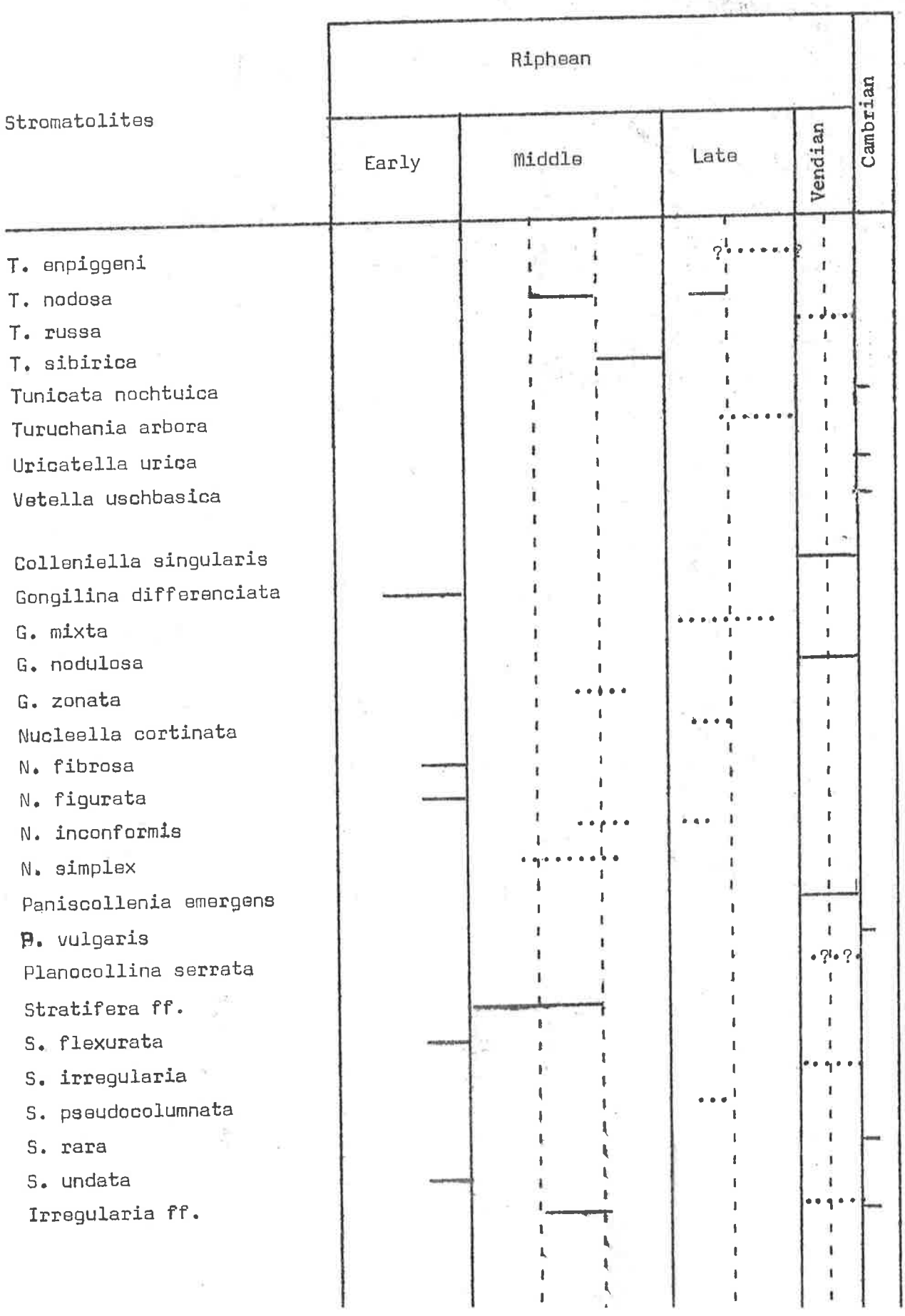
Stromatolites
Riphean
Early
Middle
Late
Vendian
Cambrian
T. enpiggeni
T. nodosa
T. russa
T. sibirica
Tunicata nochtuica
Turuchania arbora
Uricatella urica
Vetella uschbasica
Colleniella singularis
Gongilina differenciata
G. mixta
G. nodulosa
G. zonata
Nucleella cortinata
N. fibrosa
N. figurata
N. inconformis
N. simplex
Paniscollenia emergens
P. vulgaris
Planocollina serrata
Stratifera ff.
S. flexurata
S. irregularia
S. pseudocolumnata
S. rara
S. undata
Irregularia ff.

Fig.1 Locality map showing sedimentary basins discussed in the text.

Figure 2

Lamina shapes; the laminae shown are representative selections and although their orientation is the same as originally they have been spatially rearranged.

a: *Acaciella australica*.

b,f: *Boxonia pertaknurra* (b from columns with altered margins).

c: *Minjaria pontifera* (from columns with altered margins).

d,j: *Basisphaera irregularis* (j from columns with altered margins).

e: *Minjaria procera*.

g: *Kulparia alicia*.

h: *Alcheringa narrina*.

i: *Conophyton garganicum australe*.

The stromatolites a-g have parallel branching; h and i do not branch. The relationship between branching and lamina shapes is discussed in the text (p.71-73).

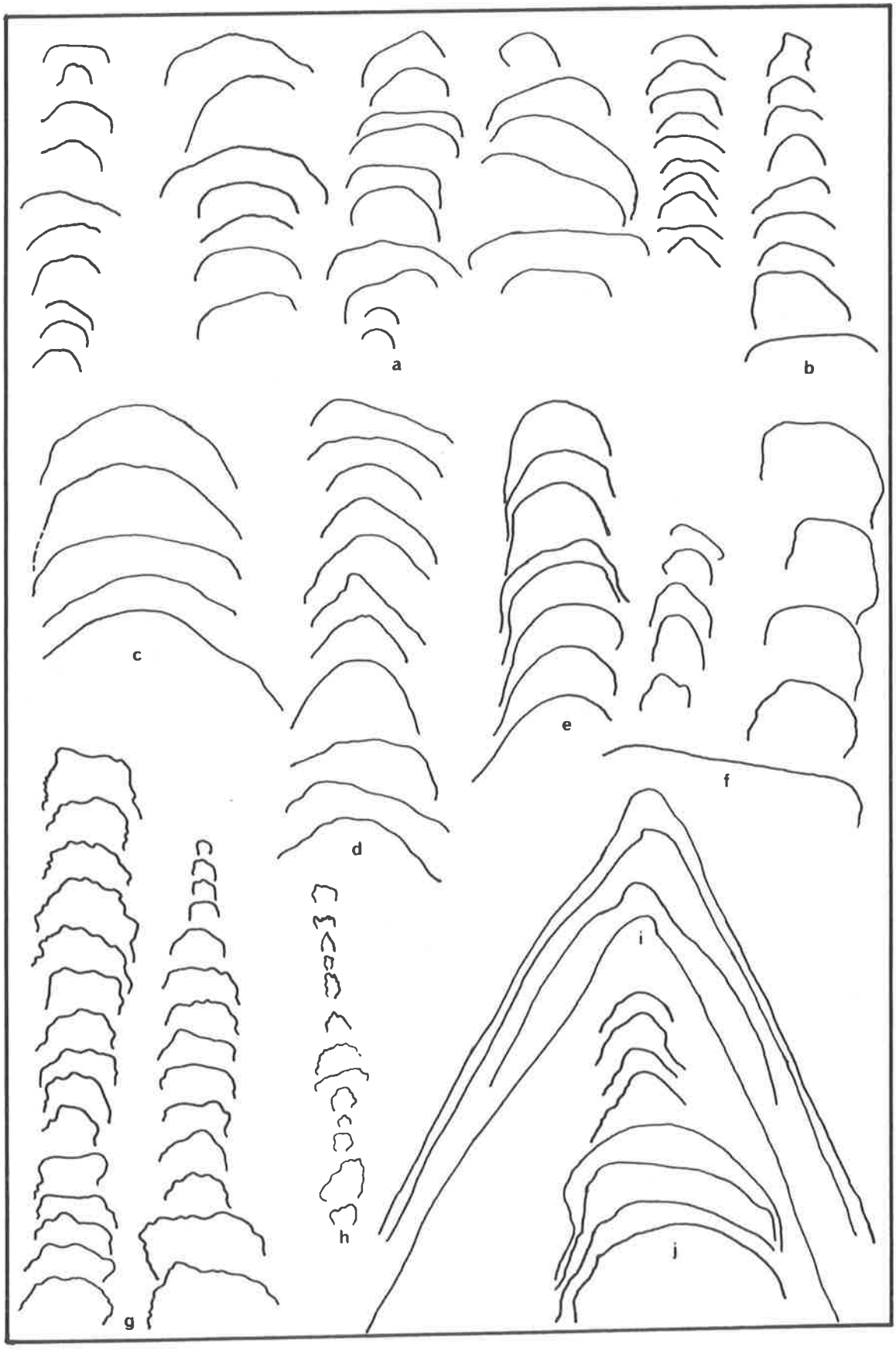

Fig. 2

Figure 3

Lamina shapes; the laminae shown are representative selections and although their orientation is the same as originally they have been spatially rearranged.

a,b: *Inzeria intia* II.

c: *I. intia* I.

d: *I. intia* III base.

e: *I. intia* III.

f: *Patomia ossica*.

g: *Linella avis*.

h: *I. intia* IV (from columns with altered margins).

i: *Pilbaria perplexa*.

The stromatolites represented here have niche-projections or nonparallel branching. The relationship between branching and lamina shapes is discussed in the text (p.71-73).

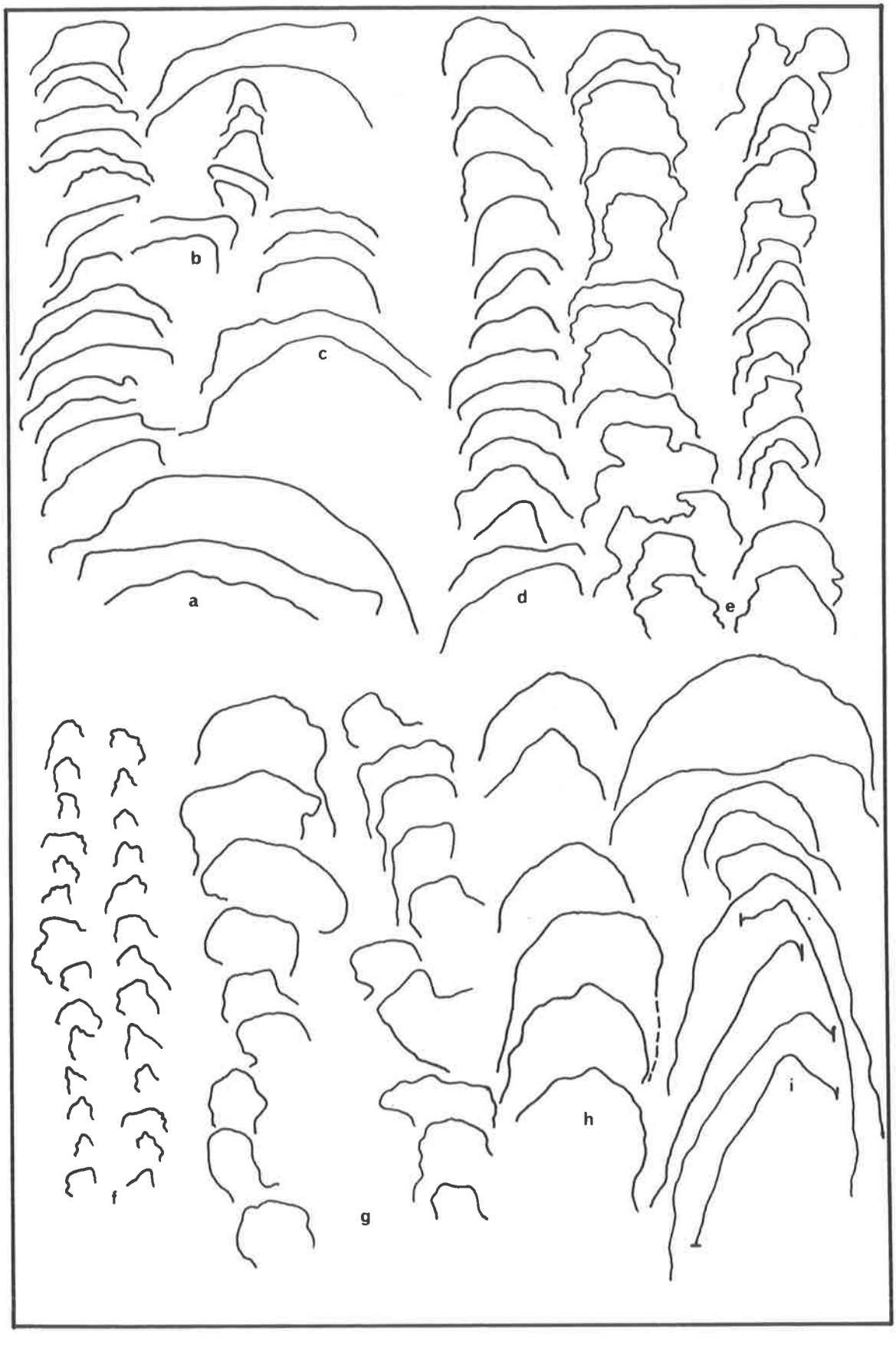
a
b
c
d
e
f
g
h
i

Figure 4

Lamina shapes; the laminae shown are representative selections and although their orientation is the same as originally they have been spatially rearranged.

a: Jurusania chewingsi.

b: Baicalia capricornia.

c: B. lacera.

d: M. mawsoni.

e: Anabaria divergens.

f: Kotuikania torulosa.

g: Tunqussia inna.

h: T. erecta (badly preserved).

The stromatolites represented here mostly have nonparallel branching. The relationship between lamina shapes and branching is discussed in the text (p.71-73).

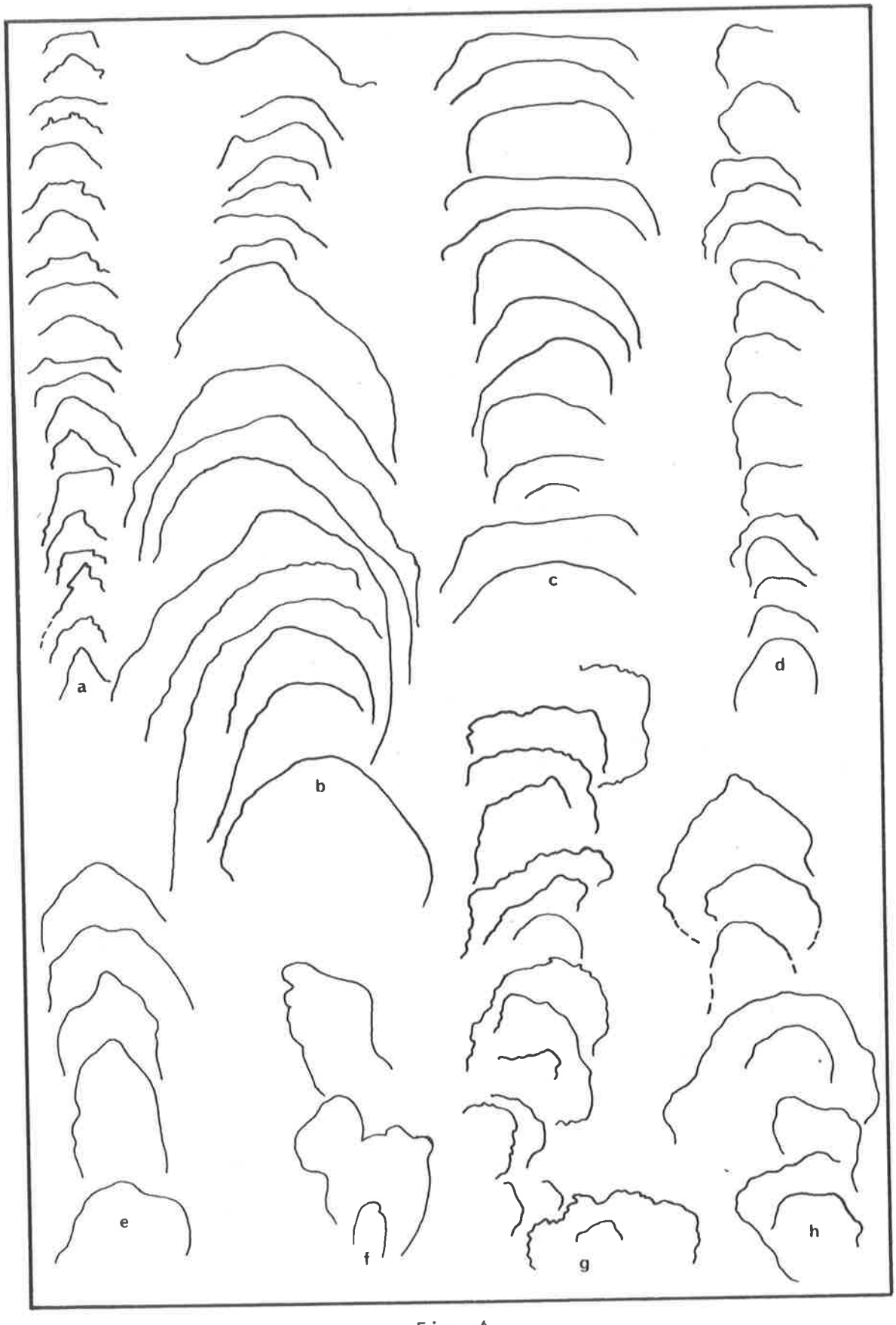

Fig. 4

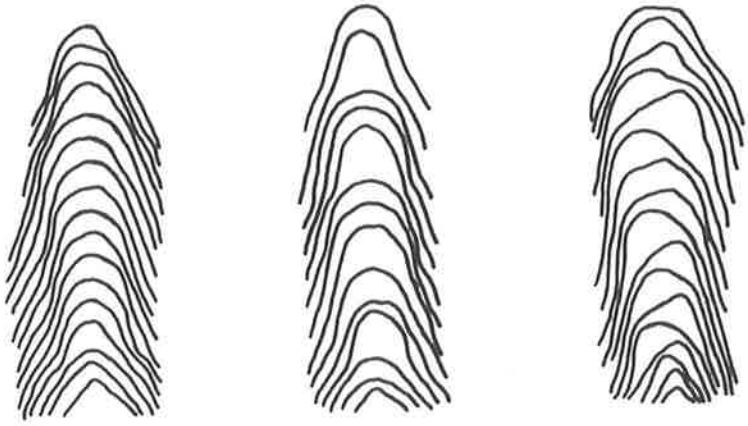

Fig. 5 Conophyton crestal zones (from Komar, Raaben & Semikhatov, 1965)

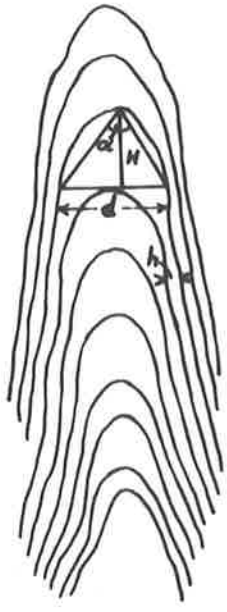

Fig. 6 The parameters used by Komar, Raaben & Semikhatov (1965) in the description of Conophyton crestal zones:

d = width of the crestal zone
H/h = coefficient of thickening
α = inscribed angle

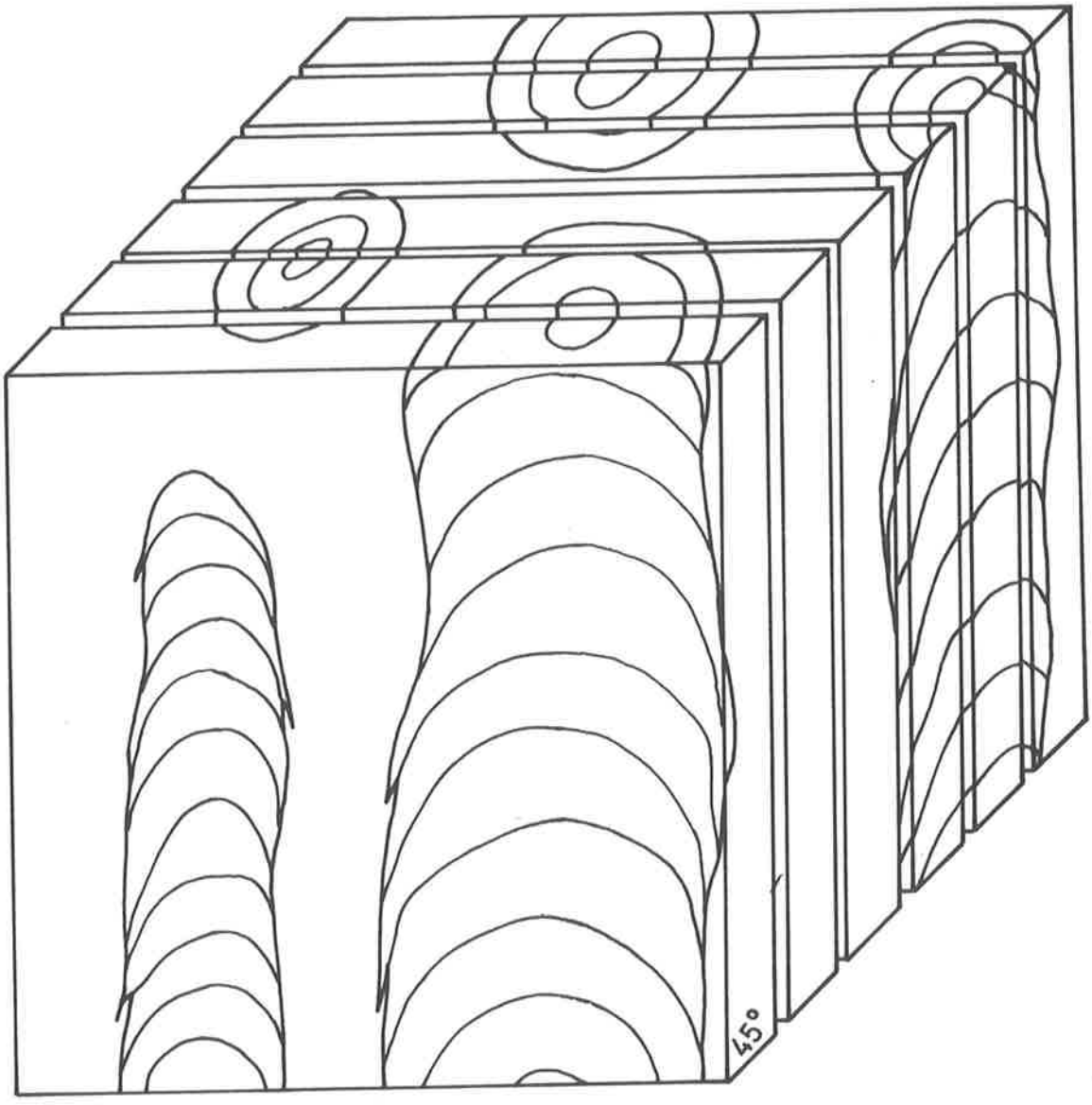

Fig. 7 Diagrammatic representation of a stromatolite specimen sectioned ready for reconstruction, with the sections arranged as in the final reconstruction (a 45° example).

OCCURRENCE

BRANCHING

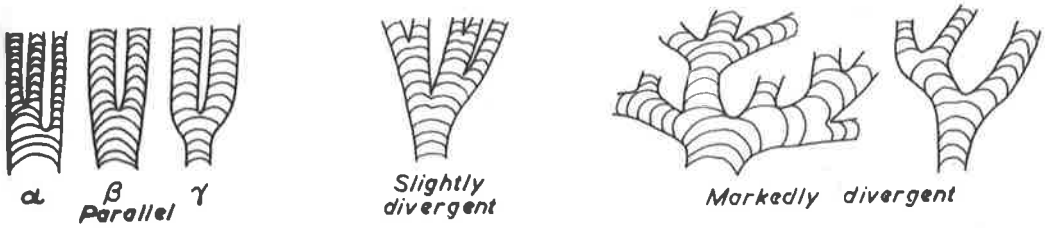

SHAPE OF COLUMNS AND MARGIN STRUCTURE

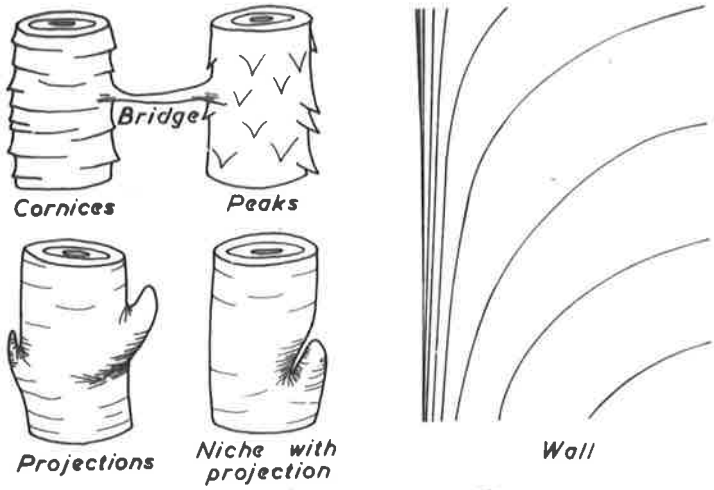

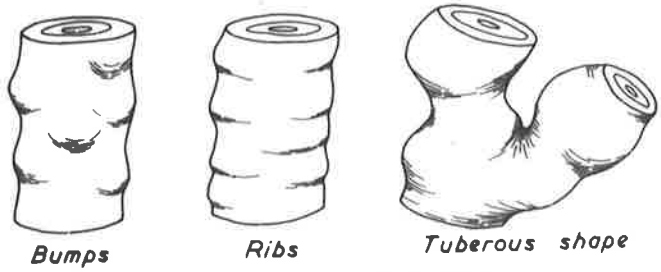

SHAPE OF LAMINAE

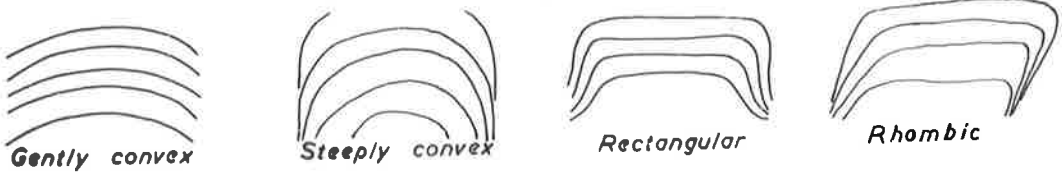

CUMULATE STROMATOLITES

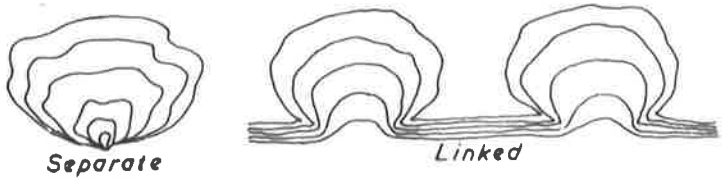

Figure 9

Conophyton garganicum australe, Irregully Formation, Irregully Creek, Nullagine Basin.

a,c: Columns in sections normal to bedding; a, from a field sketch; c, traced from a field photograph. Almost the whole of the column in c was eroded away before the next bed was deposited.

b,d,e: Reconstructions x $\frac{1}{2}$. The laminae shown on the transverse section in b were traced from the specimen. All R_1 (reliability index; see p.87).

Note In these and all subsequent reconstructions only selected laminae are traced onto the front faces. The laminae shown on transverse sections are diagrammatic, unless stated otherwise in the captions. All reconstructions are of the 45° type (p.86) unless otherwise specified.

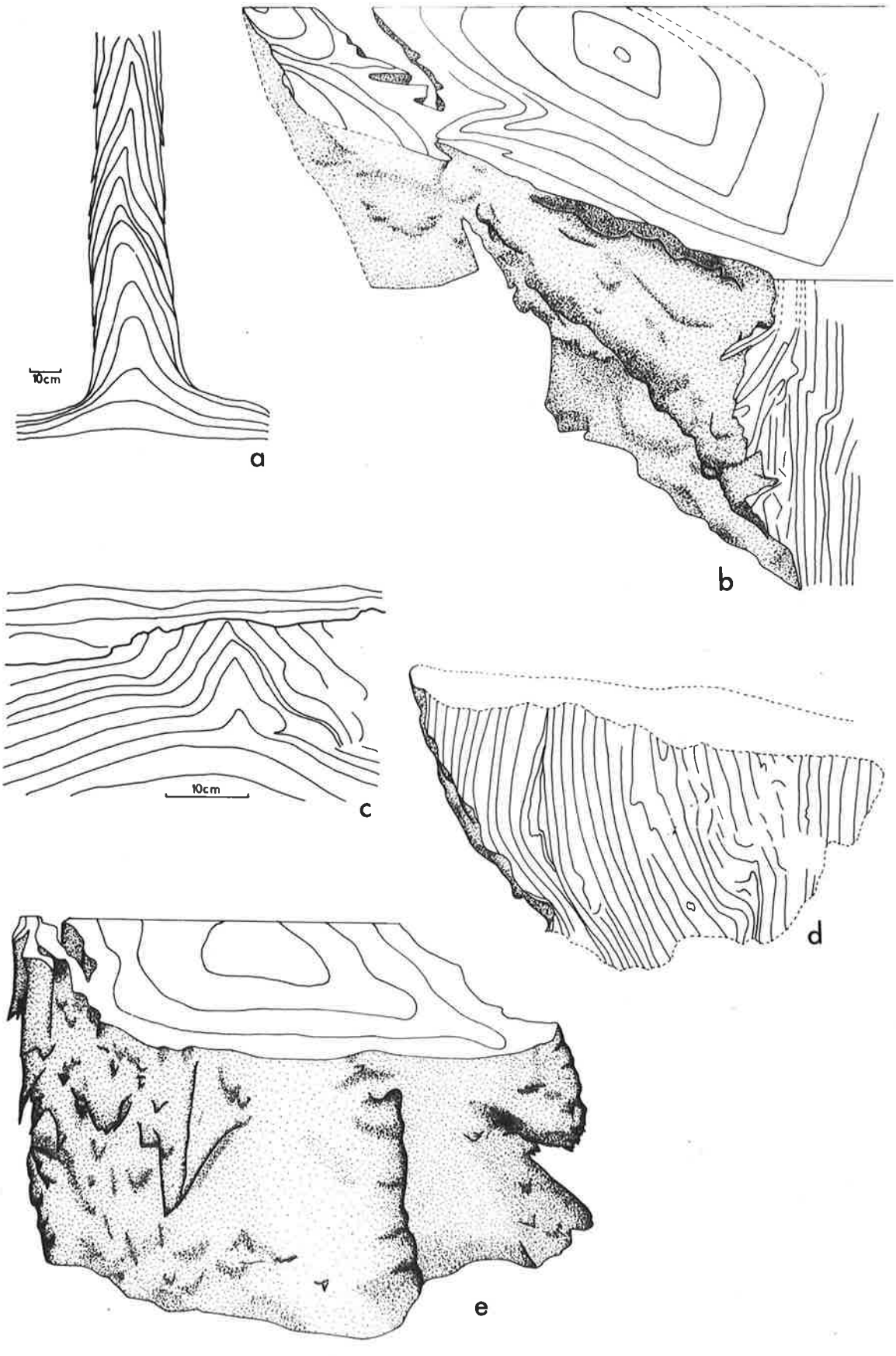
10cm
a
b
10cm
c
d
e

Figure 10

Conophyton garganicum australe statistics and comparisons; the measurements are from five specimens.

a: Frequency distribution of the ratio L_2/L_1 (thicknesses of dark laminae over those of contiguous pale laminae); class interval 0.6. On the overlay are graphs for the three other taxa in the *C. garganicum* subgroup for which statistics are available (from Komar, Raaben & Semikhatov, 1965).

b: Thicknesses of dark (L_2) laminae plotted against those of contiguous pale (L_1) laminae. Thicknesses in microns. Dots - laminae, crosses - macrolaminae. On the overlay this distribution is contoured; for the contouring the number of points within squares with sides of 5mm were counted.

c: Frequency distribution of the thicknesses of dark (L_2) and pale (L_1) laminae. Thickness in microns.

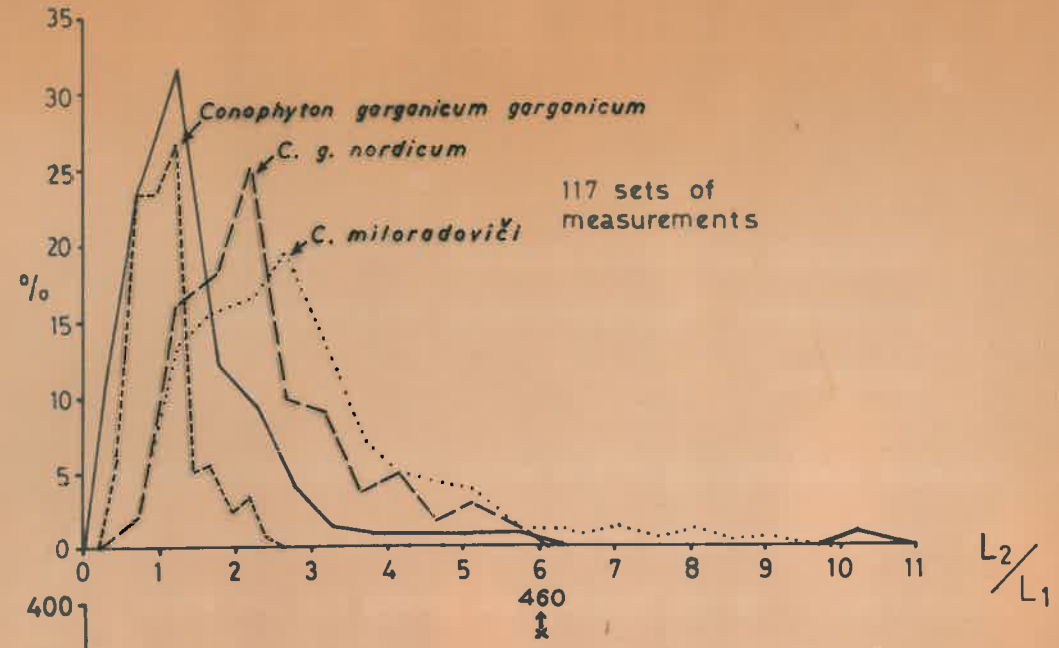
a
Conophyton gorganicum gorganicum
C. g. nordicum
C. miloradovici
117 sets of measurements
%
L2/L1
460

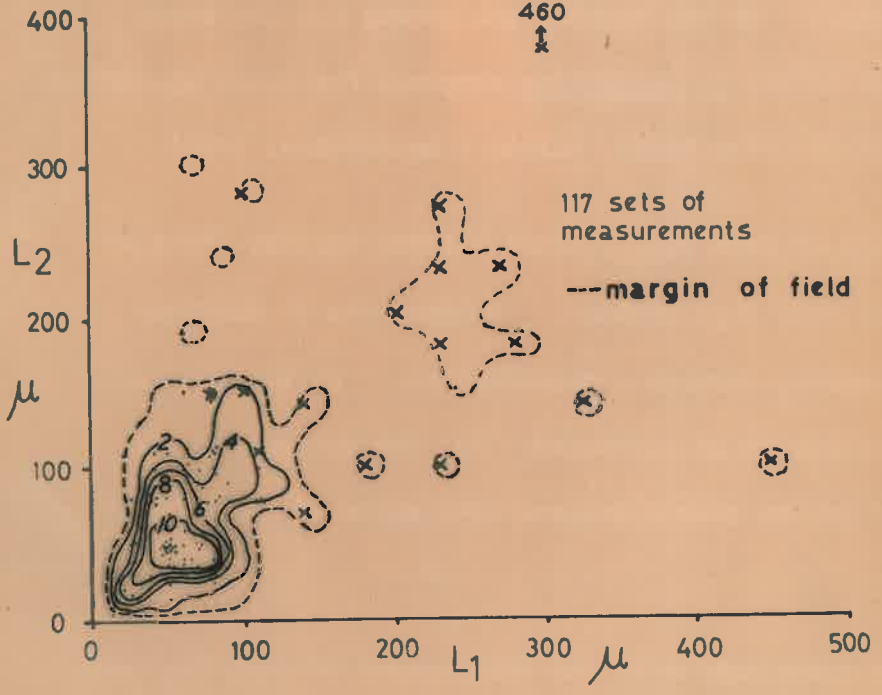
b
117 sets of measurements
---margin of field
L2
μ
L1
μ

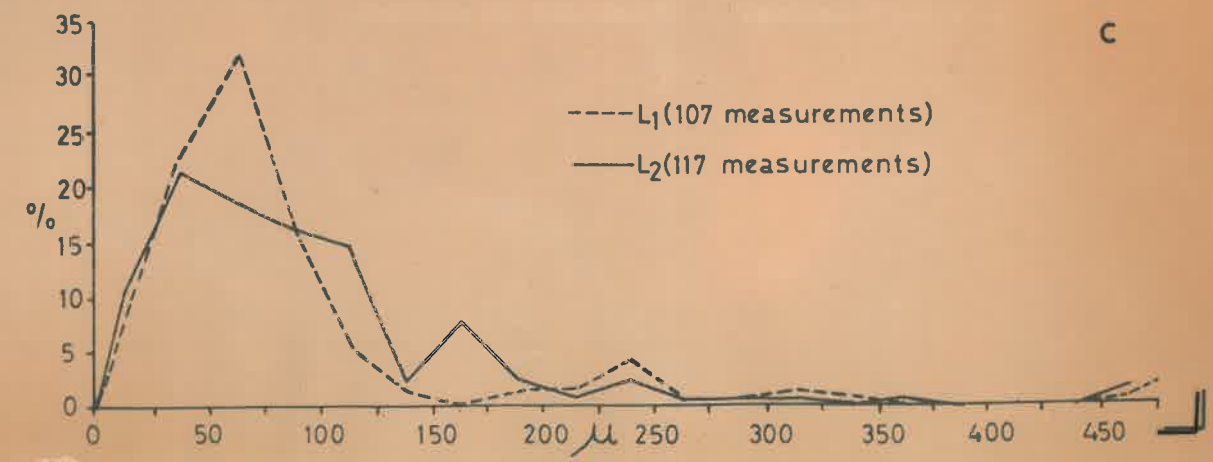
c
----L1(107 measurements)
——L2(117 measurements)
%
μ

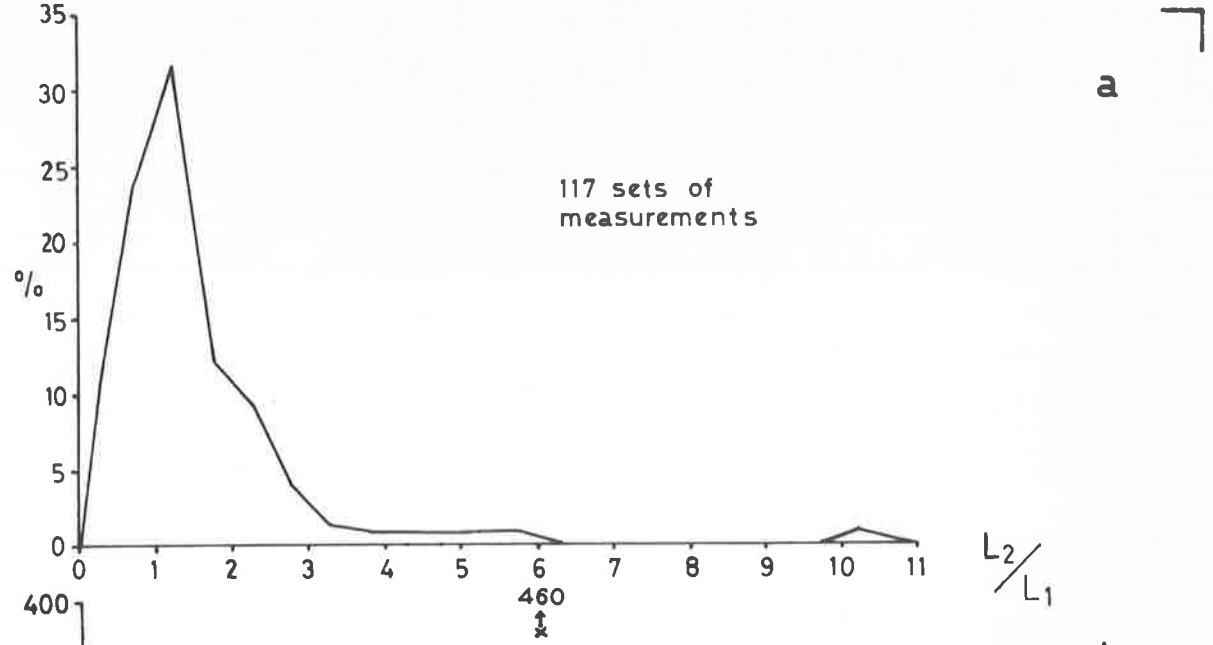
a
117 sets of measurements
%
L_2/L_1
460

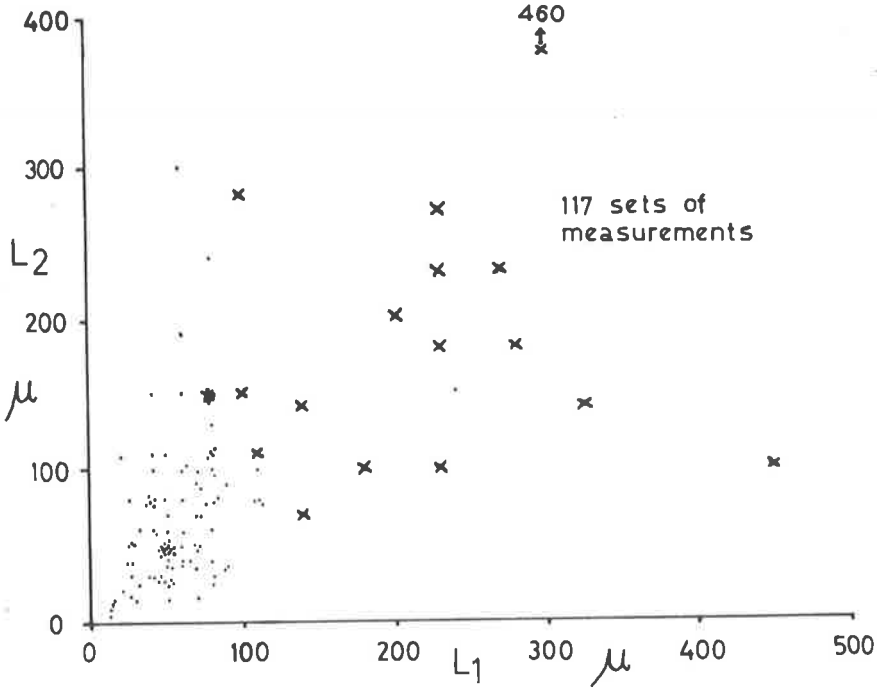
b
117 sets of measurements
L_2
μ
L_1
μ

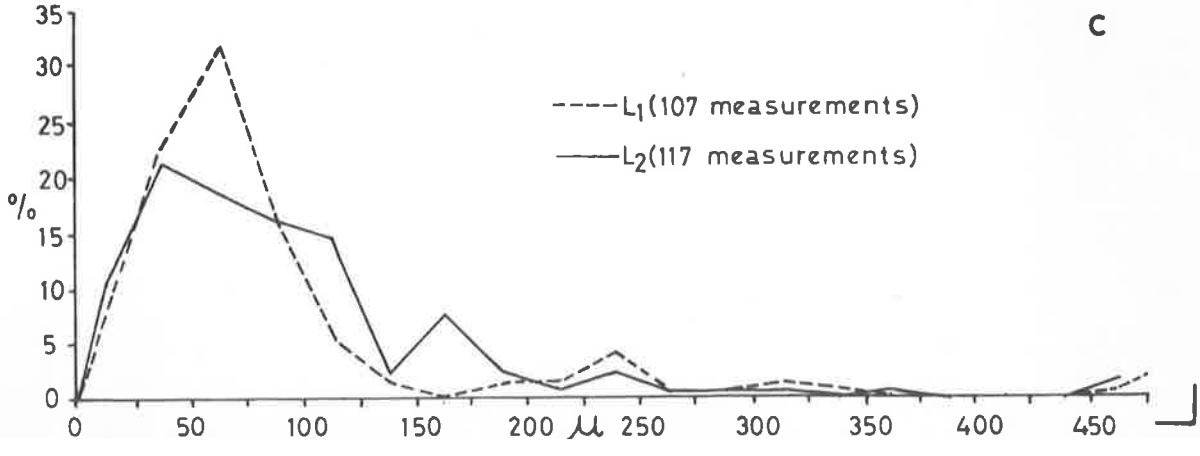
c
----L_1(107 measurements)
——L_2(117 measurements)
%
μ

Figure 11

Jacutophyton howchini, Mount Baldwin Formation, 5.5 miles southwest of Huckitta Homestead, Georgina Basin; x $\frac{1}{2}$. The columns b and c are from a small specimen and whether they are branches from another column is not known. a, CPC11316; b,c, CPC11317. All R_2.

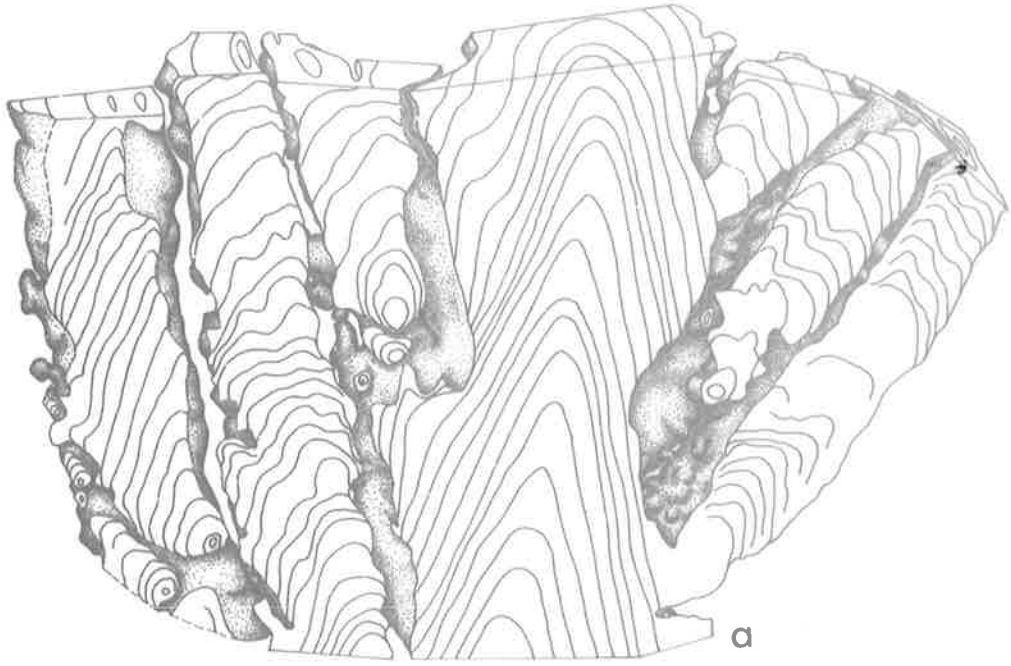
a

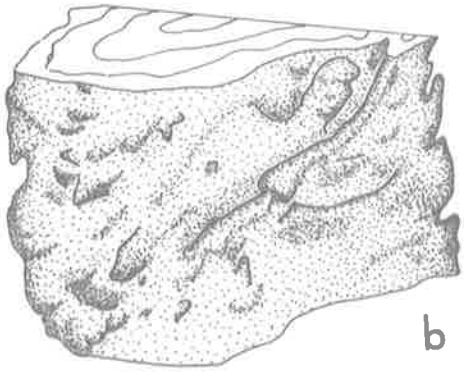
b

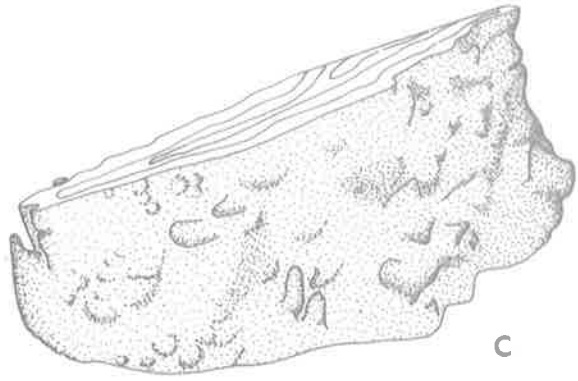
c

Figure 12

Acaciella australica mode of occurrence, Bitter Springs Formation; based on outcrops 2.3 miles WSW of Jay Creek, Amadeus Basin. The sections are perpendicular to bedding.

a: Showing contiguous hemispherical to tabular bioherms forming a domed biostrome. Diagrammatic, based on field observations, sketches and photographs.

b: Two contiguous bioherms, drawn from field photographs and sketches; that on the left is shown in plate 13d. In these particular cases the structure of the bioherm margins is poorly known but gently inclined columns often occur on bioherm margins where only queries are shown here.

c: Two contiguous bioherms, drawn from a field sketch; these are in the same biostrome as those in b. The rock between the bioherms is intraclastic limestone. Note the different form of the bioherm margins in b and c.

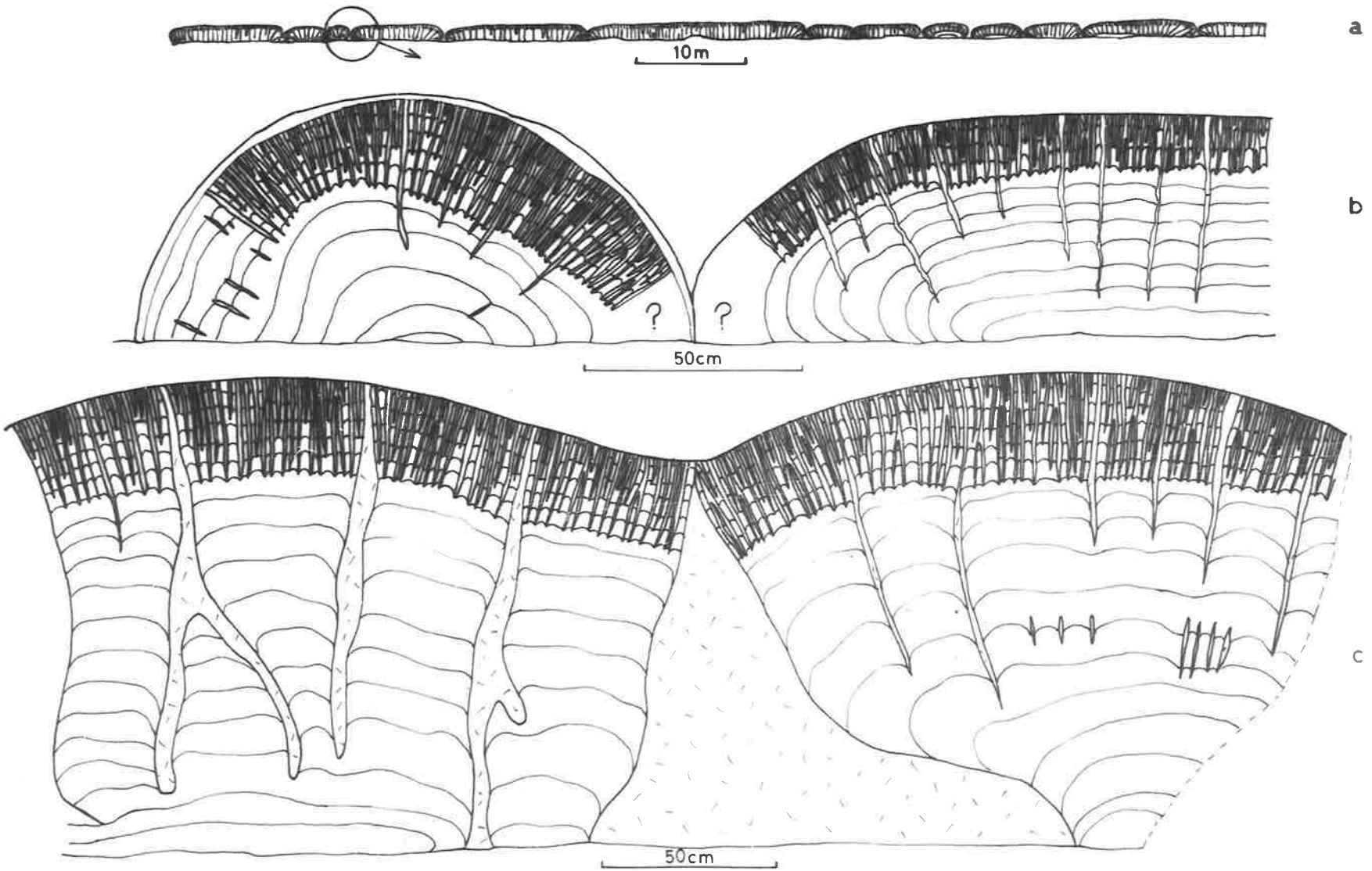
a
10m
b
?
?
50cm
c
50cm

Figure 13

Acaciella australica, Bitter Springs Formation, Katapata Gap, Amadeus Basin. Tracing of a slab cut normal to bedding but slightly oblique to the columns. The specimen (S345) is from the bioherm shown in plate 14c; the full width and height of the bioherm is not present in the specimen shown here. The stippled area represents a non-stromatolitic erosional mound.


10cm

Figure 14

Acaciella australica, Bitter Springs Formation, Amadeus Basin.

a,d,e: Katapata Gap; this is the same specimen as in figure 13. x ½ (S345).

b,c,g,i: 2.3 miles WSW of Jay Creek Settlement. x ½ (S131).

f: 2.3 miles WSW of Jay Creek Settlement. x 1 (S132).

h: 1/4 mile west of Acacia Well. x ½ (S91).

All R_1 except h, which is R_3.

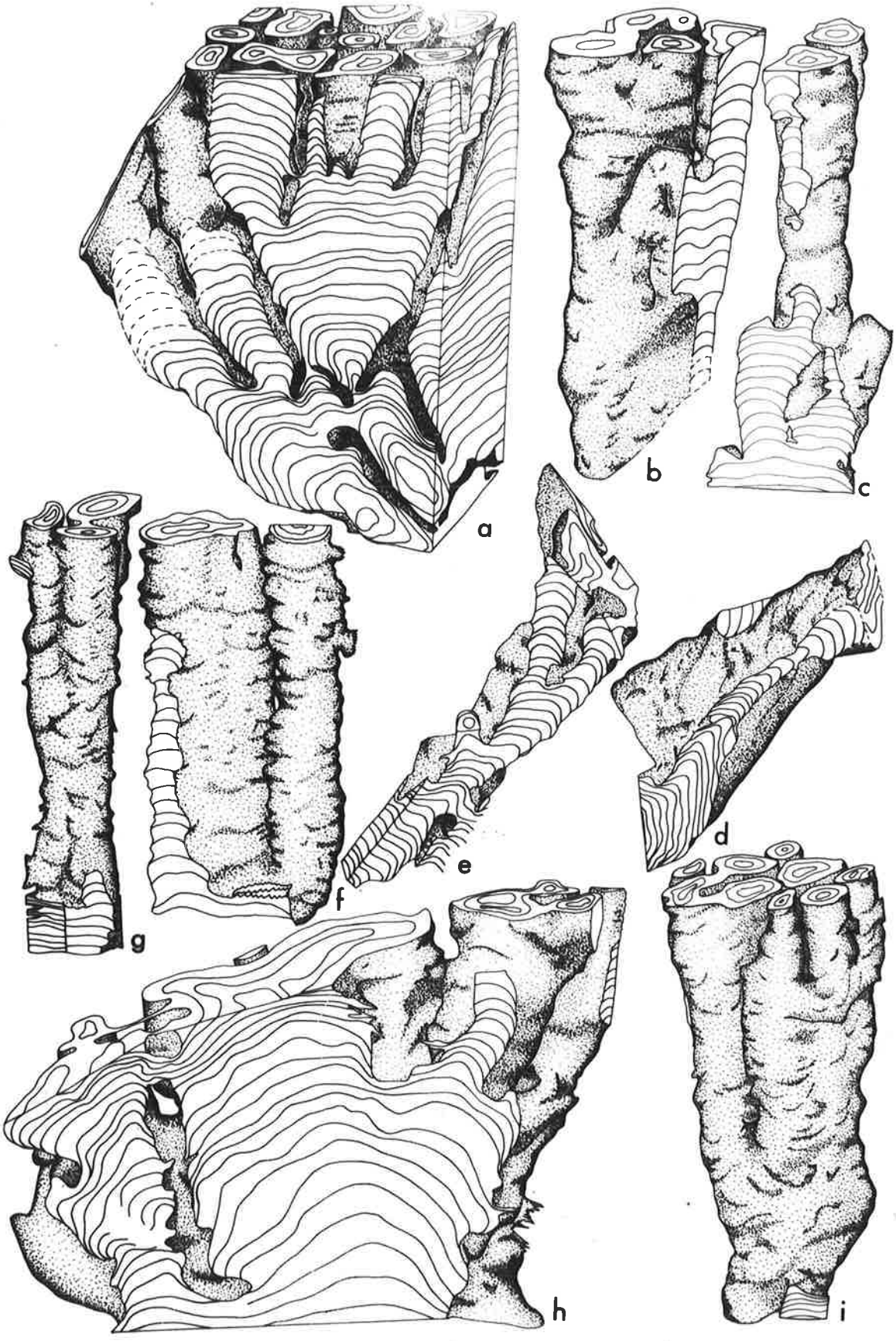
a
b
c
d
e
f
g
h
i

Figure 15

a-c: Acaciella australica, Bitter Springs Formation, 2.3 miles WSW of Jay Creek Aboriginal Settlement, Amadeus Basin. x ½ (S131). All R_1.

d-f: Alcheringa narrina, Pillingini Tuff, Mount Herbert, Nullagine Basin. x ½ (S95). d,e are R_2, f R_1.

g,h: Baicalia capricornia, Irregully Formation, 21 miles ESE of Maroonah Homestead, Nullagine Basin. x ½ (S200). R_2; h is a 60^0 reconstruction.

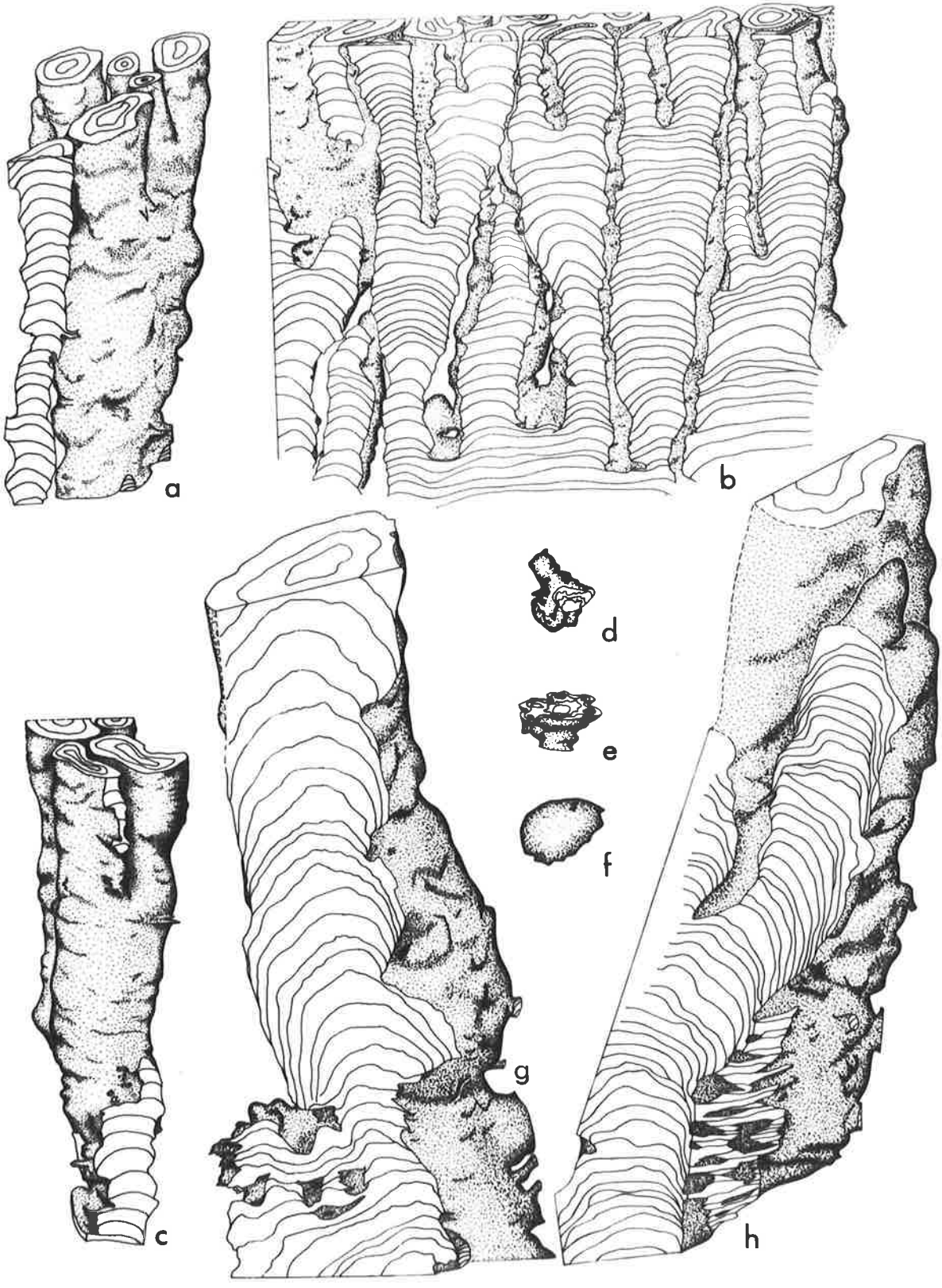
a
b
c
d
e
f
g
h

Figure 16

Baicalia capricornia, Nullagine Basin

a-d: Irregully Formation, 21 miles ESE of Maroonah Homestead. x ½ (S200). R_2. d is a 60° reconstruction of part of the column in c, drawn to show the constriction and projection about one third of the way up the column.

e: From a breccia in the Devil Creek Formation, 20 miles NNE of Coodardoo Gap. x ½ (S195). R_2.

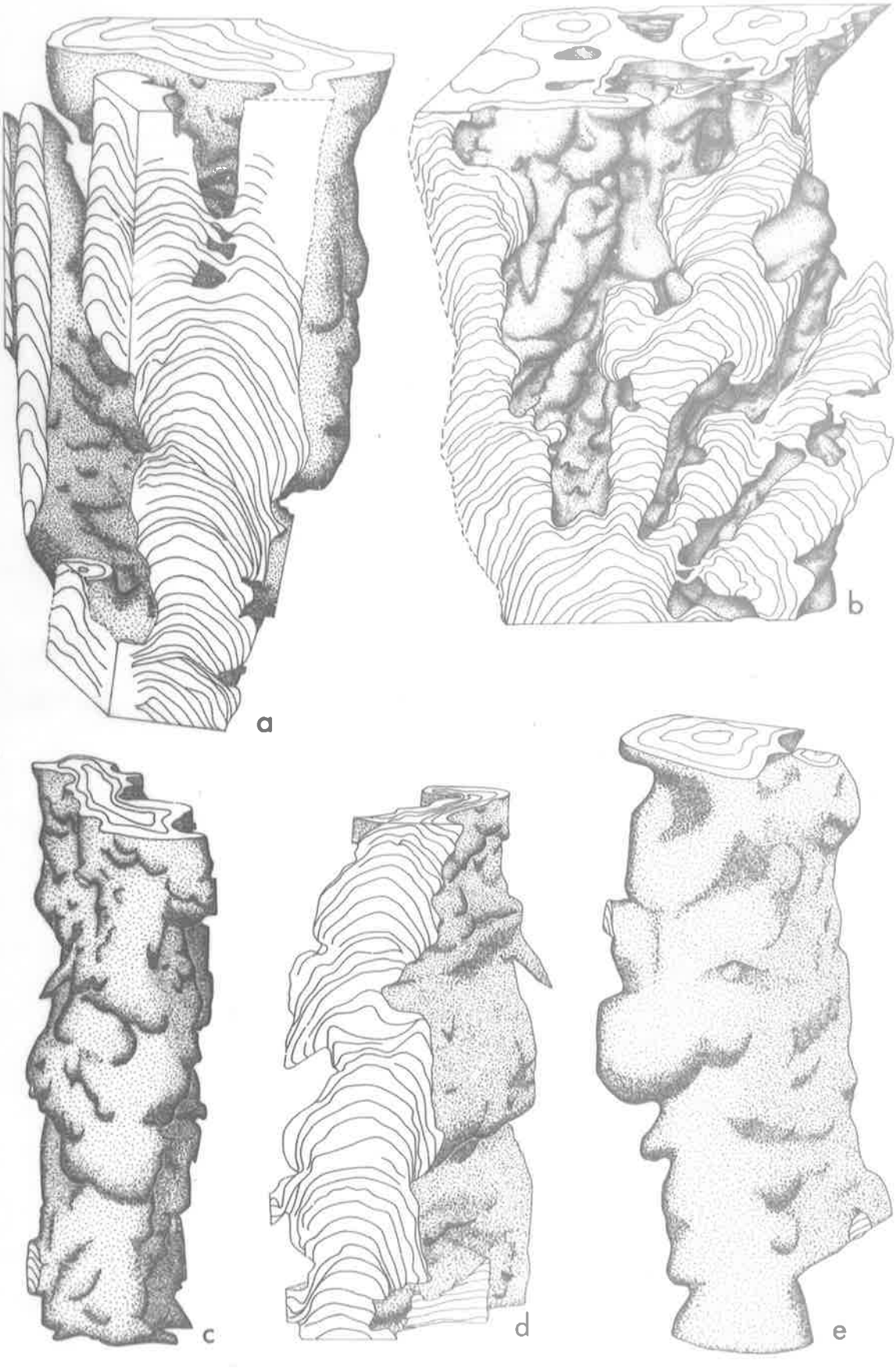
a
b
c
d
e

Figure 17

Baicalia capricornia, Nullagine Basin

a-c: From a breccia in the Devil Creek Formation, 20 miles NNE of Coodardoo Gap. × ½; a,b (S195), c (S194). R_2.

d: Irregully Formation, 21 miles ESE of Maroonah Homestead. From the uppermost part of a biostrome. × ½ (S197). R_3.

e: Locality as for d. Longitudinal section of the same columns shown in figure 16a-d. × 1/3 (S200).

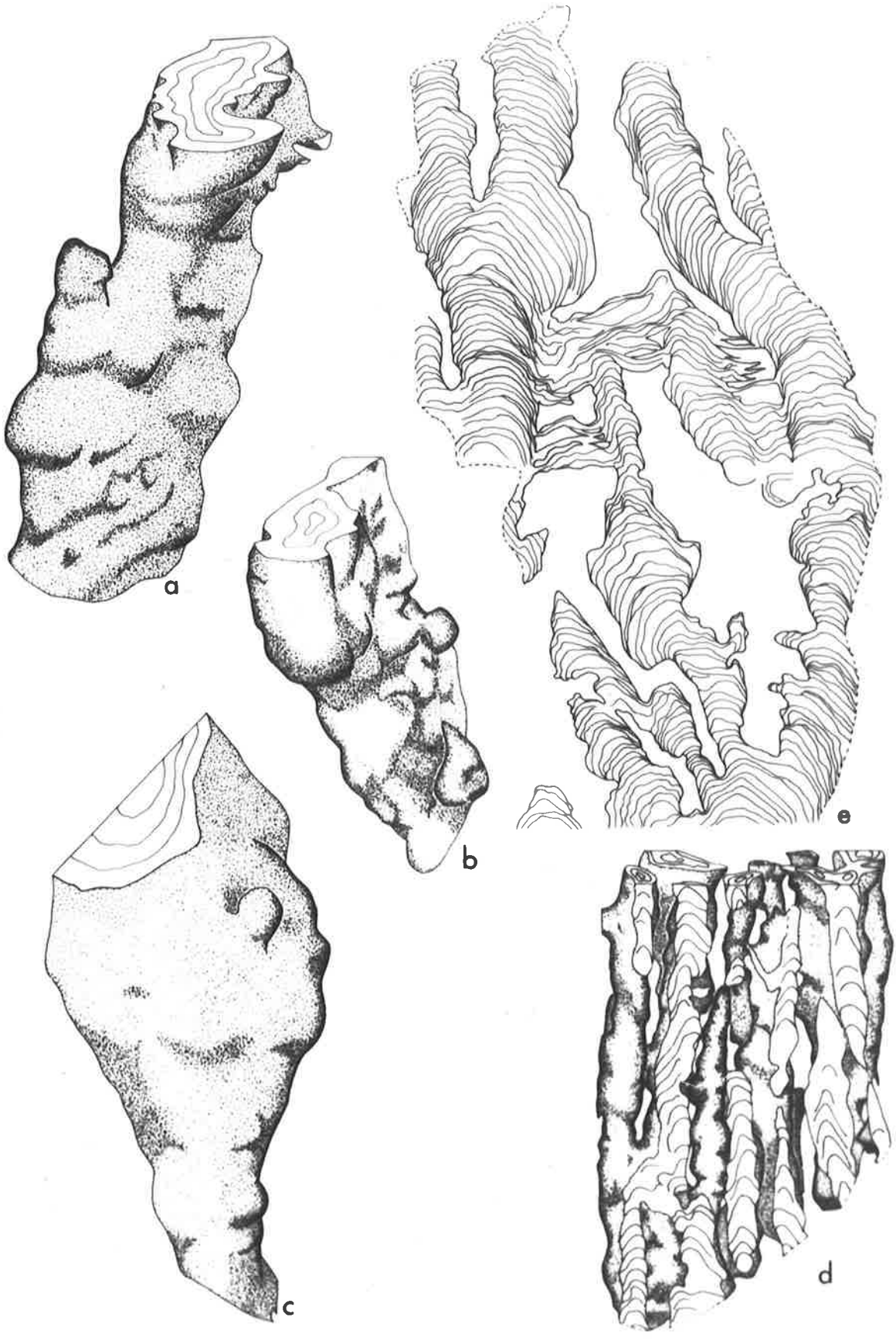
a
b
c
d
e

Figure 18

Basisphaera irregularis, Bitter Springs Formation, 2.3 miles WSW of Jay Creek Aboriginal Settlement, Amadeus Basin.

a: Diagrammatic representation of the mode of occurrence. Based on field sketches and photographs.

b: Tracing of a longitudinal section of the narrow columns. x ½ (S346).

c-f: c is from a specimen of the broad to narrow columns branching zone. In d the letter s indicates a stylolite. x ½; c (S351); d,f (S346); e (S136). R_2.

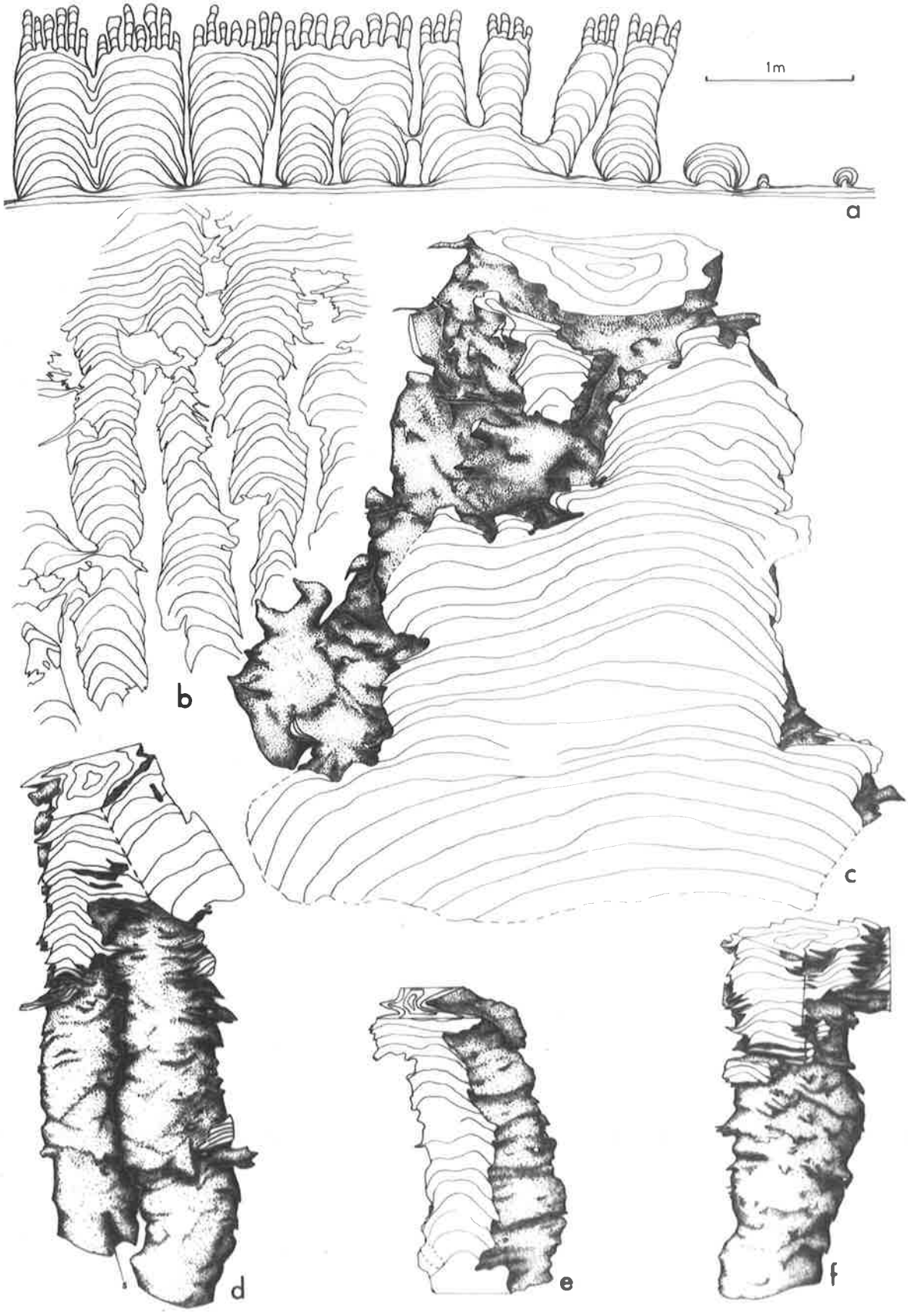
1m
a
b
c
d
e
f

Figure 19

Boxonia pertaknurra, Bitter Springs Formation, Amadeus Basin.

a-d: 2.3 miles WSW of Jay Creek Aboriginal Settlement. a and b are from the base of a bidstrome; note the absence of broad, basal columns in b. c is an excellent example of α parallel branching. x $\frac{1}{2}$; a (S354); b,c,d (S350). R_1.

e-g: 1 mile NNW of Ross River Tourist Camp. x $\frac{1}{2}$ (S391). R_3.

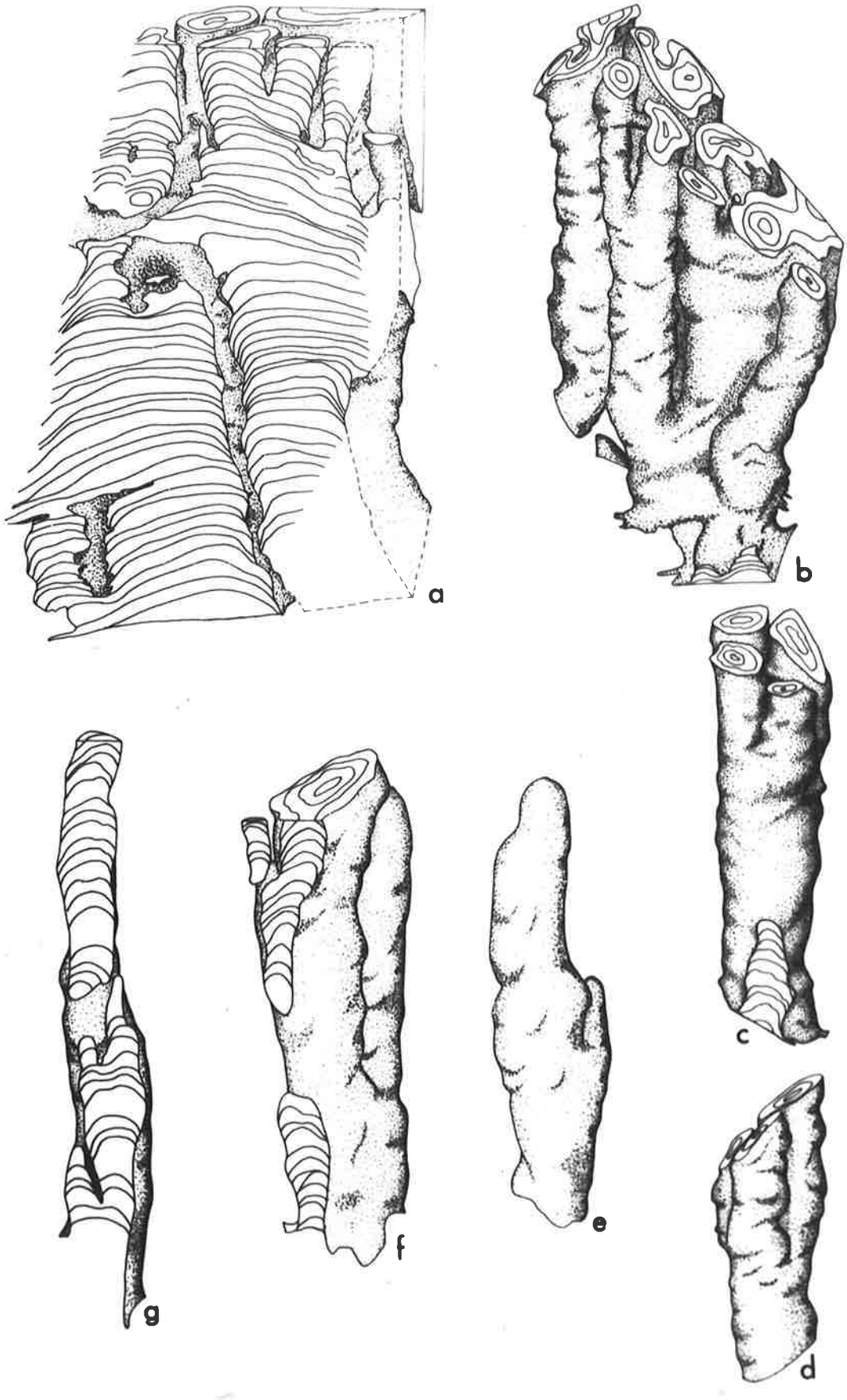
a
b
c
d
e
f
g

Figure 20

Inzeria intia mode of occurrence. Diagram based on occurrences such as that in plate 20e, showing one bioherm from within a biostrome 1 mile NNW of Ross River Tourist Camp; Bitter Springs Formation, Amadeus Basin. Stage I is frequently more complex than shown here (see plate 21d,e).

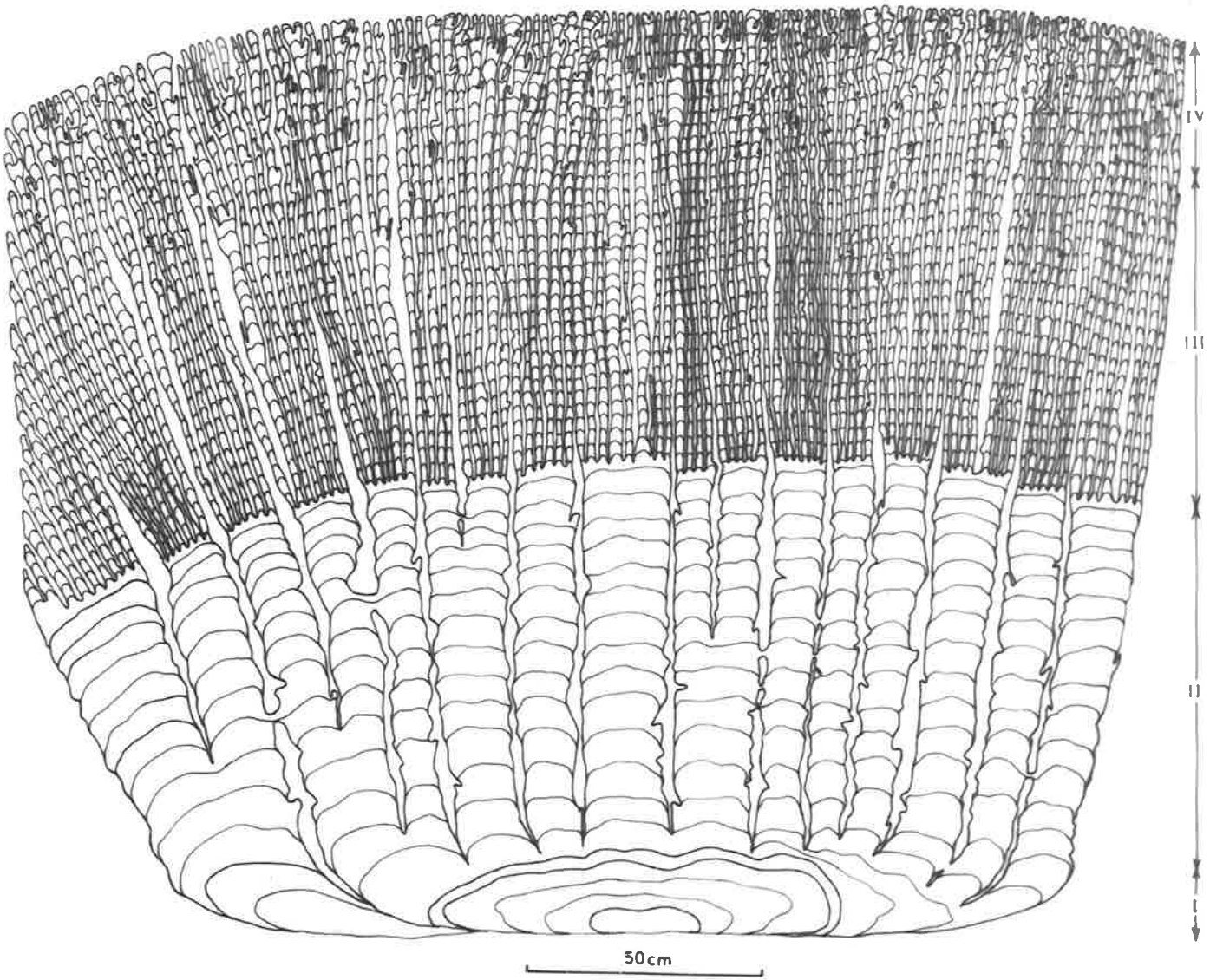
IV
III
II
I
50cm

Figure 21

Inzeria intia, Bitter Springs Formation, Amadeus Basin.

a-c,f-h: 1 mile NNW of Ross River Tourist Camp.

d-e: 1 mile N of Ross River Tourist Camp.

a,c-e,g,h: Stage II. a and c occurred separately but the others are from the complex biostrome.

b,f: Stage I. b is a tracing of a section normal to bedding. Note the niches. Both are from the complex biostrome.

a-h: x ½; a (S138); b,f (S142); c (S369); d,e (S94); g,h (S372). All R_1.

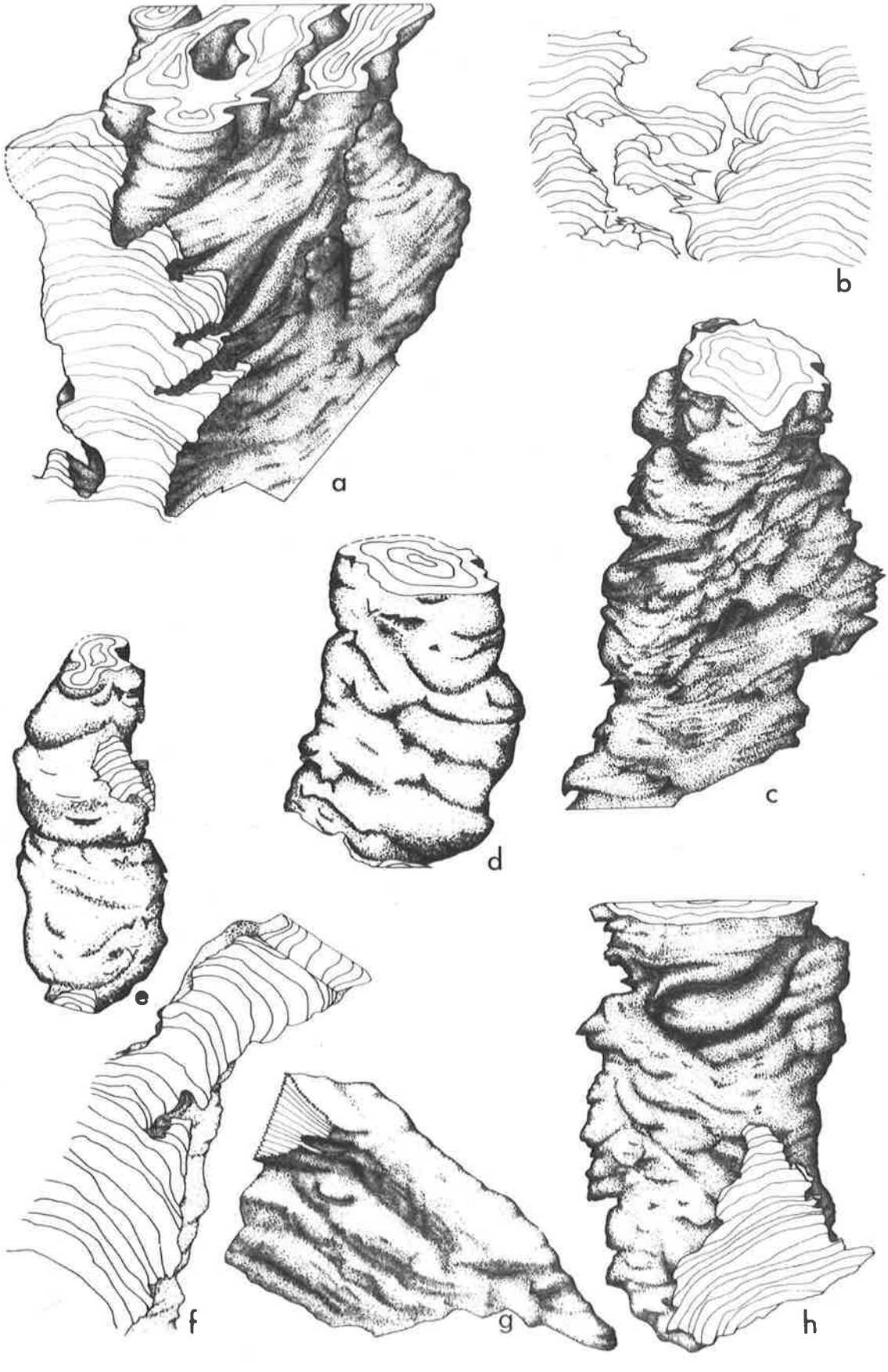
a
b
c
d
e
f
g
h

Figure 22

Inzeria intia, Bitter Springs Formation,
1 mile NNW of Ross River Tourist Camp,
Amadeus Basin.

a: Stage II specimen from a simple biostrome lacking other stages. x ½ (S369). R_1.

b: Stage IV; tracing of a longitudinal section. x 1/3 (S371).

c,i,j,k: Stage IV. x ½; c,k (S370), R_1; i,j (S371), R_2.

d,e: Stage III. No well formed niches are present in these examples but they do occur in stage III columns (see plate 22b). x ½ (S143).

f-h: Base of stage III. The branching zone from stage II to stage III columns is shown in f. The columns in g and h are from near a bioherm margin; the arrows indicate original vertical. x ½; f (S141); g,h (S379).

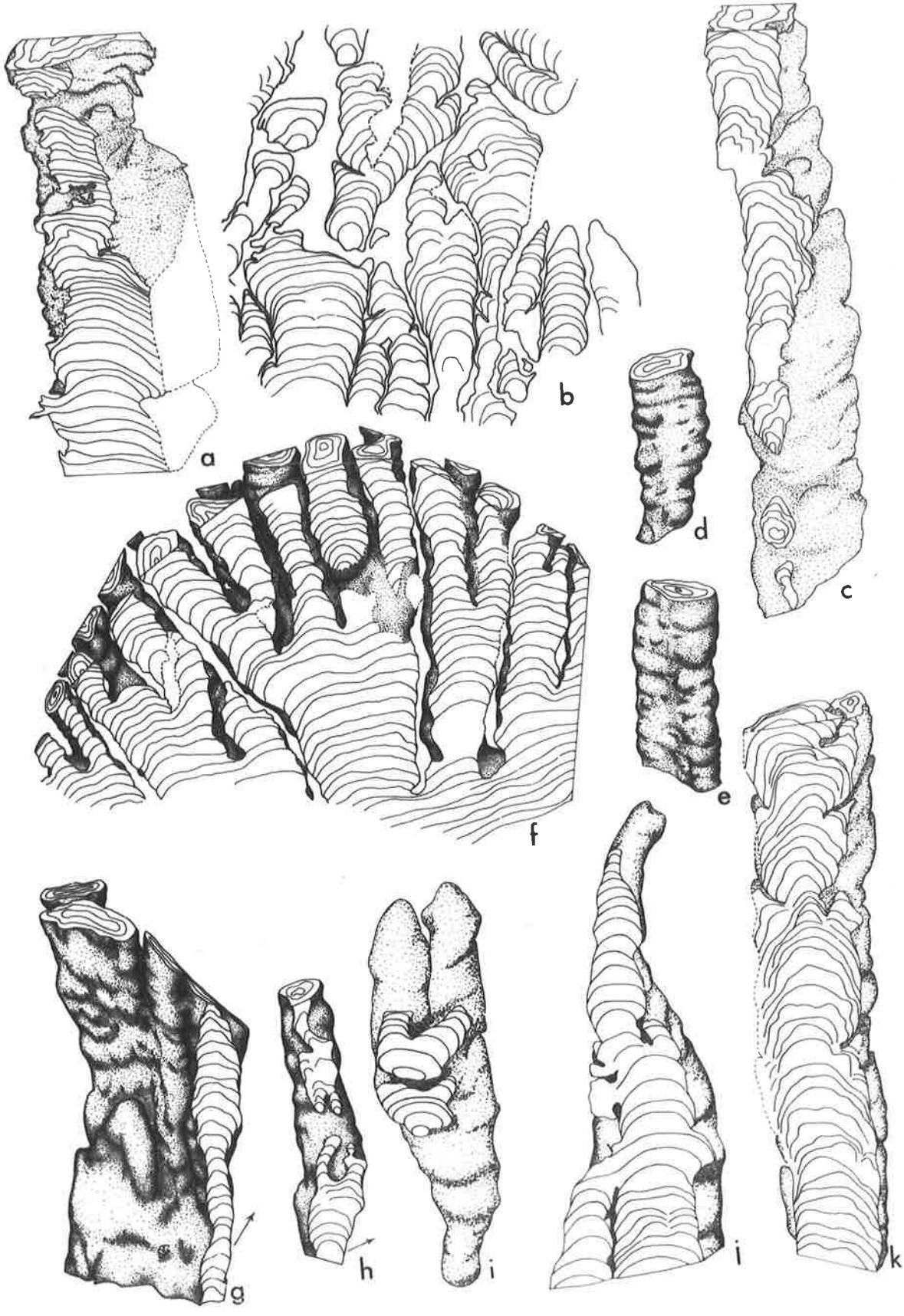
a
b
c
d
e
f
g
h
i
j
k

Figure 23

Jurusania chewingsi, Bitter Springs Formation, 2.3 miles WSW of Jay Creek Aboriginal Settlement, Amadeus Basin.

a,b: × ½ (S352). R_1. Arrow in a indicates original vertical.

c-f: × ½ (S134). R_1.

g: Mode of occurrence. Diagram based on field photographs and sketches and on laboratory examination of specimens. The bioherm on the left is that in plates 24a and 31a. The details are diagrammatic.

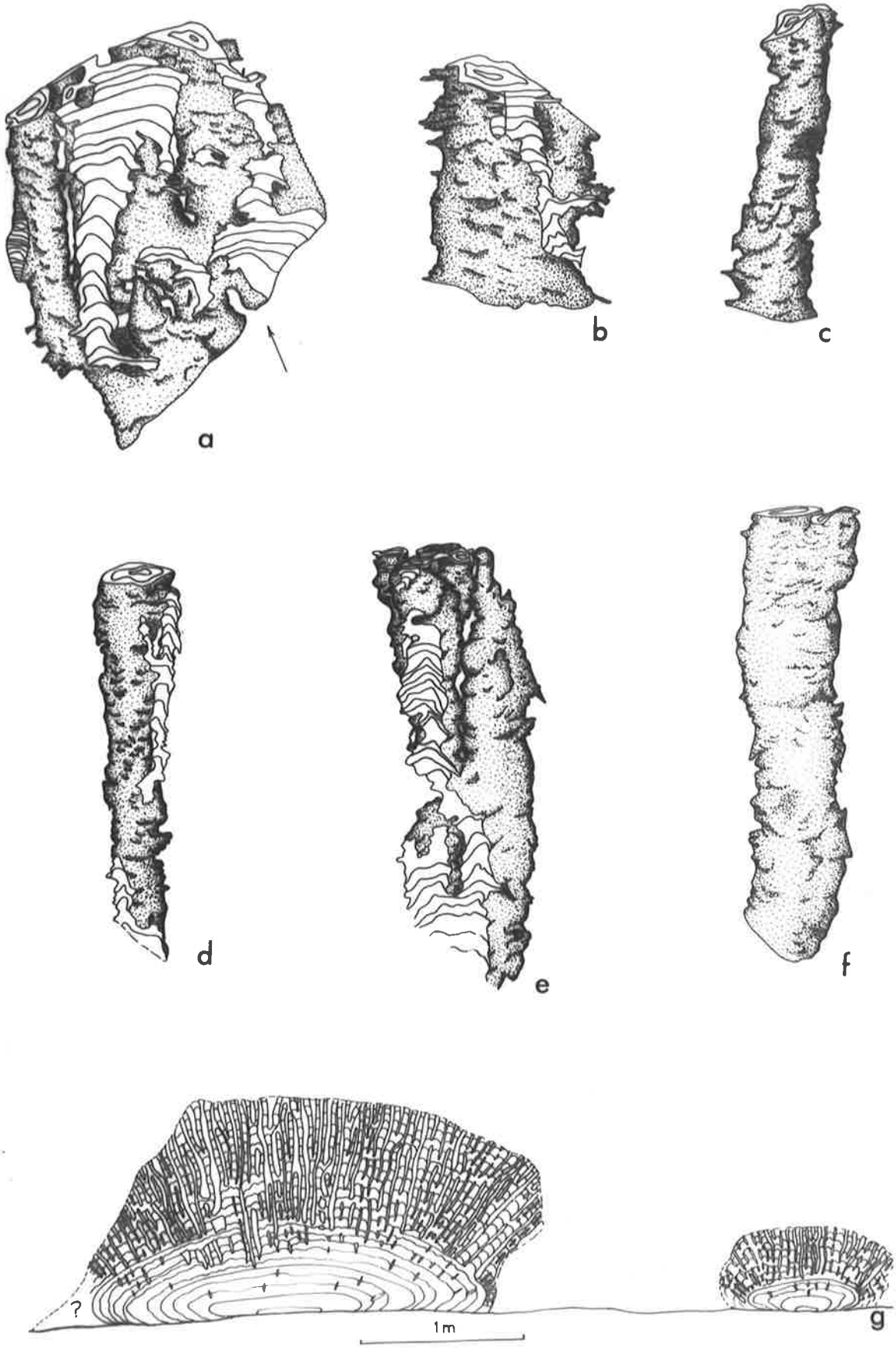
a
b
c
d
e
f
?
1m
g

Figure 24

Columnar stromatolites, Bitter Springs Formation, 2.3 miles WSW of Jay Creek Aboriginal Settlement, Amadeus Basin.

a-f: *Kulparia alicia*. × ½ (S347). R_1.

g: Possible *K. alicia* (see plate 25c). × 1 (S349). R_2.

h-k: *Linella avis*; j is from the base of a biostrome, the others from above the base. All are from the same biostrome shown in plate 26. × ½; h,i (S127); j (S377); k (S375). R_1.

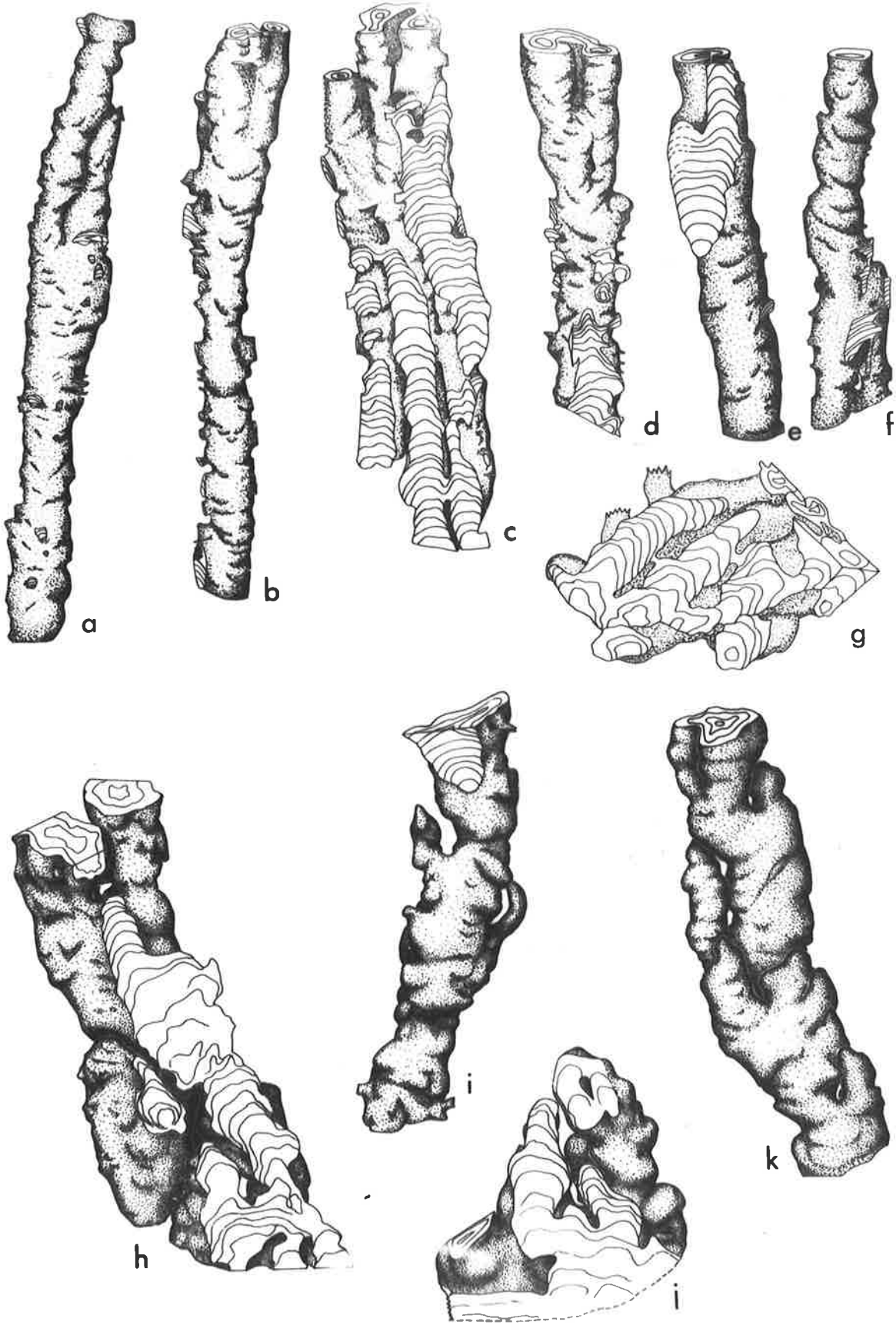
a
b
c
d
e
f
g
h
i
i
k

Figure 25

a-d: Madiganites mawsoni, Pertaoorta Group, Amadeus Basin. x ½. R_2.

a,d: Possibly Jay Creek Limestone, Jay Creek (collected by Dr C. T. Madigan). S46.

b: Shannon Formation, several miles south of the Ross River Tourist Camp. S146.

c: Jay Creek Limestone, near the junction of the Glen Helen and Hermannsburg roads (Jay Creek). Arbitrary top at a lamina. S364.

e,f: Minjaria pontifera, Bitter Springs Formation, 2.3 miles WSW of Jay Creek Aboriginal Settlement, Amadeus Basin. x ½ (S374). R_2.

g-k: Patomia f. indet., Duck Creek Dolomite, 26 miles ENE of Mount Breshnehan, Nullagine Basin. The reconstruction in k has a cut back. x ½ (GSWA A7155). R_3.

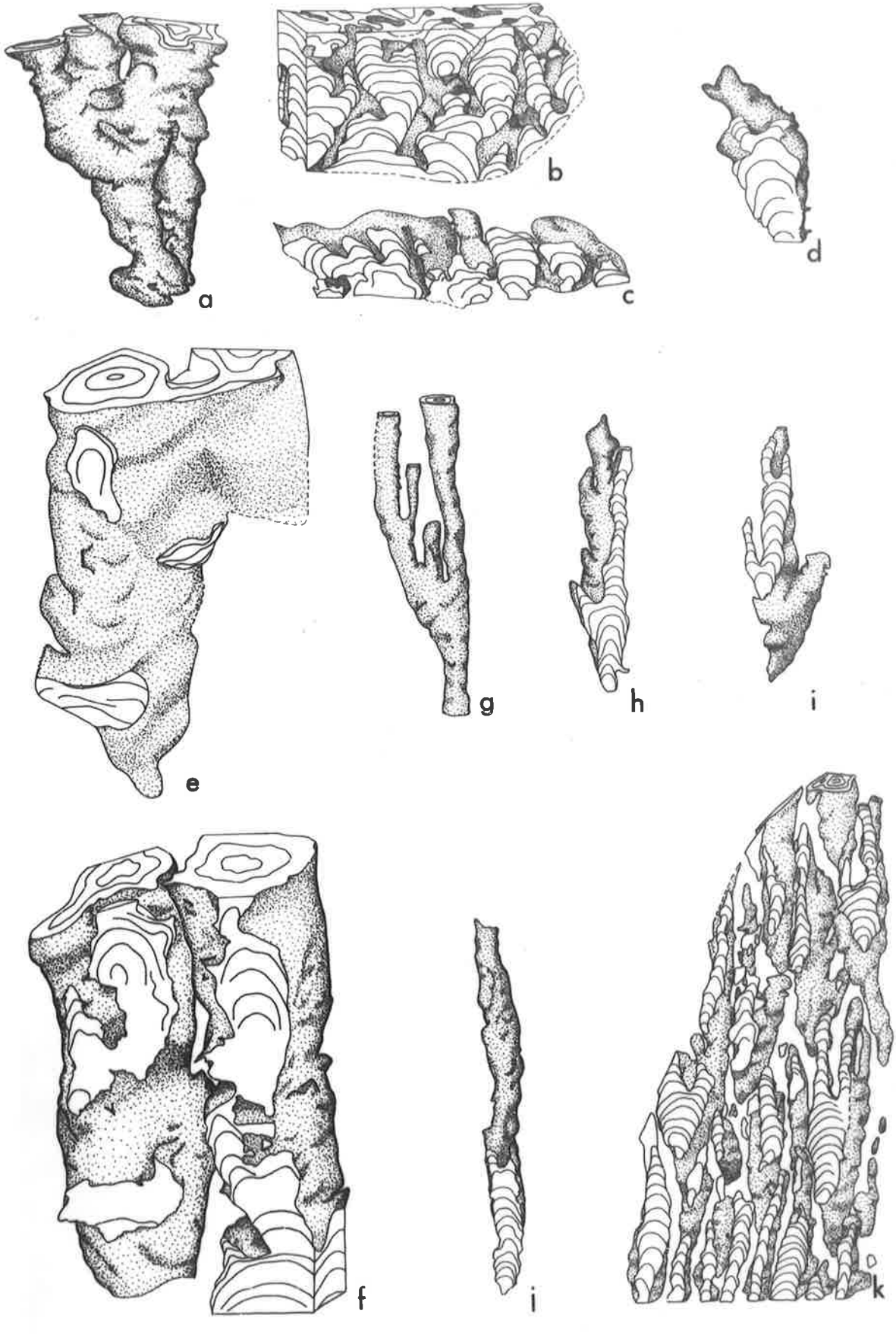
a
b
c
d
e
g
h
i
f
j
k

Figure 26

Minjaria pontifera field occurrence, Bitter Springs Formation, 2.3 miles WSW of the Jay Creek Aboriginal Settlement, Amadeus Basin. Column outlines traced from a field photograph; laminae diagrammatic. Gaps are left where no detail is visible in the photograph. The section is normal to bedding; the base of the biostrome (the same biostrome as shown in plates 26 and 28f) is marked by the dashed line; on the left there is a mound in the substrate.

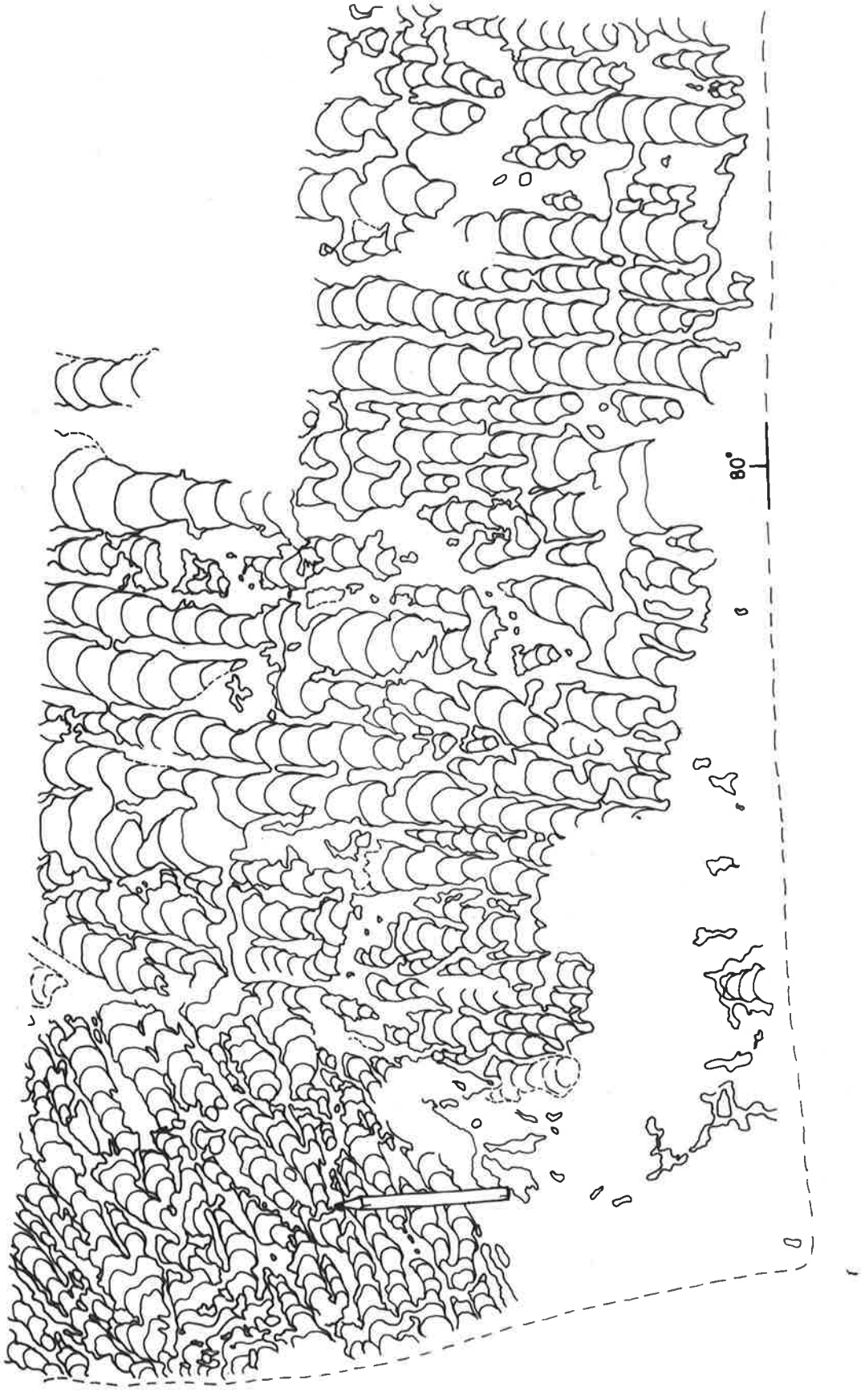
80°

Figure 27

Pilbaria perplexa, Duck Creek Dolomite, 20 miles east along the track from Mount Stuart Homestead, Nullagine Basin. x 1/3; a (S205); b,d (S201); c,e-g (S206). R_1.

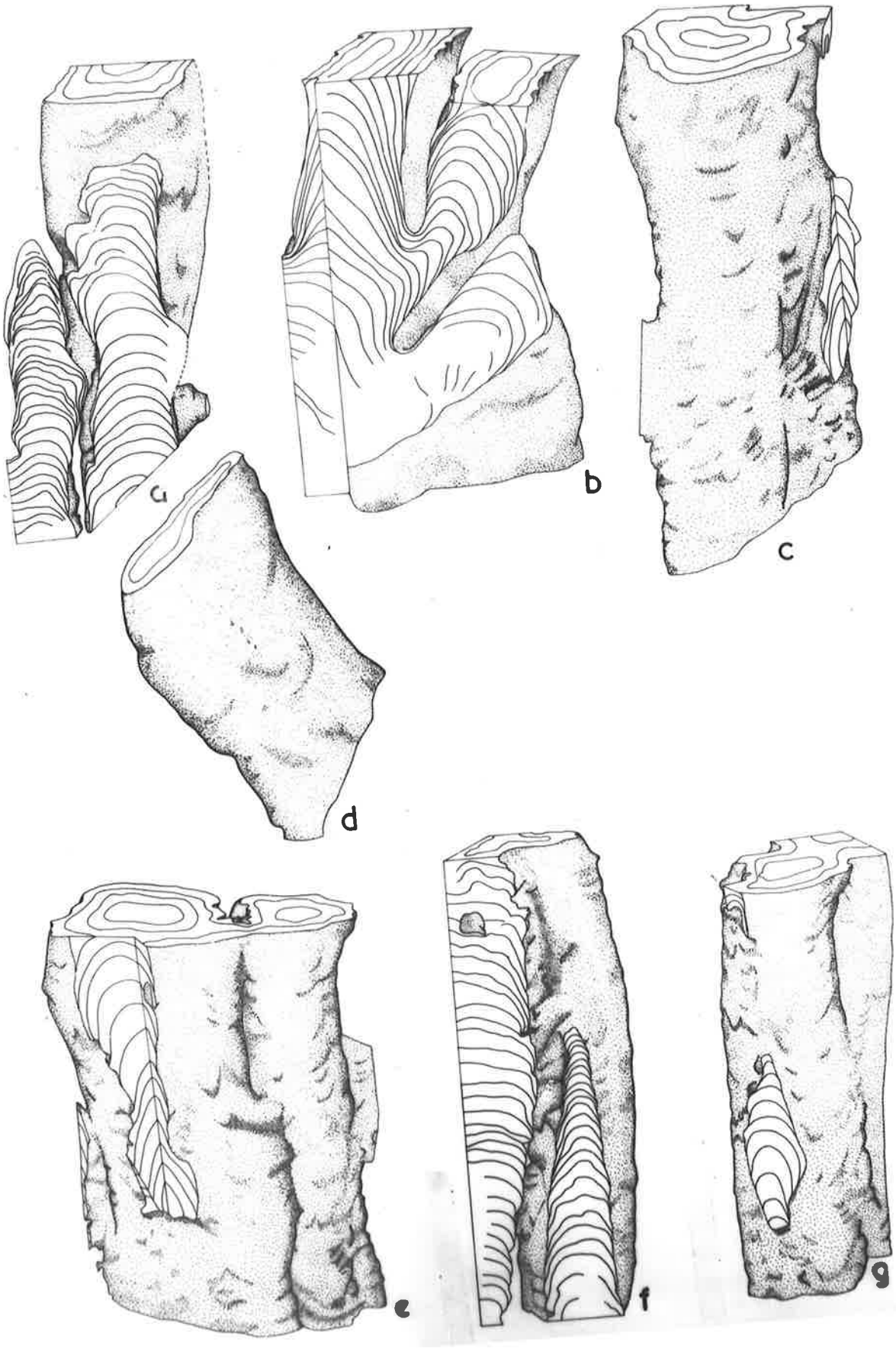
a
b
c
d
e
f
g

Figure 28

Tungussia erecta, Gillen Member of the Bitter Springs Formation, 3 miles SW of Alice Springs, Amadeus Basin. × ½. R_2.

a,d: From the upper part of the biostrome (S357).

b,c: From the lower part of the biostrome (S356). b is a tracing from a thin section cut normal to bedding. The section at the front of c is parallel to but not the same as that in b.

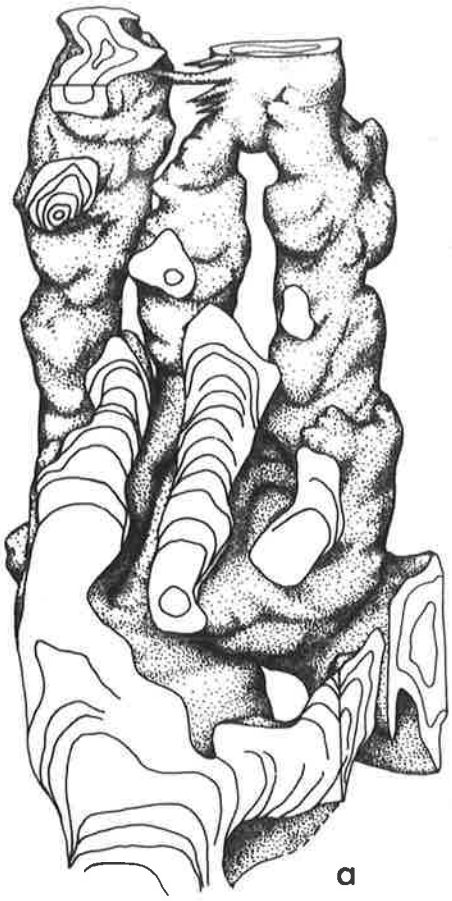

a

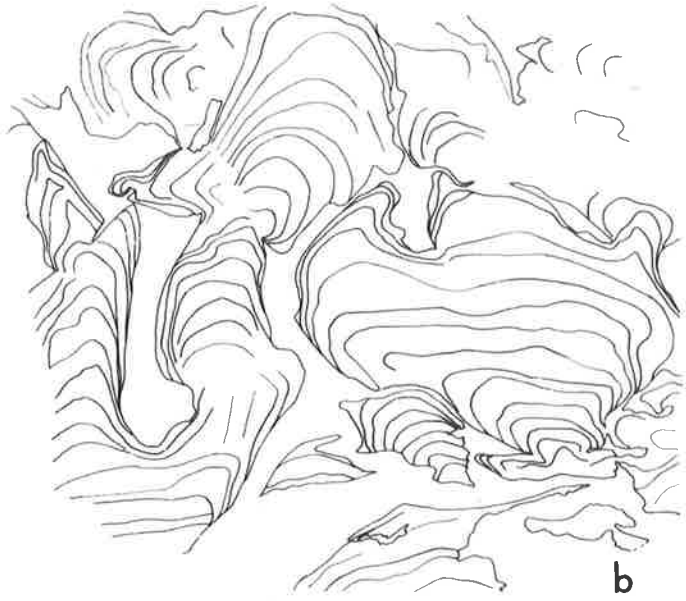

b

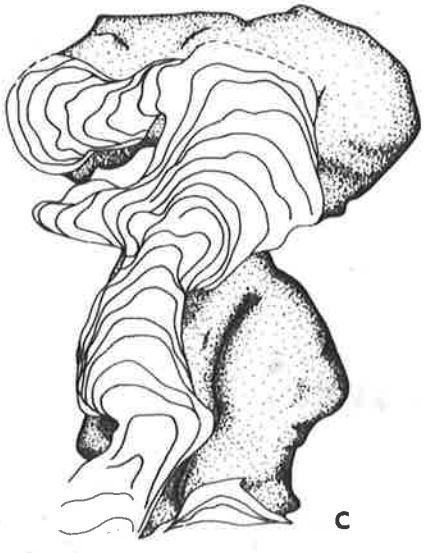

c

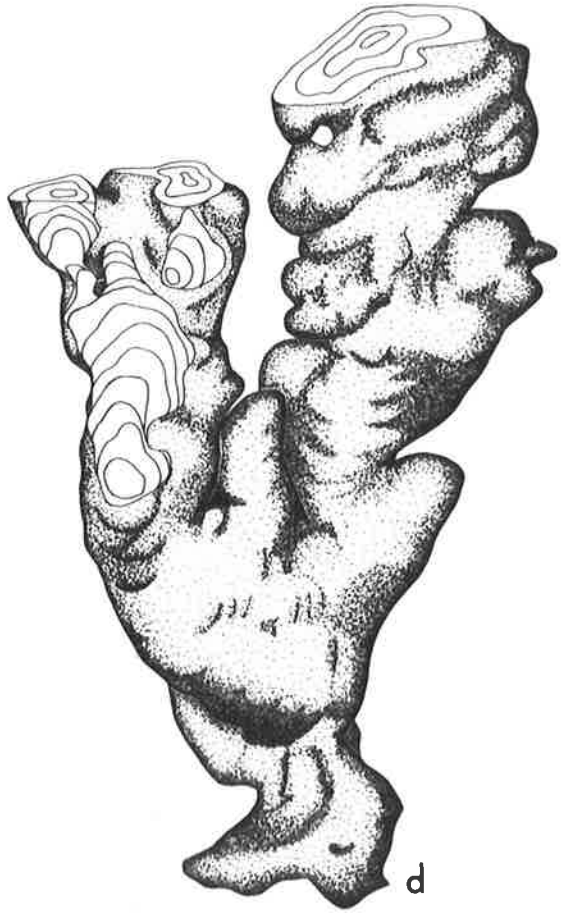

d

Figure 29

Tungussia inna, Ringwood Member of the Pertatataka Formation, Amadeus Basin.

x ½. R_1.

a: 3 miles NNW of Olympic Bore (Alice Springs Sheet area). Part of a hemispherical bioherm about 30cm wide. BMR AS78.

b-e: 5.5 miles SE of Ringwood Homestead. All four drawings represent almost the full thickness of a biostrome. e is a tracing from a section cut normal to bedding. b,c,e (S358); d (S359).

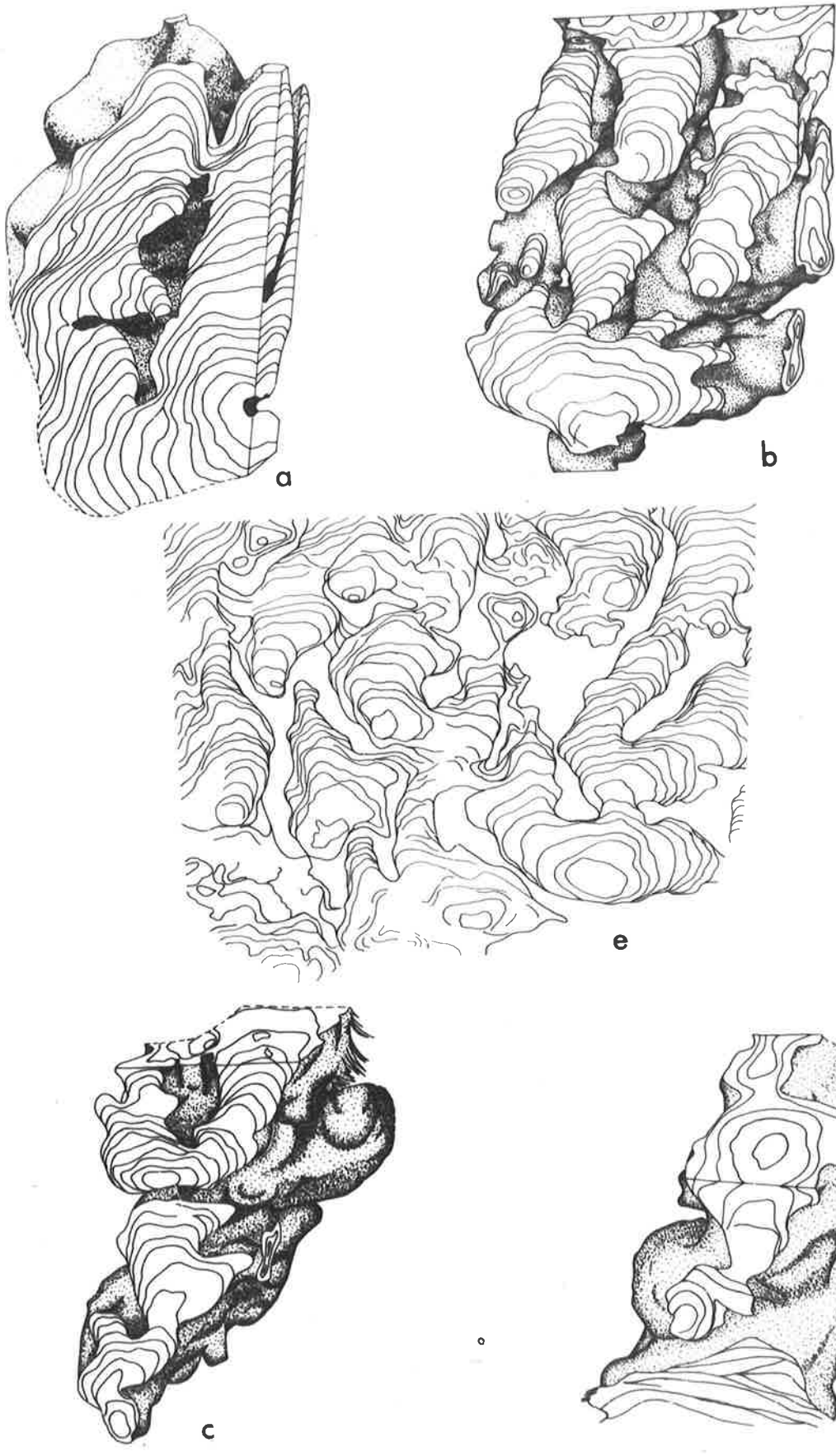
a
b
e
c
d

Figure 30

"Collenia australasica" of Edgell (1964); unnamed in this thesis. Reconstructions from the one and only specimen available and studied by Edgell. x 1 (GSWA F5015).

a: The whole specimen. R_2.

b-d: Columns from a. d is a 60° reconstruction. R_1.

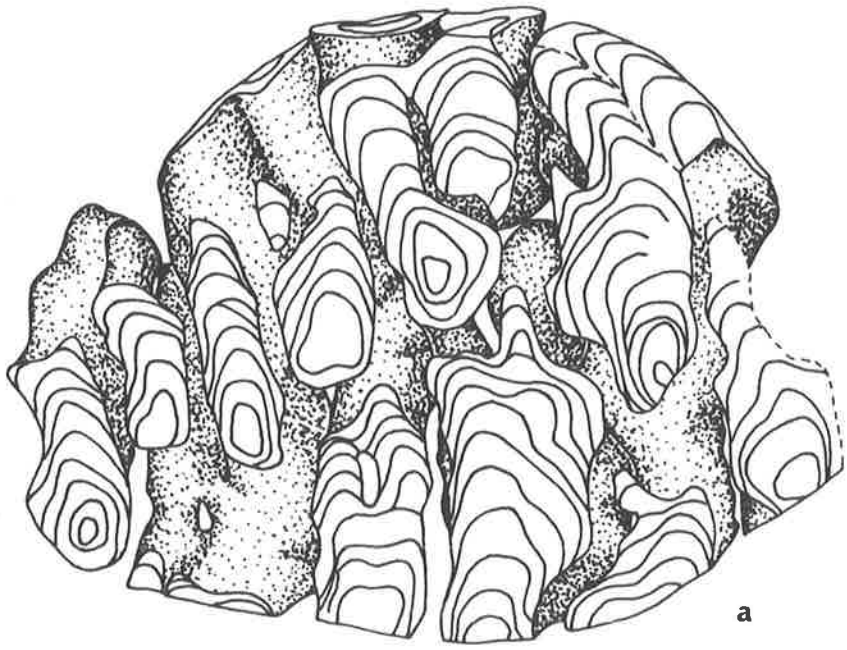

a

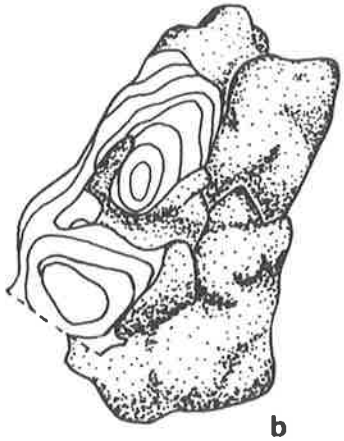

b

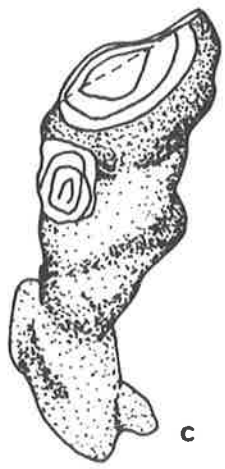

c

d

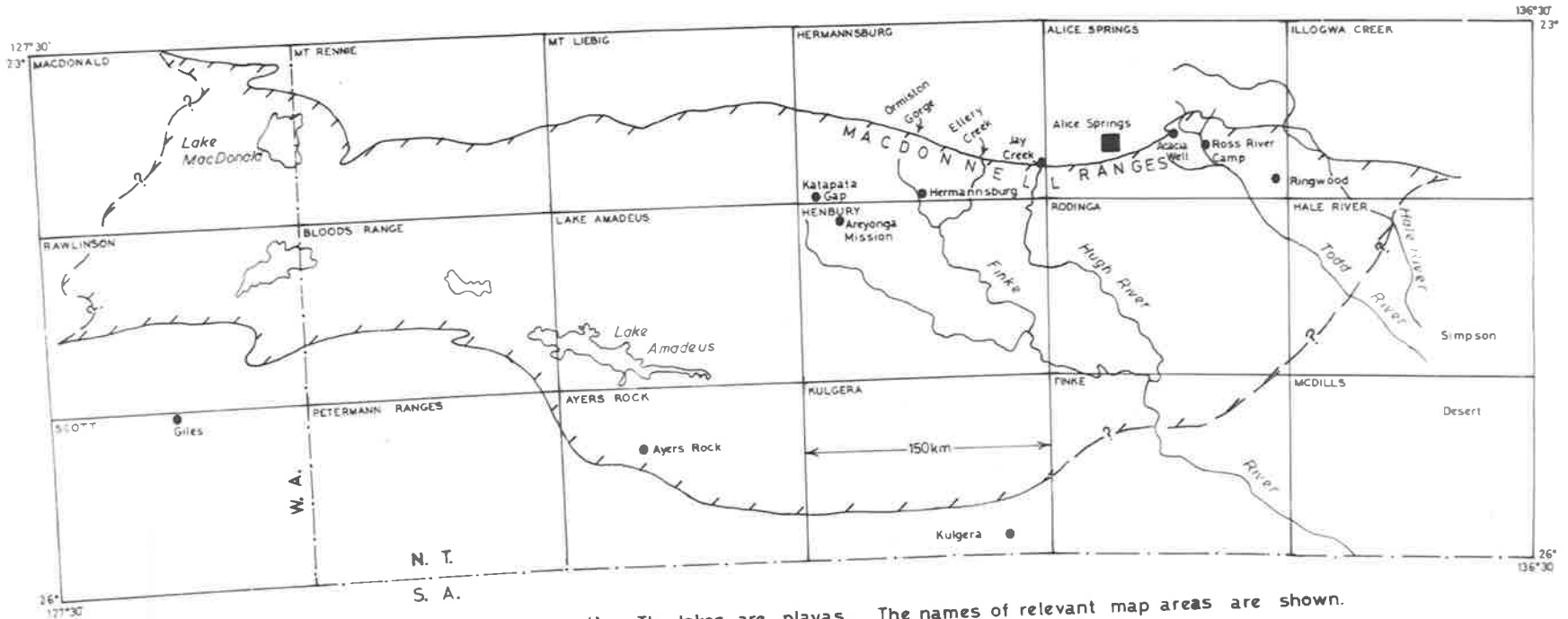

Fig. 31 Locality map of the Amadeus Basin (). The lakes are playas. The names of relevant map areas are shown.

Figure 32

Diagrammatic representation of the Precambrian stratigraphy of the Amadeus Basin (after Wells *et al.*, 1967a,b). Length of section about 800km. Facies changes shown in the west are inferential only. * Stromatolitic (vertical position of the symbol within the units has no significance).

Figure 33

Diagrammatic representation of the Cambrian stratigraphy of the northeastern Amadeus Basin (from Wells *et al.*, 1967b). Length of section about 200km. * Stromatolitic (the positions of the symbols within the formations have no significance).

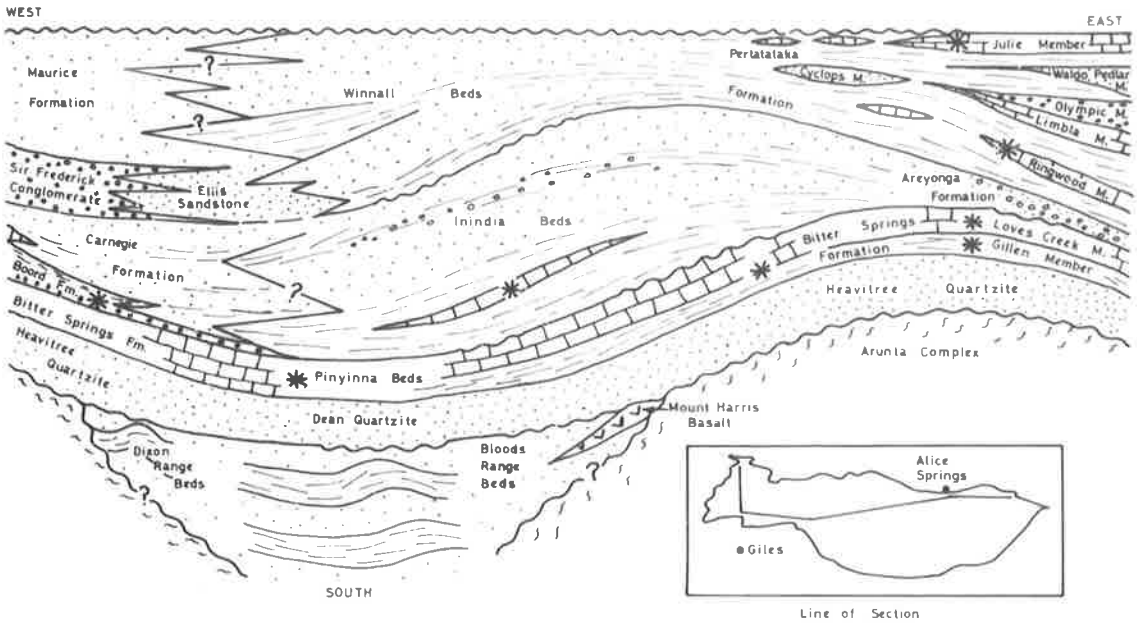
WEST
EAST
Maurice
Formation
Winnall
Beds
Pertatataka
Formation
Julie Member
Cyclops M.
Waldo Pedlar M.
Olympic M.
Limbla M.
Ringwood M.
Areyonga
Formation
Loves Creek M.
Gillen Member
Bitter Springs
Formation
Heavitree
Quartzite
Arunta Complex
Sir Frederick
Conglomerate
Ellis
Sandstone
Inindia
Beds
Carnegie
Formation
Boord Fm.
Bitter Springs Fm.
Heavitree
Quartzite
Pinyinna Beds
Dean Quartzite
Mount Harris
Basalt
Dixon
Range
Beds
Bloods
Range
Beds
SOUTH
Alice
Springs
Giles
Line of Section

32.

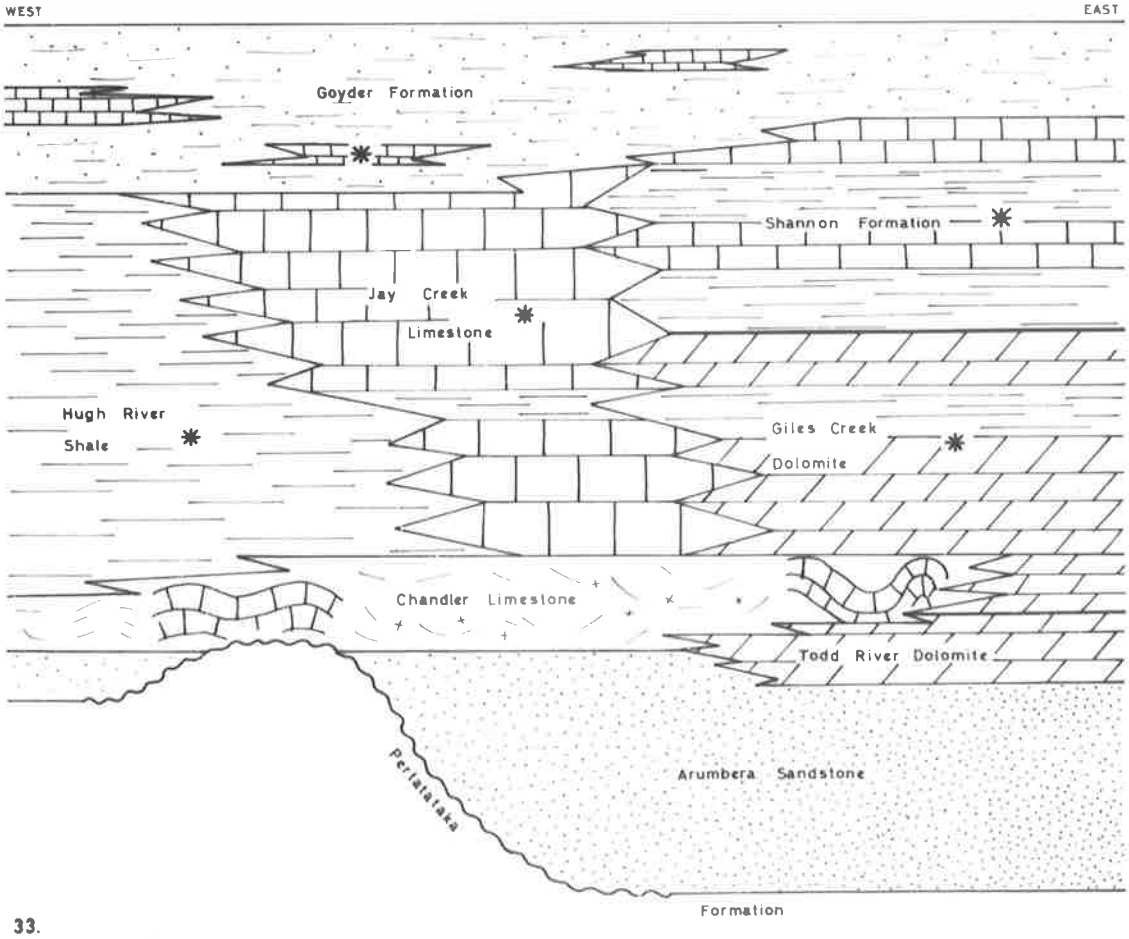
WEST
EAST
Goyder Formation
Shannon Formation
Jay Creek
Limestone
Hugh River
Shale
Giles Creek
Dolomite
Chandler Limestone
Todd River Dolomite
Pertatataka
Arumbera Sandstone
Formation

33.

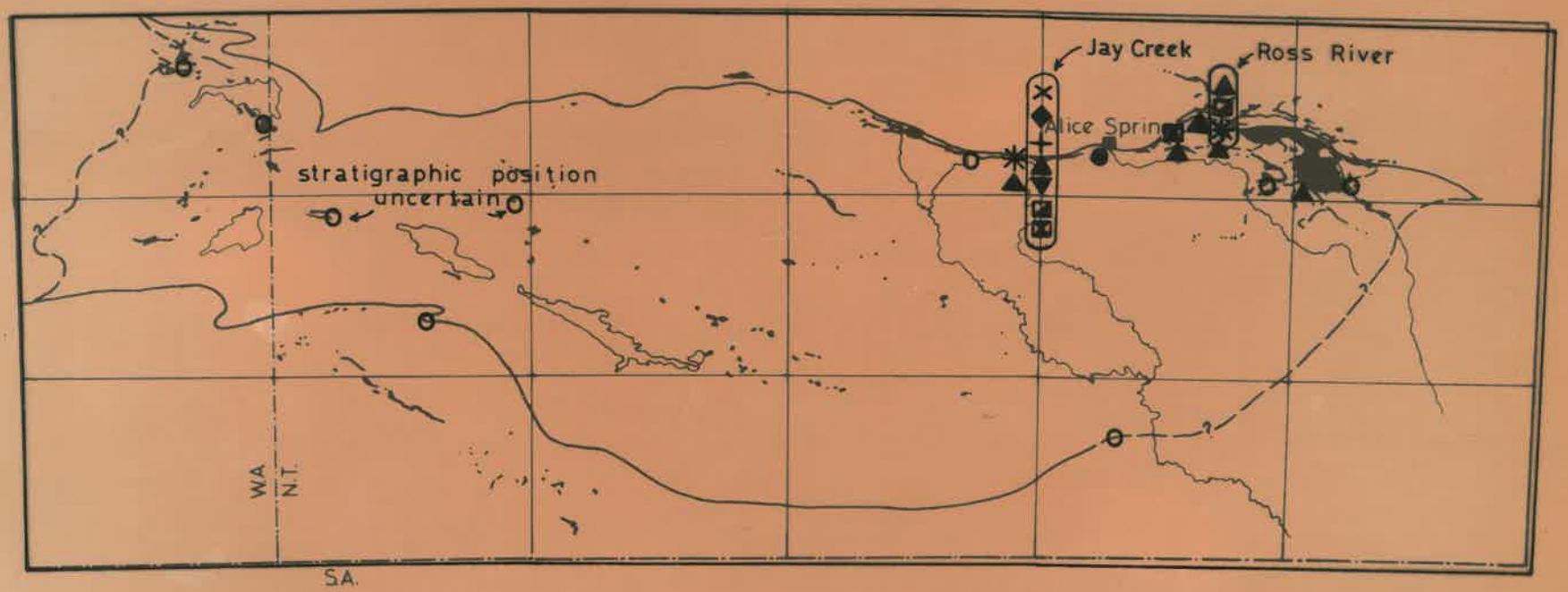

Fig.34 Outcrop distribution and (on overlay) stromatolite occurrence, Bitter Springs Formation and Pinyinna Beds, Amadeus Basin. Outcrop distribution and basin margin from Wells et al. (1967b).

- ▲ *Acaciella australica*
- ◆ *Basisphaera irregularis*
- ◪ *Boxonia pertaknurra*
- ✳ *Inzeria intia*
- \+ *Jurusania chewingsi*
- ⊠ *Kulparia alicia*
- ▼ *Linella avis*
- × *Minjaria pontifera*
- ● *Tungussia erecta*
- O *undifferentiated stromatolites*

Stromatolites are reported from the central part of the basin but as no precise localites are given they cannot be included here.

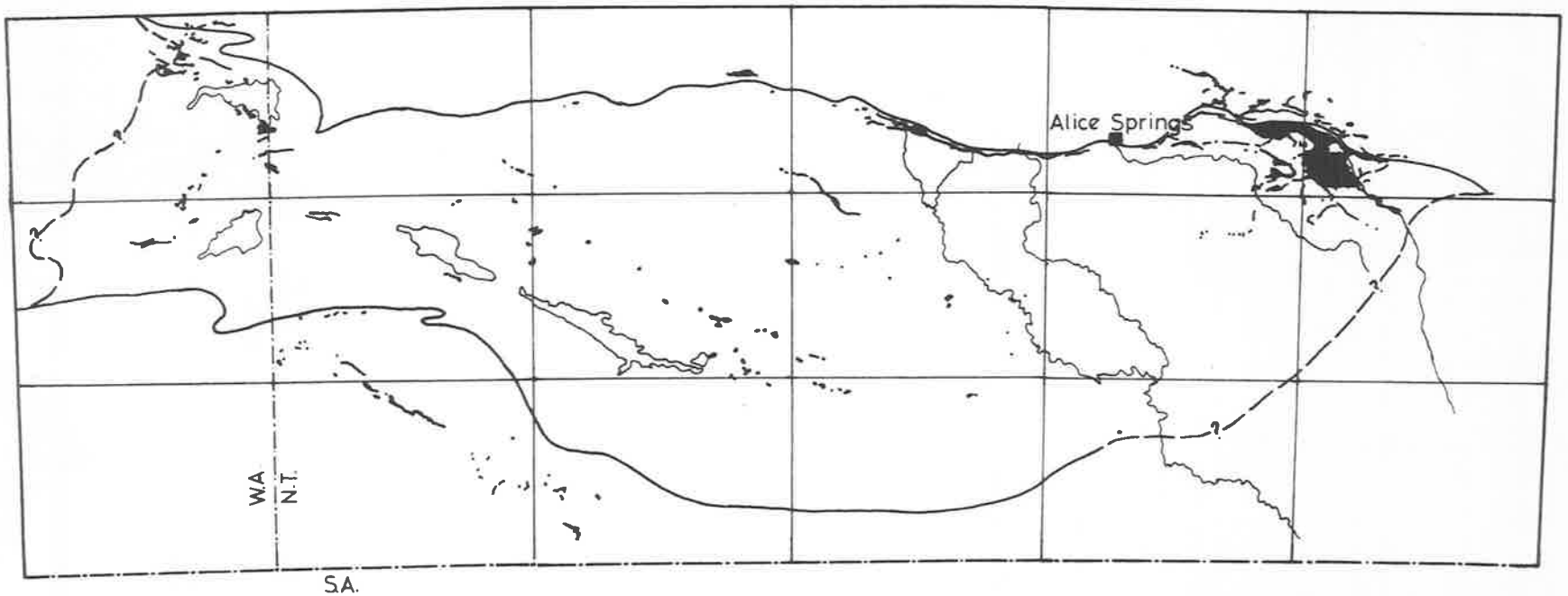

Fig.34 Outcrop distribution and (on overlay) stromatolite occurrence, Bitter Springs Formation and Pinyinna Beds, Amadeus Basin. Outcrop distribution and basin margin from Wells et al. (1967b).

- ▲ *Acaciella australica*
- ◆ *Basisphaera irregularis*
- ◪ *Boxonia pertaknurra*
- ✳ *Inzeria intia*
- \+ *Jurusania chewingsi*
- ⊠ *Kulparia alicia*
- ▼ *Linella avis*
- × *Minjaria pontifera*
- ● *Tungussia erecta*
- O *undifferentiated stromatolites*

Stromatolites are reported from the central part of the basin but as no precise localites are given they cannot be included here.

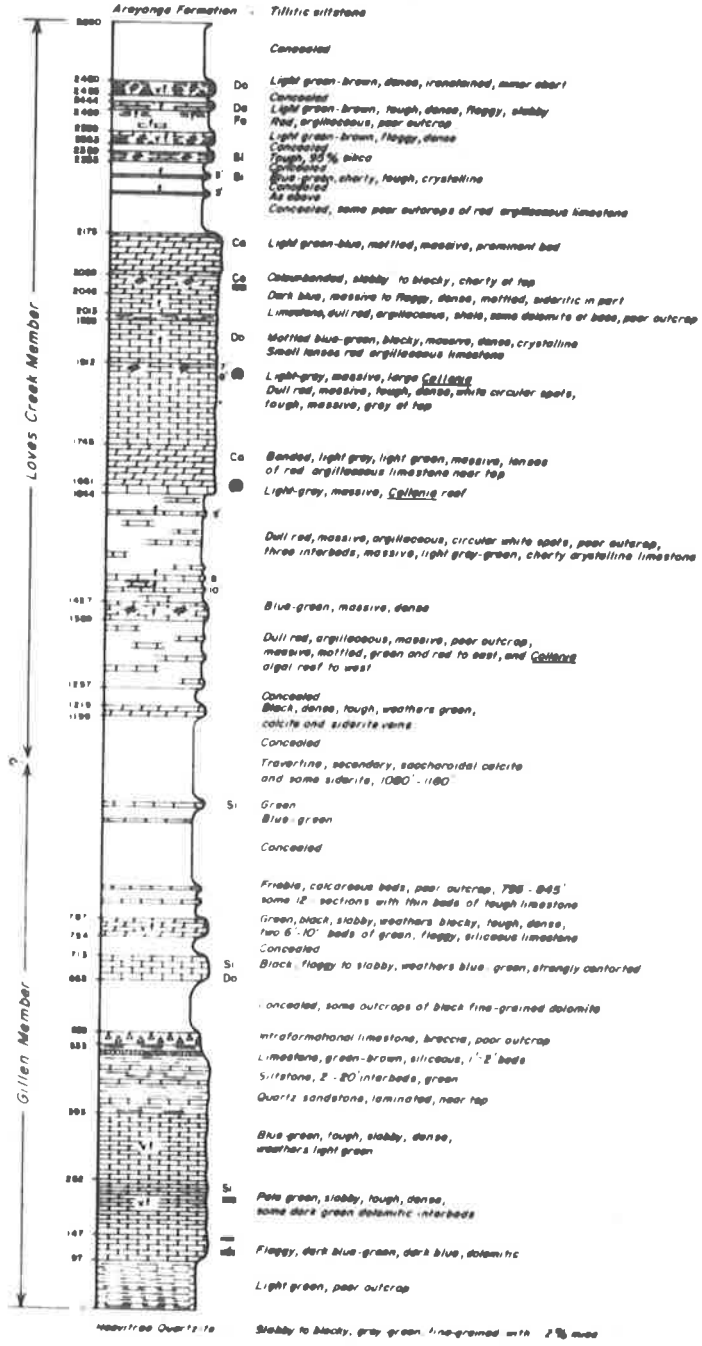

Fig.35 Reference section of the Bitter Springs Formation, Ellery Creek; from Wells et al. (1967a).

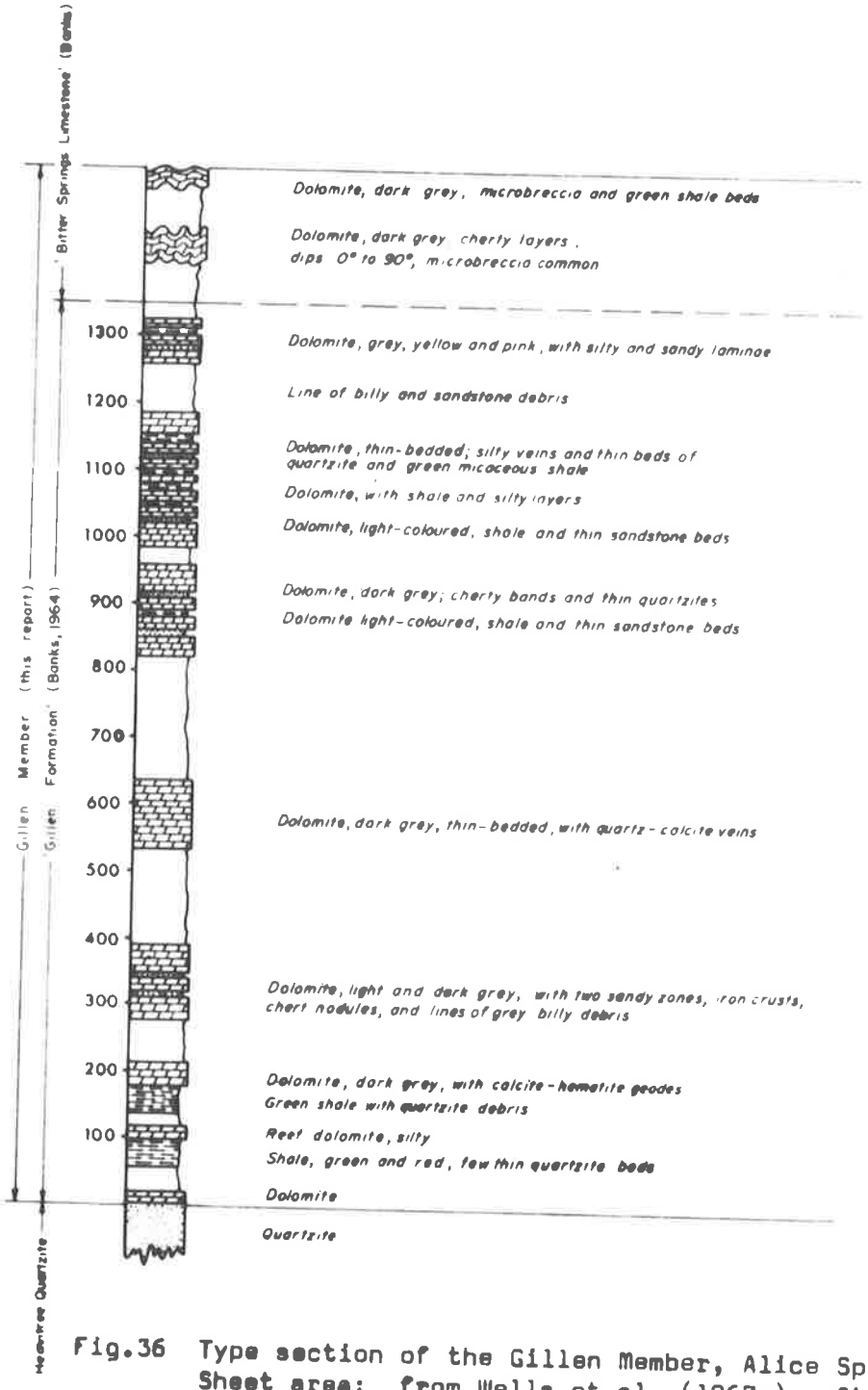

Fig.36 Type section of the Gillen Member, Alice Springs Sheet area; from Wells et al. (1967a), after Banks (1964).

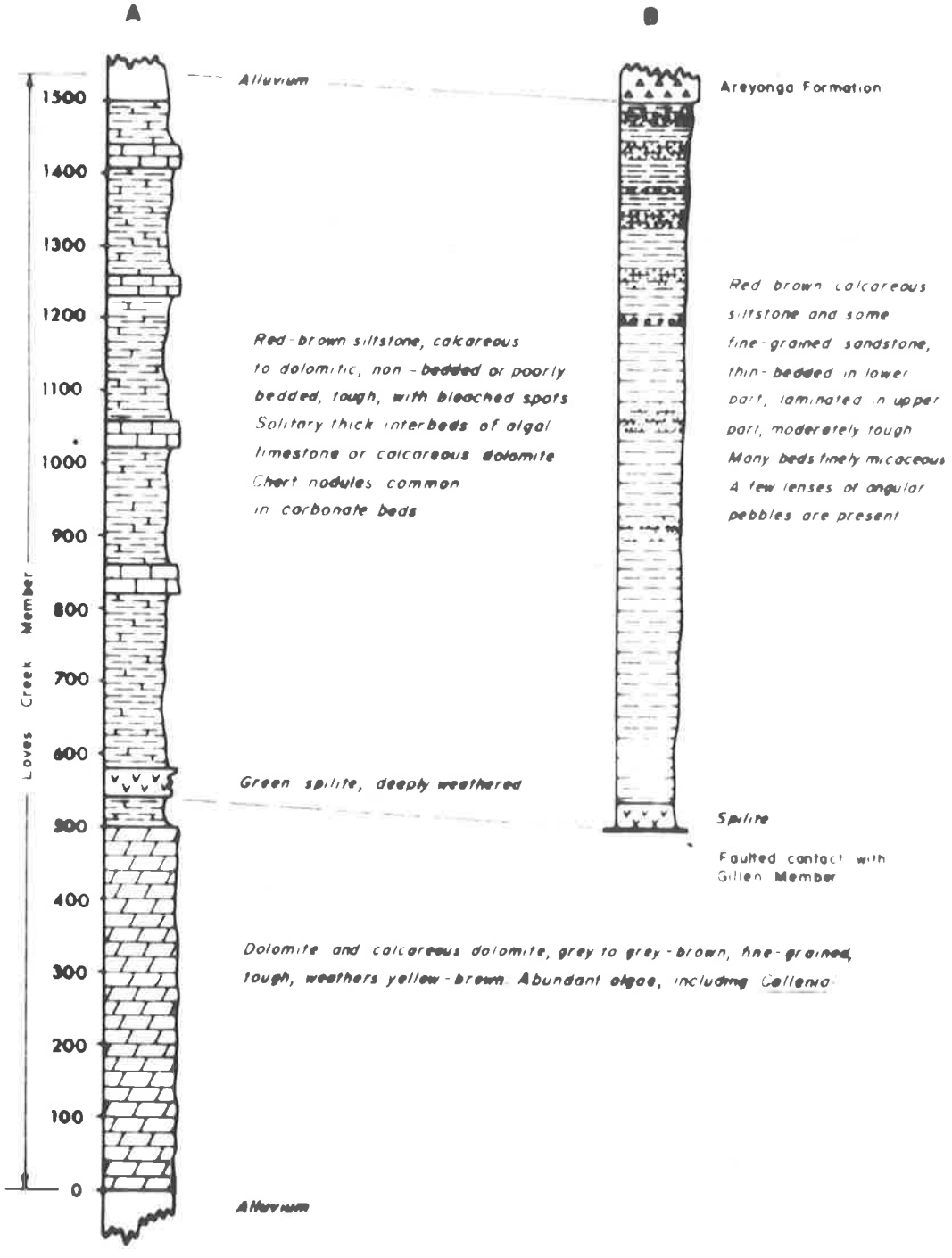

Fig.38 Generalized sequence in the Loves Creek Member; from Wells et al. (1967a).

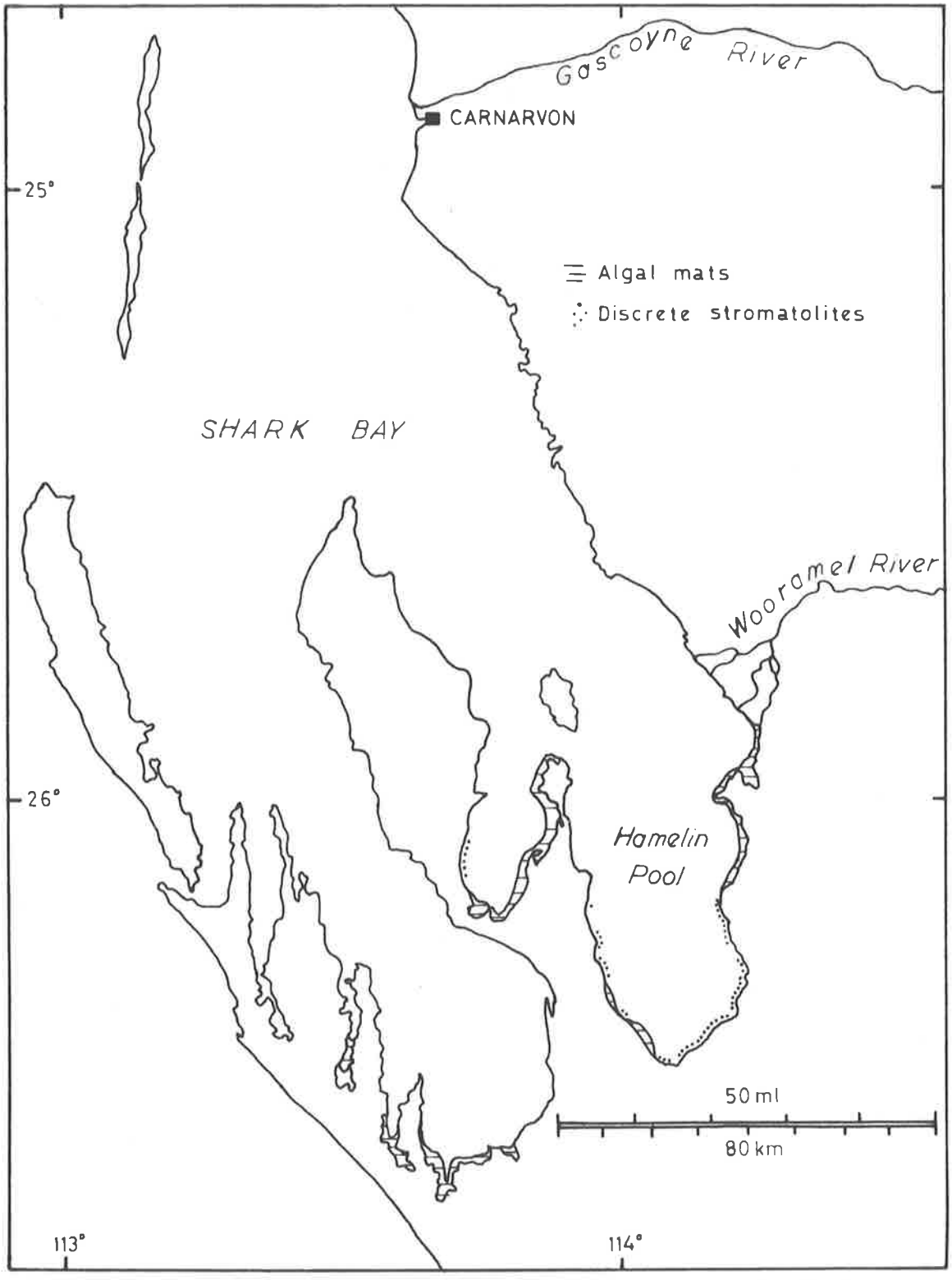

Fig. 39 Distribution of algal mats and discrete stromatolites in Shark Bay, Western Australia (after Logan, 1961). Algal mats are more extensive than shown.

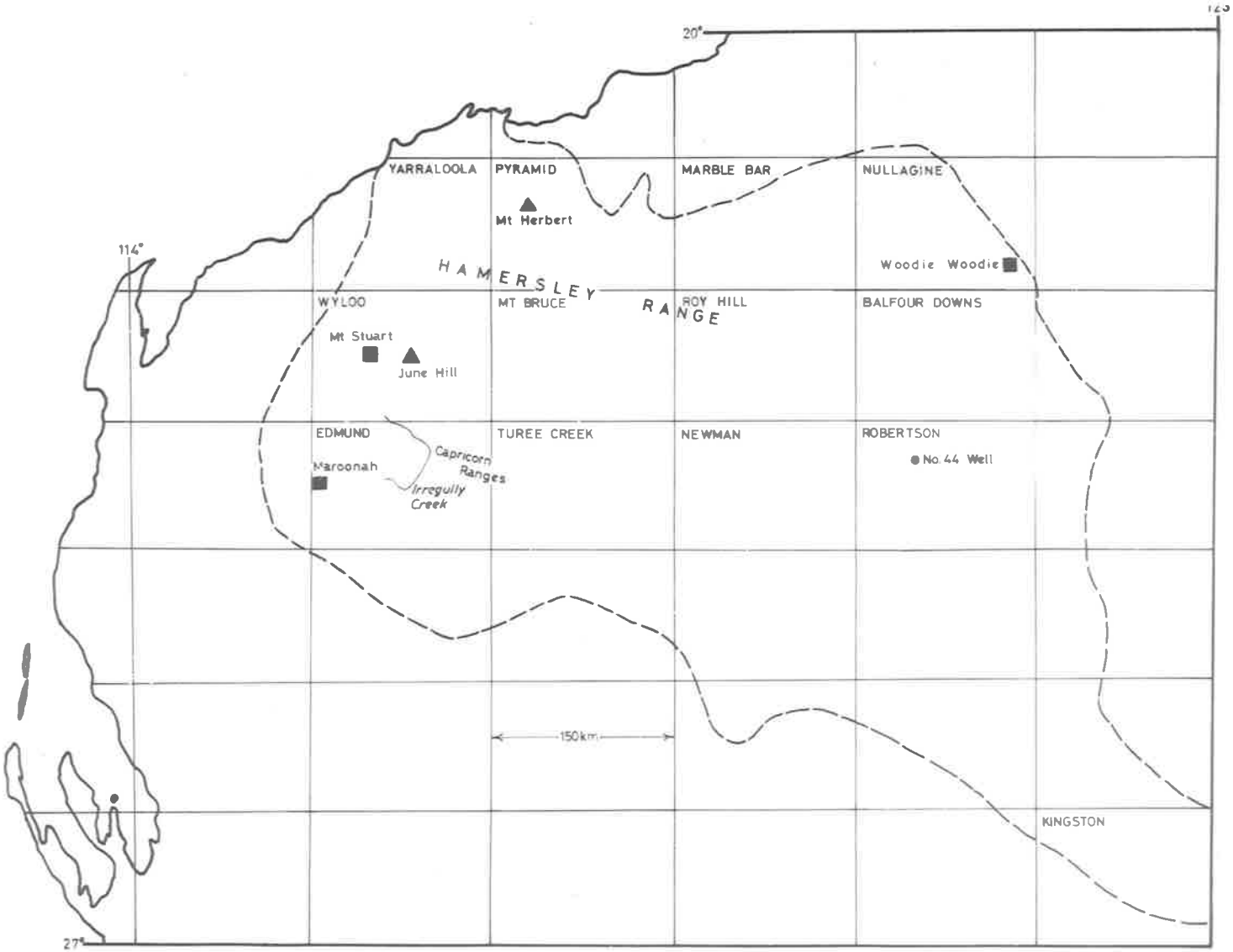

Fig. 40 Locality map of the Nullagine Basin. — — — Basin margin. The names of relevant map areas are shown.

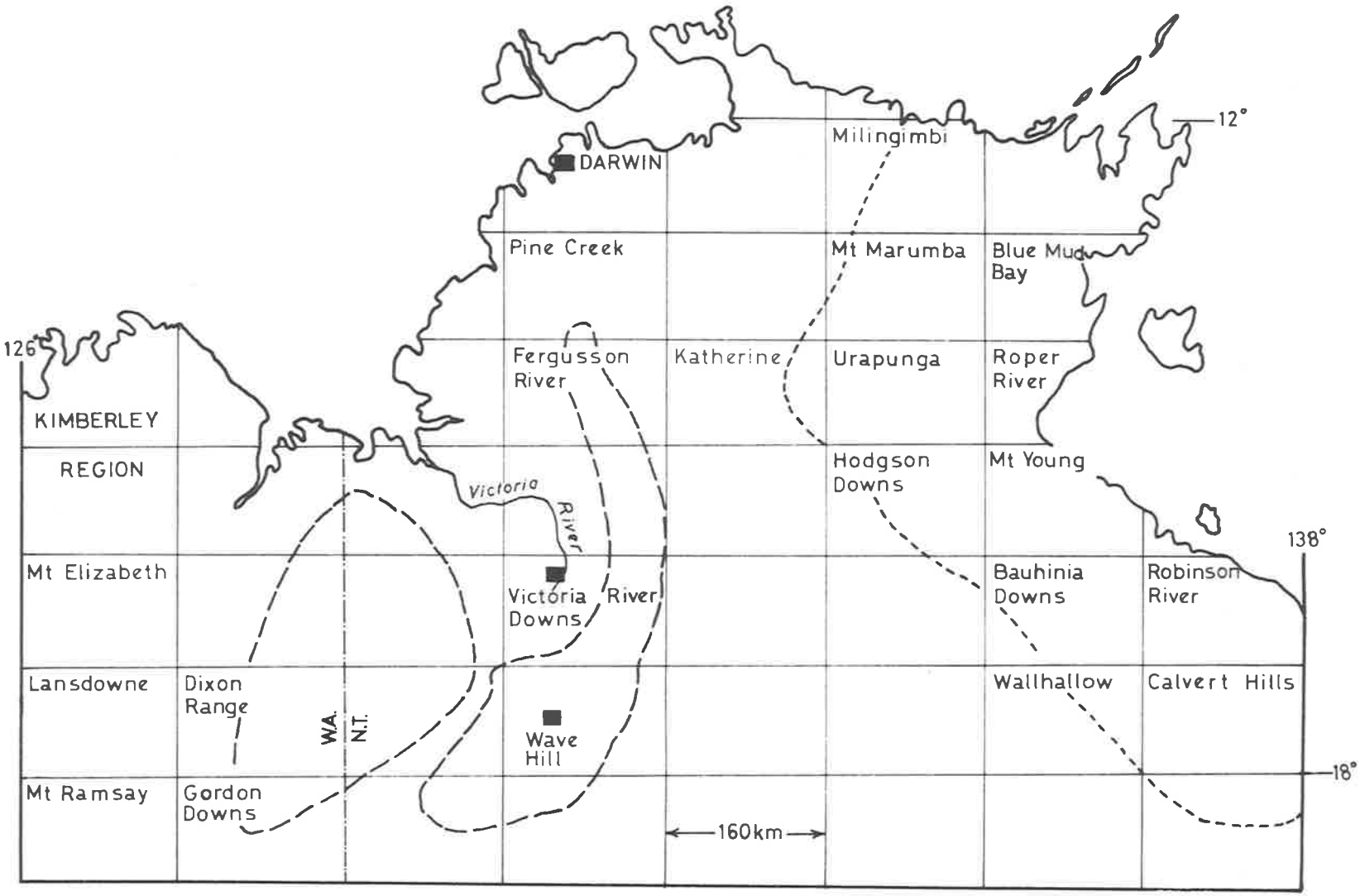

Fig. 41 Locality map of the Antrim Plateau Volcanics (———) and the McArthur Basin (------). The names of relevant map areas are shown.

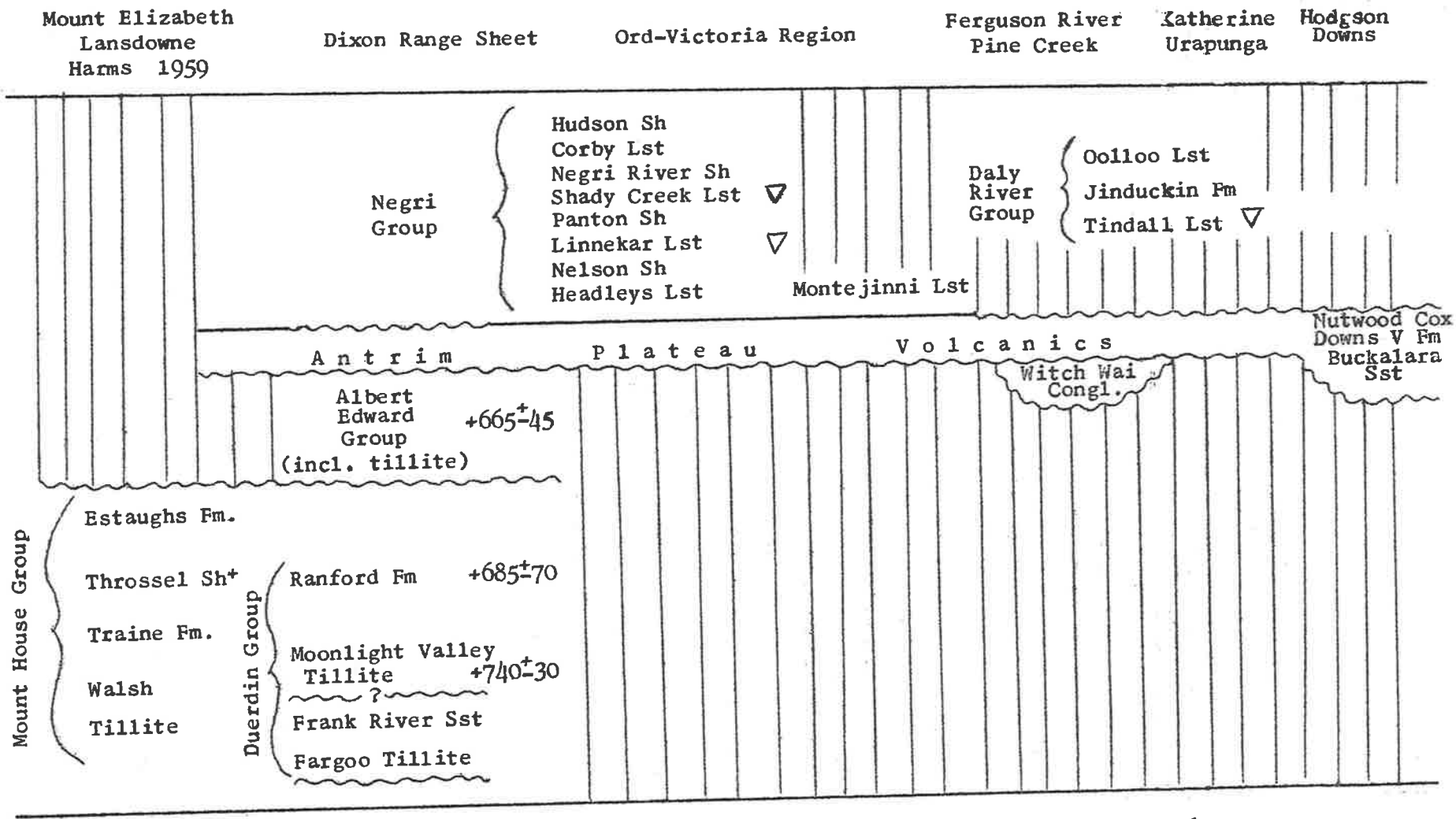

Fig.42: Stratigraphy of the Cambrian and late Precambrian deposits of the east Kimberley and northwestern Northern Territory regions.
Sh, shale; Lst, limestone; Fm, formation; V, volcanics
▽ Early Middle Cambrian fossils; + Rb-Sr shale datings

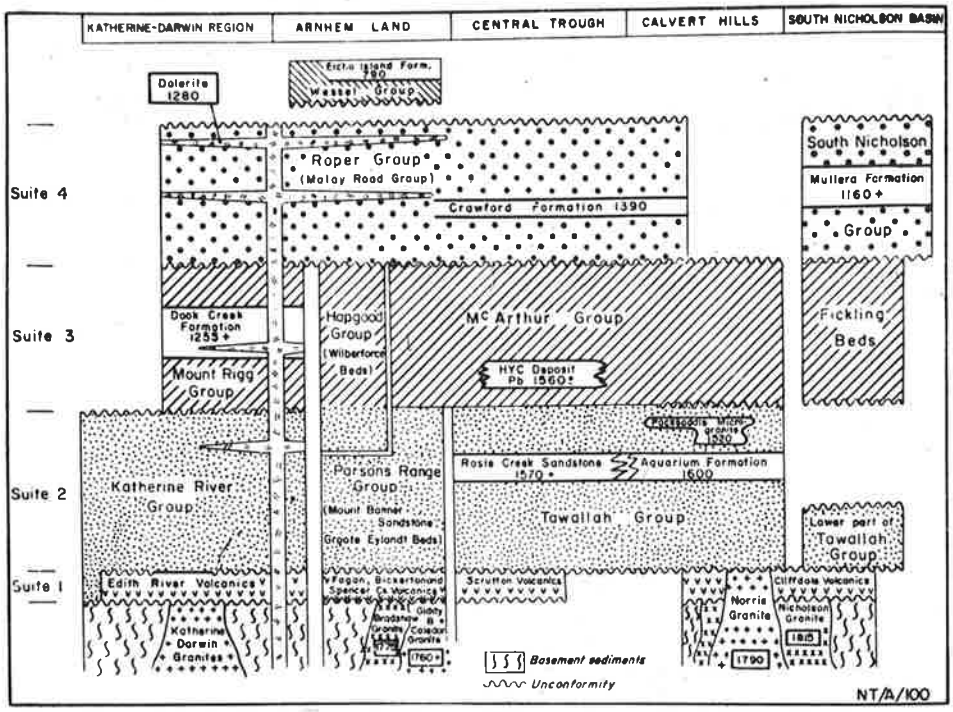

Fig.43 Diagrammatic relationships of rock units in the McArthur Basin, showing relative positions and approximate ages of dated units (age in millions of years); from McDougall et al. (1965).

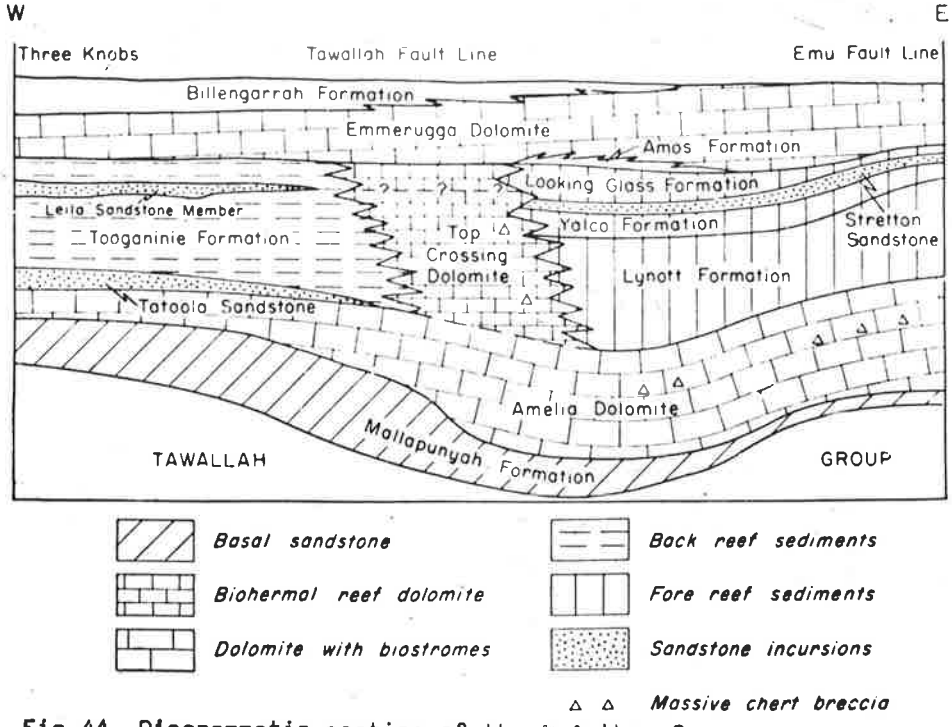

Fig.44 Diagrammatic section of the McArthur Group (Three Knobs - Emu Fault); from J. W. Smith (1964)

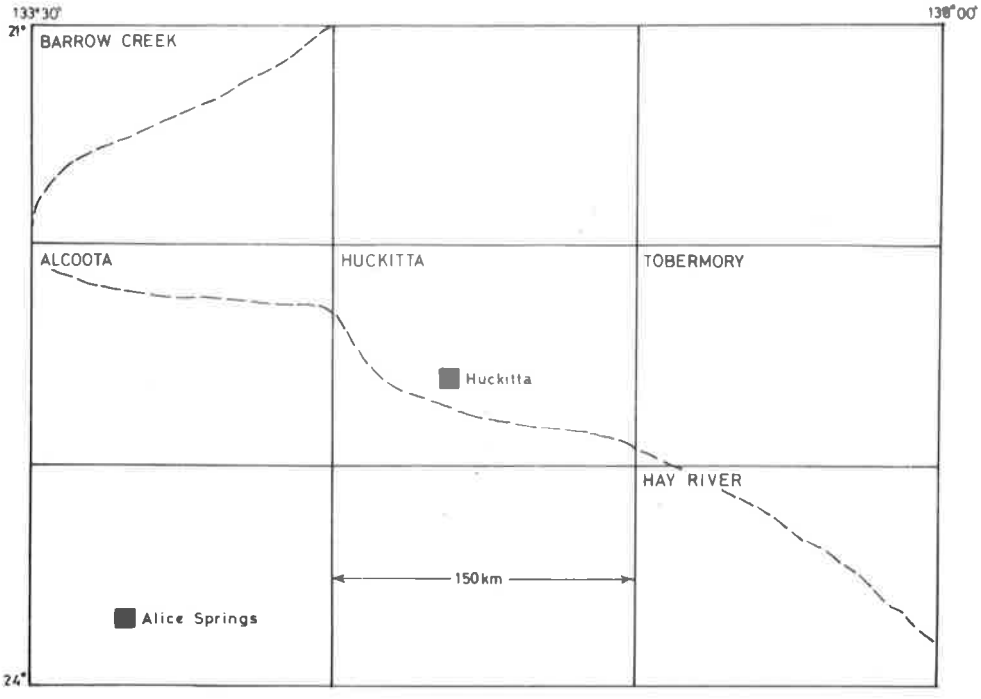

Fig. 45 Locality map for the SW Georgina Basin. The names of relevant map sheets are shown. —— Basin margin.

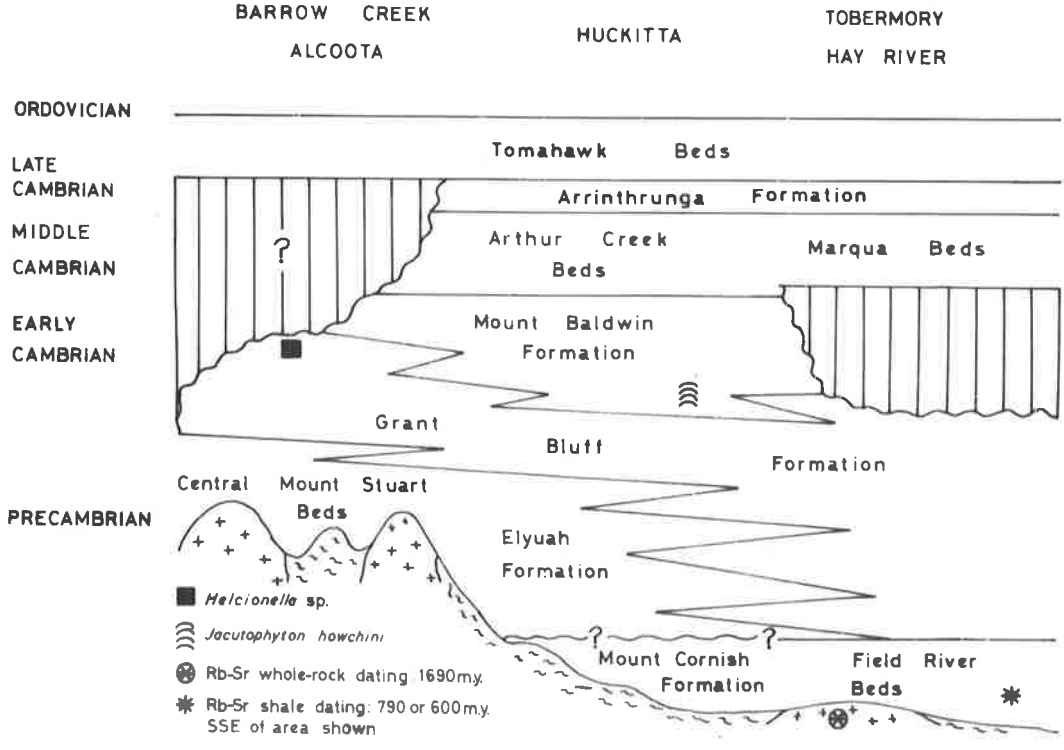

Fig. 46 Interpretation of the stratigraphy of the SW Georgina Basin. Map names are given at the top of the diagram.

Figure 47

Locality map of the Hamersley Ranges. Outcrop area of Brockman Iron Formation cross-hatched (after MacLeod, 1967 and La Berge, 1966).

Figure 48

Spacing (S) of the ridges on the larger Liesegang medusiform structure compared to that on the mechanically formed compound medusiform structures, plotted on a logarithmic scale (slightly different for the two examples). "n" represents the concentric ridges, starting at zero for the most central ridge. The ridges on the Liesegang medusiform structure are spaced in geometric progression.

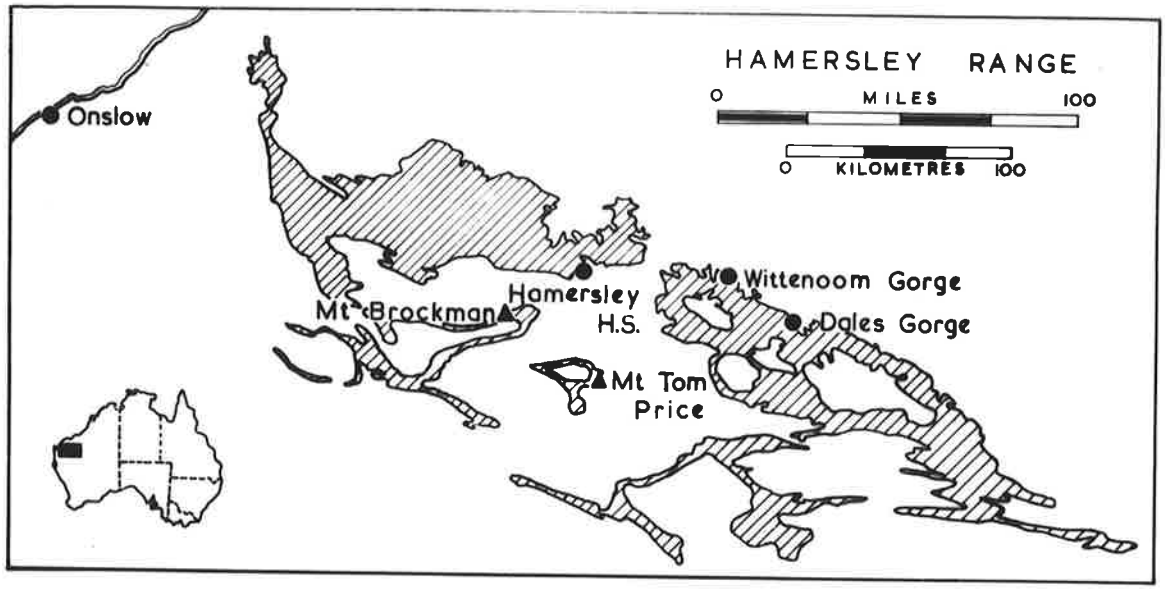
HAMERSLEY RANGE
0 MILES 100
0 KILOMETRES 100
Onslow
Mt Brockman
Hamersley H.S.
Wittenoom Gorge
Dales Gorge
Mt Tom Price

47

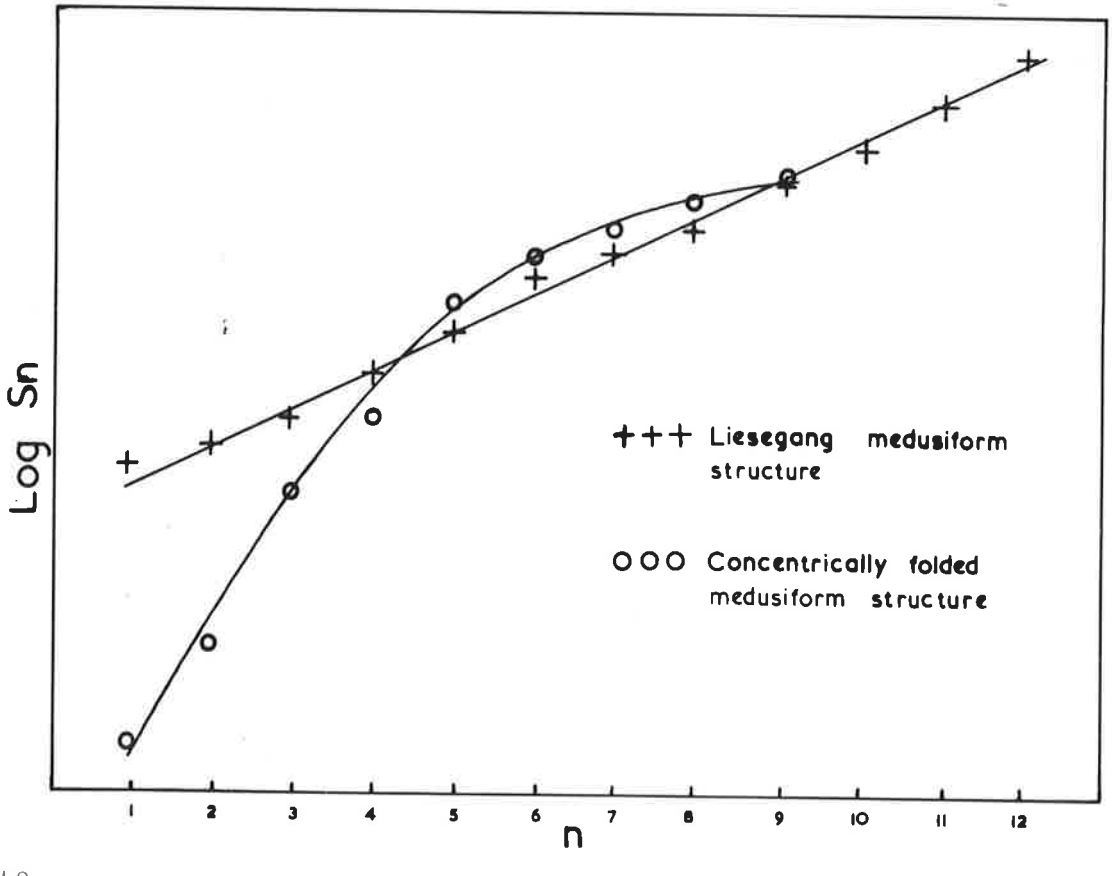
Log Sn
n
1
2
3
4
5
6
7
8
9
10
11
12
+++ Liesegang medusiform structure
OOO Concentrically folded medusiform structure

48

Figure 49

Chert pods: three variants of their shape and microband relationship with the enclosing quartz-iron oxide. Microbands are represented by thin lines, chert pod boundaries by thick lines.

Figure 50

Slightly simplified tracing of the structure shown in plate 38g. a: chert mesoband; iron oxide-rich microbands black. b: quartz-iron oxide. c: magnetite mesoband. d: several quartz-iron oxide microbands. Microbands in the basal parts of "b" are continuous with those in "a". Fractures associated with folds in "d" pass through "c" into "b".

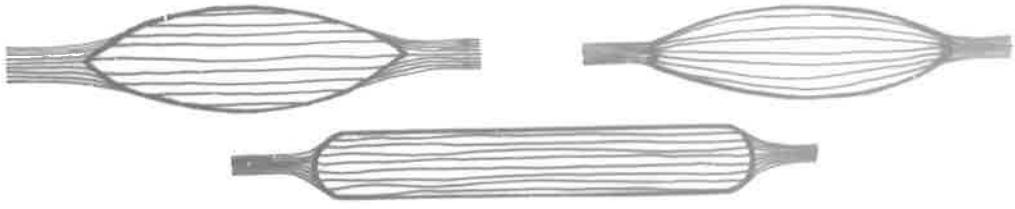

49

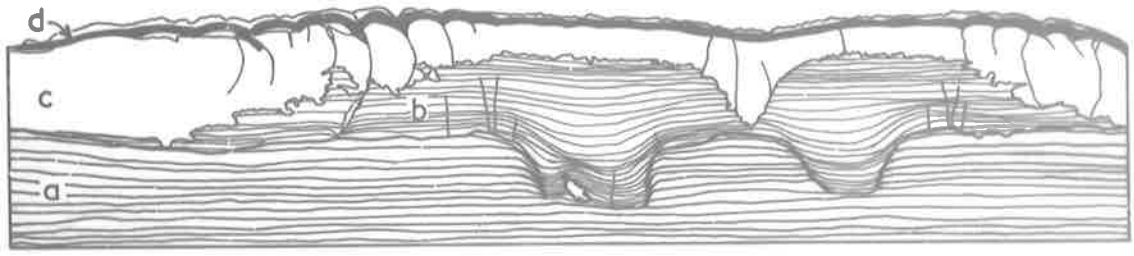

50

Plate 1

Microstructures in thin section

a,b: *Madiganites mawsoni* vermiform microstructure, grading into areas with only a grumous structure, a x 12 (S46), b x 25 (S46).

c: *Kulparia alicia*; the least altered column margins have walls; x 3.2 (S347).

1

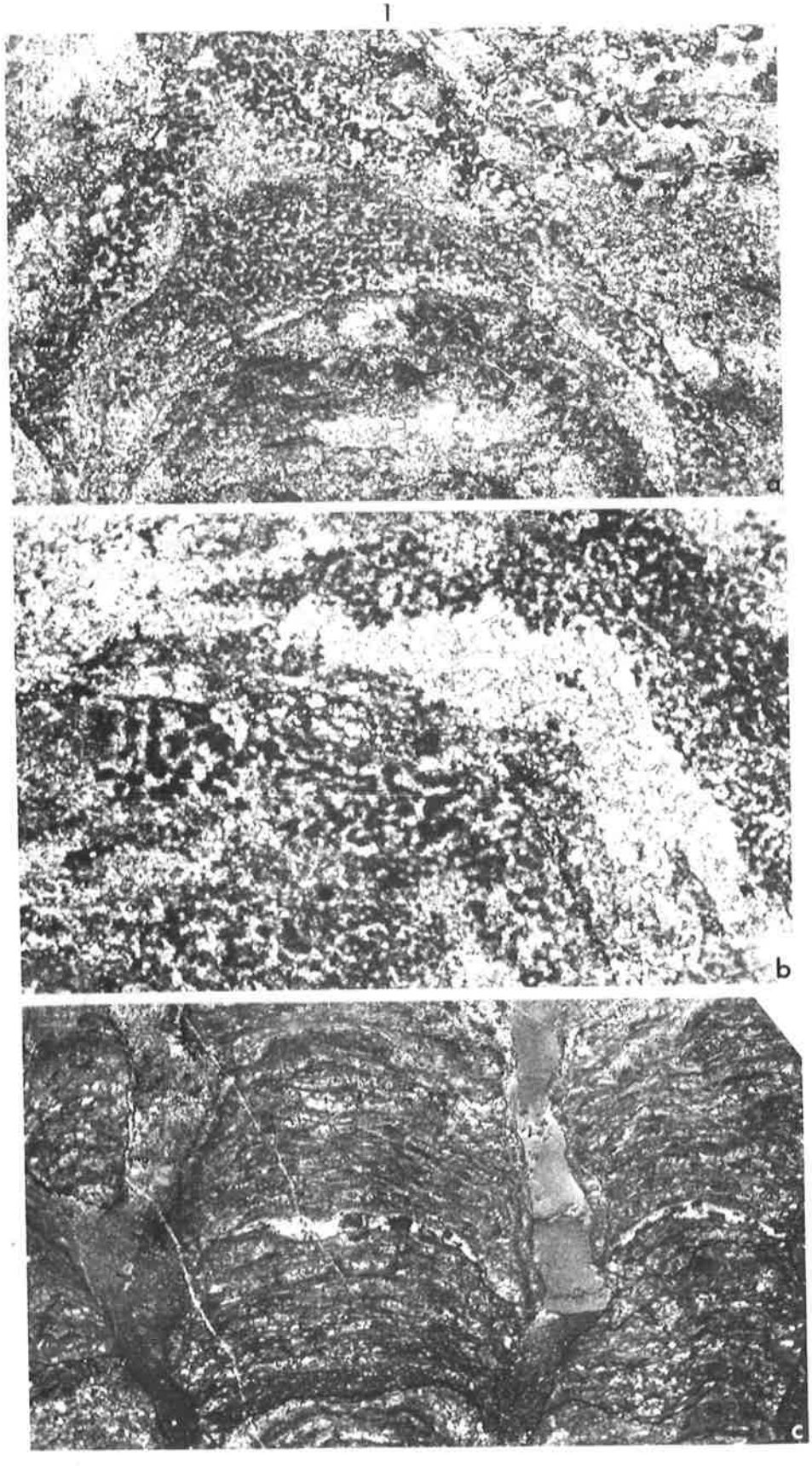

Plate 2

Microstructures in thin section; those shown here and on plate 3 are the most frequently occurring kind.

a: *Basisphaera irregularis* narrow column; x 3 (S136).

b: *Boxonia pertaknurra*; x 3 (S137).

c,d: *Acaciella australica*; c, dolomite preservation, x 3.3 (S345); d, calcite preservation - note concordant stylolites and gradations from homogeneous to grumous laminae, x 4 (S131).

e: *Minjaria pontifera*; note that laminae become parallel to or strike acutely into the altered column margin - the now patchy wall is probably the remnants of a more continuous wall; x 3.5 (S374).

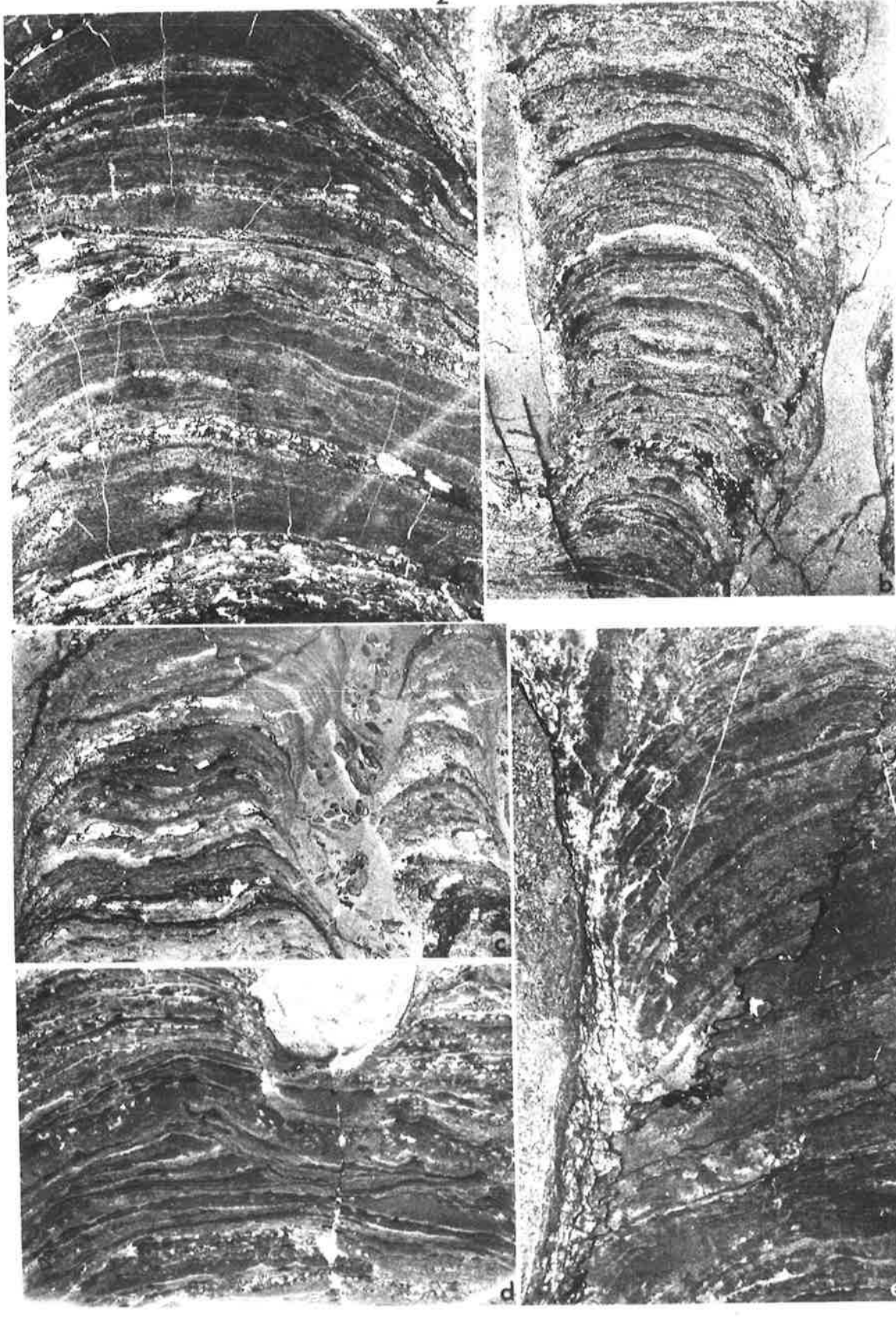
b
c
d
e

Plate 3

Microstructures of *Inzeria intia* in thin section.

a: Base of stage III; note lateral gradation from homogeneous to grumous laminae, wall, and intraclasts in the interspace; x 4 (S141).

b: Stage IV, showing a niche in one column; x 3 (S370).

c,d & e: Stage II, in differently altered specimens, e being the least altered; c & d have numerous concordant stylolites; c has a selvage; c x 4 (S138), d x 2.8 (S369), e x 3 (S372).

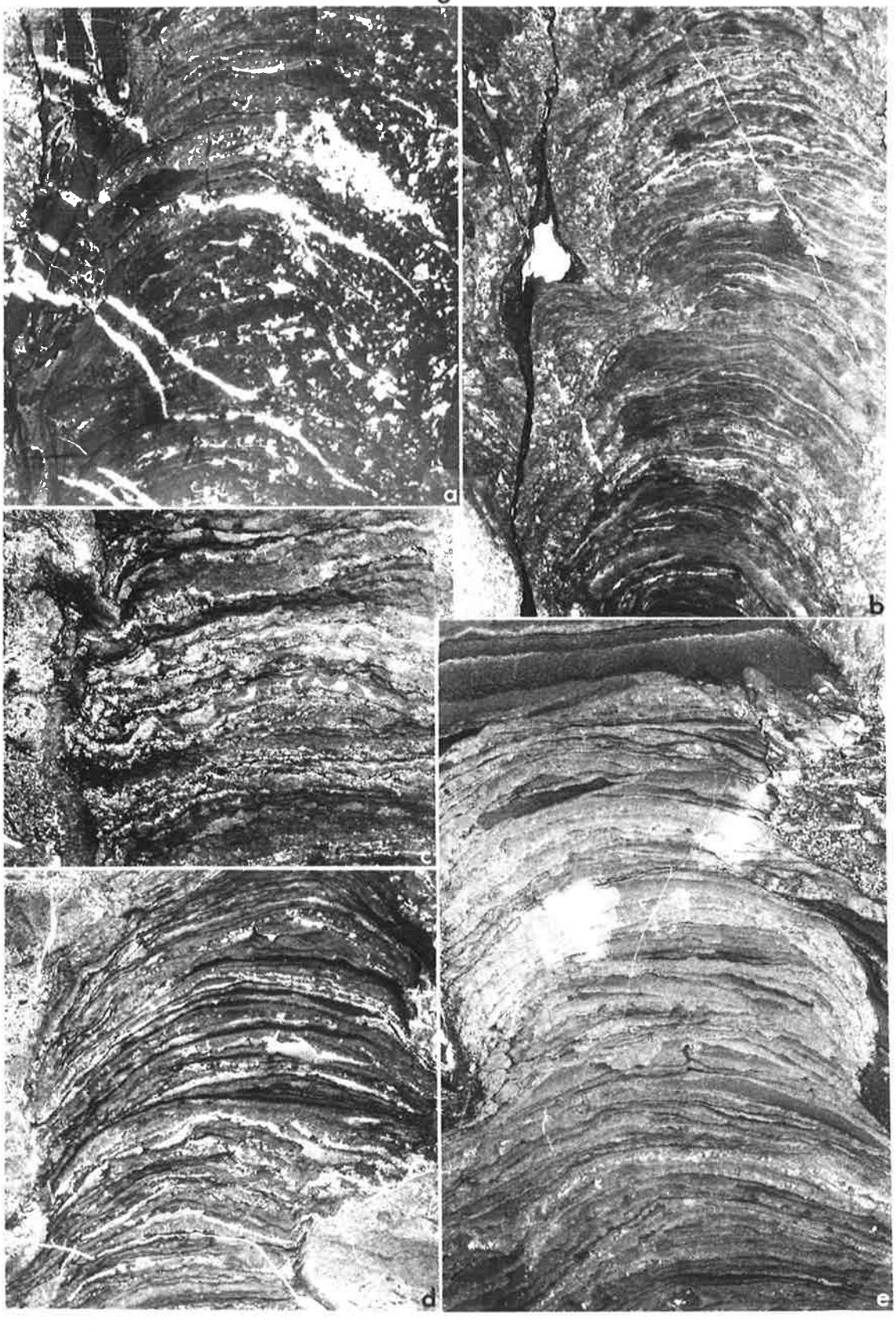
a
b
c
d
e

Plate 4

Microstructures in thin section.

a,c: Jurusania chewingsi, a from upper, columnar, part; c from lower, pseudocolumnar and many-bridged columnar part which appears to be better preserved than the other. How much of the lamina shape irregularity visible in a is secondary is uncertain. a x 3.1 (S134a), c x 3.5 (S134b).

b: Tungussia erecta, upper part; badly preserved; x 3 (S357).

d: Pilbaria perplexa; x 3.2 (S203).

e: Linella avis (Amadeus Basin) showing the microstructure, the well developed walls and bumpy column margins; x 3.2 (S127).

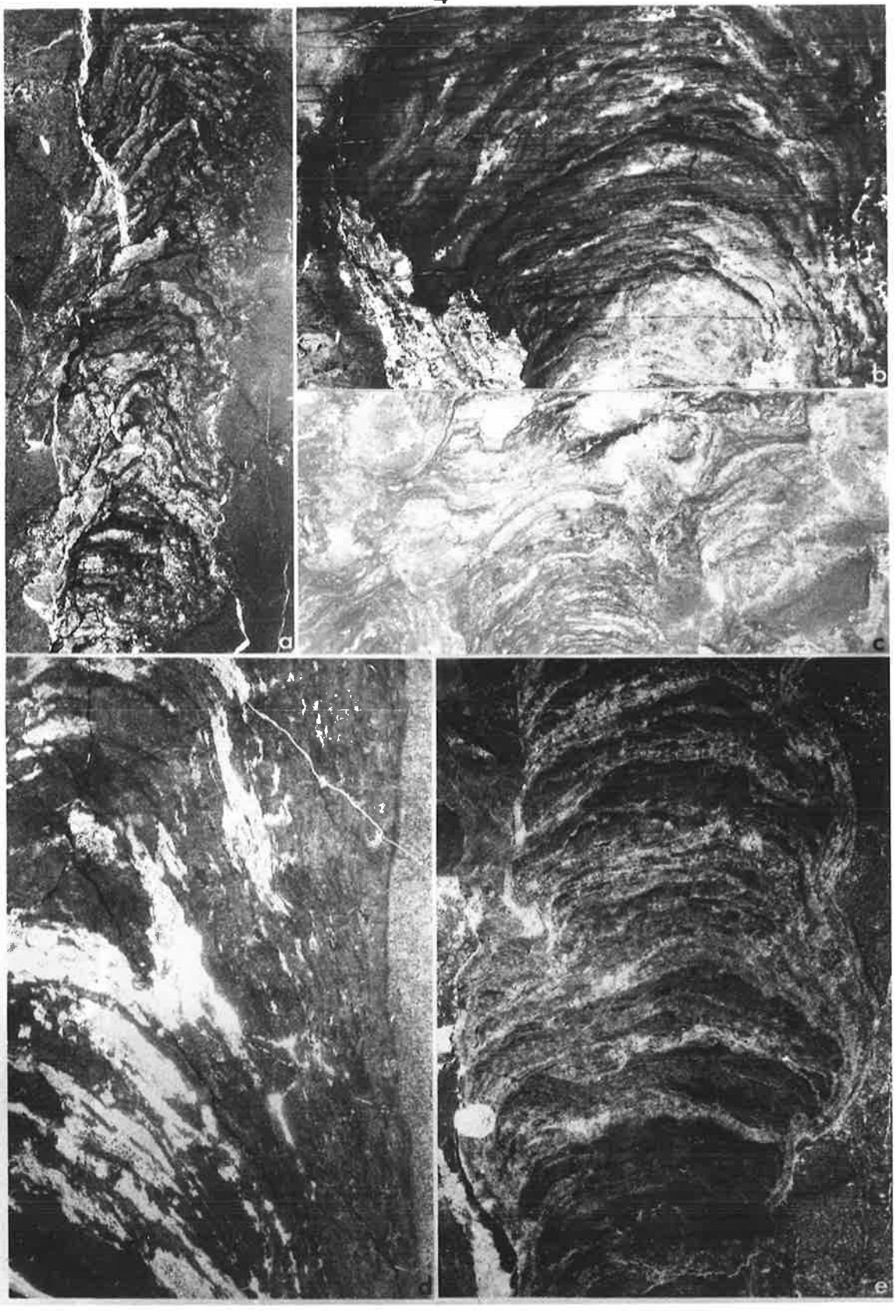
a
b
c
d
e

Plate 5

Microstructures in thin section.

a: Baicalia capricornia; note the even, continuous lamination, very similar to that in b; x 1.4 (S200).

b: Alcheringa narrina. The even, continuous laminae and radial structures are clearly visible. The speckling is caused by the inclusion of micaceous or clayey detritus, which also forms the radial structures. x 10 (S94c).

c: Conophyton cf. gaubitza; x 3.5 (GSWA F5022).

d: Conophyton garganicum (poorly preserved example from the McArthur Basin); x 7 (BMR F23519).

e: Conophyton basalticum; note the very even, continuous laminae similar to those in a and b; x 2 (CPC11314).

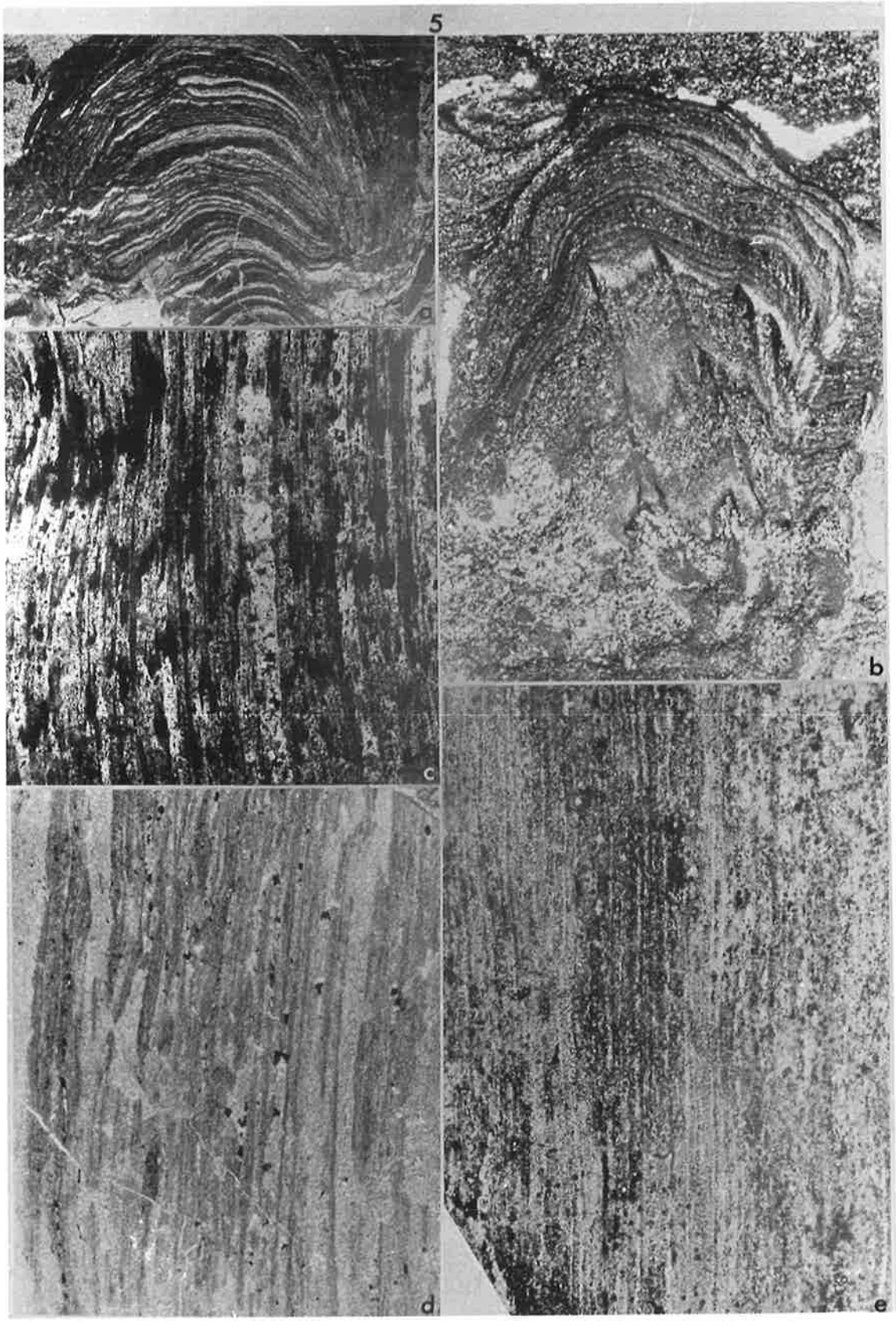
5
a
b
c
d
e

Plate 6

Microstructures in thin section

a-c: Conophyton garganicum australe. In b many lenses are visible as is much included sand-sized detritus; c shows a macrolamina. a x 1.5 (S188), b x 9 (S189), c x 20 (S188).

d: Tungussia inna; the unique, spotty microstructure of this form results from the inclusion in the columns of a large quantity of sand-sized detritus; note also the column walls; x 3 (S358).

e: Jacutophyton howchini; some thickening of laminae is visible in the crestal zone, on the left; x 4 (CPC11316).

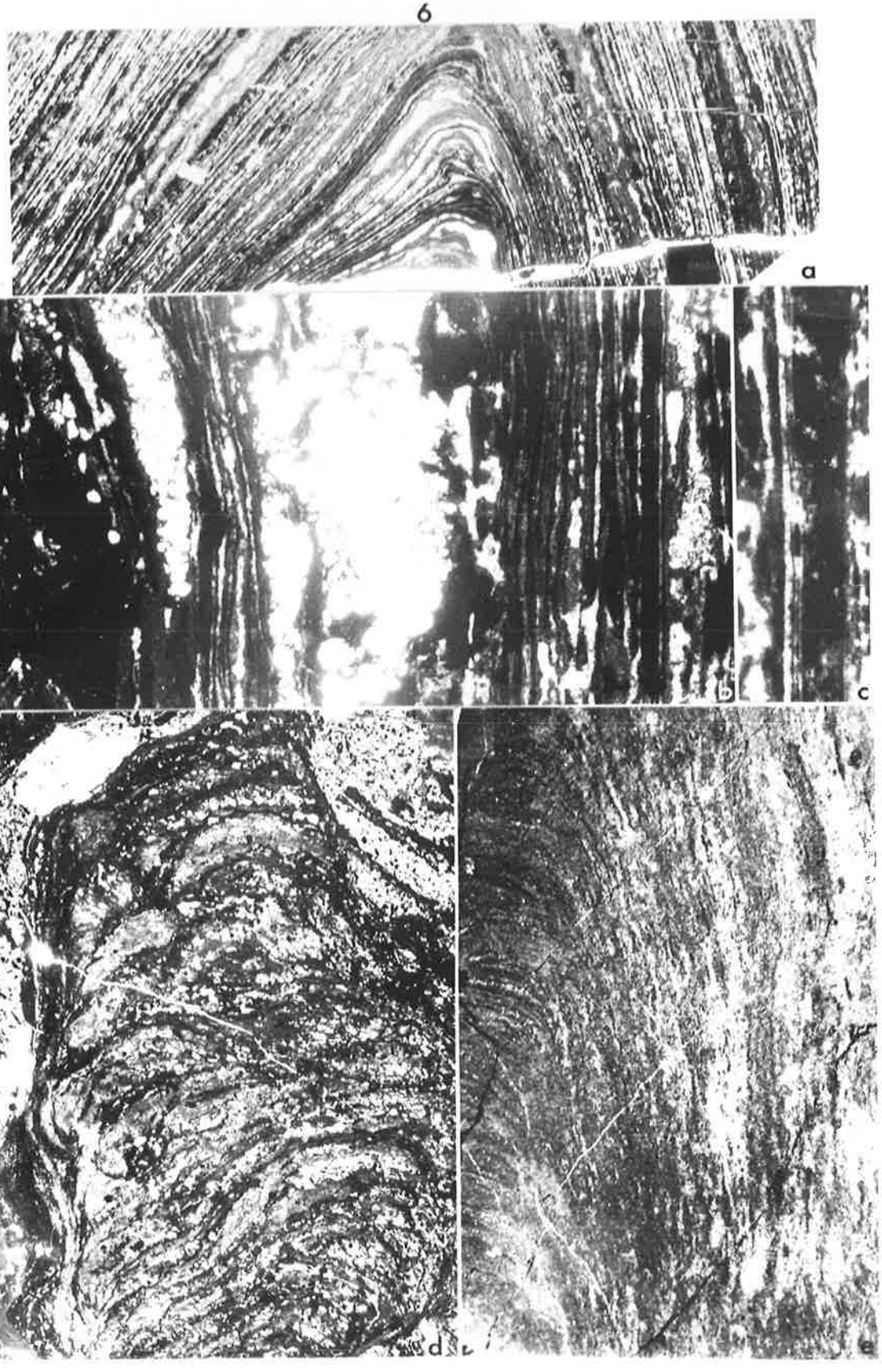
a
b
c
d
e

Plate 7

Dead stromatolites in the intertidal zone of Shark Bay, Western Australia

a: Looking baywards, north of Goat Point; elongate cumuli grade into scattered columns; there are some growing stromatolites in the foreground and middle distance.

b: Looking shorewards, north of Goat Point; the large stromatolite in the left foreground is about 2m wide and in front of it are two growing stromatolites.

c: Looking shorewards, Goat Point; the dark flats in the background are covered by algal mats such as that in plate 8c.


C

Plate 8

Growing stromatolites in the intertidal zone of Shark Bay, Western Australia.

a,b: Mamillose algal mats trapping calcilutite; Gladstone area; between the stromatolites is ripplemarked coquina and calcarenite. a, knife handle is about 15cm long. b, close-up showing foetid sediment below the few millimetres of living algal mat.

c: Eroded rugose algal mats trapping calcarenite, north of Goat Point. Here erosion of continuous algal mats leads to the formation of discrete stromatolites. Pencil for scale.

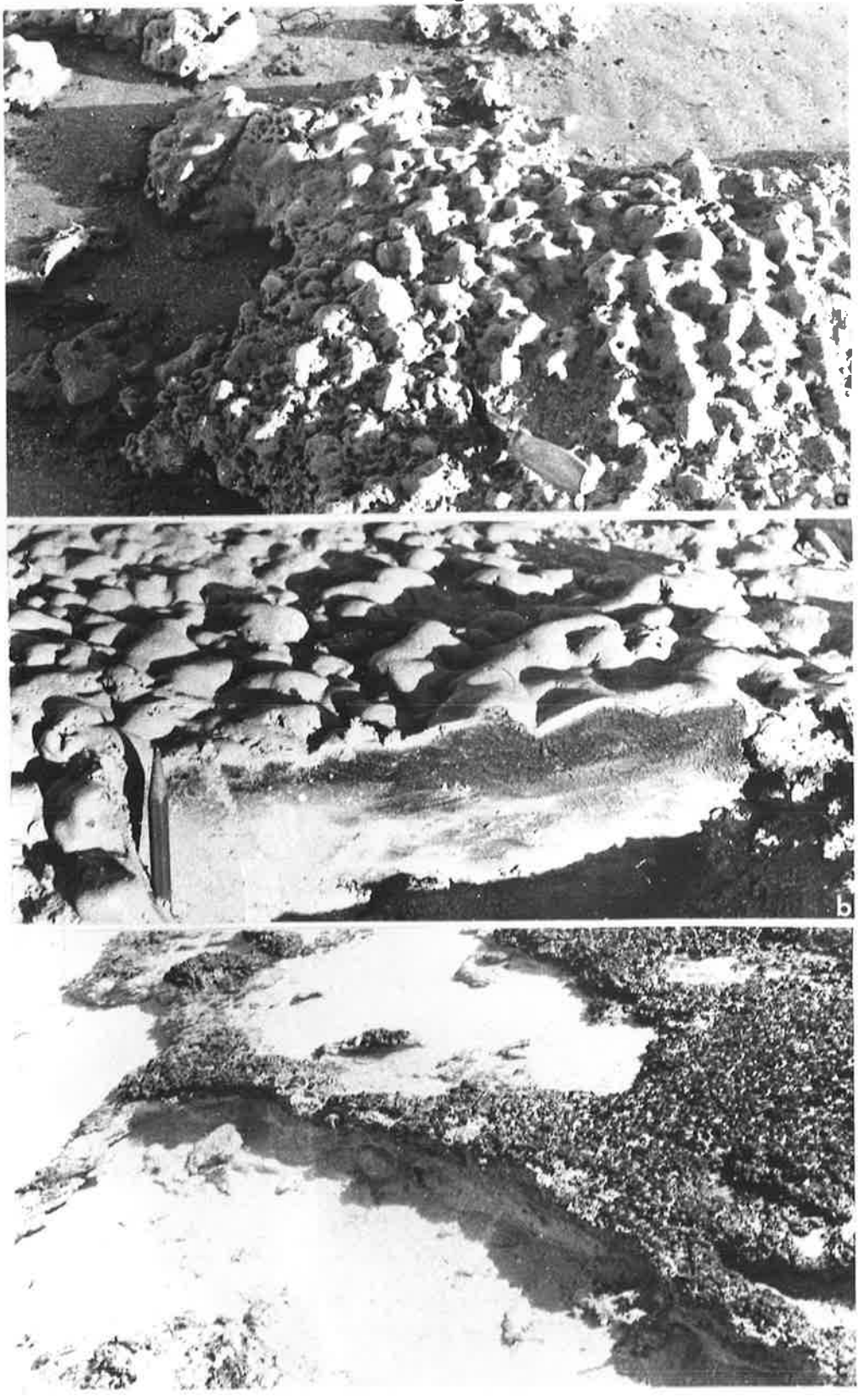
b

Plate 9

Stromatolites and sediment, Shark Bay, Western Australia.

a,b: Growing columnar stromatolites, a 33cm high, b about 30cm high; the lower quarter of the column a was buried in sediment. The dark patches are living algae. Upwardly directed surfaces are coated with calcarenite.

c: Dead stromatolite with a prominent ribbing formed by overhanging coarse laminae, north of Goat Point.

d: Eroded, dead stromatolites with large intraclasts between them, wavecut platform, uppermost intertidal zone, north of Goat Point. The notebook is 10cm wide.

e: Longitudinal section of a growing columnar stromatolite like those in a and b. Note the crude, coarse layering, included shell debris and lack of a wall. S534.

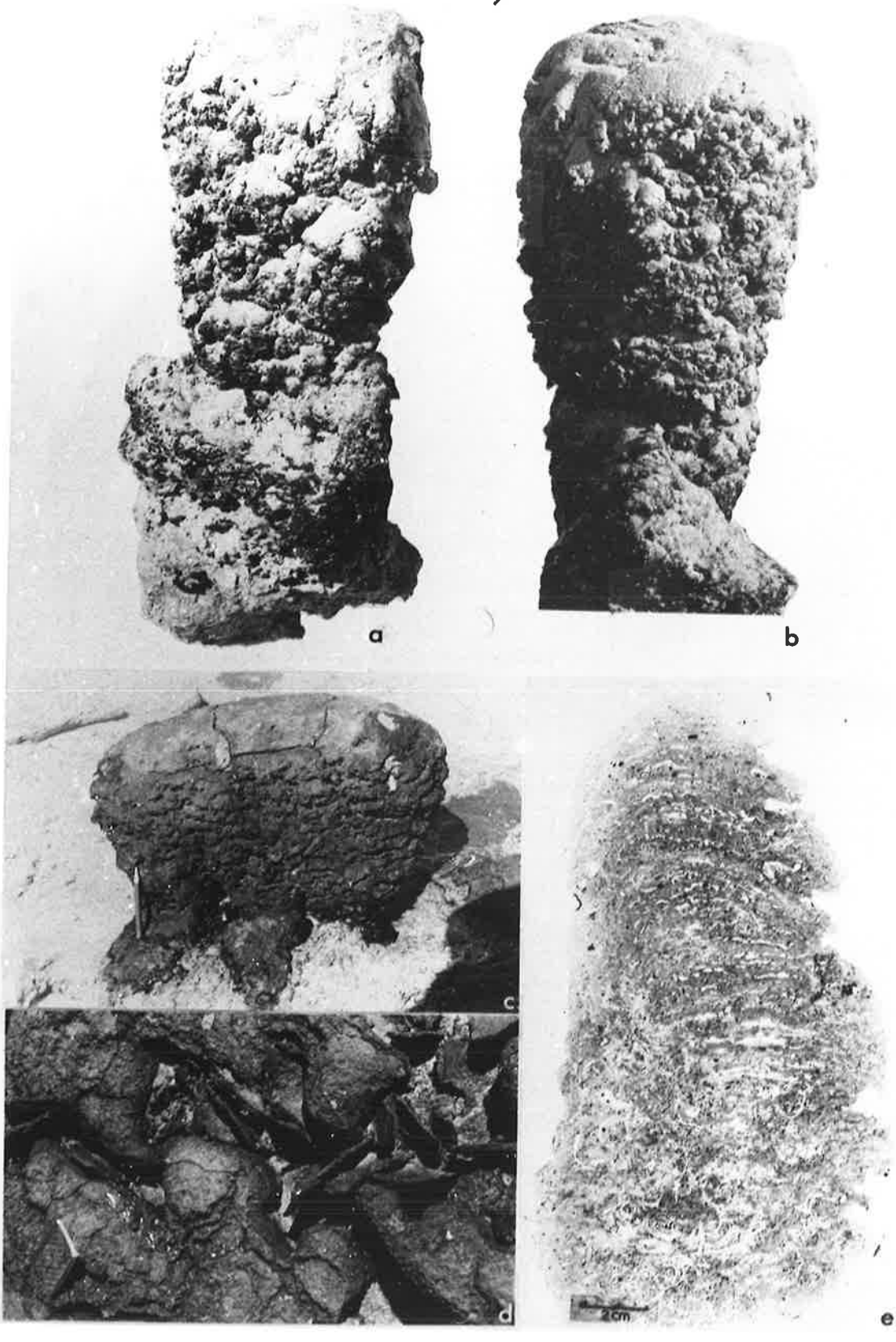
a
b
c
d
2cm
e

Plate 10

Conophyton

a-c: Conophyton basalticum, Antrim Plateau Volcanics. a, crestal zone, x 3.1 (CPC11314); despite the very poor preservation marked lamina thickening is visible. b, longitudinal section of the same specimen as in a, x 0.6. c, longitudinal section showing the full width of a column; x 0.5 (CPC11315).

d,e: Conophyton garganicum australe. e, disconformity surface almost parallel to bedding, showing transverse sections of columns. Overlying green shale bed visible in left foreground. Hammer handle 32cm long. d, close up of one of the columns in e; note the irregular lamina shape and the grit in several parts of the column.

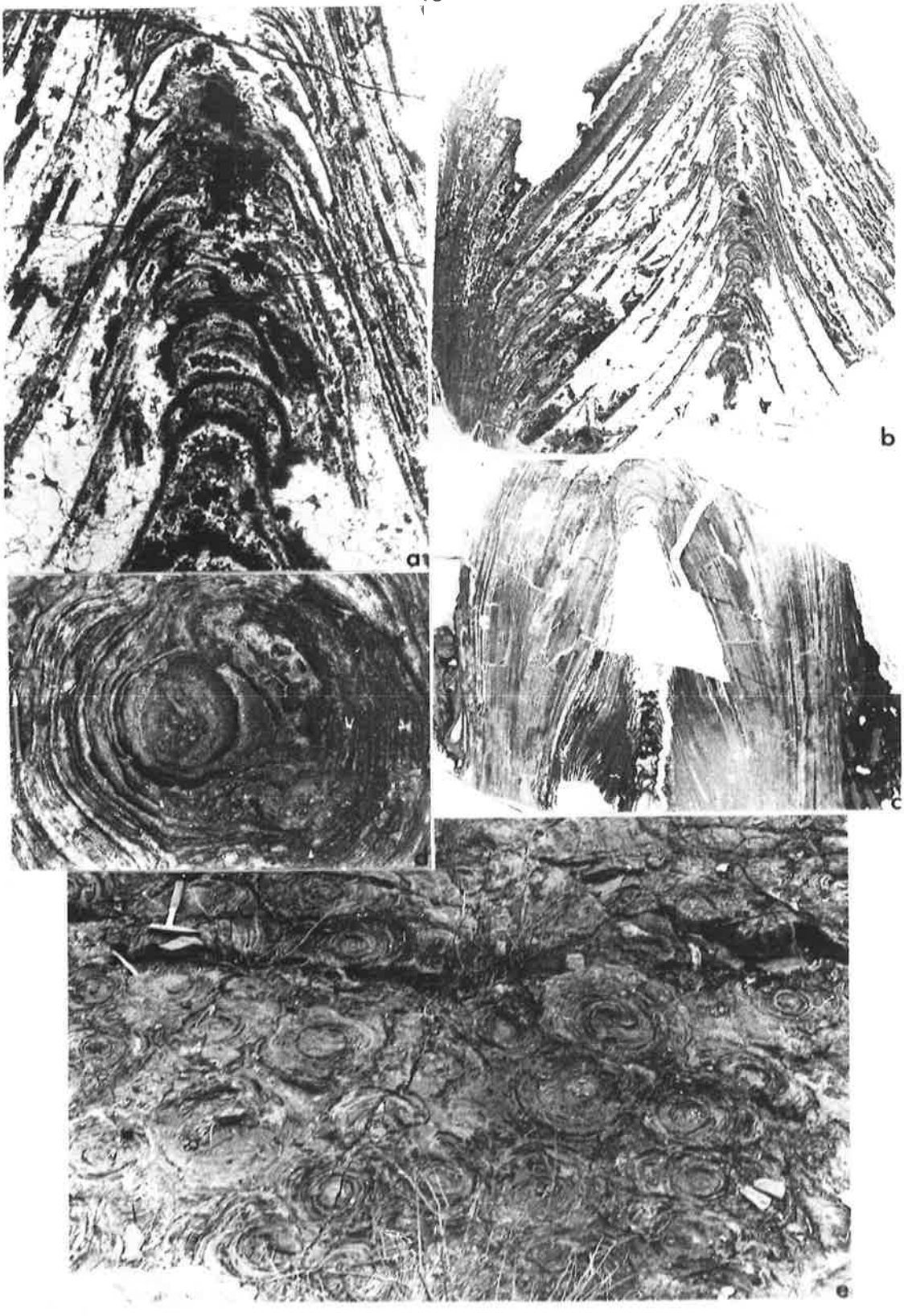
a1
b
c
e

Plate 11

Conophyton garganicum; a,b,d are thin sections, c and e cut faces.

a,b,d,e: *C. g. australe*, Irregully Formation, Nullagine Basin; longitudinal sections.

a: Crestal section; note contorted laminae and patches of coarse detritus at column margin; x 0.7 (S188).

b: Crestal section of a column with very steeply dipping and locally deformed laminae, and a very irregular margin; x 0.7 (S187).

d: Outer third of a column; note the folded laminae on the left, nappe-like fold on the right and coarse detritus along the margin; x 0.8 (S189).

e: Crestal section showing a small diapir near the top; x 1.4 (S190).

c: *Conophyton garganicum*, ?Tooganinnie Formation, McArthur Basin. The only known example of branching in conophytons. The section is not crestal. x 0.3 (F23520).

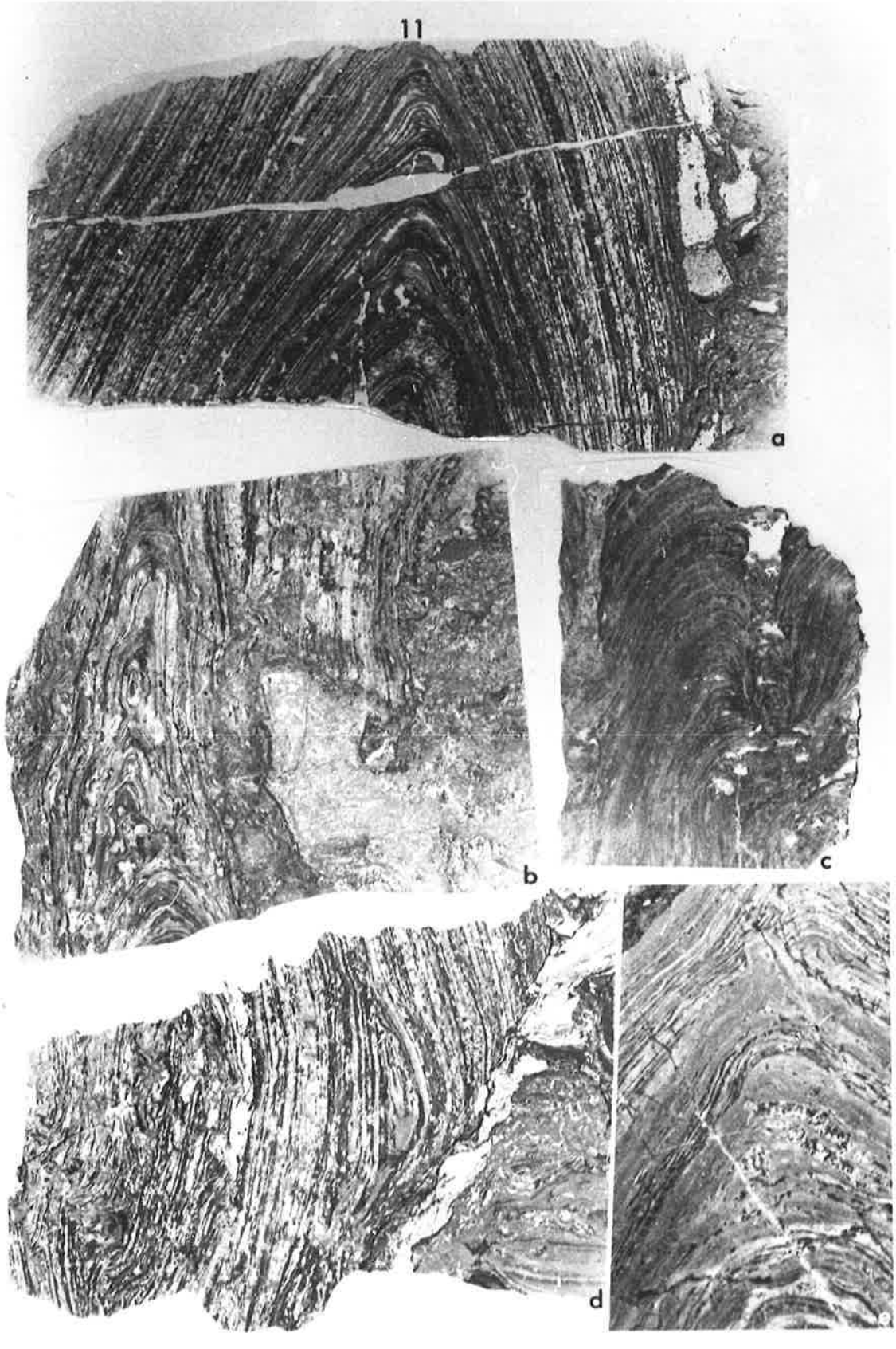
11
a
b
c
d

Plate 12

a: *Conophyton garganicum*, Reward Dolomite, McArthur Basin. Crestal section, cut face; silicified specimen. x 0.7 (CPC11319).

b,c: *Conophyton* cf. *gaubitza*, Antrim Plateau Volcanics; crestal sections. b, crestal zone; x 3.5. c, almost the full preserved width of the same column; note the lamina flexures; x 0.6 (GSWA F5022).

d,e: *Jacutophyton howchini*, Mount Baldwin Formation, Georgina Basin; longitudinal sections. e, shows central *Conophyton*-like column from which radiate branches; x 2 (CPC11316). d, column which was possibly a branch, with small digitate projections (which are not the result of secondary alteration); x 1.1 (CPC11317).

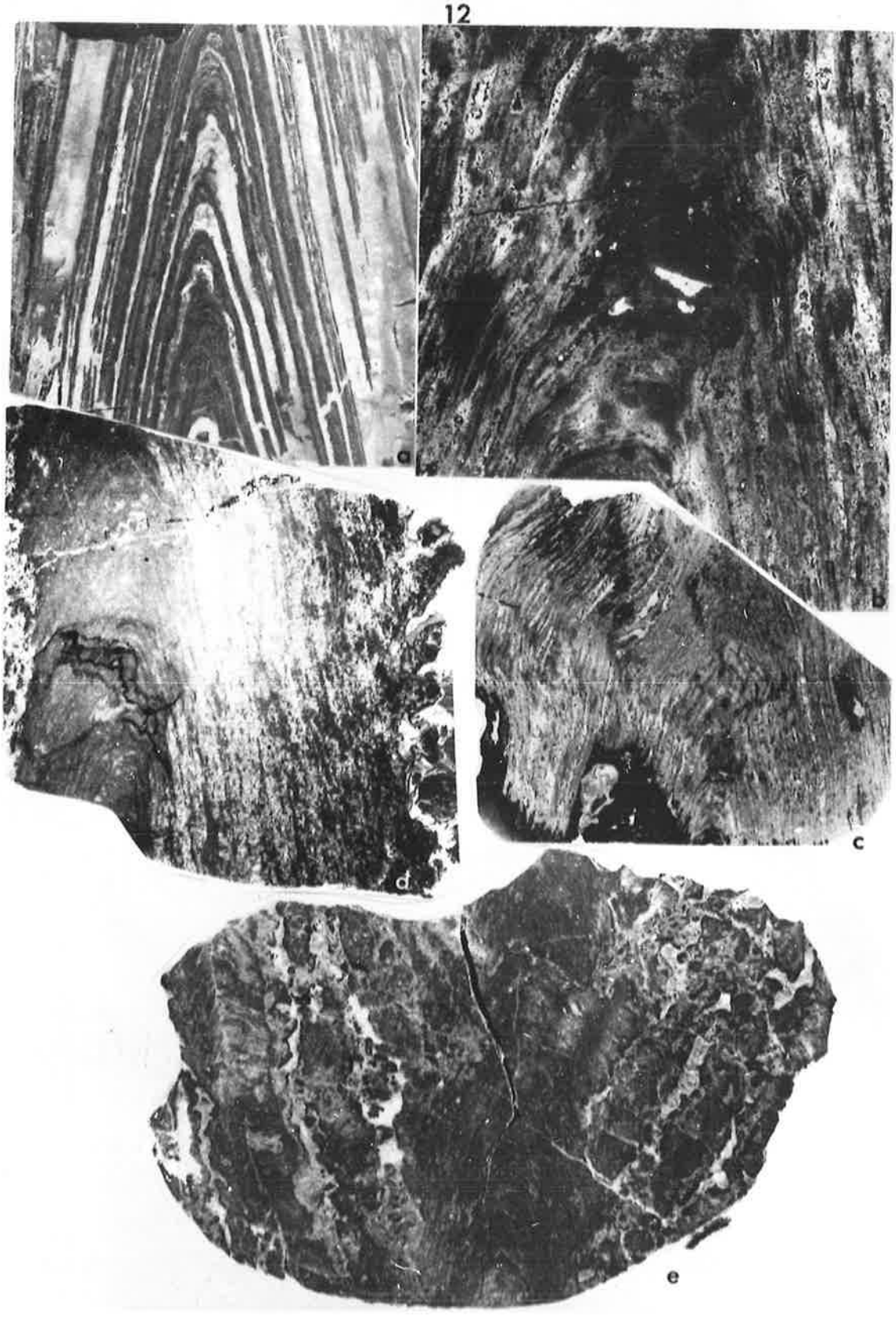
a
b
c
d
e

Plate 13

Acaciella australica in outcrop, Bitter Springs Formation, near Jay Creek, Amadeus Basin; the sections are approximately perpendicular to bedding and are all parts of one biostrome.

a,b,c,e: These all show parts of wide bioherms with broad basal columns which by α parallel branching form numerous narrow columns. Figure 12c is a sketch which includes the bioherm shown here in a.

d: A hemispherical bioherm with radially arranged columns. The sketch of the hemispherical bioherm in figure 12b is based on this photograph.

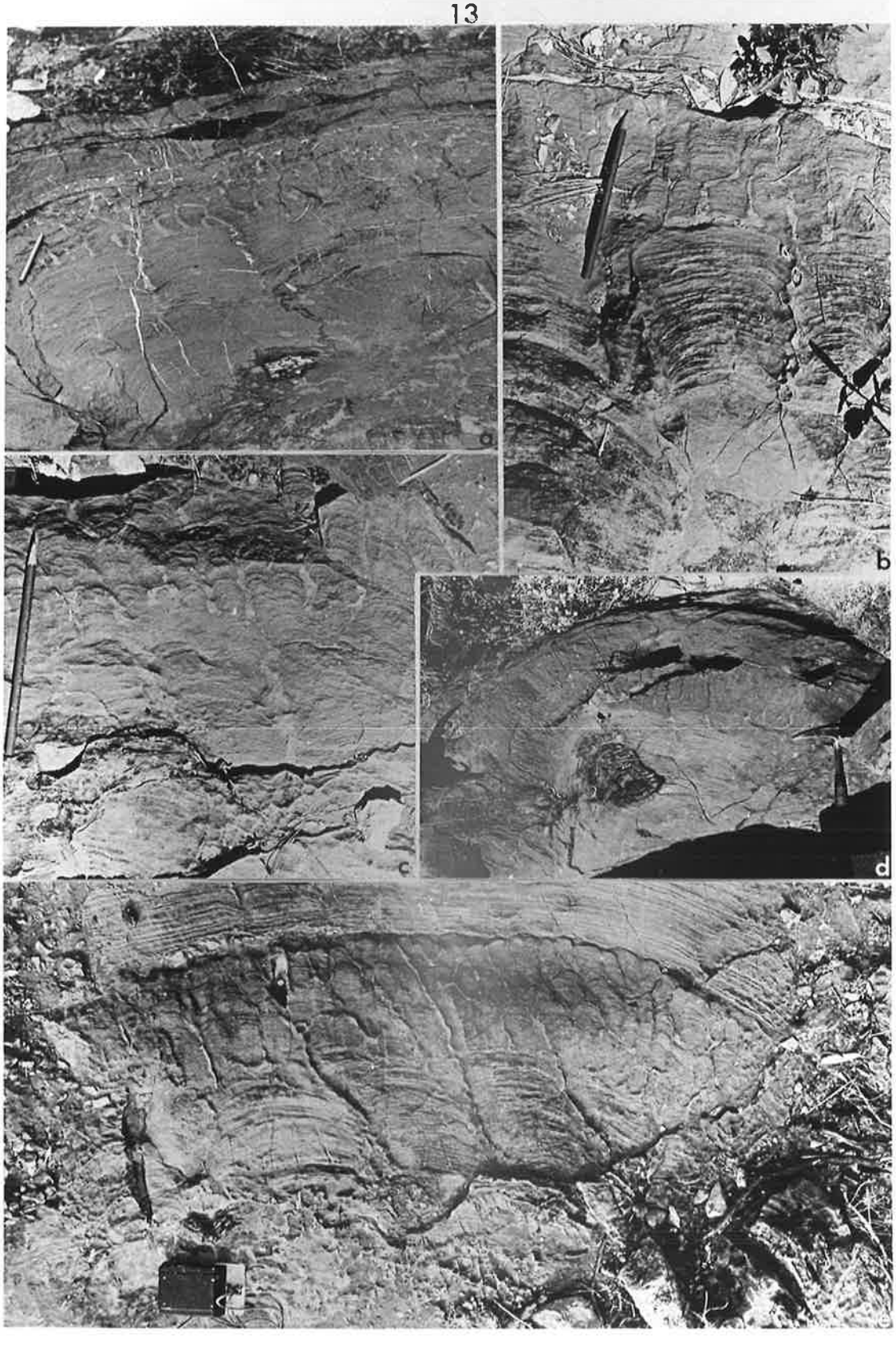
a
b
c
d

Plate 14

Acaciella australica, Bitter Springs Formation, Amadeus Basin.

a: Two contiguous bioherms near Chewings' locality, about ½ mile west of Acacia Well; section perpendicular to bedding. Hammer handle 32cm long.

b: Longitudinal thin section; specimen from near Jay Creek; x 0.5 (S131).

c,d: Bioherms in one biostrome in Katapata Gap. The specimens of figures 13 and 14a-e,i are from the bioherm in c.

e: Syntype of *Cryptozoön tessellatum*; thin section, x 1.4 (S22).

f: Syntype of *Cryptozoön australicum*; thin section, x 0.8 (S20).

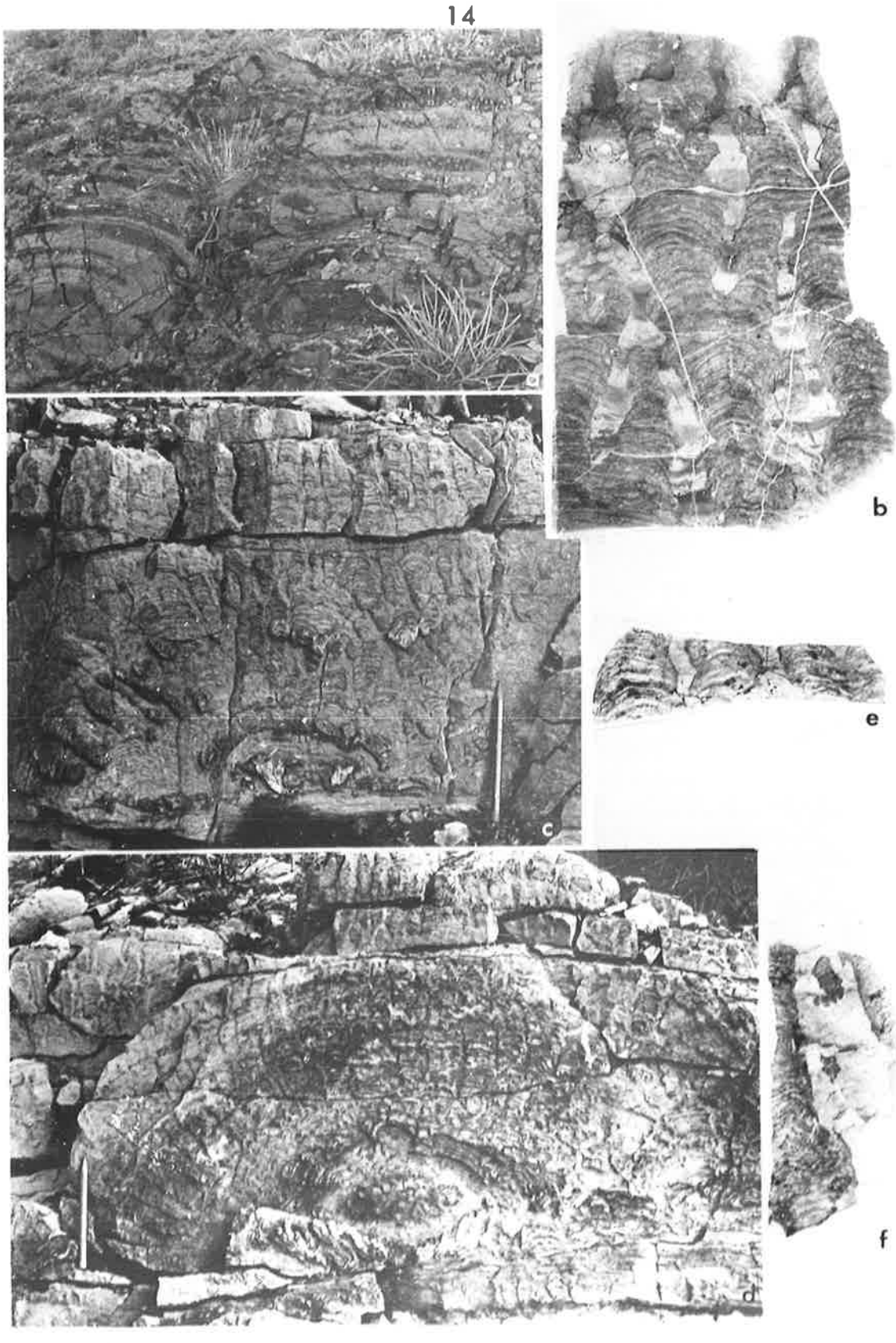
b
e
c
d
f

Plate 15

a,b: Longitudinal slabs of Acaciella australica, Bitter Springs Formation, Jay Creek, Amadeus Basin. Note the α and β parallel branching. a x 0.4 (S131), b x 0.5 (S132).

c-e: Alpheringa parrina, Pillingini Tuff, Nullagine Basin; thin sections. Note the microbioherms in d. c x 3 (S95a), d x 1.1 (S95b), e x 0.9 (S95c).

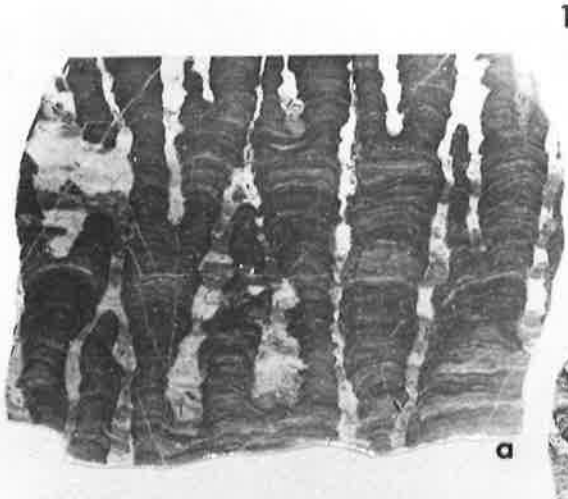

a

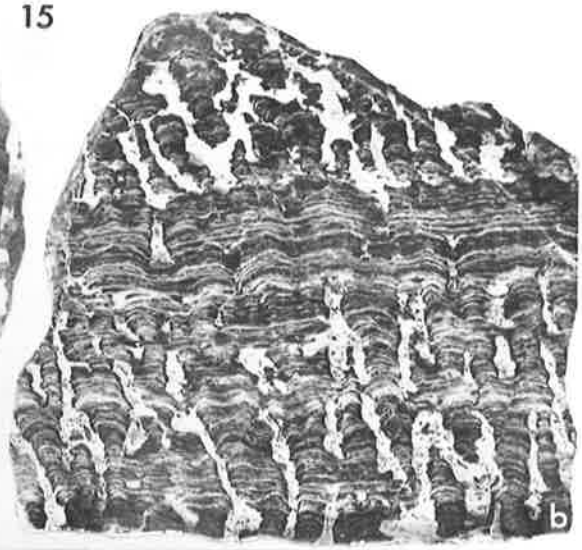

b

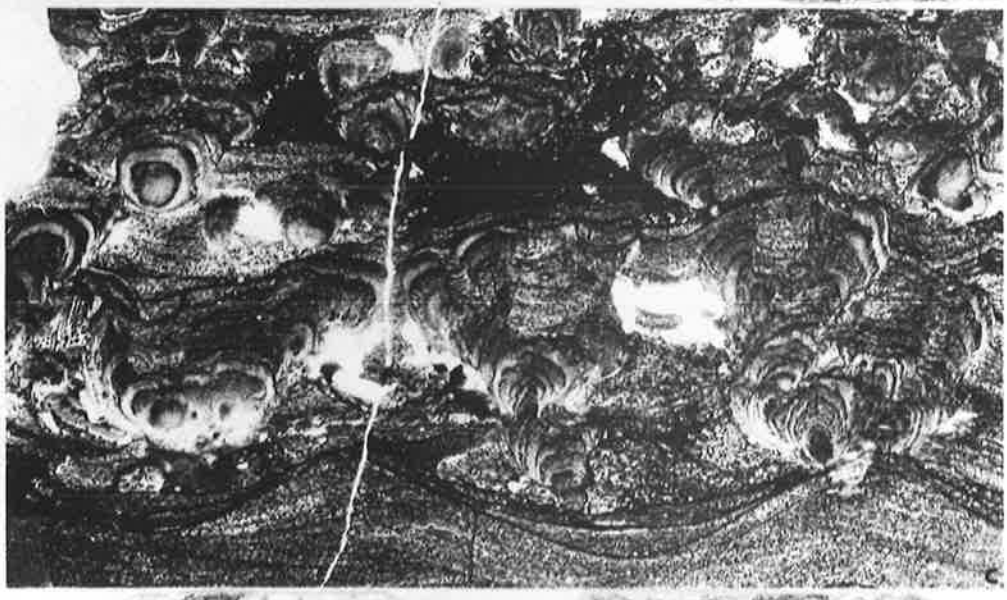

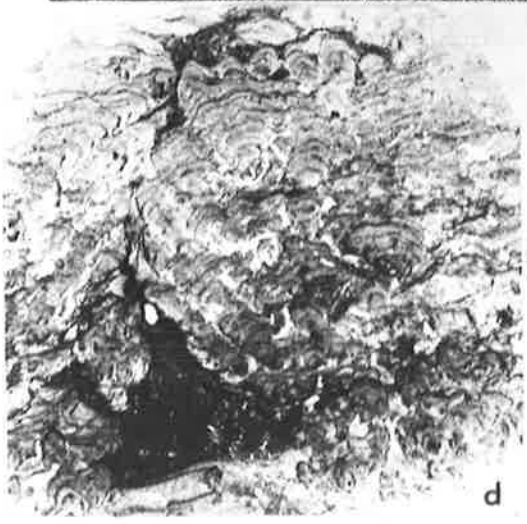

d

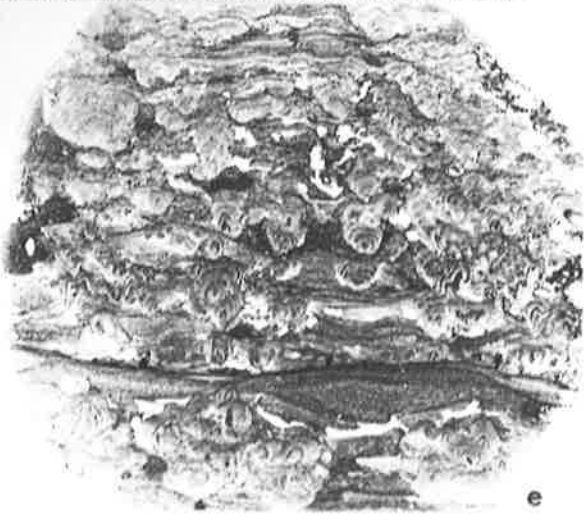

e

Plate 16

Alcheringa

a-c: Alcheringa narrina, Pillingini Tuff, Nullagine Basin. a, cut face normal to bedding showing a microbioherm; x 1.1 (GWSA 11487). b,c, thin sections, normal to bedding; b x 16 (S95b), c x 6 (S95a).

d,e: Alcheringa f. nov., Ventersdorp "System", South Africa; thin section (S535). Note the resemblance between the large cumulus in e and that in the bottom right centre of a. The pale lenses in e are coarse, sparry carbonate which probably infilled former gas cavities resulting from the life processes of the building algae. d x 3, e x 3.5.

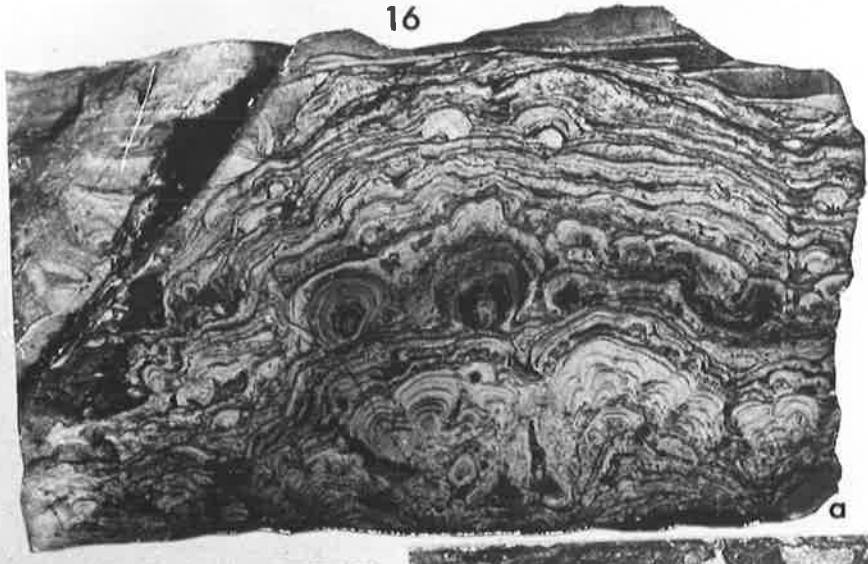
a

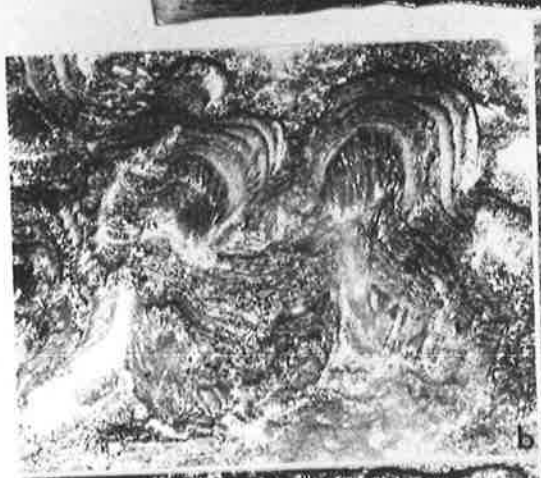
b


d


c


e

Plate 17

Baicalia capricornia in outcrop, Irregully Formation, Nullagine Basin; all sections are normal to bedding.

a,b,d,e: East of Maroonah Homestead. The outcrop in a is about 2.5m high; note the broad columns in the middle, where there are also extensive bridges. b is the upper part of a biostrome. e shows ∝ parallel branching near the base of a biostrome.

c: Northern entrance to the gorge of Irregully Creek; identity not certain.

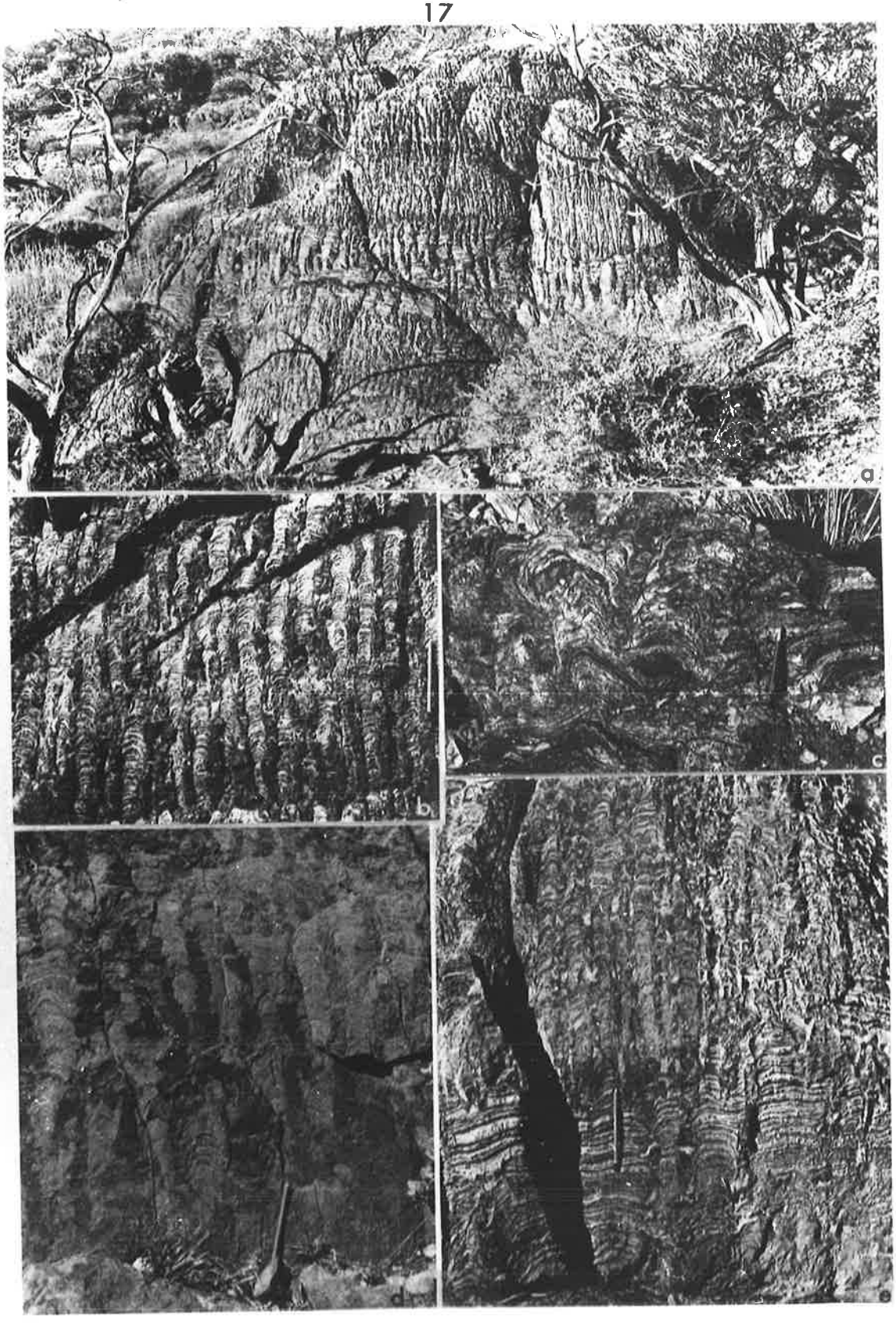
a
b
c
d
e

Plate 18

a,b: Baicalia capricornia, Nullagine Basin. a, face probably parallel to bedding showing brecciated, disoriented columns in the Devil Creek Formation. b, longitudinal thin section of a specimen from the Irregully Formation east of Maroonah Homestead; x 0.6 (S200).

c,d: Basisphaera irregularis, Bitter Springs Formation, Jay Creek, Amadeus Basin; longitudinal thin sections. c x 0.7 (S346), d x 0.1 (S136).


a


b


c


d

Plate 19

Stromatolites from the Bitter Springs Formation, Jay Creek, Amadeus Basin

a,c,d,e: Basisphaera irregularis; field and cut sections normal to bedding. a shows broad columns branching into narrow columns (all columns outlined in ink). c shows several contiguous broad columns; compass is about 6cm wide. d and e show cumulate individuals at the base of the same bed which contains the columns in a and c; d x 0.5 (S135).

b: Boxonia pertaknurra; thin section normal to bedding of broad, basal columns. Note the wall on the overhanging edge of the column on the left. x 0.8 (S354).


a


b


c

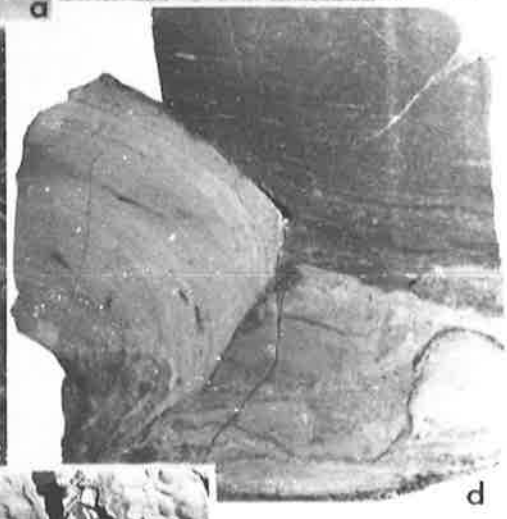
d


e

Plate 20

Stromatolites from the Bitter Springs Formation, Amadeus Basin.

a-c: Boxonia pertaknurra. a and b are sections normal to bedding of biostromes, a near Ross River Tourist Camp, b near Jay Creek. In a the column shape is greatly modified by stylolites. c is a longitudinal slab of a Jay Creek specimen showing branching from broad columns; the columns in the upper right are slightly oblique to the section; x 1 (S137).

d,e: Inzeria intia outcrops normal to bedding near the Ross River Tourist Camp. d shows contact between stages II and III. e shows a bioherm, with the broad columns of stage II outlined in ink; these branch into the narrow columns of stage III, forming the upper part of the photograph.

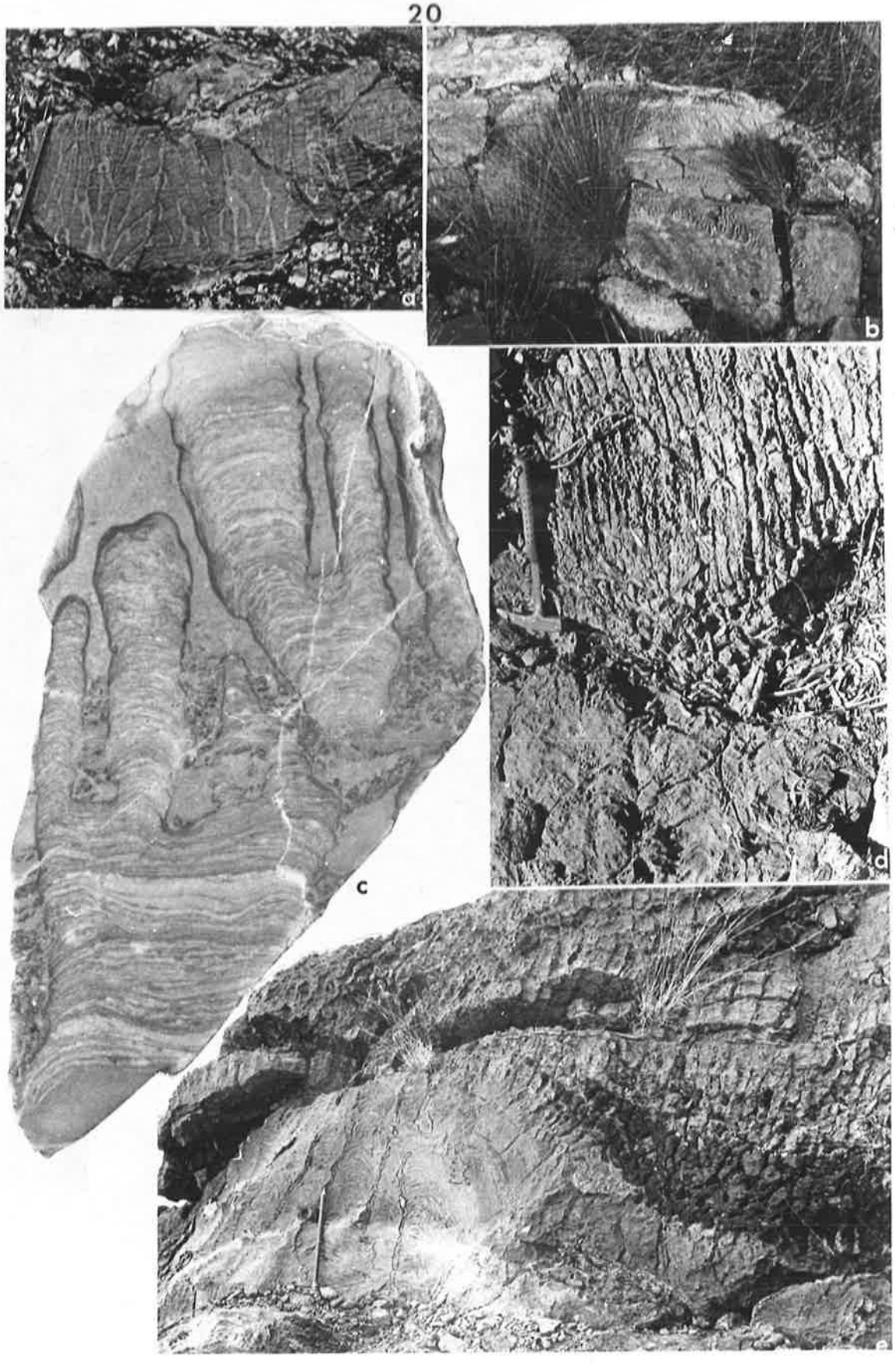
a
b
c
d
e

Plate 21

Inzeria intia in outcrop, Bitter Springs Formation near Ross River Tourist Camp, Amadeus Basin.

a: Looking west along the north side of the ridge arrowed in plate 33b. The narrow columns of stages II and III in the main *I. intia* biostrome make horizontal bands across the middle of the photograph; here they are not perpendicular to the bedding, which dips south (left) at about 40°.

b,c: Bioherms within the biostrome in a. In b the margins of two bioherms are visible; stages I and II columns are invisible. c shows stage II columns outlined in ink; the curved branching zone is visible.

d: *I. intia* I at the base of the biostrome shown in a.

e: Isolated *I. intia* I just below the main biostrome.

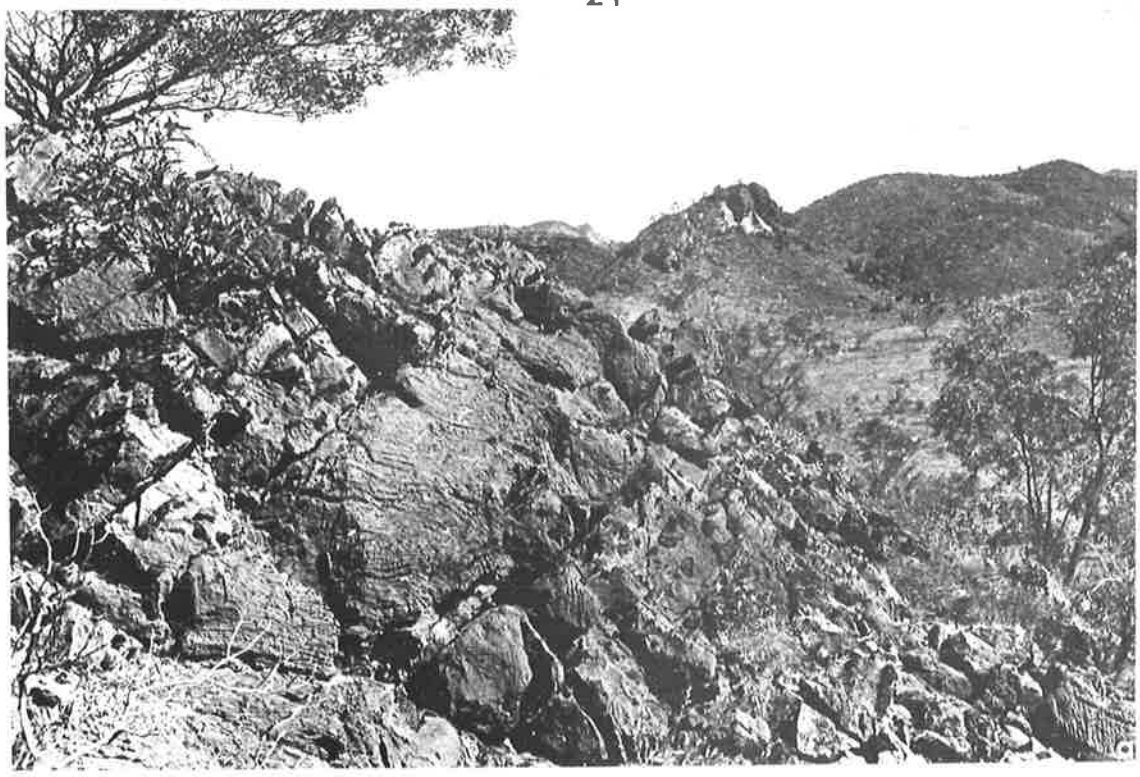

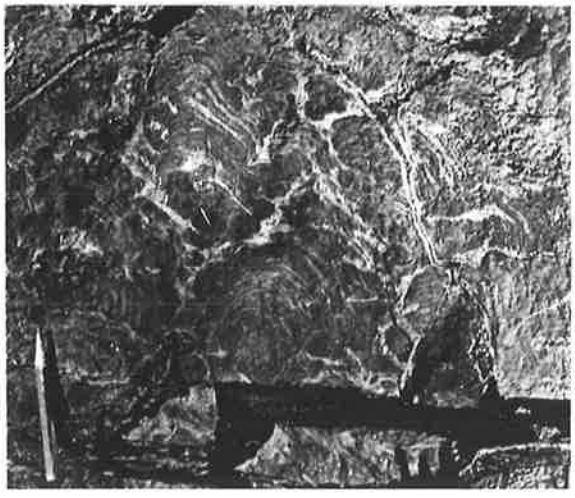

Plate 22

Inzeria intia, Bitter Springs Formation, near Ross River Tourist Camp, Amadeus Basin.

a: *I. intia* IV in outcrop, top of the main biostrome; arrows indicate projections.

b: *I. intia* III longitudinal thin section. Note walls and niches. x 0.8 (S143).

c: Outcrop showing transverse sections of *I. intia* III columns. These resemble desiccation cracks but the column laminae are convex-up, not the reverse as in desiccation cracks.

d,e: Two slabs from several centimetres apart in the same specimen of *I. intia* II reconstructed in figure 21a. d x 0.7, e x 0.7 (S138).

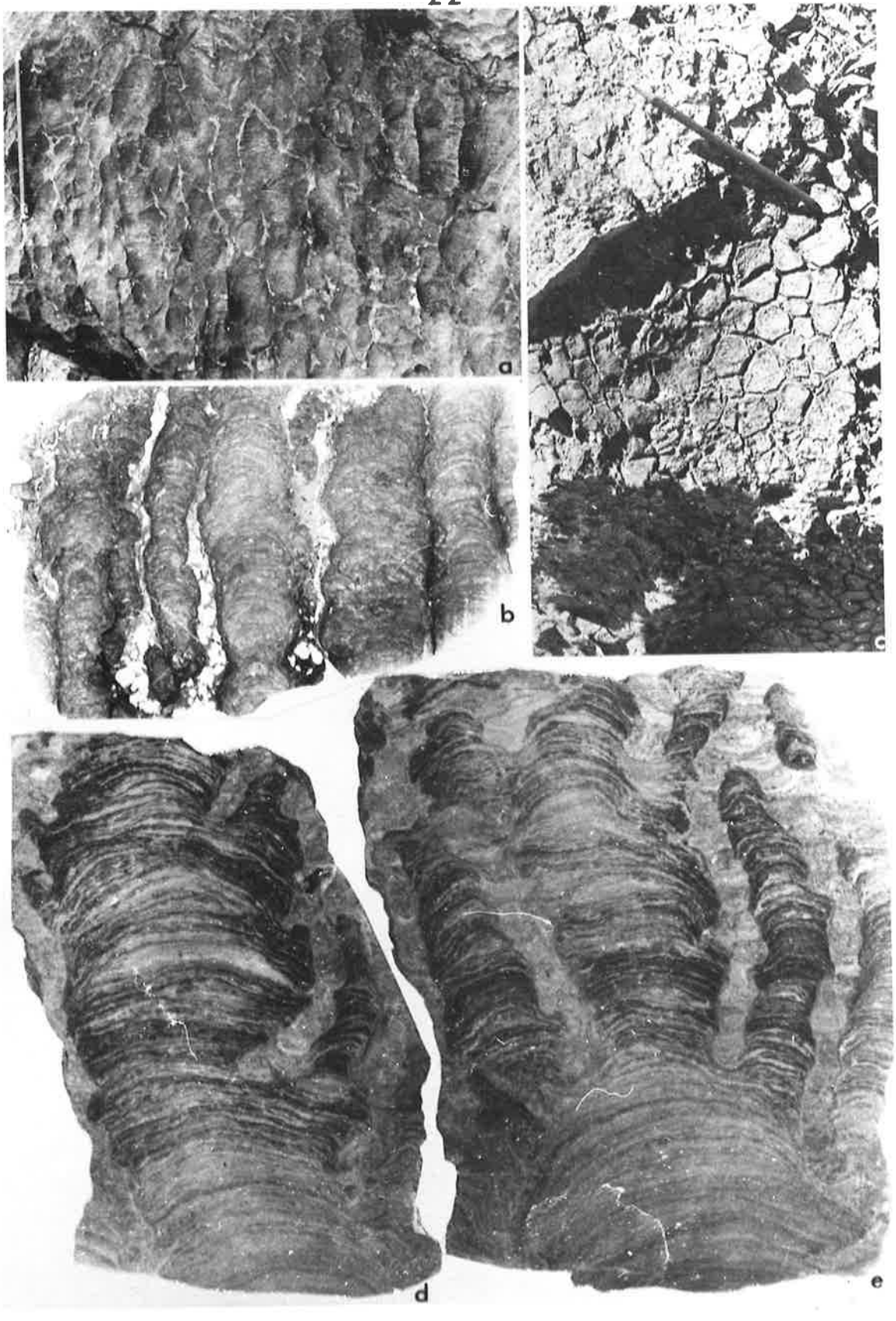
a
b
c
d
e

Plate 23

Inzeria intia, Bitter Springs Formation, near Ross River Tourist Camp, Amadeus Basin.

a: Columns from the branching zone between stages II and III shown in c. Note the wall and partial alteration from homogeneous to grumous laminae; the column on the right is greatly altered. x 3.2 (S141).

b,d: Stage IV columns. A niche is clearly shown in d. b x 0.9, d x 3 (S370).

c: Branching zone between stages II and III.

e: Example of stage II which occurred separately in a thin biostrome lacking other stages. x 0.8 (S369).

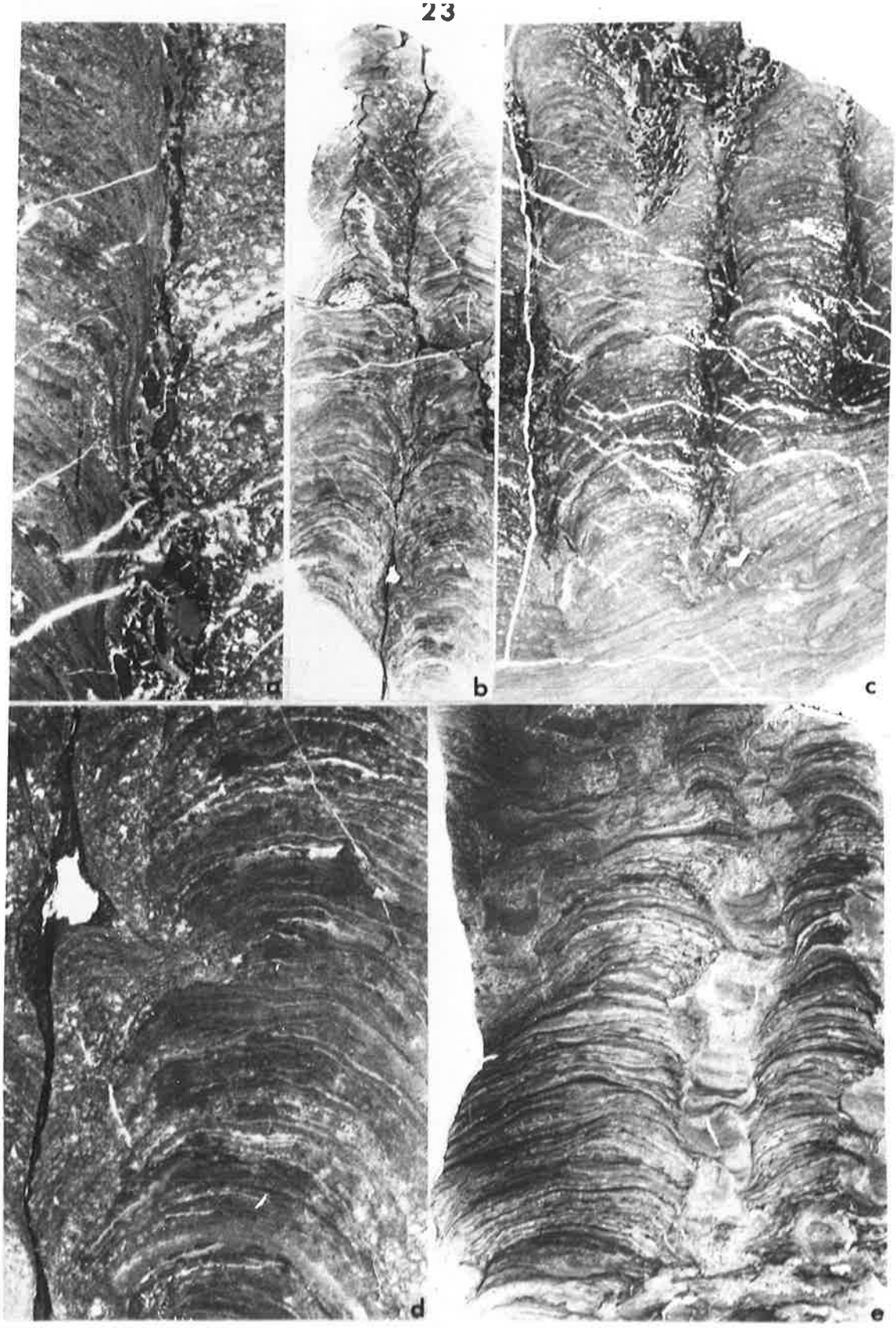
a
b
c
d
e

Plate 24

Bitter Springs Formation stromatolites,

near Jay Creek, Amadeus Basin.

a-d: Jurusania chewingsi; a and b are the same bioherm visible next to the figure in plate 31a.

a: A section of the whole bioherm normal to bedding (which dips away from the observer at about 70^{o}).

b: The gradational zone from the lower, flat-laminated part to the upper, columnar part (which forms the pale grey upper half of the photograph).

c: Thin section parallel to the columns of the gradational zone; x 0.7 (S134b).

d: Longitudinal thin section of a specimen from the columnar part of the bioherm shown in a; x 0.7 (S134a).

e,f: Kulparia alicia, in outcrop sections normal to bedding. The specimens reconstructed came from the areas shown here.

e: The bases (on at the bottom of the pencil) and junction (vertical line in the centre of the photograph) of two bioherms.

f: Columns in the middle of the bioherm on the left in e.

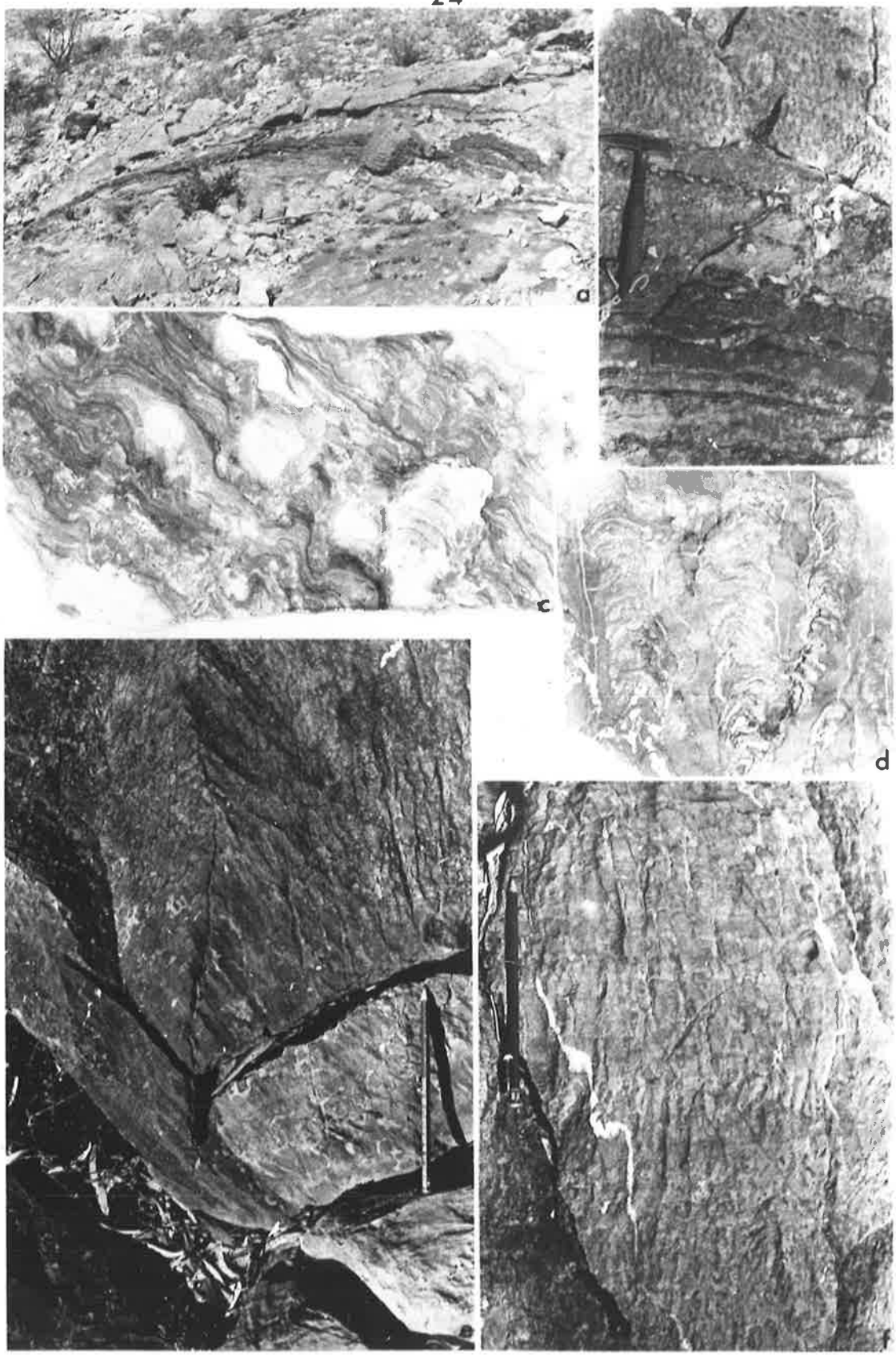
a
c
d

Plate 25

Sections of stromatolites from the Bitter Springs Formation, Jay Creek, Amadeus Basin.

a,b: Kulparia alicia longitudinal thin sections. a from near the base of a bioherm, showing narrow columns and numerous bridges; a 1 (S348). b from the central part of a bioherm; x 1 (S347).

c,d: Possible Kulparia alicia from the margin of a bioherm. There is considerable uncertainty in the identity of this specimen; note the divergence and frequent coalescing of columns; the form of the columns from the central part of the same bioherm is uncertain. The multilaminate wall is clearly visible in d. c is in approximately the same orientation as the field occurrence, i.e. a horizontal line is parallel to bedding. c x 1, d x 3.5 (S349).

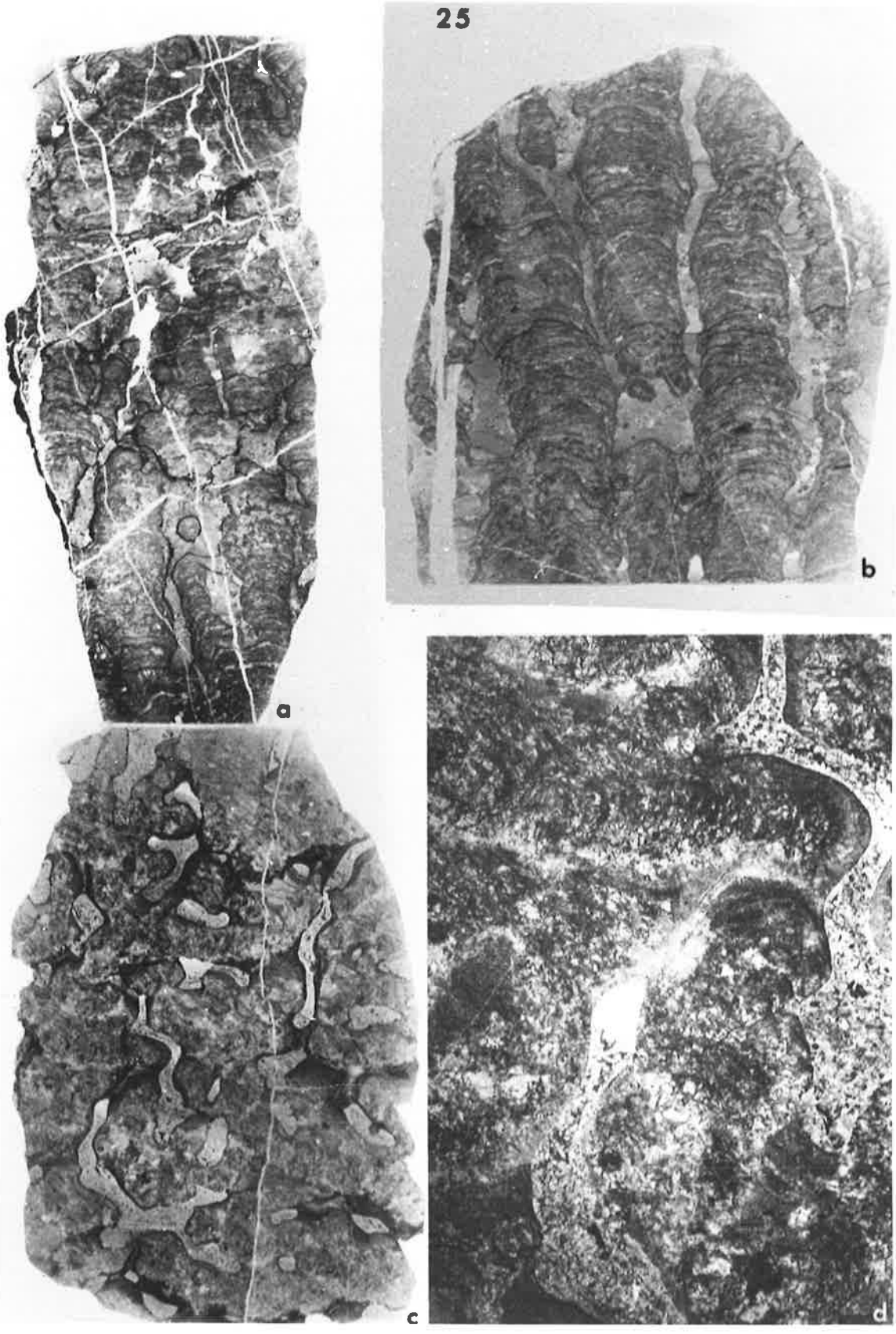
25
a
b
c
d

Plate 26

Linella avis in outcrop, Bitter Spring Formation, near Jay Creek, Amadeus Basin; all sections are perpendicular to bedding and are parts of the same biostrome.

a: Contact between two bioherms.

b: Almost the whole thickness of the biostrome.

c: The whole thickness of the biostrome, showing a flat-laminated, slightly irregular substrate.

d: Columns radiating from a mound in the substrate.

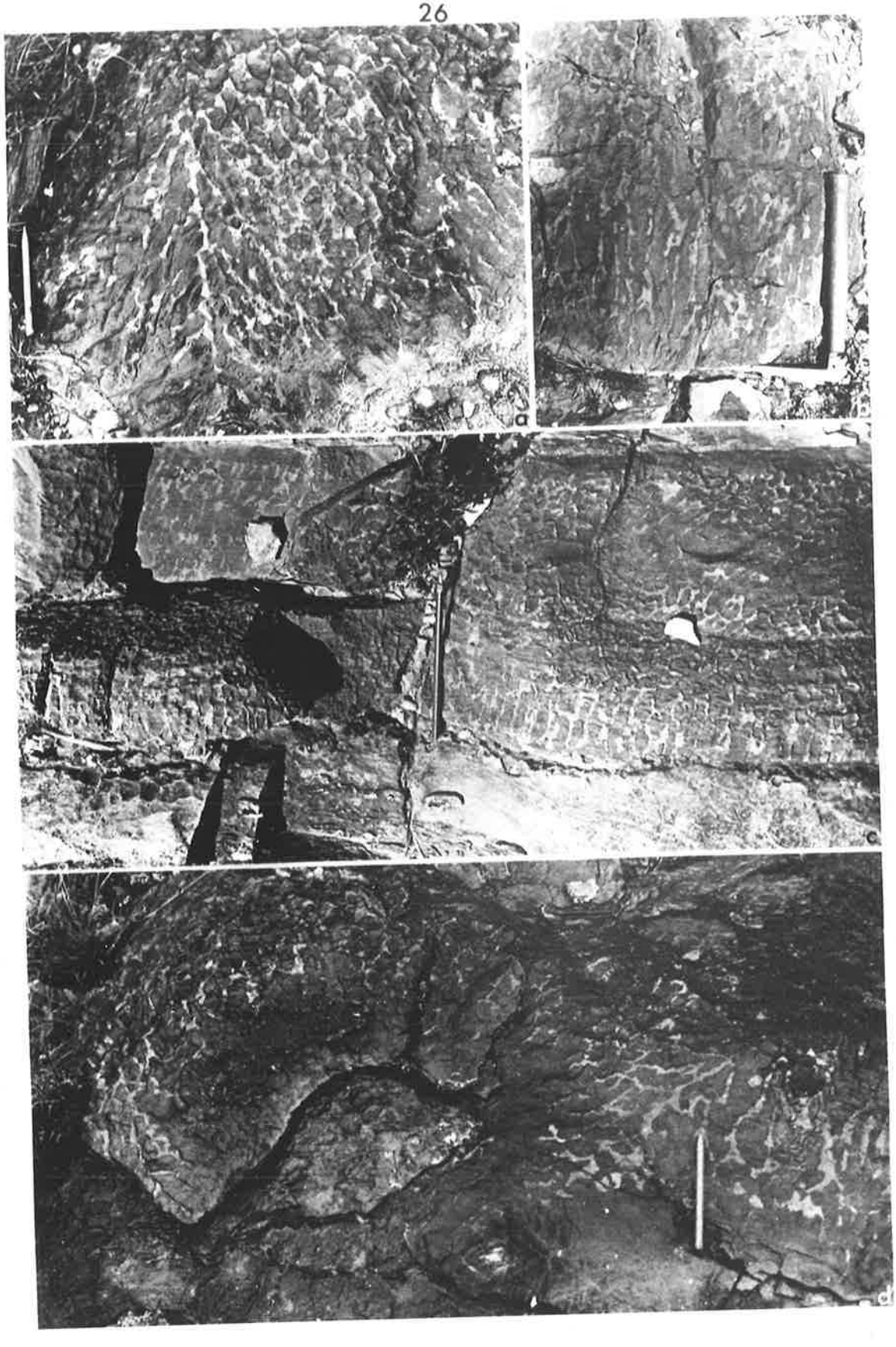
a
b
c
d

Plate 27

Linella avis, Bitter Springs Formation, near Jay Creek, Amadeus Basin.

a: Outcrop section normal to bedding, showing the top of a biostrome.

b: Slab cut parallel to columns (columns are largely calcite, interspace fillings largely dolomite); x 0.5 (S127).

c: Longitudinal thin section; note the gnarled, tuberous columns; x 0.75 (S127).

d: Cut normal to bedding, showing columns branching off a cumulus; x 0.4 (S378).

a

b

c

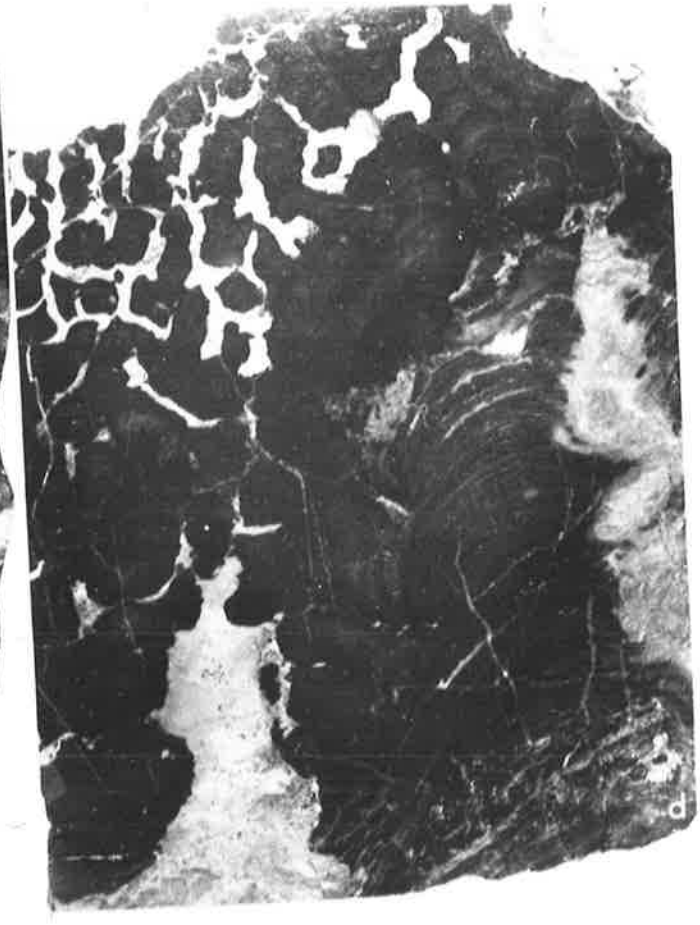

d

Plate 28

a-c: Madiganites mawsoni, Jay Creek Limestone, Pertaoorta Group, Amadeus Basin; longitudinal thin sections.

a: This is the left central column visible in c; note the thick laminae and slightly altered column margins; x 2 (S46).

b: A pseudocolumnar and many-bridged columnar specimen of M. mawsoni; x 0.9 (S364).

c: Specimen with well developed branching columns; x 0.9 (S46).

d: "Collenia australasica" of Edgell (1964) - unnamed in this thesis; longitudinal thin section. Note the steeply convex laminae; x 1.5 (GSWA F5015). Duck Creek Dolomite, Nullagine Basin.

e,f: Minjaria pontifera, Bitter Springs Formation, near Jay Creek, Amadeus Basin.

e: Slab cut parallel to the columns; the pale grey is dolomite, dark grey calcite; x 0.5 (S374).

f: Outcrop normal to bedding from within the same biostrome as shown in plate 26. Note the regularity and parallelism of the columns (on the left they are curved). The third and fourth columns left of the pencil branch from a single broad column.

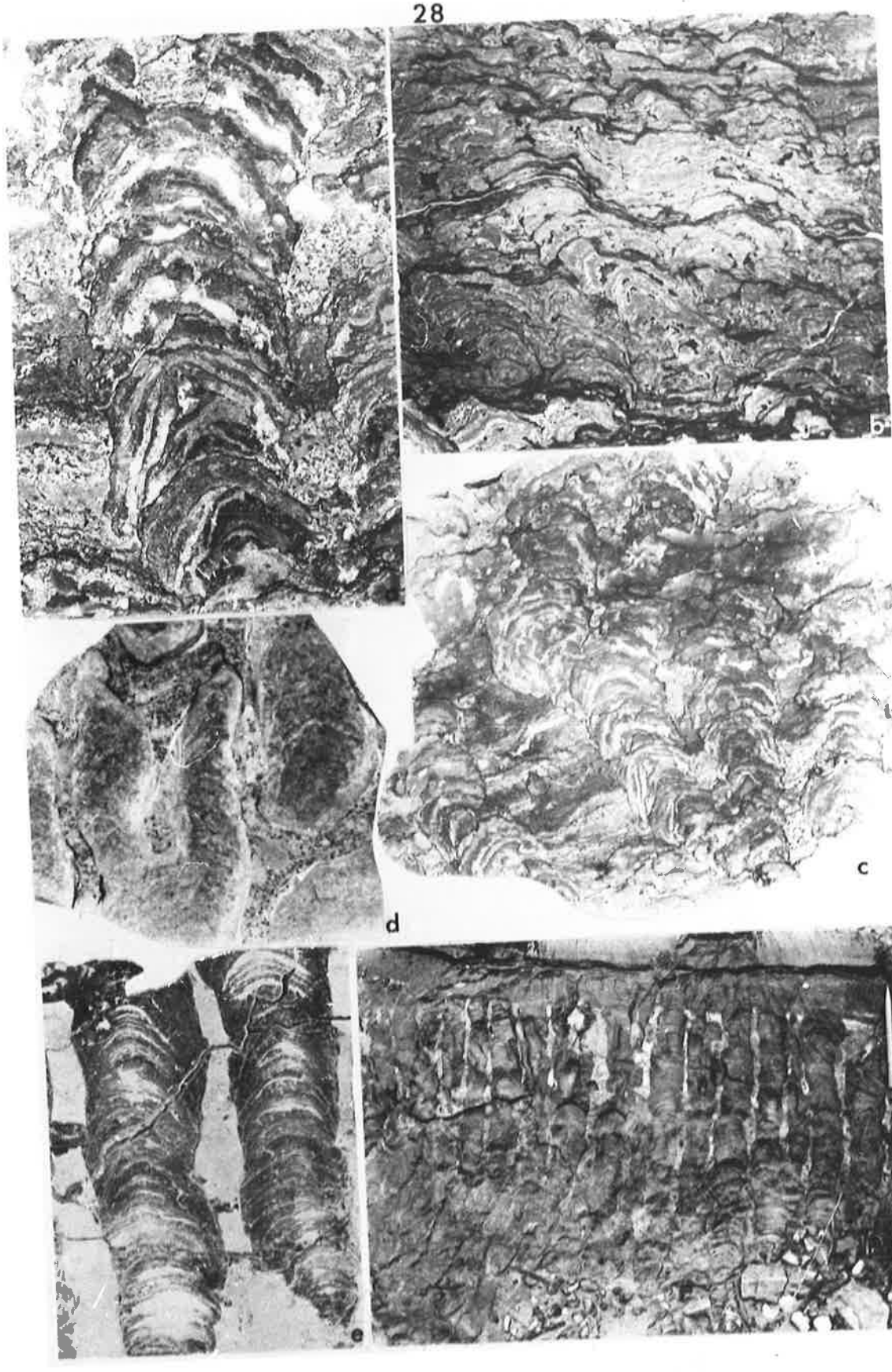
b
c
d
e

Plate 29

Columnar stromatolites, Duck Creek Dolomite, Nullagine Basin.

a,h: *Patomia* f. indet., longitudinal thin section. A patchy wall is visible in h, which is from the lower left of the section in a. a x 0.5, h x 5 (GSWA7155).

b-g: *Pilbaria perplexa*.

b,g: Longitudinal thin sections. The laminae most frequently are steeply convex but in g many are gently convex. b x 0.6 (S203), g x 0.7 (S206).

c-f: Outcrop sections normal to bedding.

a: Outcrop adjacent to a permanent large pool in Duck Creek, east of Mount Stuart Homestead.

c,d,f: Several miles east of the previous locality. Broad, basal columns are visible in e, and branching can be seen in d and f.


a
b
c
d
e
f
g
h

Plate 30

Tunqussia, Amadeus Basin.

a,c,d,e: *Tunqussia erecta*, Gillen Member, Bitter Springs Formation, near Alice Springs.

a: Outcrop normal to bedding showing almost the whole thickness of the biostrome. The specimen shown in e came from near the top of the pencil, that in d from under the bottom of the pencil.

c: Enlargement of portions of the two parallel columns on the left of d, showing the walls; x 3 (S356).

d: Thin section normal to bedding showing irregular columns and cumuli. Figure 28b,c shows other illustrations drawn from this specimen. x 0.5 (S356).

e: Longitudinal thin section of the upper, parallel column part of *T. erecta*. The column margins are greatly altered. x 0.8 (S357).

b: *Tunqussia inna*, Ringwood Member of the Pertatataka Formation, near Ringwood Homestead. Thin section normal to bedding; x 1 (S358).

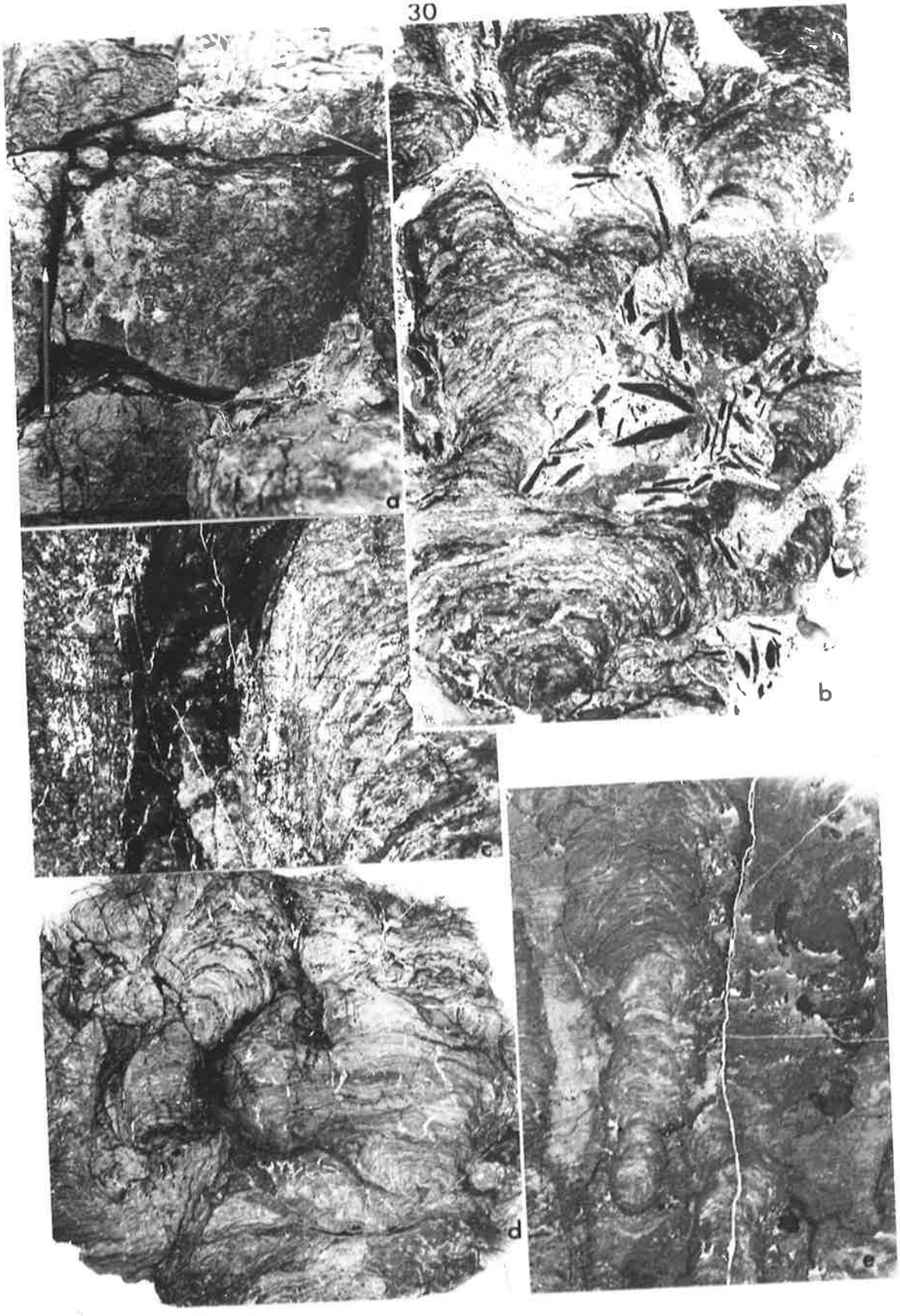
a
b
c
d
e

Plate 31

Amadeus Basin

a: Upper part of the measured section in the Loves Creek Member of the Bitter Springs Formation near Jay Creek (pl.33, fig.37). Looking slightly south of west, almost along strike. The first small valley on the left is on white-spotted red silty dolomite; the figure to the lower right of centre is next to a bioherm of Jurusania chewingsi. The Arumbera Sandstone forms the ridge on the far left.

b: An unidentified stromatolite from the Bitter Springs Formation near Jay Creek; figure reproduced from Banks (1964); scale in inches. This could be a form of Inzeria but no specimens are available for study.

c,d: Stromatolites in the Bitter Springs Formation of the Bonython Ranges, westernmost Amadeus Basin. The coin in c is about 3cm wide. Photographs by courtesy of A. T. Wells, BMR (negative nos G/3228 & G/3232).

e: Oncolites in thin section; possibly from the Inindia Beds, but poor outcrop makes this uncertain; BMR locality BR21, 24 miles north of South Range, Bloods Range Sheet area. x 3.5.

f: Oolites overlying a cumulate stromatolite; thin section normal to bedding. Loves Creek Member of the Bitter Springs Formation in the measured section near Jay Creek. x 0.9.

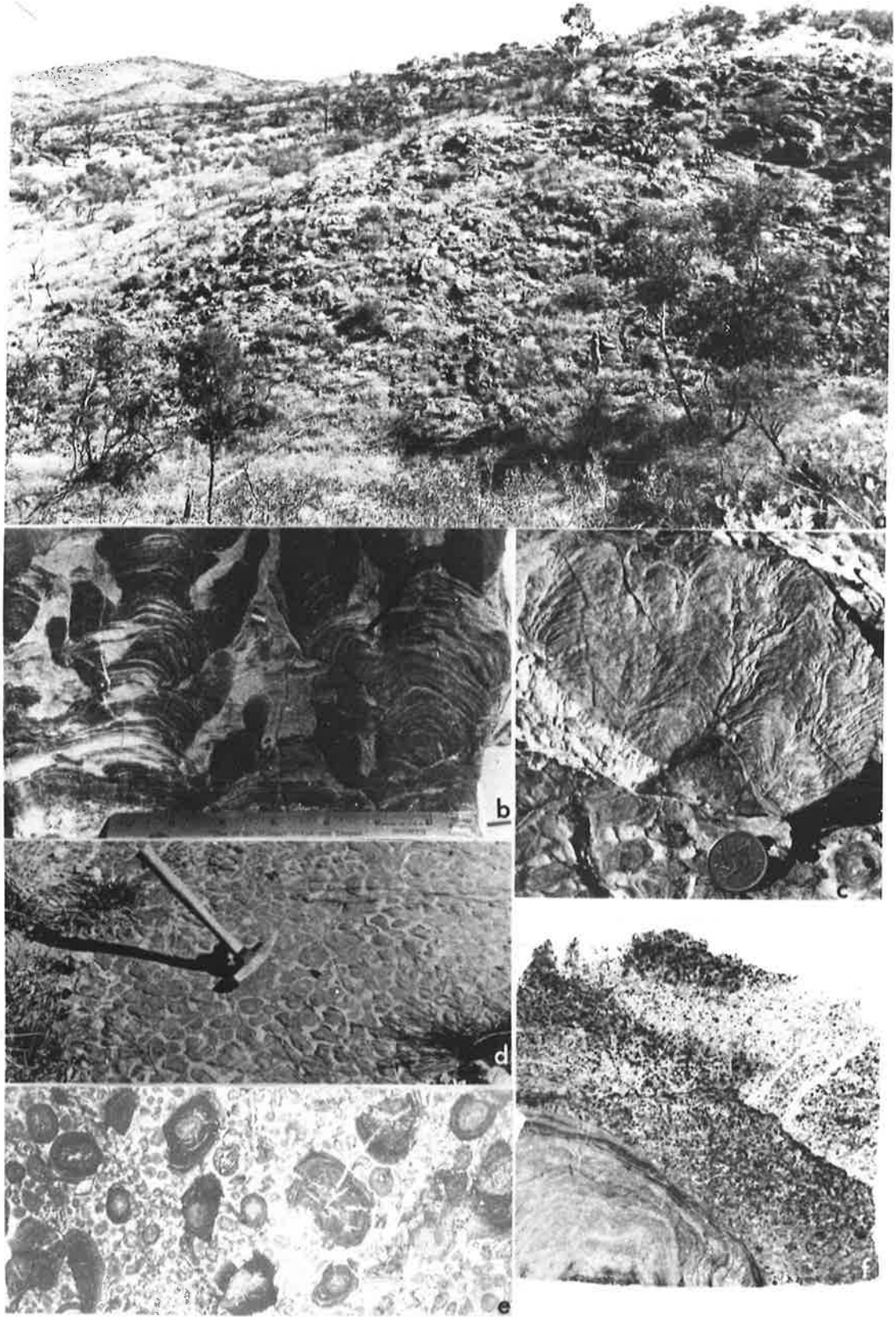
b
c
d
e
f

Plate 32

a: Cumulate stromatolites in the basal Irregully Formation, northern entrance to the gorge of Irregully Creek, Nullagine Basin. The stromatolite on the right grew over an upturned intraclast. Pencil for scale.

b: Large oncolites at the same locality as above.

c: A cumulate stromatolite in the Julie Member of the Pertatataka Formation near Acacia Well in the Amadeus Basin. Pencil for scale.

d: Linked cumuli in the Duck Creek Dolomite adjacent to a permanent large pool in Duck Creek west of Mount Stuart Homestead, Nullagine Basin. Pencil for scale.

e: Pseudocolumnar stromatolites developed on peaked stromatolites, Duck Creek Dolomite, locality as for d. Stratigraphic top towards the top of the photograph.


a


b

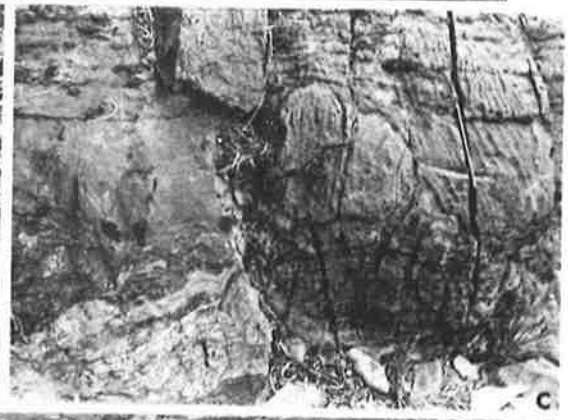
c


d


e

Plate 33

Aerial photographs of two important stromatolite localities in the Bitter Springs Formation of the Amadeus Basin. Photographs reproduced with the permission of the Commonwealth Division of National Mapping.

a: The section measured (fig.37) near Jay Creek is indicated, as is an easy access route. The whole late Precambrian sedimentary sequence is shown here, from the Heavitree Quartzite (dark ridges in the centre and upper part of the photo) to the Arumbera Sandstone (darkest ridge in the lower third of the photo). 10cm is equivalent to 4.1km. Survey 846, Hermannsburg Run 13, Photo 5038.

b: The Bitter Springs Formation on the ridge arrowed contains Inzeria intia and Boxonia pertaknurra. 10cm is equivalent to 3.6km. Survey 851, Alice Springs Run 9, Photo 5140.

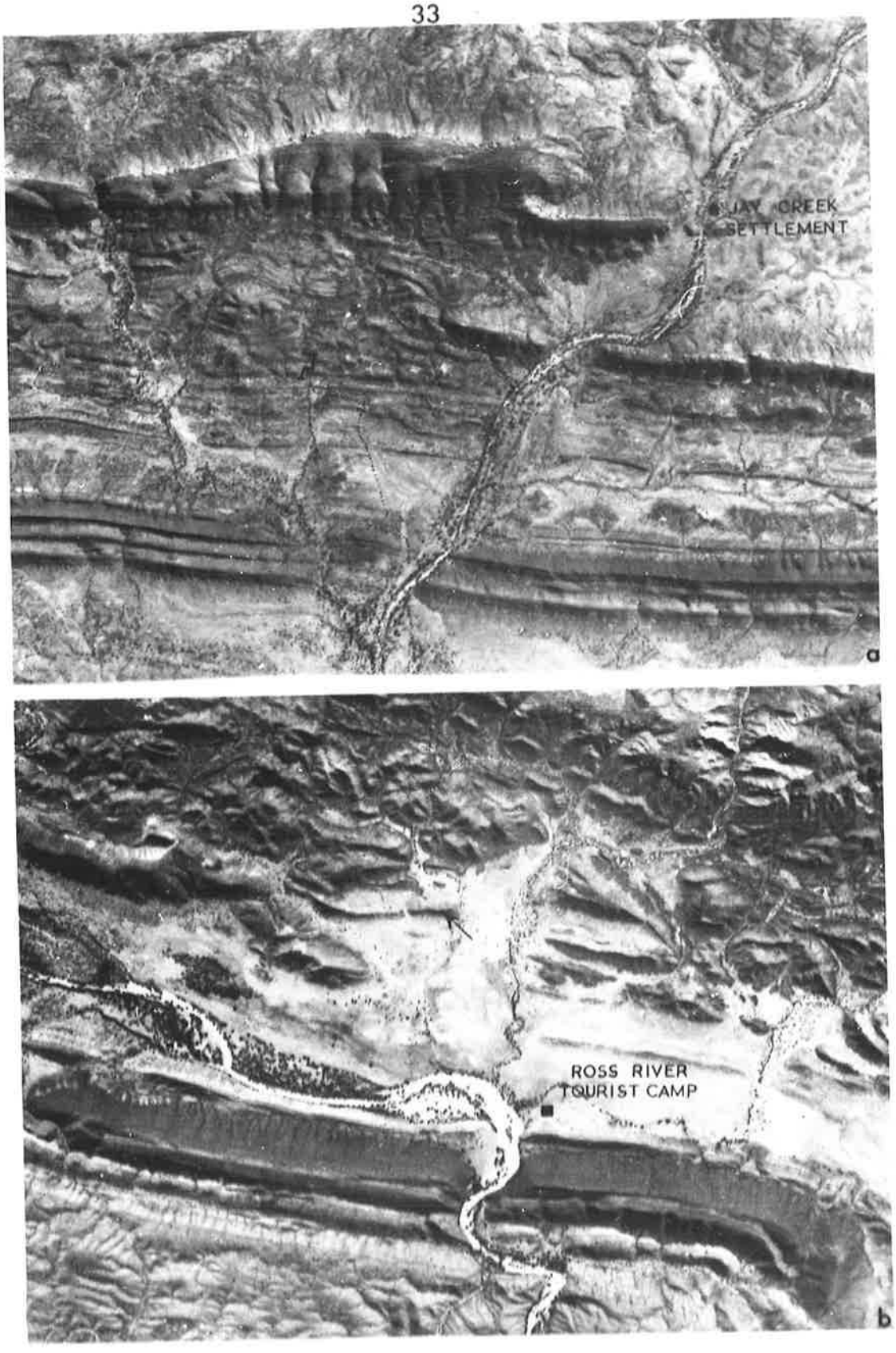
JAY CREEK
SETTLEMENT
a
ROSS RIVER
TOURIST CAMP
b

Plate 34

Brockman Iron Formation, Nullagine Basin

a: Outcrop of part of a typical iron-formation macroband within the Brockman Iron Formation. Chert-rich mesobands appear light grey; note variations in their lenticularity. Dales Gorge Member, Mount Tom Price. x 0.35.

b: Liesegang medusiform structure on the upper surface of a quartz-iron oxide mesoband. Scale about 17cm long, oriented north-south, north at bottom. Joffre Member, 6 miles east of Mount Brockman (20124).

c: Smaller Liesegang medusiform structure from near that of b (above). Note lineation trending 110° true. x 0.3.

d: Radially oriented thin-section of the medusiform structure in b, showing the prominent martite lobes and slight interlobe martite concentrations (black); chert between the lobes; gradational boundaries; fracture systems (the narrow, almost vertical, fractures are concentric with the medusiform structure; thin coat of chalcedonic quartz over uppermost surface. Polarised transmitted light. x 3.3 (20124).

e: Weathered surface of a quartz-iron oxide mesoband; exposed are partly eroded, magnetite walled, chert cored nodes within which are quartz discs, several of which are visible. Hamersley Ranges. Donated by H. F. King. x 0.75 (20130).

f: Thin-section at 90° to banding of one of the nodes shown in e. The chert core of the magnetite walled node contains ellipsoidal quartz structures, two of which are cored with chert. Limonite concentrations on the inner side of the ellipsoids are visible. Transmitted plain light. x 7 (20130).

g: Enlargement of the quartz ellipsoid in the centre of f (turned through 90°). The ellipsoid consists of elongate, radially arranged quartz grains with serrated boundaries and is set in much finer grained chert. Transmitted polarised light. x 18 (20120).

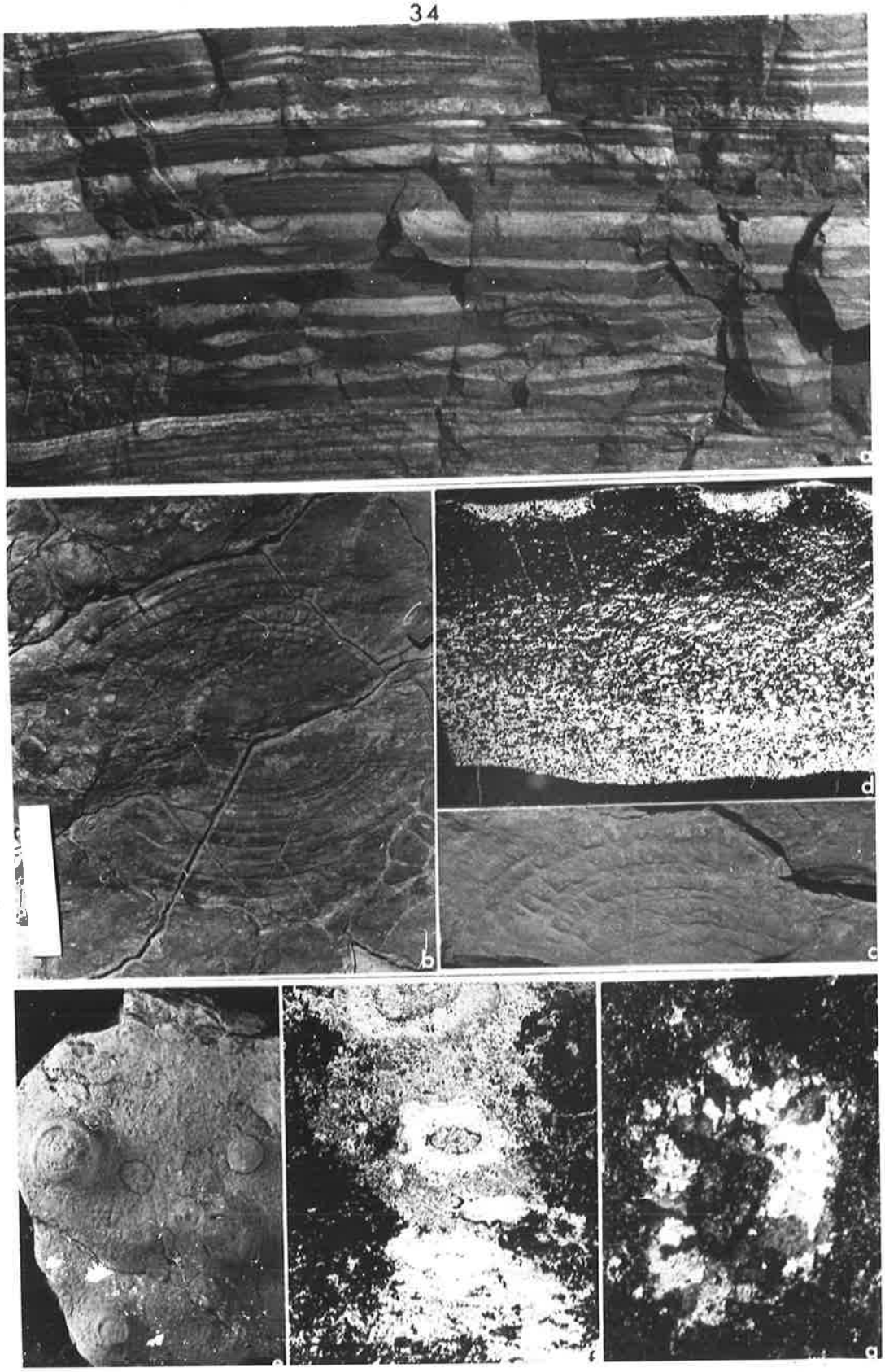
a
b
c
d
e
f
g

Plate 35

Brockman Iron Formation, Nullagine Basin

a: Diapir of quartz that has intruded into a quartz-iron oxide mesoband. Microbands are domed above it. Orientation unknown. Dales Gorge Member, 3/4 mile NNW of Hamersley Homestead. x 0.9 (20125).

b: Polished section of a medusiform structure such as those in c. On the left is an irregular body of quartz within a quartz-iron oxide mesoband. Hamersley Ranges. Donated by H. F. King. x 0.85 (20127).

c: Portions of two medusiform structures centred over quartz masses like those of a and b. Dales Gorge Member, 3 miles NNW of Mount Tom Price. Donated by H. F. King. Scale 5cm long (20126).

d: Medusiform structures possibly the impressions of the diapir kind, associated with ripple mark-like tectonic folds on the upper surface of a quartz-iron oxide mesoband. Dales Gorge Member, 6.5 miles west of Mount Tom Price. Hammer 32cm long. 20128 from this outcrop.

e: Sponge-like nodes projecting from a quartz-iron oxide mesoband into a chert mesoband, as shown in f. Mount Sylvia Formation? (below Brockman Iron Formation). About 1 mile north of Mount Tom Price. Donated by H. F. King. Orientation unknown. x 0.9 (20129).

f: Polished section of the lower of the two nodes shown in e. Note a concentration of chert in the nodes, the sharp contact of this against the chert mesoband (light grey) and the buckled microbands in the quartz-iron oxide (dark grey). x 1.2 (20129).

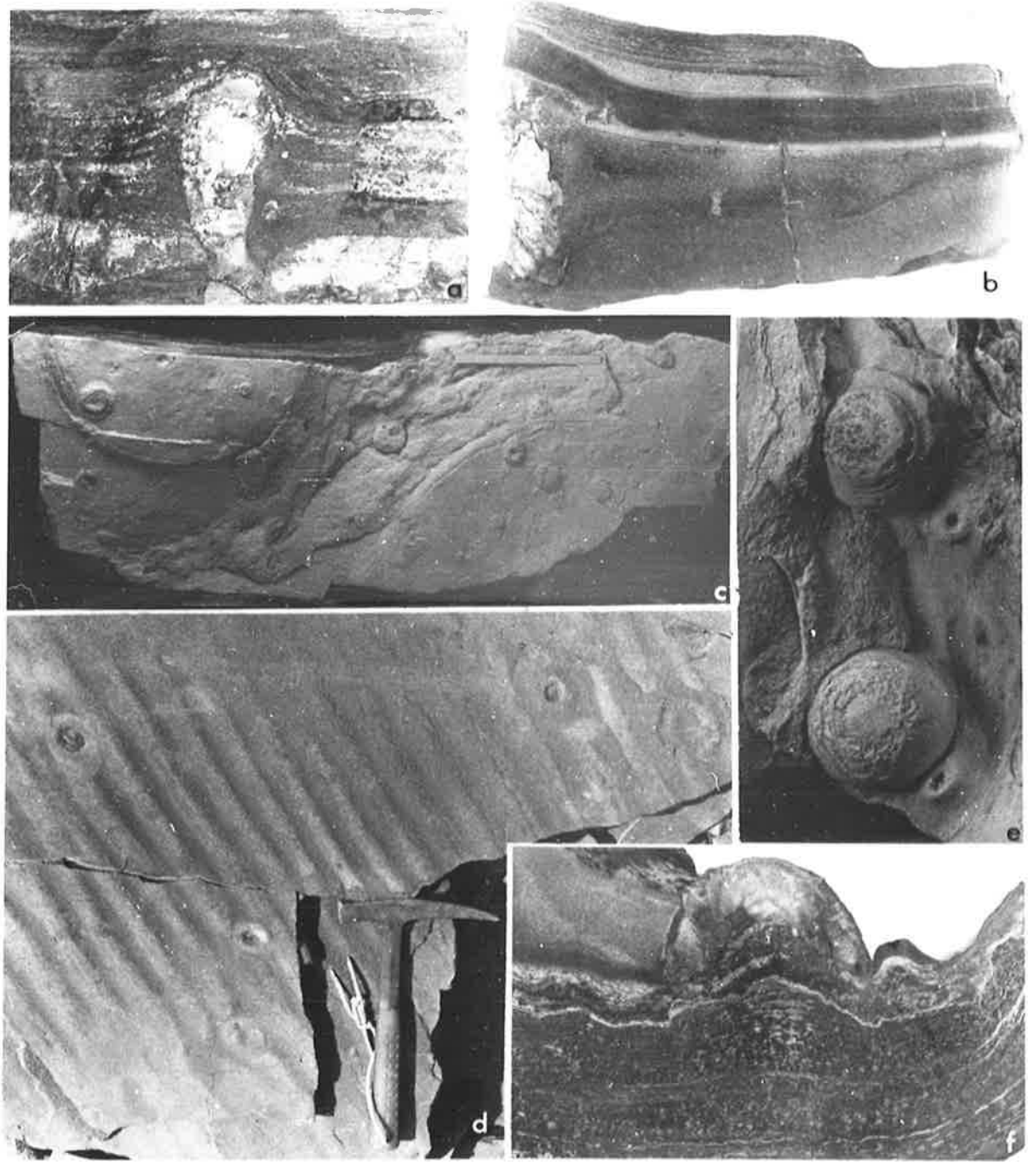
a
b
c
d
e
f

Plate 36

Brockman Iron Formation, Nullagine Basin

a: Discoidal chert pods; bedding surface. Joffre Member, 6 miles east of Mount Brockman. Hammer 32cm long.

b: Irregular chert pods; bedding surface. Dales Gorge Member, Wittenoom Gorge. x 0.15.

c: Thin section of part of a chert pod; chert microbands (light grey) alternate with iron oxide microbands - note their irregularity. Septarian cracks split the pod (the cracks were enlarged during section preparation). Brockman Iron Formation, 6 miles east of Mount Brockman. Transmitted plain light. x 2 (approx.). GSWA F5010.

d: Thin section of a part of a mesoband of "primitive chert". The light grey microbands are chert-rich, the dark grey iron-rich; note how more regular in thickness they are than those shown in c. Dales Gorge Member, 0.75 miles NNW of Hamersley Homestead. Transmitted polarised light. x 3 (20131).

e: Thin-section of the "Collenia cf. kona" of Edgell (1964, pl.2, fig.1). The microbands are depressed beneath the thickenings and not all continuous between them. Brockman Iron Formation, 31 miles NW of Hamersley Homestead. Transmitted plain light. x 0.6 (GSWA F5014).

f: Polished section showing chert pods in quartz-iron oxide. Microbands continue from the pods into the quartz-iron oxide. Dales Gorge Member, several hundred feet below the local plateau surface, within the Colonial Mine, Wittenoom Gorge. x 6 (20134). Photo by Photoservices, University of Adelaide.

g: Bulges over chert lenses (h). The "crater" rims are formed of upturned chert microbands which change to quartz-iron oxide above the chert lenses. Orientation unknown. Dales Gorge Member, Colonial Mine dump, Wittenoom Gorge. x 0.7 (20132).

h: Cross-section of a structure like those of g. The central chert lens lies within a quartz-iron oxide mesoband overlain by a chert mesoband. Brockman Iron Formation, Hamersley Ranges, x 2 (WAM 64-13).

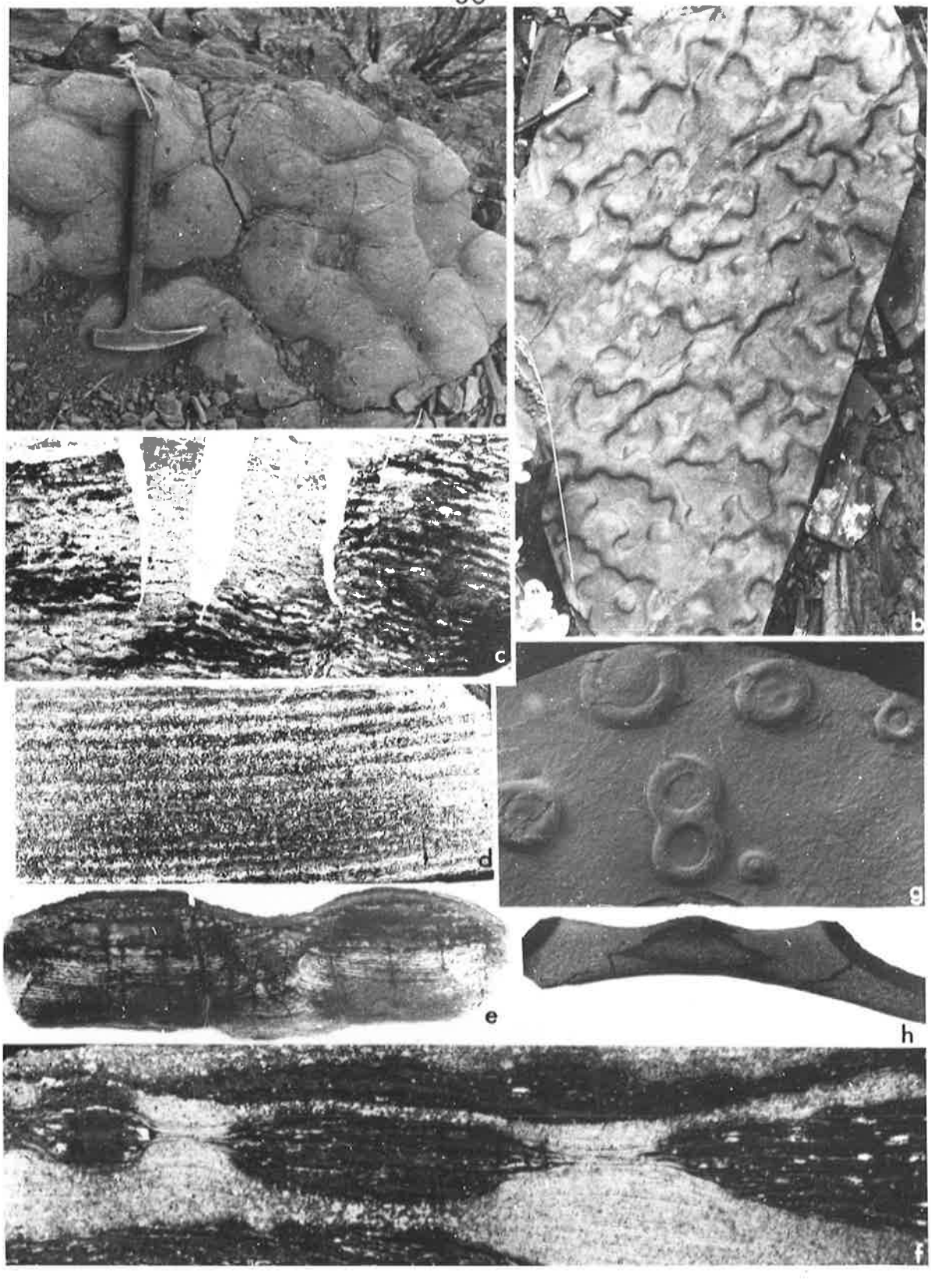
a
b
c
d
e
f
g
h

Plate 37

Brockman Iron Formation, Nullagine Basin.

a: Macule exposed in a wall of Dales Gorge. The central chert core appears pale grey. Dales Gorge Member. Pen 14cm long.

b: Surface of a magnetite mesoband with haematite-filled cracks radiating from above a diapir or macule core. Dales Gorge Member, 3/4 mile NW Mount Tom Price. x 0.6 (20133). Photograph by R. Smitt.

c: Polished section through a chert pod, the convex and concave surfaces of which are shown in d and e. Quartz-tilled septarian cracks prominent in the lower part taper upwards. Folds in the microbands conform to the convex surface. The pod is largely chert; iron oxide-rich microbands are dark grey. Brockman Iron Formation; locality not supplied. x 0.9 (GSWA F5074).

d: As c, convex surface. The surface structure is the expression of radial and concentric folds and septarian cracks, all due to shrinkage. x 0.55.

e: As c, concave surface. Weathering has left protruding the quartz fillings of septarian cracks. x 0.55.

f: Surface of a chert pod in a quartz-iron oxide mesoband. Shallow septarian cracks form an unusual pattern (cf. h). Orientation unknown. Dales Gorge Member, Colonial Mine dump, Wittenoom Gorge. x 0.8 (20134).

g: V-shaped septarian cracks centred on an irregularly deformed area in a shale bed. Donated by Mr D. McKenna. Dales Gorge Member, 2.5 miles NW of Mount Tom Price. x 0.5 (20135).

h: Natural moulds of nodules with septarian cracks, on a bedding plane in a "shale" macroband. Compare the mould in the upper right with the cracked pod of f. Dales Gorge Member, Bismark Gorge (off Wittenoom Gorge). x 0.45 Photograph by N. Beeck, courtesy Western Australian Museum (granules in the lower left are photographic artifacts).

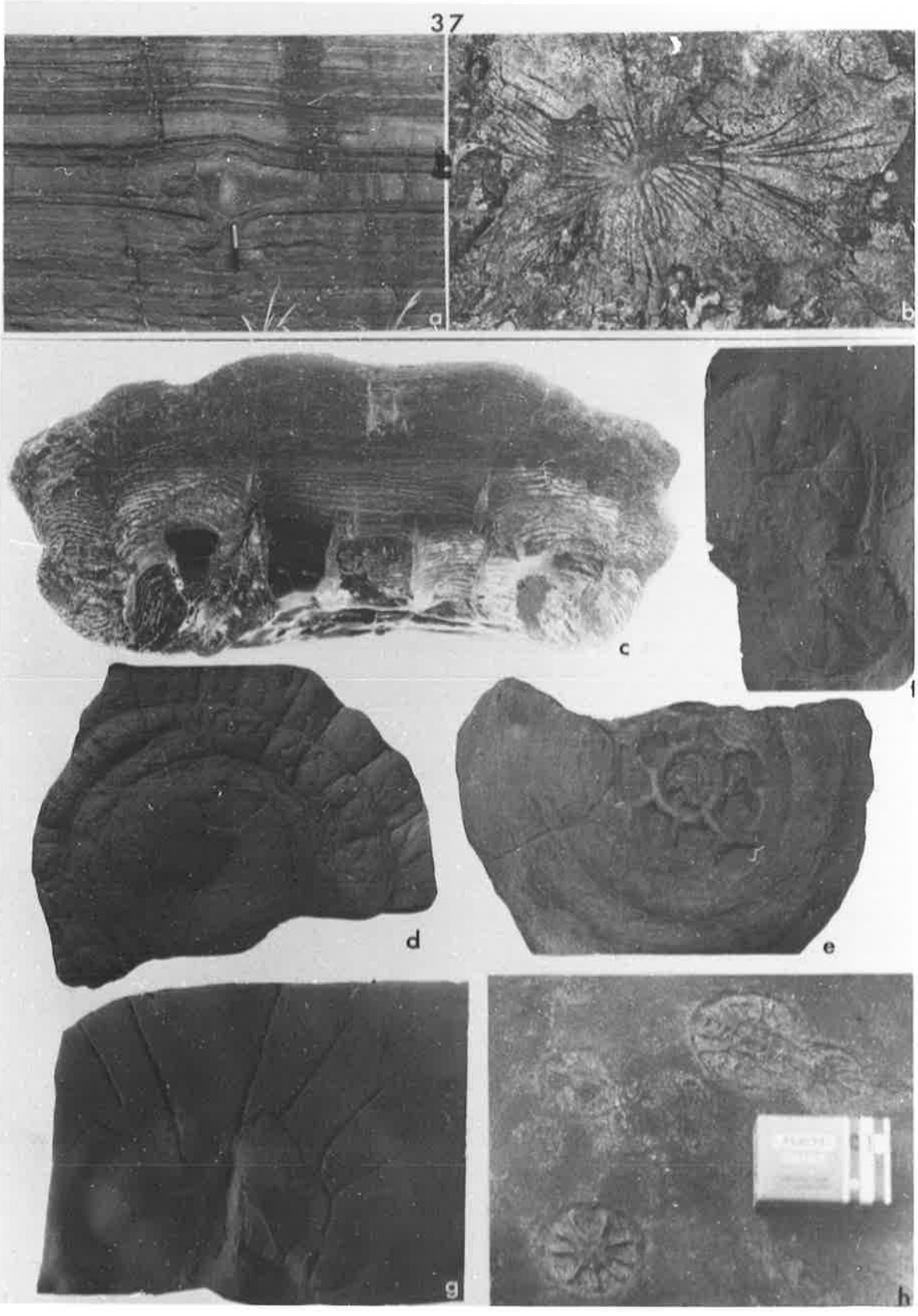
a
b
c
d
e
f
g
h

Plate 38

Brockman Iron Formation, Nullagine Basin

a: The smaller of Edgell's two "*medusae incertae sedis*". The two parallel central ridges are underlain by chert pods (b). Dales Gorge Member, 1 mile North by East of Hamersley Homestead. x 1.8 (GSWA F5001).

b: Polished section through the medusiform structure shown in a: chert concentrations forming the central ridges appear black. The rest of the structure is confined to the uppermost chert microband (pale to dark grey). The bulk of the section is quartz-iron oxide. x 2.

c: Layered, gelatinous colony of diatoms (*Nitzschia* sp., *Amphora* spp., rare *Amphiprora* sp.) from a shallow hypersaline pool. Central dark mass is rock to which the colony is attached. Lake Eliza, southeastern South Australia. x 1.1 Identifications by Dr V. Cassie. Photograph by R. Smitt.

d: Numerous compound medusiform structures on the upper surface of a magnetite mesoband. Dales Gorge Member, 1 mile North by East of Hamersley Homestead. x 0.15.

e: Two of the structures shown in d. The granular texture is due to the weathering into relief of magnetite octahedra. x 0.8 (20136).

f: Portion of a medusiform structure on the surface of a magnetite mesoband. The small "crater" is due to a deformation about a quartz concretion. Dales Gorge Member, 6 miles NNE of Mount Brockman. x 0.8 (20138).

g: Polished section through the centres of two adjacent medusiform structures of d, similar to those shown in e. See figure 50 for explanation. x 1.5 (20137).

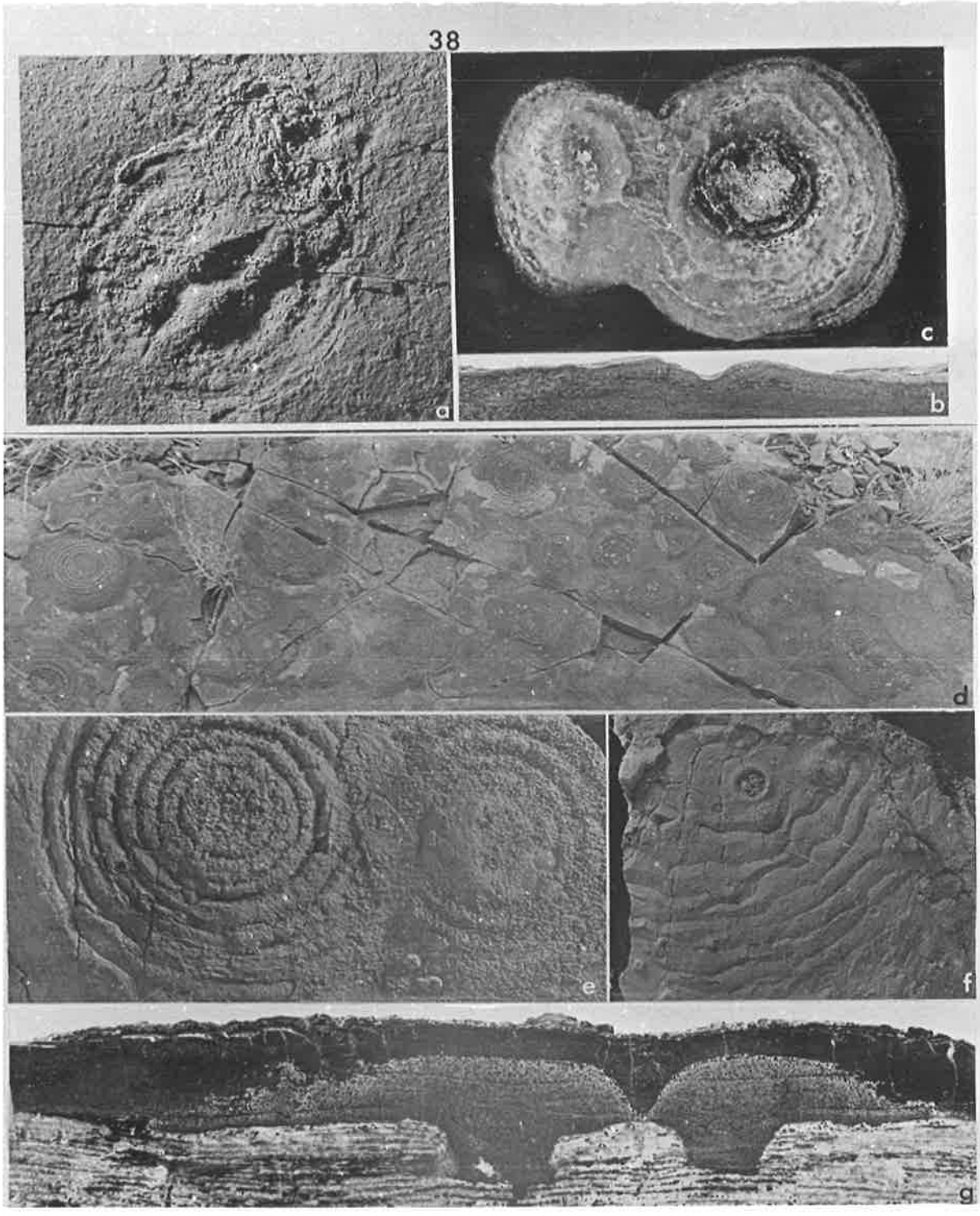
a
b
c
d
e
f
g

Plate 39

Tectonically deformed sand volcanoes from the Noltenius Formation, Pine Creek Geosyncline, Northern Territory.

a: Upper surface of a greywacke bed at the George Creek locality. Note the weakly developed foliation trending from the upper left to lower right. Pencil for scale.

b: Transverse thin section of a small sand volcano (i.e. parallel to bedding) from George Creek. Note the coarse grained core and the grain size gradation in the cone from coarse in the centre to fine at the periphery. During section preparation grains were lost from the fractures. Ordinary light x 0.7.

c: Outcrop transverse section of a cone with nine cores, Tumbling Waters locality. Photograph by R. Smitt. x 0.3.

d: Two of the volcanoes on the same bedding plane as in a. Note the very numerous radial fractures and the cross cutting quartz vein. George Creek.

e: Bedding plane exposure of two contiguous cones; the small cone appears to have deformed the larger, and to have deflected the fractures in the large cone. George Creek.

f: Joint surface showing oblique longitudinal sections of the volcanoes. Tumbling Waters locality.

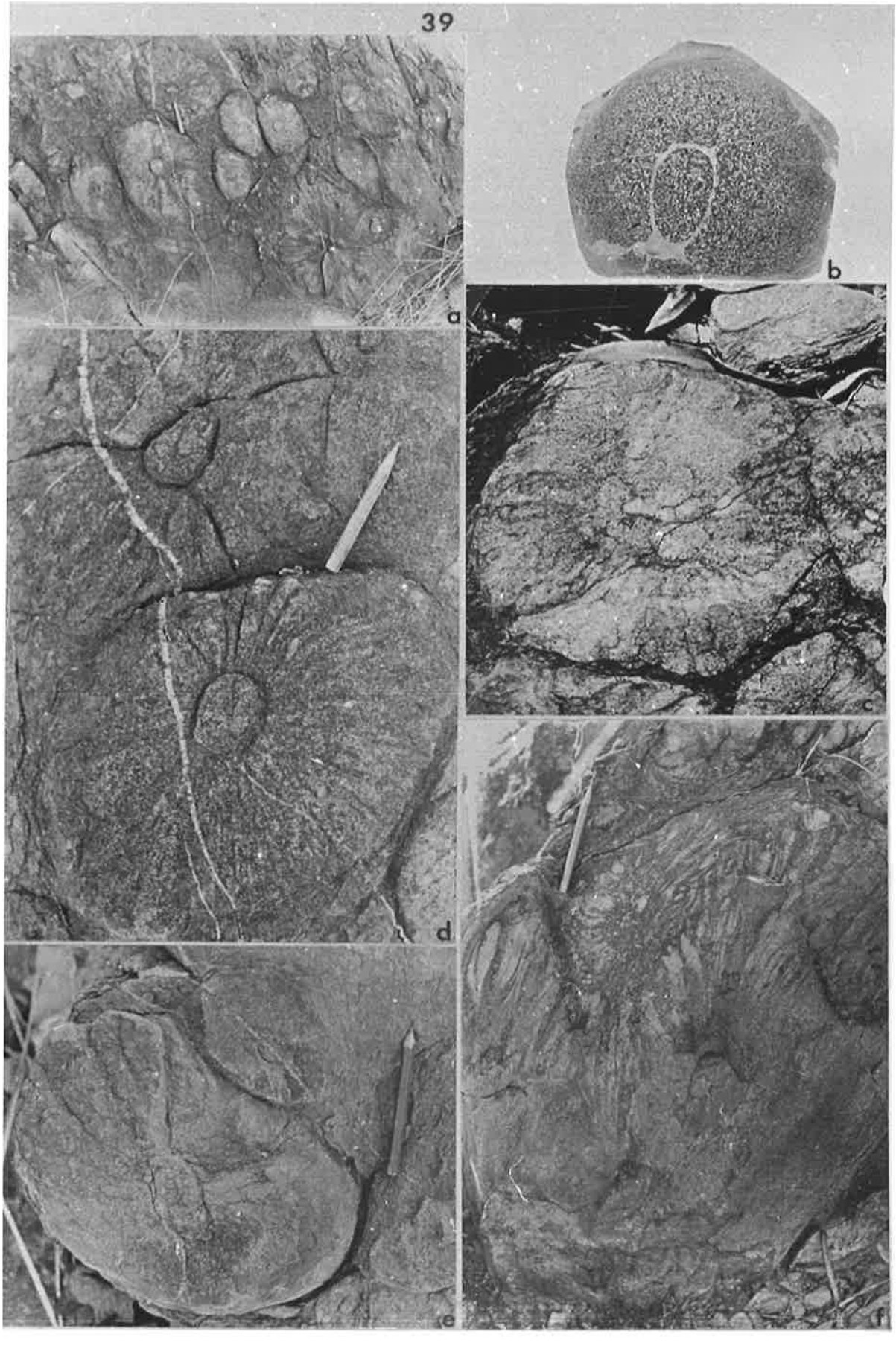
39
a
b
c
d
e
f

Plate 40

Thin sections of tectonically deformed sand volcanoes, Noltenius Formation, Pine Creek Geosyncline, Northern Territory.

a: Axial section parallel to the core. Half of the core shows on the extreme right. The fracture on the left circumscribes the whole cone. Note the decrease in grain size from the centre to the margin of the cone. Laminae in the cone are gently convex upwards but are sharply deflexed at the core and at the outer margin of the cone. Crossed nicols, x 2. Specimen from the George Creek locality.

b: Axial section parallel to core; the core is not present but was parallel to the right hand edge of the photograph (and normal to bedding). Note the intertonguing of fine and coarse layers, with general fining outwards, and the concave upwards laminae. Crossed nicols, x 1.5. Specimen from the George Creek locality.

c: Transverse section of part of the core. Most grains were lost from the concentric fracture zone on the core margin. Ordinary light, x 4. Specimen from the George Creek locality.

d: Section normal to one of the radial fractures. The main fracture zone crosses the section in the upper right, but most grains were lost during section preparation. Parallel fractures split quartz grains. Crossed nicols, x 25. Specimen from the George Creek locality.

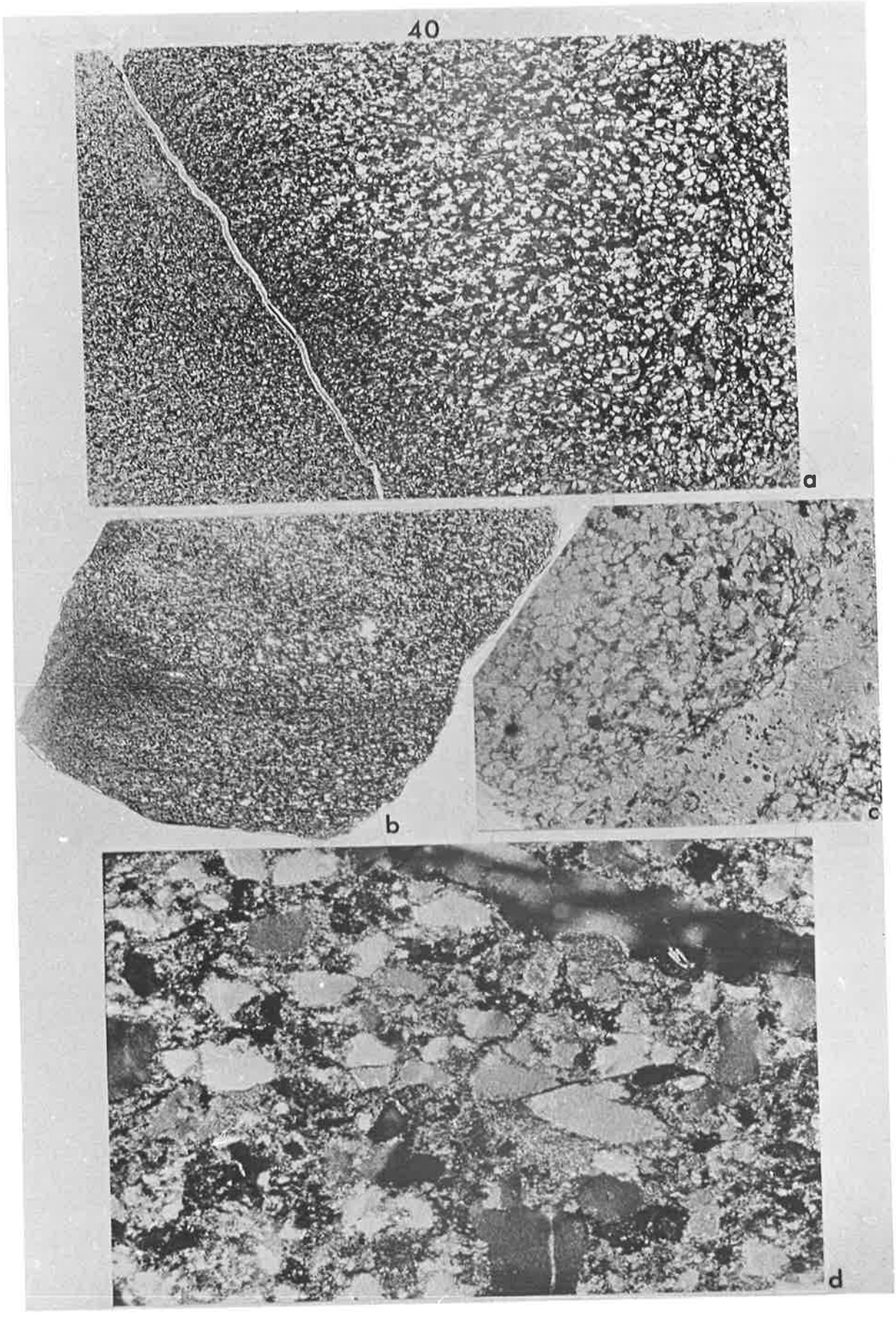
a
b
c
d

Table 5:

The distribution of stromatolites in Australia and correlation with the sequence in the USSR, combining data from this thesis with that in Glaessner, Preiss & Walter (1969) and Cloud & Semikhatov (1969) and with additional information about stromatolites in the Adelaide Geosyncline from W. V. Preiss (pers. comm., December, 1969). Single horizontal lines represent constraints on the age of the sediments provided by isotopic dating, dating with conventional fossils or tillite correlations. The position of the horizontal line beneath the Loves Creek Member (Amadeus Basin) is based on stromatolite correlations. Where isotopic datings are uncertain the probable limits to the ages of the sequences, as determined by the isotopic dating of contiguous igneous or metamorphic rocks, are shown by converging lines within the columns. The lower limit to the age of the Amadeus Basin sequence, as determined isotopically, is very uncertain but the most likely possibility is shown by a dashed line with queries. The upper limit of the age of the Burra Group (Adelaide Geosyncline) is uncertain but the possibility of a long break below the lower tillite is shown by a dashed line. Cloud & Semikhatov (1969) report Inzeria tjomusi Krylov from the Dook Creek Dolomite from near the McArthur Basin; this is not listed because as they state the identification is doubtful.

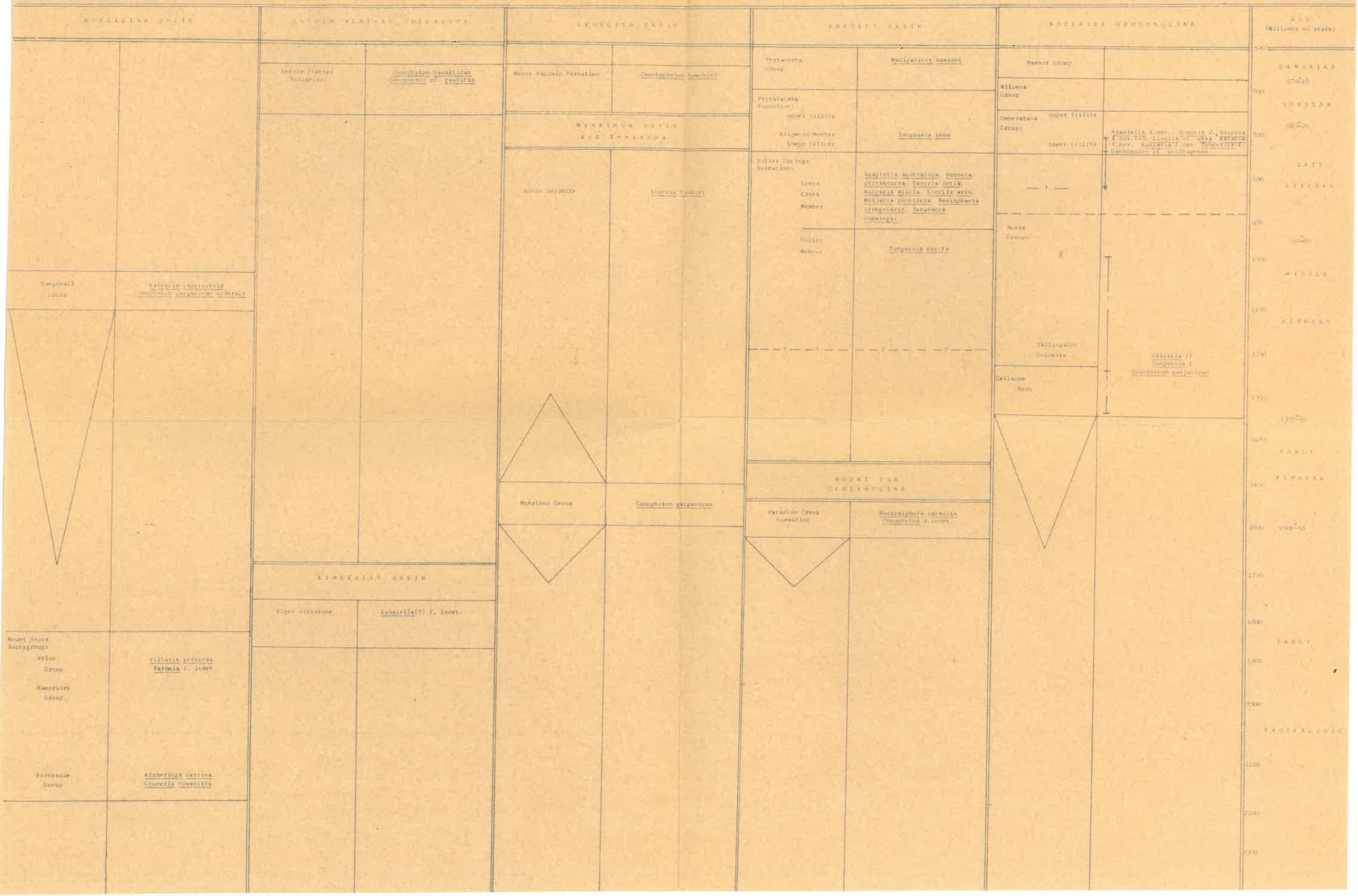
NULLAGINE BASIN
ANTRIM PLATEAU VOLCANICS
GEORGINA BASIN
AMADEUS BASIN
ADELAIDE GEOSYNCLINE
AGE (Millions of years)
Antrim Plateau Volcanics
Conophyton basalticum
Conophyton cf. gaubitza
Mount Baldwin Formation
Jacutophyton howchini
Pertaoorrta Group
Madiganites mawsoni
Hawker Group
Wilpena Group
Pertatataka Formation:
upper tillite
Ringwood Member
lower tillite
Tungussia inna
Umberatana Group:
upper tillite
lower tillite
Acaciella f.nov., Boxonia f., Inzeria f.nov. 1-3, Linella cf. ukka, Katavia f.nov., Kulparia f.nov., Tungussia f., Gymnosolen cf. confragosus
McARTHUR BASIN and Environs
Mara Dolomite
Inzeria tjomusi
Bitter Springs Formation:
Loves Creek Member
Acaciella australica, Boxonia pertaknurra, Inzeria intia, Kulparia alicia, Linella avis, Minjaria pontifera, Basisphaera irregularis, Jurusania chewingsi
Gillen Member
Tungussia erecta
— ? —
Burra Group
?
Bangemall Group
Baicalia capricornia
Conophyton garganicum australe
Skillogalee Dolomite
Baicalia ff
Tungussia f
Conophyton garganicum
Callanna Beds
MOUNT ISA GEOSYNCLINE
McArthur Group
Conophyton garganicum
Paradise Creek Formation
Eucapsiphora paradisa
Conophyton f. indet.
KIMBERLEY BASIN
Tiger siltstone
Kussiella(?) f. indet.
Mount Bruce Supergroup:
Wyloo Group
Pilbaria perplexa
Patomia f. indet
Hamersley Group
Fortescue Group
Alcheringa narrina
Gruneria biwabikia
500
CAMBRIAN
570±15
600
VENDIAN
680±20
700
LATE
800
RIPHEAN
900
950±50
1000
MIDDLE
1100
RIPHEAN
1200
1300
1350±50
1400
EARLY
1500
RIPHEAN
1600
1600±50
1700
1800
EARLY
1900
2000
PROTEROZOIC
2100
2200
2300

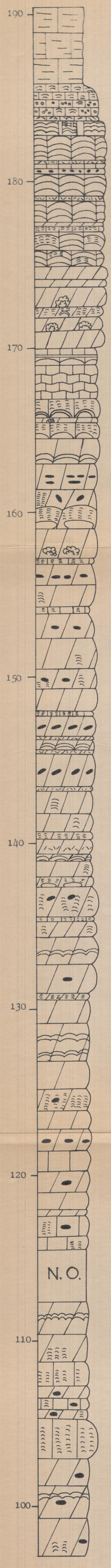

Massive red silty dolomite with white spots

Dark grey stromatolitic limestone

Light buff oolitic stromatolitic limestone
Intraformational conglomerate
Light yellow and grey stromatolitic limestone: small linked cumuli, poor Acaciella australica

Dark grey limestone

Flat-laminated, yellow-weathering, grey-green dolomite
Dark grey limestone: small A. australica+

Dark grey limestone: some large A. australica

Yellow-weathering grey-green dolomite: scattered cumuli, some A. australica, many flat-laminated beds

Dark grey limestone: mostly flat-laminated, large cumuli about 10m wide. some small A. australica

Pale grey-green wavy laminated limestone

Dark grey limestone: large A. australica+. Continues for at least 2.5km
Grey wavy-laminated limestone and dolomite: scattered cumuli
Dark grey limestone: Linella avis+ (Minjaria pontifera+ about 90m E of section. Continues for at least 2.5km

Yellow-weathering pinkish grey to grey-green dolomite: much flat-laminated, much poorly laminated. Separate and linked cumuli and A. australica

Jurusania chewingsi

Dark grey limestone: Linella avis
Yellow weathering grey-green dolomite: mostly flat bedded, poorly laminated, parts cherty. Scattered unbranched columns

Greenish-grey limestone: A. australica

Yellow weathering pale grey-green dolomite: some large and small unbranched columns, much flat-laminated carbonate

Dark grey limestone: A. australica

Yellow-weathering grey-green dolomite: A. australica, rare oncolites

Yellow-weathering grey-green dolomite: Basisphaera irregularis+

Yellow-weathering grey-green dolomite

Yellow-weathering grey-green dolomite

Yellow-weathering grey-green dolomite: large A. australica

Dark grey limestone: A. australica
Bright yellow dolomite(?): red siltstone float, red stromatolitic carbonate float
Yellow and grey-green weathering pale grey dolomite

Bright yellow dolomite(?): A. australica

Yellow-green weathering pale grey dolomite

Grey-green weathering grey dolomite: A. australica

Yellow and grey weathering, grey flat-bedded dolomite and limestone

Grey dolomite: large A. australica
Grey dolomitic limestone: small irregular columnar stromatolites

Yellow-weathering grey dolomite: A. australica?

Dark grey limestone: small A. australica

Yellow-weathering pale grey limestone and dolomite

Dark grey limestone: Kulparia alicia+

Yellow-weathering pale grey laminated dolomite. Mainly flat-laminated, some small linked cumuli, large A. australica near base

Pale grey dolomite: Boxonia pertaknurra offset from section - in creek; position uncertain but in lower part of no outcrop interval

Yellow-weathering grey dolomite: A. australica

Dark grey limestone: A. australica

Yellow weathering grey dolomite
Beds with A. australica (and perhaps some Boxonia pertaknurra other than that specified) alternate with flat-laminated dolomite

Boxonia pertaknurra+ W off section about 80m

Lens of dark grey limestone with possible Kulparia alicia+ and large A. australica

Yellow weathering grey dolomite
A. australica and possibly also B. pertaknurra

Base of Loves Creek Member

Barren, fractured, grey dolomite (Gillen Member)

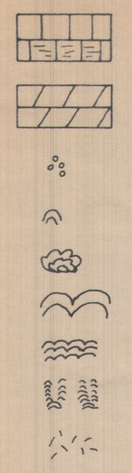

Limestone (silty)
Dolomite
Oolites
Stromatolites: undifferentiated
" cumulate
" large laterally linked hemispheroids
" pseudocolumnar
" columnar
Intraformational breccia
Chert - as nodules or disseminated
+ Stromatolite specimens studied in the laboratory
N.O. No outcrop

Figure 37 Lower part of Loves Creek Member, Jay Creek
Scale in metres